Human Serum Albumin Characterisation and Binding Studies by Spectroscopic Techniques

Banfield, Beulah

Awarding institution:
King's College London

Human Serum Albumin
Characterisation and Binding Studies
by Spectroscopic Techniques

by

Beulah A. Banfield

Submitted to King College, University of London, in partial fulfilment of the requirements for the degree of Doctor of Philosophy

December 2010

Abstract

Human Serum Albumin (HSA) is a plasma protein of great significance with an ability to bind numerous endogenous and exogenous ligands, having a single polypeptide chain of 585 amino acids constructed in three domains of relatively equal size. Although HSA's existence has been known for many years, its characterisation and ability to bind ligands still remain enigmatic. Only in 1992 was the crystal structure of HSA reported (*Carter and Ho, 1992*). Effective crystallisation and the determination of meaningful crystallographic data and structure had proven difficult. The 1992 report concerned HSA crystals grown using zero gravity conditions.

The objective of this project is the characterisation of recombinant and native HSA using Ultra-violet (UV) & circular dichroism spectroscopy (CD) and involved HSA conformational changes, which altered the ability to bind or off-load ligands. Changing environment, together with the use of characteristic "marker ligands," influences binding to provide a handle that can be utilised and monitored. This enables the assignment of binding sites and the study of perturbating conditions.

Changing conditions such as pH, temperature, ionic strength and solvents in the presence and absence of ligands were employed to extract further information on this elusive protein. Fragments of recombinant HSA were also used (namely domain I and domain I + II) under identical conditions as the whole protein in order to help elucidate and assign binding sites.

To my family Lawrence, Amanda and Rebecca for your continued patience, support and understanding. Your willingness to adapt to the changes throughout this project has meant that I have been able to spend the time needed to complete.

This project is also dedicated to my mother (Rosalina Leona Thornhill) and late father, without their continued presence, encouragement and support I would not have completed.

This war is over, this battle won.
This thesis is completed.
I thank the Lord
In Jesus' name
Amen

In loving memory of my father, Mr Cleveland Edbert Thornhill

Acknowledgements

Firstly I would like to express my thank to Dr A. F. Drake, my supervisor, for his continued guidance and support throughout my PhD, always being available when the inevitable problems arose. Thanks are also sent to Dr John Woodrow and colleagues at Delta Biotechnology (Nottingham, UK.) for their continued interest and for providing me with the samples of albumin (human, defatted and recombinant albumins, also the domain fractions) as well as supplies.

I would like to thank Frank Boretto and Les Spencer at Birkbeck College (University of London) for the provision of chemicals, equipment and their general assistance without which would have made the preparation of some samples difficult.

Thanks are expressed to Dr Simon Senior, Dr Antje Nordmann (both former students of Birkbeck College, London) for their support and words of encouragement.

Last I would like to thank Dr Tam Bui (Kings College, London) for her support and ever ready proverbial boot dispensed as and when required. Dr Bui has given her unreserved encouragement especially throughout the latter part of this project.

Thanks to all concerned.

Index

Index **Page:**

Index **Page:**

Index **Page:**

Index **Page:**

List of Figures Page:

List of Figures **Page:**

CHAPTER 3 Spectroscopy

CHAPTER 4 Spectroscopic Characterisation of HSA

List of Figures **Page:**

CHAPTER 5 Small Ligand:HSA Interaction

List of Figures **Page:**

List of Figures **Page:**

CHAPTER 6 Large Ligand:HSA Interaction

List of Figures **Page:**

List of Tables Page:

CHAPTER 1 Structure and Properties of Human Serum Albumin (HSA)

CHAPTER 2 Ligand Binding

CHAPTER 3 Spectroscopy

CHAPTER 4 Spectroscopic Characterisation of HSA

List of Tables **Page:**

CHAPTER 5 Small Ligand:HSA Interaction

CHAPTER 6 Large Ligand:HSA Interaction

Introduction

The ubiquitous nature of human serum albumin (HSA), sometimes referred to as albumin, has ensured that it is a much studied protein, and its reluctance to relinquish all its structural characteristics has tantalised the curiosity of scientist for many years. However, persistency has paid off with a plethora of information resulting in the first crystal structures of albumin being determined by Carter in 1989, and more recently by scientists such as Curry *et al* 1998, Carter *et al* 1999, Sugio *et al* 1999, Bhattacharya *et al* 2000 and Yang *et al* 2007. There has been an explosion in the crystallographic information available on HSA and slowly its structural information is being revealed. Albumin, once thought to be a scavenger with no specific binding function other than to "mop up" and transport excess ligands is now thought to be responsible primarily for the transport of unesterified fatty acids (FA) together with the ability and capacity to bind numerous drugs and metabolites (covered in more detail later) (*Curry et al, 1998*). FA is an essential component in the body and is used in membrane lipids, hormones as well as being an important source of metabolic energy. Albumin aids in the transport of FA which have a low solubility and are stored as triglycerols in the body's adipose tissue (*Bhattacharya et al 2000*). There is between 0.1 – 2 moles of FA bound to albumin through hydrophobic interactions which although bound tightly is in rapid exchange with the solution (a more detailed account to follow). Albumin's high ability to bind, transport and off-load FA makes it an ideal facilitator for the transport of FA (*Muravskya et al, 2004*). As many as twelve FA binding sites have been detected on HSA, the number of sites found are determined by the chain length of the FA with a certain degree of unspecificity shown by albumin as to arrangement of binding sites. An asymmetrical distribution of FA sites is observed.

HSA is a plasma protein with an *in vivo* concentration of approximately 50mg/ml and a molecular weight of 66500D, whose existence together with haemoglobin and fibrin were

recognised as far back as 1916 (*Peters, T. Jr., 1996*). Many attempts have been made to isolate and characterise serum albumin, however, it was the medical applications in World War II that prompted the biggest achievements in albumin purification. The sequence and structural similarities between bovine serum albumin (BSA) and human serum albumin (HSA) prompted the use of bovine serum albumin in place of human. The huge demands on albumin during the war together with the availability of bovine albumin made it an ideal substitute for human serum albumin. Unfortunately, small differences between the two plasma proteins were sufficient to produce deleterious effects in some patients, and proved fatal in others (*Peters, T. Jr., 1996*). The use of BSA in humans was terminated. Cohn and co-workers, during the 1940's, purified BSA from cold alcohol, producing a flocculent white precipitate. The protocol revolutionised albumin purification with the removal of alcohol by evaporation at low temperature, thus removing the need for salt to precipitate (salting-out) the protein. This method had the benefit of suppressing bacterial growth in the absence of salt (*Cohn et. al., 1941*).

Albumin, being the major blood plasma transport protein binds numerous different endogenous and exogenous compounds that would be toxic in the unbound state but rendered non-toxic by virtue of its bound state (*Olsen et al, 2004*), a mode of action that has enabled albumin to act as an extracellular antioxidant (*Kragh-Hansen, 1990, and Halliwell, 1988*). Albumin's high concentration is responsible for buffering the blood to pH 7.4 and maintaining 80% of the bodies colloidal osmotic pressure, 30% due to the presence of HSA itself and the other 50% due to the presence of cations like sodium and potassium associated with the negative surfaces of albumin (*Tavirani et al, 2006*). HSA is the most abundant secreted protein found, and belongs to a class of proteins which share the same multigene deriving from 190 amino acids (aa) (others include α-fetoprotein and the vitamin D-binding protein) (*Peters, T. Jr., 1985, and Kraig-Hansen, 1990*). The gene for albumin is located on chromosome 4 that is 16,951 nucleotides long from the

putative “cap” site to the first poly (a) addition site. It is split into 15 exons which are distributed throughout the three domains that are the result of triplication of a “single primordial domain” (*Wikipedia, 2007*).

Albumin is found in all secretions, including concentrations of between 0.1 - 0.5mg/ml in the gastrointestinal track. Trace amounts have also been detected in sweat and tears, with about 30mg excreted in urine per day (*Rosenoer, 1977*). As one of several transport proteins found in the body, albumin is unlike the other proteins that show great specificity binding only one or two ligands. HSA will bind numerous ligands reversibly with high affinity, particularly those with limited solubility in blood that include long chain fatty acids (LCFA) and bilirubin (*Blaur et. al., 1978*). HSA can also transport ligands such as haematin, thyroxin and some steroids whose specific transport proteins are saturated (*Seery, et. al., 1977*) It is said that more than 70% of drugs can be transported by albumin (*Kratochwil et al., 2002*). Clean albumin appears white, but bound ligands such as bilirubin induces a yellow colour with an intensity dependent upon the amount of the ligand bound.

HSA, compared to other proteins of similar molecular weights has proven to be atypical; this may explain some of the diversities of the protein. The content of tryptophan is unusually low, one in human and two in bovine, the average found in proteins generally is around seven. The hydrophobic amino acids, Methionine (6 residues), glycine (12 residues) and isoluecine (8 residues) are also atypically low (*Peters, T. Jr., 1996*) for proteins with MW ~ 65000. Conversely, the numbers of cystine, leucine and ionic residues like glutamic acid and lysine are unusually high giving a large number of ionisable residues, estimated to be around 185 charges per molecule of HSA at pH7. Since there are more negative charges present (i.e. more acidic residues), HSA has a high negative charge. At pH7 the charge number lies between -12 and -17 which facilitates the solubility of the protein. Albumin is the most acidic plasma protein found in

the body, essentially not glycosylated, it is one of a few proteins to have little to no association with carbohydrates. Only 1% of glucose is bound to albumin in the average person. The inability of albumin to bind carbohydrates is thought to be associated with the lack of the sequence:

Asn - X - Ser / Thr

where X is any amino acid other than proline that inhibits the functionality of this site; the low presence of carbohydrates is an ideal marker for the quality control of HSA purity (*Hughes, W. L., 1954*). The purity of HSA is based on having a carbohydrate concentration of less than 0.05%; the integrity of HSA is determined by electrophoresis which shows albumin to be essentially a single species.

In the body there exists in equilibrium two pools of albumin, vascular and extra-vascular pools of 140g and 180g respectively, with the vascular pool being the more important metabolically. The heterogeneous nature of the extra-vascular pool exhibits exchanges of varying rates. Exchanges between, for example, the lymph and metabolically active organs are fast, whilst exchanges with muscles and skin are slow. The vascular pool circulates around the body once every minute only spending between 1-2 seconds exchanging transported substances with cells. Albumin is replaced at a rate of 14g/day and has a half-life of between 19-20 days (*Blaur et. al., 1975*). The synthesis of albumin is primarily affected by nutrition, but is also influenced by osmotic pressure, state of health and hormones such as thyroxin, cortisone, insulin and growth hormones. Hormonal influence can stimulate synthesis by up to 30%, but this effect causes an automatic increase in the rate of catabolism by the same amount keeping the relative overall concentration the same (*Roseneor et. al., 1977*).

Small amounts of HSA are present in infants under the age of two. However, studies have shown albumin production increases dramatically during the last month of gestation, reaching levels of up to 40mg/ml. Specific to infants is a protein called α-fetaoprotein (AFP) which is similar to

HSA but contains 5 extra residues (590 as opposed to 585) giving a molecular weight of 68950D (as opposed to 66500), and belongs to the same group derived from the same multigene (*Peters. T. Jr, 1992*). AFP contains five more residues in the region of 1-10 in loop 1, and has very similar physical properties to HSA, sharing a similar size, shape and ability to bind numerous ligands. But unlike HSA, AFP has a weaker ability to bind long chain fatty acids (LCFA), having only three binding sites as opposed to albumin that has been reported as having up to ten. AFP has 32 cysteines compared to HSA's 35, 30 of which show similar sequence alignment to HSA (*Peters T. Jr 1996*). The disulphide forming loop six in HSA is missing in AFP, and there is a half cystine at position 18 which will not form a free thiol. One significant difference between AFP and HSA is that AFP has an n-glycosylated site in subdomain IIA that enables it to bind 4% of carbohydrates (*Krusius et al, 1982*). There is only a 39% sequence homology between the two. Both AFP and HSA are synthesised in the liver, but many questions remain unanswered about the mechanism. The biosynthesis of HSA is thought to occur in the hepatocytes in the liver, and is secreted into the hepatic plasma where it enters the circulatory system (*Glaumann, H., 1970, Peters et al, 1971*). The initiation of synthesis is triggered by a hydrophobic 'signal peptide', 18 residues long (Figure1). Transcribed mRNA affixes itself to cytoplasmic ribosomes where synthesis takes place. The signal peptide guides the nascent 'preproalbumin into the cytoplasmic secretary canals where cleavage leads to 'proalbumin' (*Blaur et al. 1975)*, where molecular folding occurs. The proalbumin is cleaved further with the loss of a basic amino-terminal hexapeptide just before secretion from the hepatocytes, cleaving (Arg-Gly-Val-Phe-Arg-Arg) sequence in most mammals. Not much is known about the propeptide, but it is thought to be responsible for the correct alignment of the Cys prior to S-S formation, and is also believed to be responsible for protecting the nascent protein against enzymatic cleavage. Chaperonins are thought to bind to the partially folded protein, protecting it and completing the folding process (*Ellis et. al. 1991*).

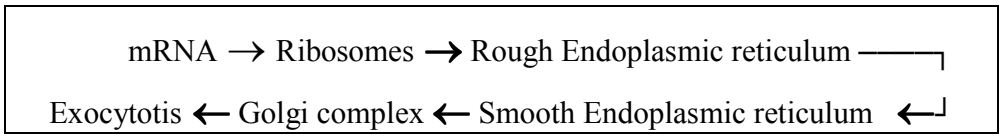

Figure 1. Schematic Representation of the Synthetic Route of HSA

The liver is the primary site found for albumin production, and the synthetic cycle takes on average 25mins to complete. However, albumin is not secreted immediately on synthesis but is retained for 20-30mins prior to secretion., HSA is not stored but synthesised as and when required. Unlike its metabolism, the catabolism of HSA is vague. Neither the mechanism nor the site of catabolism are known. During its 27day journey around the body, albumin picks up many small ligands that stick to the molecule. Structural damage also occurs with 'nicks' and tears appearing. The rate of degradation is proportionally linked to the rate of synthesis, ensuring the overall concentration remains constant. The manner in which albumin molecules are selected is not fully understood, but it is believed that criteria such as oxidation, additions and S-S interchanges play an important part in the selection process. HSA is broken down into its constituents and released into the body for further peptide formation. 14g/day of albumin is replaced, of which 5% of the body's nitrogen is supplied by albumin in this way. Degradation is thought to occur in the cytosol where most of the peptidases are concentrated.

This thesis endeavours to provide a closer understanding of the characteristics, behaviour and binding capabilities of HSA, to reduce some of the ambiguity surrounding the protein and to postulate further advances on the road to discover our most illustrious protein. A lot of work as been carried out in recent years that has brought us ever closer to unlocking albumin's illusive structural characteristics, but with any reluctant protein, albumin still remains as complex as ever showing diverse characteristics when cocktails of ligands are considered. There is still a lot of work left before we can eventually say that this protein has been "studied to death."

CHAPTER 1

Chapter 1: Structure and Properties of Human Serum Albumin (HSA)

1.1 Introduction

Albumin is one of a few specialised proteins that exhibit non-specific polyligand binding phenomena; its veracity to bind numerous ligands with great affinity is unprecedented as no other protein in the body binds with such indiscrimination (*Zunszain et al, 2003*). The ability of albumin to bind stems from an unusual distribution of amino acids together with conformational abilities strongly influenced by environment (*Rosenoer, 1977*). The conformation of albumin is pH dependent (*Peters, T. Jr., 1996*); observed pH induced changes are reversible in the range of pH 2 – pH 12, with the formation of five defined structural states that will be discussed later (*Basir et al, 2007*). The conformational characterisation of albumin has been fraught with difficulties. Although a much studied protein, the structure of HSA in part has challenged scientists, made difficult by its relatively large size, which has made the determination of qualitive data by conventional means difficult (*Fanall et al, 2007*).

One contentious area in the structural elucidation of albumin has been the number, availability and location of binding sites, be they pockets or tunnels. This has caused much debate. He and Carter were the first to have initial success in not only managing to obtain decent crystals that yielded measurable X-ray diffractions, but also obtaining meaningful diffraction patterns from them, enabling the elucidation of secondary and more importantly tertiary structure. The determination of the X-ray structure (*Carter, 1989*) has provided a greater understanding of the size and shape of albumin and its binding sites. However, the routine determination of the albumin structure remained difficult; NMR is restricted as the tumbling rate of such a large molecule is slow which causes broadening of the resonances.

1.2. Amino Acid content and Primary Structure of Albumin

HSA is a negatively charged, unglycosylated single polypeptide of 585 amino acids (MW ≅ 66,500D), with an *in vivo* concentration of approximately 50mg/ml (*Peters, 1985*) and is responsible for approximately 80% of the colloidal osmotic pressure in the body (*Carter, 1994*). Although albumin is unglycosylated, nature allows for approximately 10% formation by non-enzymatic glycosylation involving the ∈-amino group of lysine 525 (*Shaklai et al, 1984*). This site specific glycosylation results in a change in the conformation that affects the way in which some ligands bind to glycosylated albumin, with the result of reduced binding of some ligands such as fatty acids. However, haemin binding remains unaffected. This effect has implications when looking at albumin from diabetic patients, who as a whole have detectable levels of glycosylated albumin.

The molecular structure of albumin divides into three domains that can all be further sub-divided generating six subdomains. The complete amino acid (aa) sequence of HSA was determined by Meloun (*Meloun et al., 1975*) and is shown in Figure 1.1., complementing the work of J. R. Brown on his sequence determination of bovine serum albumin (*Brown, 1975*). The comparison of bovine and human albumin shows great similarities. However, the differences are significant to make the use of bovine albumin in humans non-compatible. Table 1.1 shows the distribution of amino acids within human albumin in comparison to BSA. There are great similarities between the two in terms of both structure and sequences, giving 76% sequence homology (*Peters, 1985 and Carter et al, 1993*). As an alternative to native human serum albumin, the production of the recombinant product is now in development and the initial results look promising.

Figure 1.1. Amino Acid Composition of Human and Bovine Serum albumin. *(Rosenoer, 1977)*

Amino Acid & Single Letter Code	Human		Bovine		HSA/BSA
	N° of Residues	% Composition	N° of Residues	% Composition	Fractional Difference
Aspartic Acid (D)	36	6.2	40	6.9	0.9
Asparagine (N)	17	2.9	14	2.4	1.2
Threonine (T)	28	4.8	34	5.8	0.8
Serine (S)	24	4.1	28	4.8	0.9
Glutamic Acid (E)	62	10.6	59	1.1	1.1
Glutamine (Q)	20	3.4	20	3.4	1.0
Proline (P)	24	4.1	28	4.8	0.9
Glycine (G)	12	2.1	16	2.7	0.8
Alanine (A)	62	10.6	46	7.8	1.3
Valine (V)	41	7.0	36	6.2	1.1
Cysteine (C)	35	6.0	35	6.0	1
Methionine (M)	6	1.0	4	0.7	1.5
Isoleucine (I)	8	1.4	14	2.4	0.6
Leucine (L)	61	10.4	61	10.5	1
Tyrosine (Y)	18	3.1	20	3.4	0.9
Phenylalanine (F)	31	5.3	27	4.6	1.1
Lysine (K)	59	10.1	59	10.1	1.0
Histidine (H)	16	2.7	17	2.9	0.9
Tryptophan (W)	1	0.2	2	0.3	0.5
Arginine (R)	24	4.1	23	3.9	1.0
Total	585	100.1	583	99.7	

Table 1.1 Comparison between the amino acid content of human and bovine HSA.
(U. Kragh-Hansen, Danish Medical Bulletin, 37, 1990, 57 – 88)

The amino acids in albumin form nine loops arranged into a distinctive pattern. Each domain contains three loops arranged with one long, one short and one long loop. The arrangements of the loops in relation to the nomenclature of the domains are as follows;

Loop	1 – 2	4 – 5	7 – 8
Domain	IA	2A	3A

Loop	3	6	9
Domain	IB	2B	3B

Although the domains show some structural similarities with some degree of sequence conservation, there is only between 18-25% sequence homology at best (Table 1.2). The differences in sequence are sufficient to show differences in the domain activity especially where binding is considered.

Domain I	Versus	Domain II	25% Identical
Domain II	Versus	Domain III	20% Identical
Domain I	Versus	Domain III	18% Identical

Table 1.2. Comparison of Identical Residues in each Domain.

Protein folding is an intricate and complicated process that yields a biologically active product. This is further complicated if the protein contains domains that are able to fold independently and interact with one another (*Wetlaufer, 1981*). The X-ray crystal structure of intact albumin has shown how HSA divides into three homologous domains. With that in mind, Dockal and coworkers have determined the crystal structure of the individual domains of albumin by means of cloning and expression (*Dockal et al, 1999*). Conventional methods to separate the domains using chemical cleaving or proteolytic techniques have shown to produce defective domains; the reagent used dictates the cleavage products. Often the fractions generated by such methods are non-representative of the domains in the intact protein, and result in "unimpaired structural integrity," which in turn can lead to a debilitation in domain functionality. The cloning and expression of HSA creating fractions of domain I (1 - 197), domain II (198 – 385) and domain III (386 – 585), with partial overlapping of some regions of the domains, creates fractions with intact domains cleaved at natural boundaries. The ability to produce stable intermediates and determine their conformation has aided in elucidating the tertiary structure and function of the whole protein. Figure 1.2. shows consistency in both the secondary and tertiary structures of the three domains of albumin. Unlike the sequence homology, the secondary and tertiary structural homology shows very close agreement, but contains subtle differences sufficient to affect the functionality of the domains with domain I being the least active in terms of ligand binding.

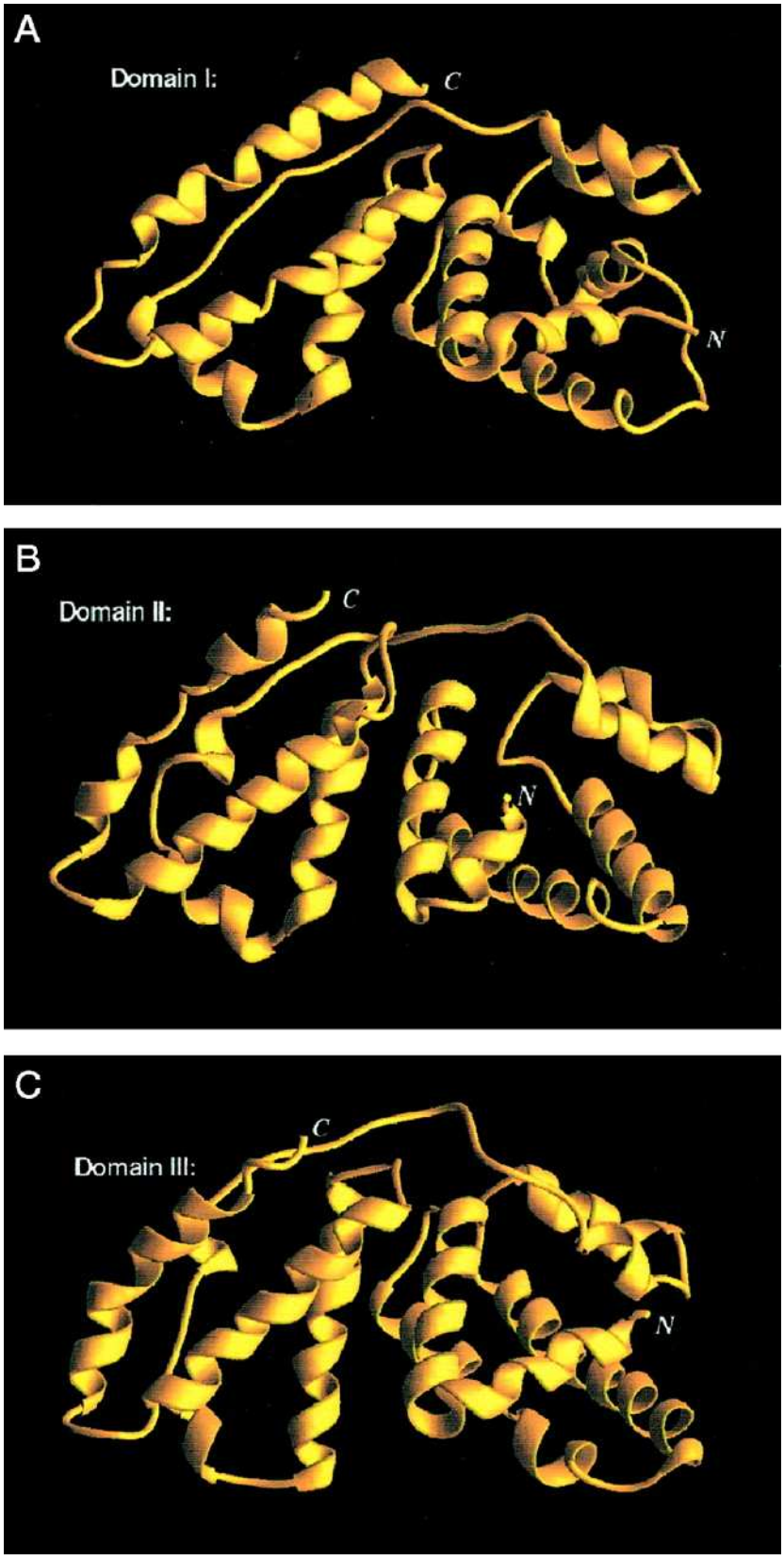

Figure 1.2. X-ray Crystal Structure of the recombinant domains of HSA.
(Carter et al, J. Biol Chem, Vol 274, Iss 41, 29303 – 29310, 1999)

Human albumin contains only one tryptophan at position 214 found in the long loop 4, (BSA has two), lower levels than that found for most proteins of similar size that would more typically contain seven tryptophans (*Kraigh-Hansen, 1989*). The number of methionines, glycines and isoleucines are also atypically low, 6, 12 and 8 respectively, with a high abundance of cystines, leucines and ionic amino acids like glutamic acid and lysine that produce a high charge on albumin facilitating its solubility in aqueous solutions. A pH 7 there are potentially 185 charges/molecule (*Peters, 1985*). The high abundance of acidic residues compared to basic residues gives HSA a net charge of 12^- at pH7, making it a very acidic plasma protein.

Albumin contains 35 cysteine (cys) (17 cystine) residues, of which 34 pair to form a distinct disulphide bridge pattern (*Foster et al*, *1977 and Carter, 1992*). The disulphide pattern makes the albumin molecule both flexible and resistant to extreme conditions, by ensuring a cys-cys trans peptide bond that prevents adjacent cysteines from forming disulphide bridges with each other. The disulphide bridges fix the spatial orientation of the helices and constrain the protein domain structure (*Blaur et al., 1978.*). In domain I is an omission at position 34 of one of the disulphide bonds, leaving a free cys often partially blocked by covalently bound ligands. In domain I, there are also two cys residues "missing" that should be found at positions 8 and 54 (refer to Figure 1.3) and may account for the lack of binding ability in this domain when compared to domains II & III.

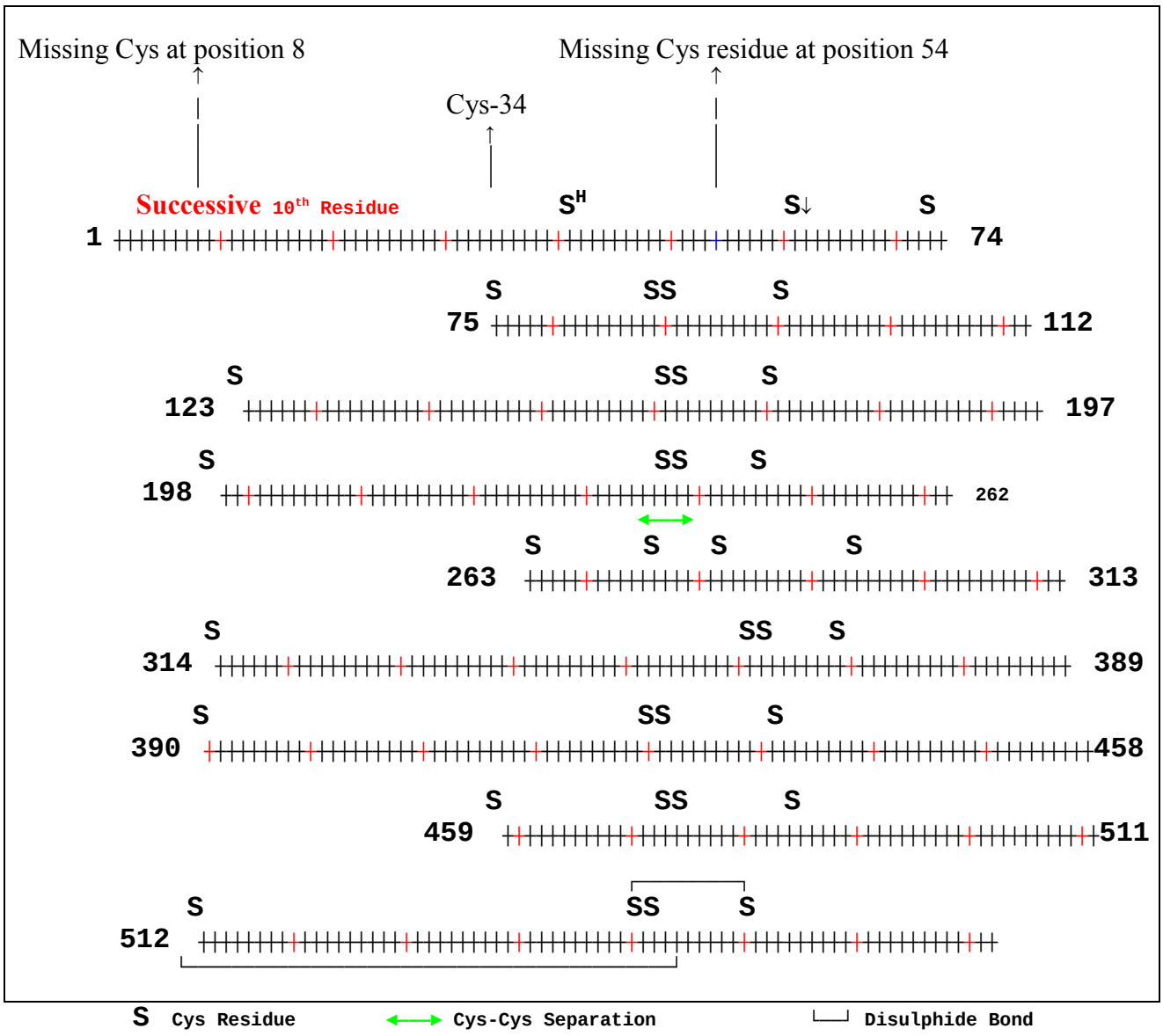

Figure 1.3. Diagrammatic Representation of the Disulphide Pattern in HSA forming 9 loops.
(Rosenoer, 1977)

Another structural difference can be located within domain II with the separation of the cysteine pairing that is not adjacent but separated by three residues (Figure 1.3). Since domain III binds preferentially first with respect to that of domain II, a contributing factor may result from the cysteine separation found within domain II, or at least this factor may contribute to the possible lower disulphide constraint that may exist within that binding pocket (*Peters, 1985*). There are no disulphide bonds formed between adjacent cysteine residues (*Foster, 1977*). The formation of cys-trans peptide bonds together with a 100° rotation between adjacent cys-cys groups ensures non-compatibility with the adjacent SH groups.

HSA contains 18 tyrosine and 31 phenylalanines, which together with the single tryptophan make up the aromatic residues responsible for the observed UV and CD spectrum. There is a

large population of tyrosines distributed within loops 3 and 6. Loop 3, a short length of 24 residues contains 7 tyrosines (*Peters, 1996*). Traditionally, the absorption of a protein at 280nm is ascribable to tryptophan (ε_{280} = 5540). However, the combined contributions of 18 tyrosines will be significant (Tyr residue, ε_{280} = 1480); disulphides ε_{280} = 134 will also make a small contribution (*Peters, 1985*). Although there is a high concentration of phenylalanine compared to the other aromatic residues, its ε_{280} = 0 offers no contribution in terms of absorption. Absorption in the far UV (i.e. below 240nm) is dominated by the peptide bond (Rosenheck & Doty, 1961).

1.3. Secondary, Tertiary and Quaternary Structure of Albumin

Initial secondary structure calculations, based on several techniques including circular dichroism (CD) spectroscopy, found HSA to contain 44-48% α-helix, 16% β-sheet with the remainder as irregular structure (36-40%). The early consensus on the quaternary structure of HSA was that albumin was ellipsoidal, with dimensions of 140Å along the x-axis and 40Å along the y-axis (Figure 1.4); the results were based on many techniques including hydrodynamic studies (*Hughes, 1954, and Squire et al, 1966*). At pH 3.6, the ellipsoid consists of three spheres of diameters 38Å, 53Å and 38Å (*Broomfield et al, 1966*), which represent the three domains. The separation of the spheres is affected by pH; at pH 2.2 the separation was found to be as much as 34Å.

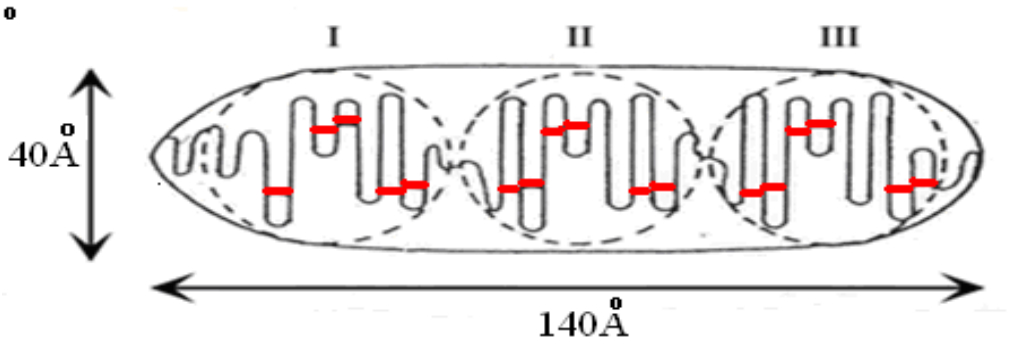

Figure 1.4. Model of HSA based on its Physical Properties.
(Rosenoer, 1977)
The broken circles represents the domains, I, II and III, within the polypeptide, the horizontal red bars represent the 17 disulphide bridges.

Within each domain there are six helices, three in each subdomain, X, Y and Z which run anti-parallel to one another and are held in place by the extensive disulphide bridging (with the exception of domain I that has only one connecting disulphide bond). The concept of a "trough-like" structure or "well" was forwarded as illustrated in Figure 1.5.b. The subdomains are held together by strands of polypeptide chains called hinge regions, separating subdomain A & B from subdomain C (Figure 1.5.). A polarity separation exists within the protein with all the hydrophobic residues located inside or between the helices and the hydrophilic residues located on the surface (*Kragh-Hansen, 1989*).

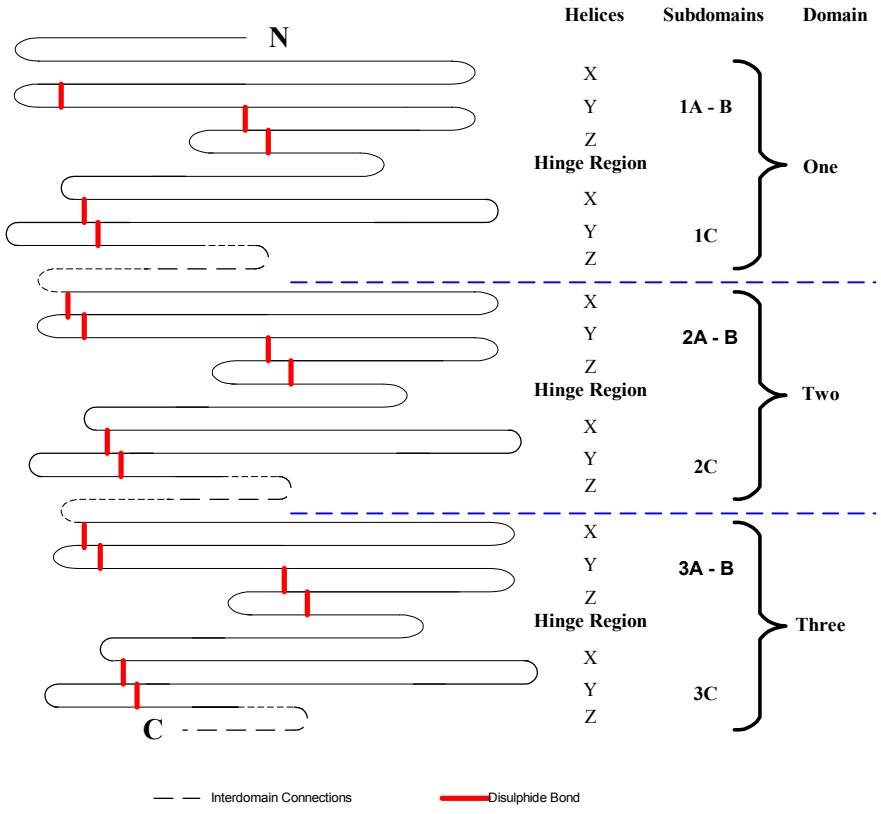

Figure 1.5.a. Schematic representation of HSA showing the helices, subdomains and domains. *(Rosenoer, 1977)*

The N-terminal and C-terminal ends of the molecule are represented by N and C respectively.

The arrangement of the helical bundles in the sundomains (depicted as X, Y and Z as shown in Figure 15.a.) was first highlighted by Brown when determining the sequence of albumin in 1975, and further supported by Meloun and coworkers soon after, as shown in Figure 15.b. Of the nine loops, eight form a double loop due to the arrangement of the Cys-Cys repeating sequence of eight of the 17 pairs, only the first loop does not form the pairing and this is most likely due to the missing Cys at position 8.

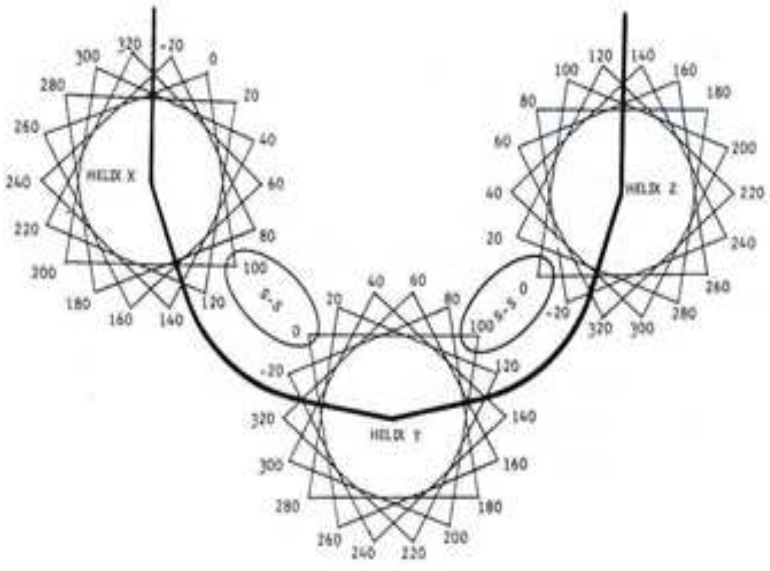

Figure 1.5.b. Schematic representation of one of HSA's subdomain, showing the trough like arrangement of the helical bundles.
(Rosenoer, 1977)

Two possible approaches to the ways in which the adjacent Cys-Cys pairing could bond have been determined, these are shown in Figure 1.5.c. Of the two possibilities, by common consensus, the arrangement shown in Figure 1.5.c.(II) is the more likely. The arrangement that includes the adjacent Cys is the most likely configuration as it introduces an extra residue into the loop. This arrangement also has the effect of reducing the possibilities of any steric contributions that could exist on the exclusion of the Cys when considering the smaller loop of each pairing, limiting possible rotations that could be created with the α-carbon bonds between adjacent Cys-Cys residues.

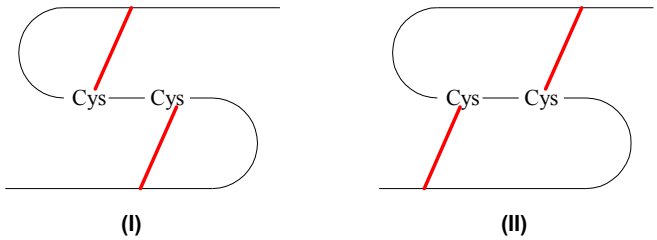

Figure 1.5.c. Schematic representation of two possible arrangements of disulphide pairing.

1.4 X-Ray Crystal Structure of Human Serum Albumin

Determining the X-ray crystal structure of HSA has proven over the years to be problematic, with the production of inferior crystals, too small to study and incredibly soft, possibly due to the high water content of around 55%. The crystal shape, size and consistency varied dramatically resulting in conflicting information. In 1989, the first crystal structure determination was reported (*Carter et al., 1989*) with crystals that gave meaningful diffraction patterns that were both detected and analysed. The new crystals were difficult to grow, growing with continuous solvent channels running throughout. The solvent content of the crystals was 78% and although the crystals showed weak scattering of X-rays, diffraction patterns in the recombinant form of human serum albumin (rHSA) was measured at a resolution of 2.8Å. rHSA crystals were grown from polyethylene glycol (PEG) at neutral pH and recrystallized under a microgravity environment. The real advances in structural determination of albumin came in 1992 (*Carter et al., 1992*) that showed the cigar shaped structure that was previously accepted as the standard shape was in fact inaccurate, at least where the crystal structure was concerned at physiological conditions. He and Carter found HSA to be heart shaped, similar to that of an equilateral triangle, with sides of around 80Å and a depth of around 30Å. The work carried out by He and Carter has prompted enormous advances in the structural analysis of albumin (*Carter et al, 1994; Curry et al, 1998; Sugio et al, 1999, Bhattacharya et al., 2000, Qin et al, 2007*). Figure 1.6 shows the extent of the information with the high resolution X-ray crystal structure of HSA compatible with that

determined by He and Carter, and shows how domain I is situated perpendicularly to domain II forming a T-shaped configuration. Conversely, there is a 45° angle between domain II and domain III forming a Y-shaped configuration. It is this arrangement of the domains that gives albumin its characteristic heart shaped structure, with very little interaction between domain I and domain III. It should be noted that the recombinant form of albumin exhibits the same structural conformation as the native form based upon the X-ray crystal structure with an r.m.s deviation of 0.24Å for all C_α atoms (*Sugio et al, 1999*).

Crystallographic studies show HSA to contain 67% α-helix, distributed in 28 helical bundles. Earlier predictions by Pearson (*Pearson, 1990*) found HSA to contain 19% β-sheet. Recent studies have shown HSA to contain 23% extended chain conformation with the remainder, ~10% existing as turns. In accordance with earlier findings, He and Carter found the evidence of three domains, domain I, II and III (starting from the N-terminal), and each domain was formed from two subdomains A and B (*Sugio et al, 1999*).

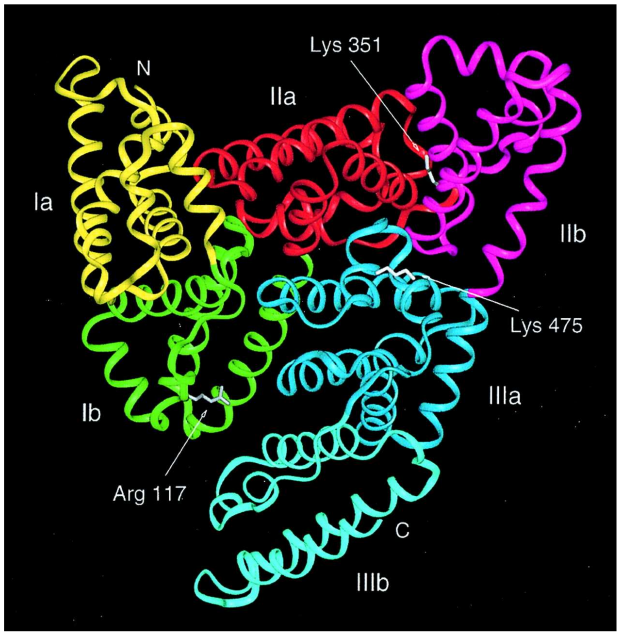

Figure 1.6. X-ray Crystal Structure of HSA first reported by He and Carter in 1992.
(Sugio et al, Protein Engineering, Vol 12, No 6, 439 – 444, 1999)

Diagram is colour coded to show the subdomains, domain IA is coloured yellow, IB is in green, IIA is in red, IIB is in magenta, IIIA is in blue and IIIB is in cyan (Sugio et al, 1999).

The structural arrangement of each domain was identical regardless of the primary sequence and composed of ten helices labelled h1-h10 (Figure 1.7.). The subdomains, A and B share a common motif with helices h1, h2, h3 and h4 in subdomain A identical to those of h7, h8, h9, and h10 in subdomain B with two exceptions. Firstly, the disulphide bridge joining h1 and h3 in subdomain 1A does not exist. Secondly, subdomain A contains two additional short helices running anti-parallel to one another, helices h5 and h6. These are linked together by a pair of disulphide bridges forming a small double loop that ensures the continuity of the helices throughout subdomain A, and contributes to a network of four interhelical disulphide bridges (refer to Figure 1.7.). Subdomain B is complementary to that of subdomain A for helices found, but it also contains the N- terminal portion of the extended polypeptide chain that links the domains together.

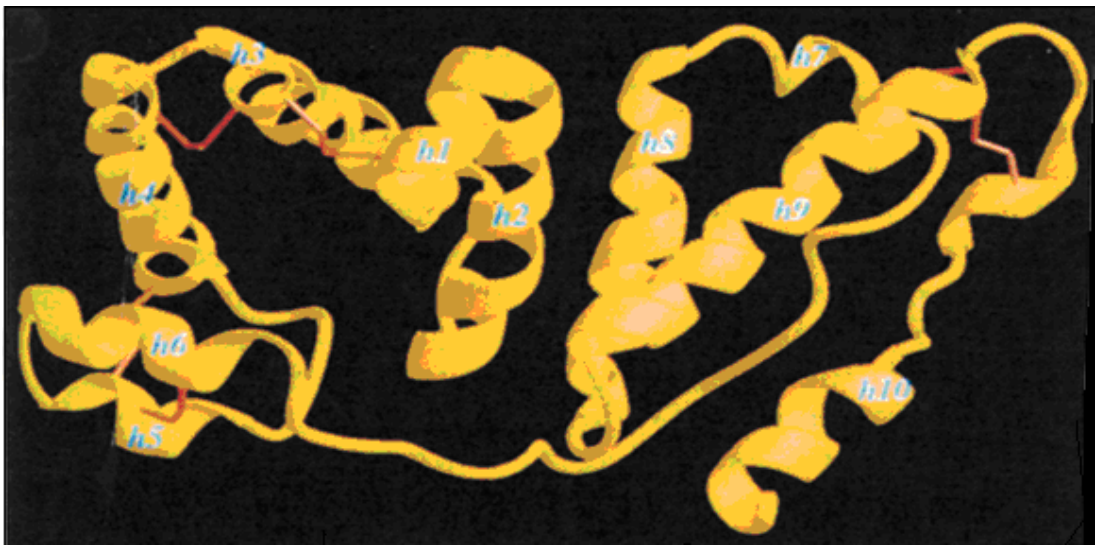

Figure 1.7.i. Ribbon diagram of domain II, (disulphides are shown in red).
(Carter et al, Nature, Vol 358, 209 – 215, 1992)

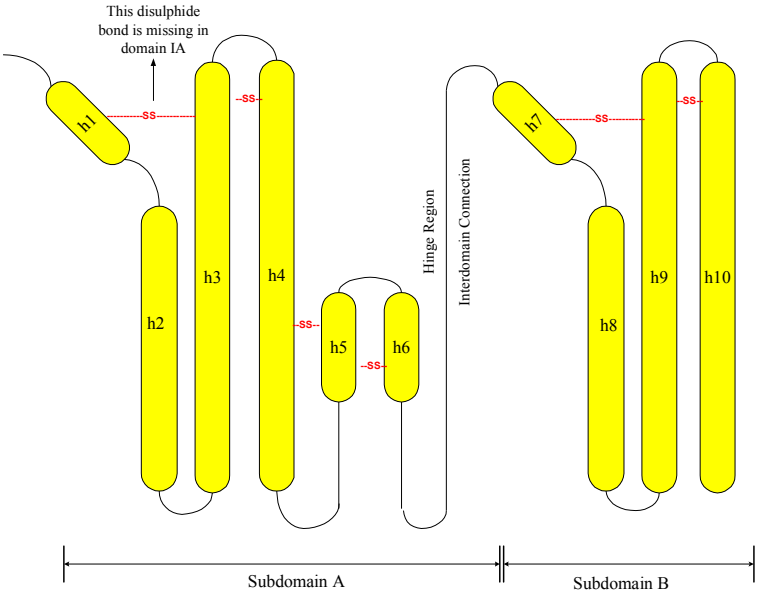

Figure 1.7.ii. Representation of Domain II, showing the 10 helices as determined by X-ray crystal structure.
(Carter et al, Nature, Vol 358, 209 – 215, 1992)

Linkages joining the subdomains IA-IB, IIA-IIB and IIIA-IIIB are referred to as interdomain connections or hinge regions, and exist as extended polypeptide chains found between residues Lys 106 to Glu 119, Glu 292 to Val 315 and Glu 492 to Ala 511 in domains I, II and III respectively. There are exceptions, the structural conformation of the interdomain connection between IB and IIB are helical, extending from the C-terminal portion of the helices to the N-terminal portion of IIA and IIIA respectively. Subdomains IIA and IIIA are also helical, (helices: h10(I) - h1(II) and h10(II) - h1(III)), and the longest helix is found between subdomain IB-IIA, extending over 31 residues. The charge distribution across the domains is uneven, -9, -8 and +2 for domains I, II and III respectively in human HSA. In view of the uneven charge distribution, the acid/base distribution seems less problematic. There does not seem to be any significant patterns of acid versus base distribution throughout albumin except in one area on the surface of domain I that is basic in nature (*Carter*, *1994*). Conversely, there seems to be distinct areas of uncharged amino acids, thought to be associated with long chain fatty acid (LCFA) interactions. The X-ray structure confirms

Brown's predictions (*Brown, 1975*) on the arrangement of the 35 cysteine residues with a unique arrangement of disulphide pairing, 16 of the 17 cystines present forming disulphide linkages. The disulphide linkages are found to be predominantly gauche-gauche-gauche as predicted by Raman spectroscopic studies, with a typical $C\beta_1$-S_1-S_2-$C\beta_2$ torsion angle clustered around ±80°(*Aoki et al, 1973*), and are located between helical segments in most cases. The unique network of disulphide pairing gives HSA its exceptional abilities not seen in other proteins, with the disulphides well protected and relatively inaccessible to solvents. The disulphide bridges are arrangement within albumin as follows:

Domain I	**Domain II**	**Domain III**
	200 – 246	392 - 438
53 – 62	245 – 253	437 - 448
75 – 91	265 – 279	461 – 477
90 – 101	278 – 289	476 - 487
124 – 169	316 – 361	514 – 559
168 – 177	360 – 369	558 - 567

The free cysteine residue, Cys34 is located between the helices of IA-h2 and IA-h3. In practice, between 30 – 40% Cys34 residues in albumin are oxidised by residues of cysteine or glutathione contained within other regions of the molecule to form an intermolecular disulphide linkage (*Peters, 1985*). Cys-34 is located on the surface of the albumin molecule. However, its Sγ is directed towards the interior of the molecule and is surrounded by the side chains of Pro 35, His 39, Val 77 and Tyr 84. This arrangement of the residues stops the sulfhydryl group within the molecule from coupling with another external cysteine residue from neighbouring molecules. Blocking the free thiol, Cys-34, adds to the stability of the protein, preventing mixed disulphide formation and dimerization (*Peters, 1985*). Cys-34, has an unusually low pK_{SH} (pK_{SH} = 5), compared to cysteine and glutathione (pK_{SH} = 8.5 and 8.9 respectively) allowing it to catalyse reactions by forming intermediates (*Pedersen et al., 1980*).

1.5. Properties of Human Serum Albumin

The chemical nature of HSA ensures a high buffering capacity resisting small changes in pH. When dissolved in water, HSA attains a neutral pH between pH 6.5 - 7.0. However, changing pH results in conformational changes that are both distinctive and indicative of that pH and result in protein unfolding with the possible cleavage of some of the disulphides, all of which are reversible once physiological conditions are re-established (Figure 1.8). Five transitions (or forms) have been defined when the pH is changed: the N-form (normal), F-form (fast), E-form (extended), B-form (basic) and the A-form (aged), as shown in Table 1.3. Each form has an associated change in structural conformation in the protein resulting in tertiary and quaternary changes. Along with the structural changes are physical changes. Lowering the pH to below pH3.5 causes a dramatic increase in viscosity together with an increase in hydrodynamic volume. There is also an increase in electrostatic repulsion with the moving apart of disulphide loops. Intermediate transitions have also been detected, for example at pH4, with smaller changes in intrinsic viscosity resulting in other physical changes that are not as dramatic (*Luetscher, 1939*). The effect of pH changes are considered important as it allows conformational changes to aid the loading and off-loading properties of the protein. A study of HSA rigidity will provide a better understanding of how the protein functions and adapts.

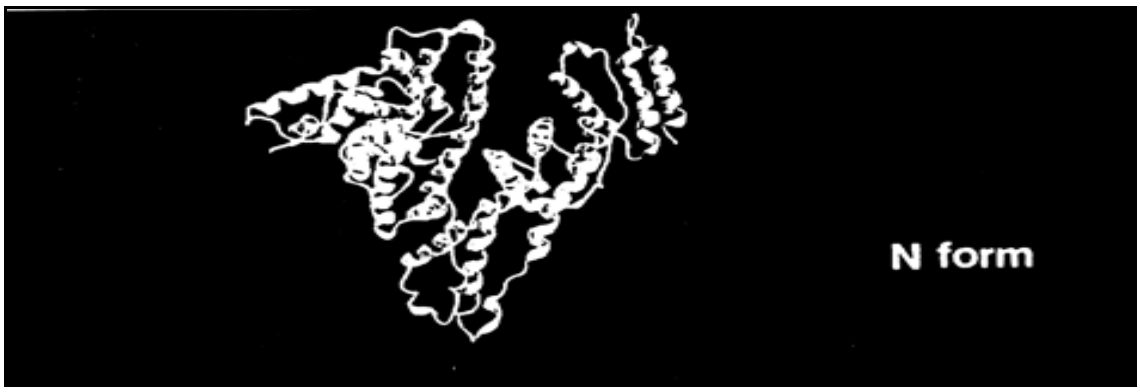

pH7.0

pH4.0

pH<3.0

Figure 1.8. Structural representation of HSA showing its pH dependence.
(Carter et al, Adv in Prot Chem, 45, 153 – 203)

Different Forms of HAS	State	pH	Physical Characteristics
N-Form	Neutral	5-7	Natural form, heart shaped
F-Form	Fast	~4.0	Viscosity starts to increase, partial unfolding of domain III, loss in contact between domain III and domain II due to loss in hydrophobic contact
E-Form	Extended	<3.0	Increase in viscosity, loss in helical content, decrease in solubility
B-Form	Basic	~8.0	Loss of helical content, increase affinity for small ligands, changes that are of physiological importance
A-Form	Aged**	~10	

Table 1.3. Conformational Changes of HSA with respect to pH.
(** Occurs over time).

A decrease in pH promotes the sequential unfolding of the albumin molecule that originates from the N-terminal, with domain III unfolding first, followed by domain II and concluding with domain I (*Fanali et al, 2007*).

Table 1.4 Schematic Representation of the Physical Properies and Chemical Changes in Albumin in responce to pH.

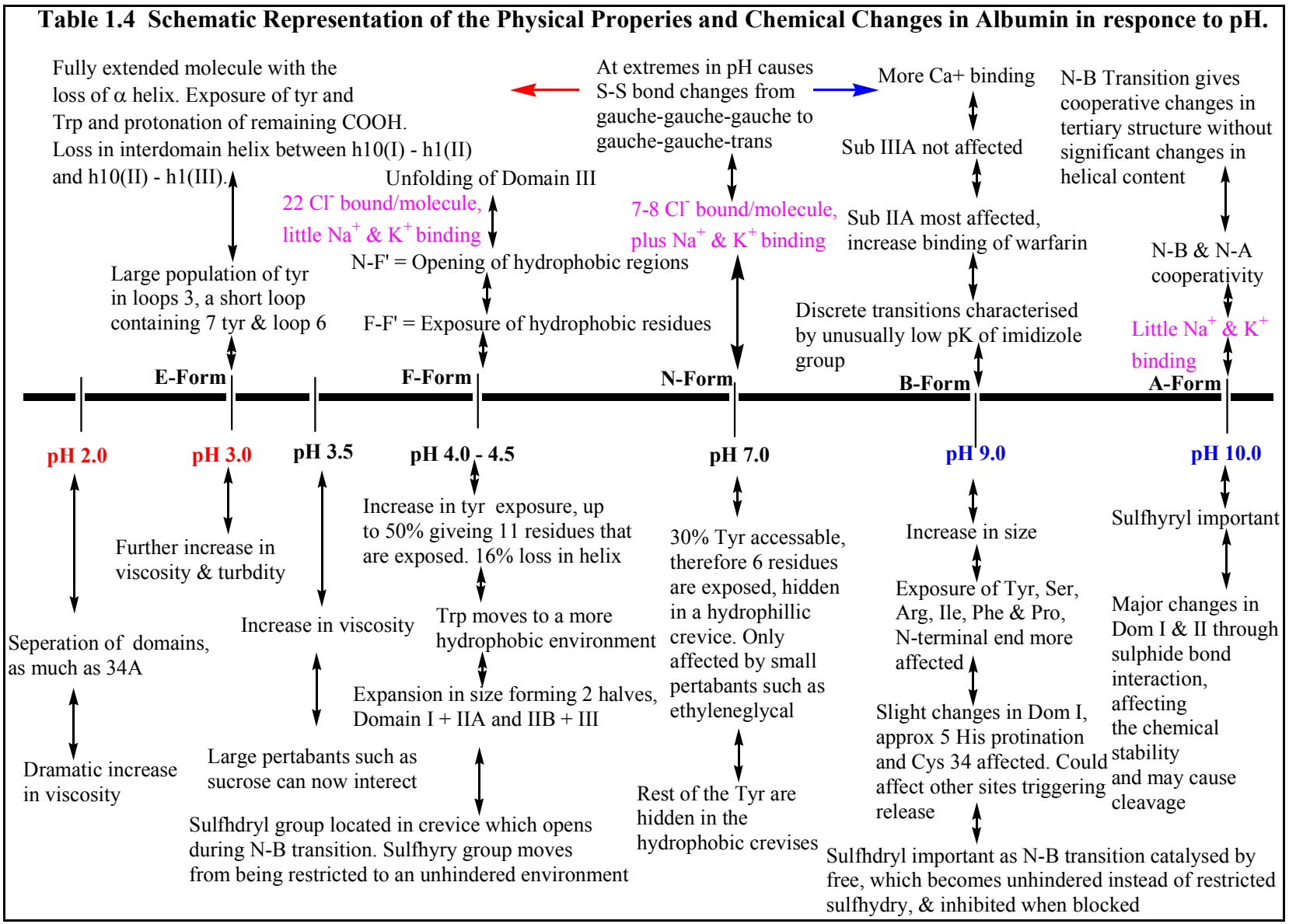

1.5.i. Fast -form Transition of Albumin (F-form)

The formation of the F-form within the pH range pH4 to pH4.5 involves transitions involving at least three cooperative steps (*Leonard, 1961*), with some intramolecular dissociation of the subdomains with possible secondary structural rearrangements. 20% more tyrosyl residues become accessible to environmental perturbations, increasing the existing 30% normally found at pH7 to 50%. Binding affinities are affected similarly in the F-form showing a reduction that can be correlated with the increase in viscosity observed. Foster and co-workers (*Foster et al, 1957*) believed the N-F transition occurs in two stages involving an intermediate F' state that can be represented by $N \rightarrow F' \rightarrow F$. Associated with this transition is the loss in percentage α-helical content reflected in the cooperative forms, the N-F' transition shows a reduction in helix from 51% to 44% and the F' - F transition presents a further reduction from 44% to 35% resulting in a total loss of 16 % of helical content (*Leonard, 1961*), as shown in Table 1.4. The N-F' transition is thought to be the opening of first the hydrophilic regions with the F'-F transition reflecting the exposure of the hydrophobic residues. Towards pH4, there is an expansion in size with the HSA molecule becoming more extended, more asymmetric with more of the molecule becoming accessible to the solvent. Carter and He suggested that during this transition, HSA separates into two halves, defined by domain I + IIA and domain IIB + III, (refer to Figure 1.8).

A pH change from pH7 to pH3 sees the neutralization of approximately 40 COOH side chains with a collective $pK_a = 3.7$. Glutamic residues normally show a $pK_a = 4.1$, aspartic residues typically give $pK_a \sim 3$. It has been possible to isolate the F-form by gel electrophorisis (*Foster et al, 1957*) at a pH between pH3 – pH4. Foster found that there was a certain amount of insolubility associated with this state, the F-form has a solubility

<<1μ/ml in 3M KCl as opposed to the N-B form (neutral-base form) which is totally soluble. In the F-form, HSA becomes more extended and more asymmetric, attributed to the changes in the ionisation status of the COOH groups and the accessibility of three of the five tyrosine side chains. A blue shift in the UV absorption is observed. Changes in helicity have also been inferred at 333nm by fluorescence excitation studies of HSA tryptophan (*Foster et al, 1957*).

1.5.ii. Extended-form Transition of Albumin (E-Form)

Below pH 3.0, HSA undergoes further quaternary structural changes due to the further loss of α-helix conformation; a fully extended structure prevails. There is a dramatic increase in solution viscosity and turbidity increases. Fluorescence studies have shown an increase in the exposure of the tyrosine and tryptophan residues. All the remaining carboxyl residues have become protonated (*Leonard, 1961*). Like the F-form, formation of the E-form is completely reversible. The loss in secondary structural conformation is thought to be due to the loss of structure in the interdomain helices between h10(I) - h1(II) and h10(II) - h1(III) (*Peters, 1996*).

1.5.iii. Base-form Transition of Albumin (B-Form)

At pH≥9.0 (alkaline conditions), HSA undergoes another transition that is more subtle than the lower pH changes but nevertheless of physiological importance (*Dockal et al, 2000*). There is evidence suggesting that this transition occurs in discrete steps with a loss in helical content *(Hart et al., 1986*). This transition is characterised by the unusually low pK_a value of the imidazole groups. There is an expansion in size of the HSA molecule with the exposure of buried residues, especially Tys, Ser, Arg, Ile, Phe and Pro. The amino-terminal end of the molecule is most affected. Structural changes affecting subdomain IIA (Site I) are evident with increased binding for warfarin detected, but with no significant observable

effects seen in subdomain IIIA (Site II). Small structural contributions are observed in domain I. NMR studies have confirmed some of the histidines (~5) become protonated, and Cys-34 is also affected (*Zurawski, 1974*). Although domain I does not contain any major binding sites, changes in conformation could be a factor in triggering the release of bound ligands from HSA bound drugs at their target sites. The N-B transition is catalysed by the presence of the free sufhydryl residue and is inhibited when the sufhydryl residue is blocked (*Stroupe et al., 1973*); in this form, an increase binding of calcium ions is detected.

1.5.iv. Aged-form Transition of Albumin (A-Form)

The A-form exists at pH≥10 and like the B-form is reliant on the sufhydryl residue. Its formation involves two cooperative states, the neutral-base transition (N-B form) and the base-aged form (B-A-form) with the release of protons. There is an expansion of the protein molecule with the major changes occurring within domain I and II through disulphide bond interchange. High pH affects the chemical stability of the S-S bond making them unstable with possible bond breakage.

1.5.v. Additional Aspects of Serum Albumin Structure

There are several transitions associated with the different forms of HSA, which involve unfolded intermediates that are detected as the protein undergoes internal reorganisation. Albumin responds differentially to chemical perturbations in the N-form and the F-form. The effect of adding salts like potassium chloride (KCl) results in the N-form requiring high concentrations before precipitation occurs. Conversely the F-form can be "salted" out in 3M KCl, this is possibly due to the exposure of hydrophobic regions that are normally buried within the protein in the N-form. The ability of albumin to bind at low pH is also compromised with the F-form showing reduced binding ability when compared to the N-form, this could be perceived as facilitating off-loading at an interface with target tissues.

The forms are the conformational structures that are attained after the transitions are completed. The N-F transition is thought to involve the unfolding of domain III (*Geisow et al., 1977*). Considering the fragments of albumin, no changes have been observed in either domain I or domain II. When albumin is in the N-form there are six tyrosyl residues exposed, when the pH is reduced to below pH4.5 (F-form) the amount of perturbed tyrosyls increase by a further five. In the N-form the tyrosyls are hidden in a hydrophilic crevice and can only be affected by small pertubants such as ethyleneglycol, sufficiently small enough to penetrate the crevice (*Herskovitz et al., 1962*); Tryptophan is also affected by reduced pH as it moves from an aqueous environment to a more hydrophobic one in the F-form. The extended structure of the F-form will allow larger purtubants such as sucrose to interact.

The charge distribution across albumin is uneven at pH7 with a charge of -6 at the apex, -9 at the base, -14 on the left and –1 on the right (*Peters, 1996*). The net charge on the albumin (-15) is also affected by changing pH. Bound salts are also affected; on average HSA has 7-8 chlorides (Cl^-) bound / molecule. Decreasing the pH increases the amount of bound Cl^- ions to 11 (Cl^-) bound / molecule at pH5.2 and 22 (Cl^-) bound / molecule at pH4.2 (*Figge et al.*, 1991). Conversely, monovalent cations such as Na^+ and K^+ only bind significantly at pH 7.4.

CHAPTER 2

CHAPTER 2: Ligand Binding to Human Serum Albumin

2.1. Introduction

HSA can bind numerous ligands with high affinity. However, there is still ambiguity surrounding the actual number of binding sites that may be present within the protein. As many as nine sites for long chain fatty acids (LCFA)) has been reported, (*Kragh-Hansen, 1990*). The challenge to determine just how many sites albumin has will always be influence by the environment in which the albumin molecule finds itself in at the time of binding, the degree of saturation of the ligand in question and/or the influences of other ligands that may bind at the same time and may add to the cocktail.

Frequently there is a "connection" or linkage between the ability to bind at different sites. Linkage can be defined as the effect of binding ligands in relation to one another that can show positive or negative facilitation *(Wyman & Gill, 2000)*. Linkage can also characterise or affect the way in which binding is attained. Linkage effects may be exhibited in the form of chemical linkage, physical ligand linkage, polysteric linkage and/or polyphasic linkage. When considering chemical linkages two principle possibilities exist, homotrophic chemical linkage where the ligand site in question binds the same ligands, or heterotrophic chemical linkage where the site binds different ligands. It is also possible to have a situation where the two different ligands interact with the protein and competitively bind simultaneously with respect to each other, this is referred to as identical linkage. A negative facilitation will inhibit binding; conversely, a positive facilitation gives rise to enhance binding.

Physicochemical considerations can also influence the ability of the protein to bind ligands. Factors such as temperature and pressure (*Peyrin et al, 1999*) can influence and affect binding, giving binding curves that will be dictated by and reflect those changes. Polysteric effects involve aggregation, which usually relates to the concentration of the

protein. Polyphasic linkages involve more than one phase. An example of this is demonstrated by aqueous sickle-cell haemoglobin binding gaseous oxygen. In both polysteric and polyphasic processes solvent effects are also a major consideration.

2.2. Structural Effects and Functionality

A prerequisite to understanding binding is to understand the structure of the macromolecule under investigation. However, macromolecules that have similar amino sequence can show diverse variations in terms of binding ability and molecular shape. Often binding will invoke a conformation change in the macromolecule either at a local level or on a more global scale (see later for a more detailed account of the binding of myristate to HSA) which may in turn affect the functionality of the remaining binding sites, this can be referred to as an allosteric mechanism. A macromolecule can be seen as a "molecular transducer" that will, under certain circumstances, respond to, and can be considered to be effectively controlled by the modulating effects of the ligand in question. A binding ligand will control the macromolecular shape and response to subsequent ligands *(Wyman & Gill, 2000)*.

When considering the locations within a macromolecule that are responsible for the attachment of ligands, the terms binding sites and binding regions have been used in the literature. The two are clearly different and do not necessarily refer to the same position on HSA (refer to Table 2.2). The binding of most ligands is reversible. Association constants (K_{ass} or K_a) for ligands binding to albumin are usually quoted as being of the order of 10^4 to $10^6 M^{-1}$. Ligand binding can cause conformational changes in both the protein and the ligand as the ligand binds (*Peters, 1985*). This may be to preserve the characteristics and functionality of both the protein and the ligand, or it may be a feedback mechanism to prevent further binding or offloading of the ligand or other ligands that may be in the vicinity at that time.

2.3. Location of Binding Sites on Serum Albumin

The recent developments in the determination of the crystal structure of HSA have enabled the study of albumin in more depth with a distinction and discrimination between binding sites. Importantly, FAs are shown to be important in maintaining the binding functionality of the protein. The use of myristate in the formation of the crystal has enabled better crystal formation that gives rise to better diffraction of the X-rays. Myristate seems to stabilise the crystal structure which would concur with the fact that HSA is the main vehicle for carrying FAs (*Curry et al, 2006*). The presence of myristate has enabled the dramatic increase in data determination, obtained from crystallographic studies of HSA drug binding. The binding of drugs causes several effects, resulting in altering distribution, lowering the rate of clearance and increasing the half-life of the drug in the blood.

2.3.i. Metal ion and anion binding

The main metal binding site for ligands such as copper (Cu^{2+}), nickel (Ni^{2+}), zinc (Zn^{2+}), gold (Au^{+}) and silver (Ag^{+}) is located at the N-terminal of subdomain IA involving the first three amino residues, Asp-Ala-His, with histidine at position 3 playing a pivotal role (*Sadler et al., 1994*). A second metal binding site involving the free sulfhydryl residue, Cys-34, has also been found.

Chloride (Cl^{-}) ions can affect the binding abilities of some ligands; its K_{ass} in plasma is low (K_{ass}=720M^{-1}). There are between 7-8 Cl^{-} ions bound to HSA at pH7.4 attracted to residue pairs such as Lys-Lys and Arg-Arg (detected by NMR) (*Honoré et al, 1988*). Albumin contains 9 such pairs, 5 are located in subdomain IIIA at positions 413, 444, 484, 524 and 573. All are found in the helical stretch of the protein. Cl^{-} is attracted to the C-terminus and is known to reduce the binding of warfarin, Trp and octanoic acid, (*Honoré et al, 1988*). For this reason, it is imperative when undertaking fundamental bindings studies

to make sure that the protein is as pure as possible so that influences such as Cl^- do not interfere with the binding ability of the ligand under investigation. All samples are dialysed and freeze dried to ensure purity and stored in sealed containers in the refrigerator. Ionic effects from sodium chloride, sodium sulphate and sodium acetate were investigated for their effects on the structural and binding abilities of albumin, the results of which can be found in Chapter 4 of this thesis.

2.3.ii. Ligand (Drug) Binding

The binding mechanisms of ligands are specific, invoking the interaction of different residues within albumin depending on the ligand in question, even though, in the majority of binding situations, the same locations are involved (IIA and IIIA). Reversible conformational changes occur as well as allosteric effects that remain as long as the ligand is bound. Albumin is an important determinant of the pharmacokinetic behaviour of many drugs. For example, albumin limits the free drug found in the plasma to between 1-10% depending on the drug. It is the free drug that is active in blood (*Peters, 1996*). Thus the drug concentration is controlled by albumin if albumin is the binding receptor in the circulation. The limiting factor of drug binding is the binding affinity to the protein. Although binding of ligands to albumin may be considered desirable for ligands of low solubility, thus preventing aggregation of the ligand, a strong affinity to albumin would mean that a higher dosage, in the case of drugs, would have to be used to obtain the effective free dosage in the blood (*Curry et al, 2005*). The binding of drugs is never simple in *vivo* as the drug has to compete with endogenous metabolites producing a cocktail. It is worth noting that in excess of 90% of drugs bind to HSA. In this way, HSA acts as a depot for ligands (*Yan-Jun Hu et al, 2005*). There also seems to be some degree of overlap of binding sites between the major drug binding sites and other ligands, especially when the sites for FAs are included in the mix (*Curry et al, 1998*). The binding efficiency of albumin

is so great that some drugs become sequestered by HSA, leaving very low levels of therapeutic drug for active distribution (*Curry et al, 2001*).

Subdomain IA, located in domain I, is not renowned for its binding abilities, as very few binding locations exist. There is the possibility of a binding pocket located within the stretch of polypeptide that includes Cys-62, the first disulphide, located in a nonhelical stretch. However, the lack of disulphides in this location allows the helical stretch h3 to increase its packing angle with h4 (Figure 1.7. in Chapter 1.) effectively eliminating a pocket (*Carter et al., 1994*) and may explain the effective inability of ligands to bind within this region. There was speculation about a long chain fatty acid (LCFA) binding site allocated within subdomain IB; this has now been verified (see later).

Two principal ligand (drug) binding sites on albumin have been observed for major ligand binding located within domains II & III. The first is often referred to as the Sudlow Site I. Sudlow characterised the site located in subdomain IIA that binds hydrophobic (*Sudlow et al., 1976*), bulky, heterocyclic molecules with a centrally located negative charge (e.g. warfarin) (*Fanali et al, 2007*). The second site, referred to as the Sudlow Site II, is found in subdomain IIIA and binds aromatic carboxylic acids with a negative charged at one end of the molecule (e.g. diazepam and ibuprofen). Table 2.1. and Figure 2.1. & 2.2. shows the possible ligands and their binding sites within albumin. The distribution of amino acids that line both binding site cavities are similar with an asymmetrical distribution of hydrophobic residues lining one half of the surface, and either basic or positively charged residues on the other. Subdomain IIIA is the most active or dominant binding site, an elongated "sock-shaped" cavity with mostly hydrophobic residues at the foot, hydrophilic residues located along the leg (*Carter et al., 1994*) and solvent accessibility at the opening. Subdomain IIA binds more specifically.

Binding Region	Binding Sites	High Affinity Binding Ligand	Amino Acid Residue	Comments	Binding Locations (He & Carter)
I	1	Long - chain fatty acid ions	390 - 450	Primary binding site is between 377 - 582. Several sites exist specifically for 1°,2° & 3°FA.	IIIA
II	2	Diazepam 0ctanoate L- and D-Tryptophan Chlorazepate L-Thyroxine p-Iodobenzoate Chloride ions	306 - 386	Positively charged amino acids, probably lysine residue are part of this binding region. as is histidine. The HSA tertiary structure is also important for this site.	IIIA 380 - 450
III	3	Bilirubin Several dyes (Phenol Red) Iopanoate	182 - 283	Large number of basic amino acids, lysine - 240, arginine and histidine ,and possibly tyrosine.	IIA
	4	Cu2+ Ni2+	1 - 3 +	The three amino terminal residues, Asp-Ala-His, His-3 is essential.	IA
	5	Haemin	124 - 298	This binding site is close to region 3. Several expts. have shown a separate and distinct binding site, and that the C-terminal part of albumin is important for the spatial conformation of the haemin binding site.	
IV	6	Salicylate Digitoxin Sulphaethidole Chlorpropamide Tolbutamide Indomethacin	124 - 298	Lys - 199 important where acetylation occurs, acetyl group transferred by the aspirin. Overlap between this group and group V.	IIA & IIIA
V		Warfarin	124 - 298	Lys 199 may be important, Trp-214 residue is essential.	IIA

Table 2.1. Representation of the binding regions in HSA.

(U. Kragh-Hansen, Danish Medical Bulletin, 37, 1990, 57 – 88)

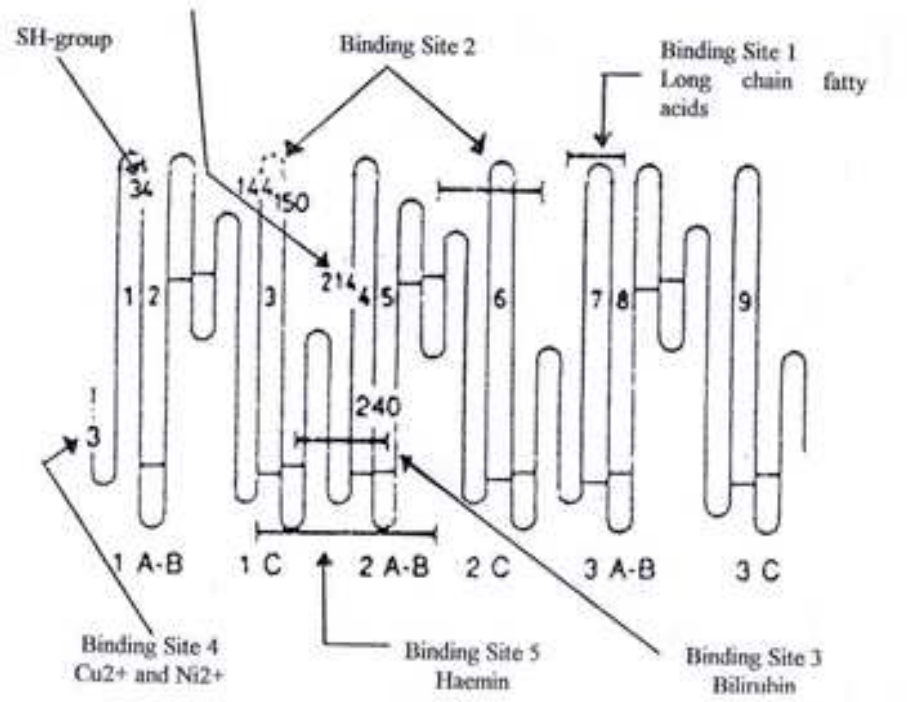

Figure 2.1. Location of binding sites on HSA.
(U. Kragh-Hansen, Danish Medical Bulletin, 37, 1990, 57 – 88)

2.4. Site Specific Marker Ligands

The ability of HSA to bind numerous ligands has made it a topic of study for many years. Inevitably, binding site locations on albumin with specific ligands have been discovered and used as markers for that specific binding site, (Figure 2.1. and Table 2.2.). Markers can be used as a valuable aid to locate, track and mark possible sites for ligands whose characteristics are not fully known or understood. The markers are diverse and their binding has been specifically located on albumin. Examples of some markers used in investigations in this thesis (refer to Table 2.1.) have been chosen to represent the diversities exhibited by albumin binding, as well as the distribution and susceptibility of binding pockets in the molecule. Figure 2.2. gives a more realistic view of how the marker ligands are distributed throughout the albumin molecule and the special orientation of the molecules relative to each other, as well as the close proximity of the fatty acids in relation to the other ligands.

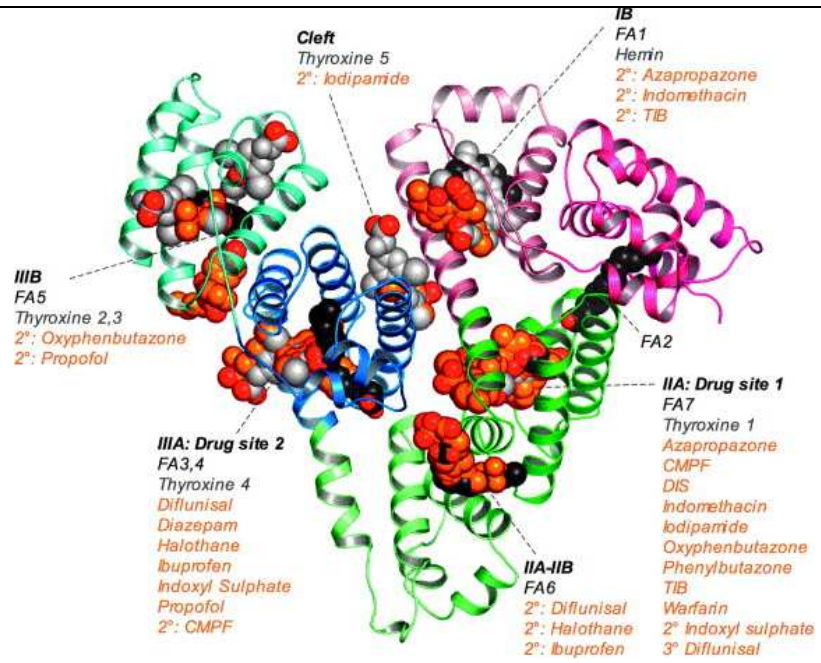

Figure 2.2. Tertiary and quaternary structure of HSA showing binding locations.
(Curry et. al, Journal of Mol Biol, vol 353, issue 1, 2005, page 38 – 52)

The ligands are shown as space-filling representation with oxygen shown in red, all others atoms are the FA (myristic acid). Endogenous ligands of haemin and thyroxin, and drugs are colour coded dark grey, light grey and orange respectively.

Some markers exhibit more than one binding site as in the case of salicylic acid, although they may prefer a dominant site at lower ligand concentration. Such marker ligands can be used to determine which site on albumin an unknown ligand might occupy if used in a cocktail with a marker ligand of known binding site location. This, however, is not as simplistic as stated as other effects need to be considered such as competition effects, feedback effects whether positive or negative and environmental effects such as pH and solvents.

Drugs	Dyes	Ions	Fatty Acid
Warfarin (War) IIA	Phenol Red (PR) IIA	Sodium Chloride Multiple occupancy	Octanoic Acid (FA) IIA & IIIA + Multiple occupancy including unknown sites
Diazepam (Daiz) IIIA	Bromophenol Blue (BPB) IIA	Sodium Sulphate	
Salicylic Acid (SA) IIA & IIIA	Bromocresol Green (BCG) IIA	Sodium Acetate	
5-Iodosalicylic Acid (5ISA) IIA & IIIA			
3,5-Diiodosalicylic Acid (DIS) IIA & IIIA			

Table 2.2. Examples of Site Specific Markers used and their Binding Sites.

2.5 Mechanisms of Binding to Human Serum Albumin

There is an inordinate number of bindings sites recorded for medium chain fatty acids (MCFA) and LCFA but quite where they may be located is yet to be exactly determined. What is known is that the chain length of the fatty acid (FA) is imperative to the determination of the numbers of binding sites found, the longer the chain length the more binding sites that have been detected.

2.5.i. The Effects of Myristate Binding to Albumin

FA binding is one of the most important interactions of HSA in the body as it is the only way FAs are transported around the body. The effects of myristate (Myr) binding has already been stated previously. Myr is a medium chain fatty acid (MCFA). However, what has not been clarified is the total number and location of binding sites myrisate has on HSA. However, there seems to be agreement that there are at least 5 long chain fatty acid (LCFA) sites on albumin (Figure 2.3), 3 strong or primary sites and 2 weak or secondary sites giving rise to an asymmetric distribution of the FA on albumin.

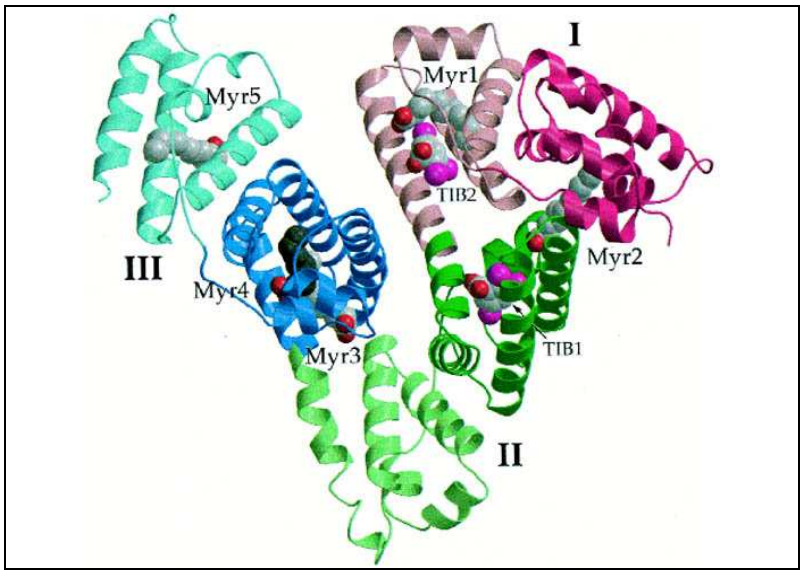

Figure 2.3 Schematic representation of 5 Myristate molecules bound to HSA.
(Curry et al, Nature Structural Biology, 5, 827 – 835, 1998)

Domains I, II & III are represented in colours magenta, green and blue respectively. Subdomains A & B are the dark and light shades respectively in each domain. Myristate is shown as, carbon in grey, oxygen in red and iodine in light magenta.

FA binding sites are characterised by being hydrophobic pockets with positively charged residues (Arg, Lys) or polar side chains (Ser, Tyr) at the entrance to the pocket. Where possible, H-bonding occurs to the FA carboxyl group holding the FA more strongly than just hydrocarbon chain interactions. Numbering the binding sites of FA is arbitrary and bears no significance to the magnitude of the binding affinities. The FA binding sites are shown for each domain in Figure 2.4 and Table 2.3.; all were determined by X-ray crystallography (*Muravskya et al, 2004*).

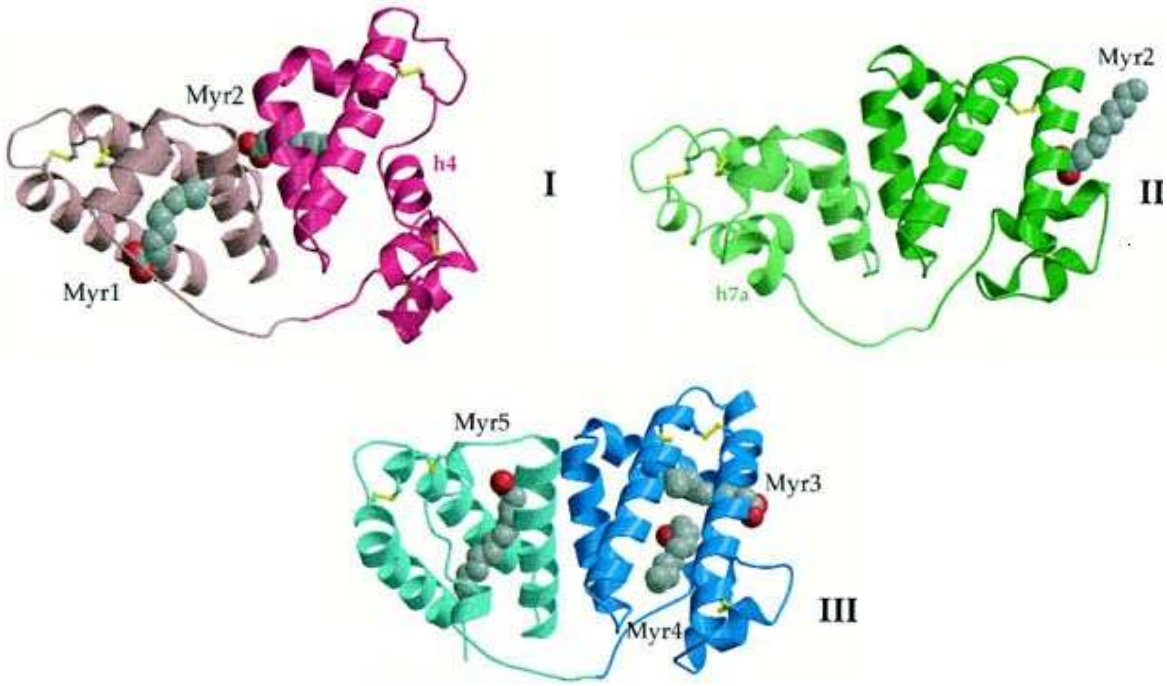

Figure 2.4. Schematic representation of the individual domains of albumin showing Myristate binding.

(Curry et al, Nature Structural Biology, 5, 827 – 835, 1998)

The colour coding is as described in Figure 2.3. for the domains, subdomains & Myr, with 2 molecules of Myr in domain I, 1 molecule in domain II and 3 molecules in domain III.

Myristate	Location on HSA	Affinity
Myr 1	Located in subdomain IB	Low
Myr 5	Located in subdomain IIIB	High
Myr 2	Located in the interface between subdomain IA & IIA	High
Myr 3	Located in subdomain IIIA with contributions from IIB that anchors the carboxylate	Low
Myr 4	Located in subdomain IIIA	High

Table 2.3. Location of the myristate binding sites on albumin.

These five sites are the main FA binding sites to albumin, but there are four further putative FA sites that have not yet been shown in the X-ray crystal structure of Figure 2.4. A 6th possible site is located between subdomains IIA & IIB with interaction with Arg 209 from IIA and H-bonding to Asp 324 & Glu 354 in IIB; this binding site is located close to IIB. Little is known about the 7th site other than it appears to be a low affinity site located entirely within the binding pocket of site IIA. The binding of FA induces a rotation of the domains (*Curry et al, 1998*). Domain II remains essentially the same, however, domain I & domain III move (Figure 2.5). Conformational changes result from FA binding, resulting in the rotation of domains I & III with respect to domain II, said to be driven by FA binding in the junction between subdomains IA & IIA (*Curry et al, 2006*).

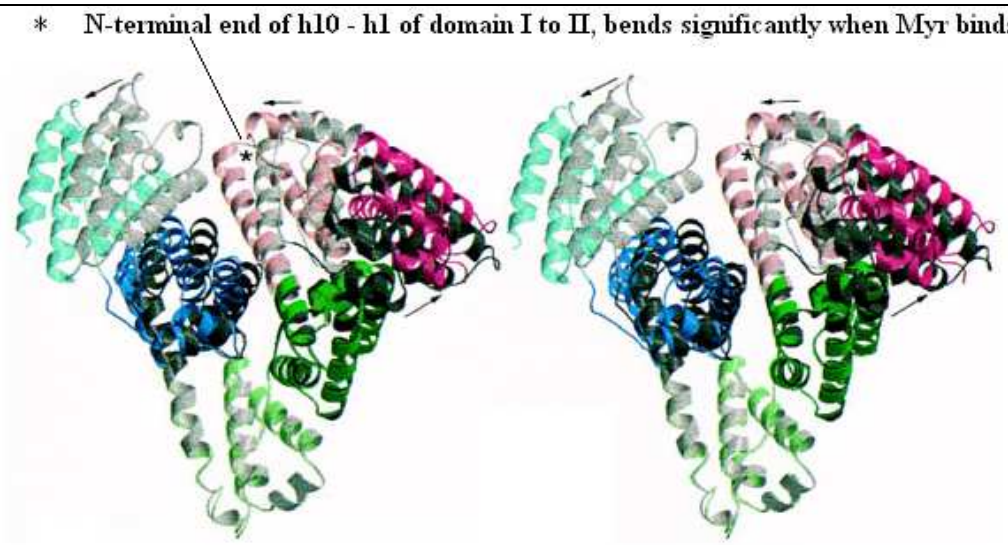

Figure 2.5. Schematic representation of the conformational changes resulting in Myr binding.
(Curry et al, Nature Structural Biology, 5, 827 – 835, 1998)

The colour coding for albumin domains with bound Myr is the same as described in Figure 2.3. HSA only is colour coded grey with dark and light grey representing subdomains A & B respectively. The coloured helices indicate how much the albumin conformation changes when Myr binds, and the arrows show the direction that both domain I & III move with respect to domain II. The Cα of HSA with and without Myr are superimposed at domain II as this is the only domain that does not change.

Although the binding of myristate exposes the asymmetrical properties of the domains, similarities in domain IB & IIIB exist with the myristate binding site existing within these regions as tunnels, open at both ends and spanning the width of the subdomain of

approximately 1.7Å that runs perpendicular to the axes of helices h9 & h10. Differences are also observed in the way Myr 1 & Myr 5 are bound within subdomains IB & IIIB respectively in that the Myr molecules are inverted with respect to each other within these subdomains (refer to Figure 2.4.). No binding sites for Myristate has been determined in subdomain IIB, as although this tunnel exists it is highly restricted at its centre by aromatic residues, namely Phe 309, Phe 330 and Tyr 353. There also exists a possible block at one end of tunnel IIB where the carboxylate residue of the FA would dock and bind (*Carter et al, 1992*). The interaction of myristate occurs in two stages. Firstly there is an ionic interaction of the FA carboxyl group with the albumin surface. The second stage is the carbon chain (C-chain) attraction of the FA to the interior of the protein globule that results in the dissociation of the carboxyl group (*Muravskya et al, 2004*). It is inevitable that albumin undergoes conformational changes with each addition of Myristate.

2.5.ii. Chain Length Dependence of Fatty Acid Binding to Albumin

There is a relationship between the number of binding sites on albumin and the chain length of the FA, with an increase detected in primary association to high affinity binding FA sites associated with increase in chain lengths that are not linear (*Kragh-Hansen et al, 2006*). FAs such as octanoate, decanoate, laurate and myristate are all examples of MCFAs. The principal site of octanoate and decanoate is a single site in domain III. Laurate binds to IIIA & IIIB and myristate binds to IB & IIIB. The primary binding sites were found to be affected by amino acid mutation in other regions of the protein. Of the MCFAs studied, only the X-ray crystal structure of the octanoate remains unknown (*Bhattacharya et al, 2000*). Site IIA is the site for shorter chain FAs like octanoate and decanoate. It should be noted that MCFAs constitutes only a small fraction of the FAs found in blood. For the longer chain FAs up to five principal high affinity binding sites have been detected. LCFA are known to control the binding of ligands to HSA, by competitive and allosteric mechanisms that are found to mainly involve domain I (*Chuang*

et al, 2006). In vivo, FAs are stored as triacylgycerols in the adipose tissue, released into the circulation with transportation by albumin. The solubility of FA in the body unassisted is <1μM. HSA will carry normally concentrations of FA between 0.1 – 2M/mol of HSA (*Frederickson et al, 1958*). However, there are some occasions, such as after exercise or adrenergic stimulation, or extreme fasting, or in patients with diabetes, liver or cardiovascular decease when this concentration can increase to as much as 6M/mol of HSA. Not all FAs produce inhibitive or deleterious effects on the binding of other ligands to albumin. Indeed, the presence of FA (3M/mol of FA:HSA) has been shown to increase the binding of warfarin to albumin, bringing about as much as a 3 fold increase in the binding constant. Higher concentrations of FA produce competition between the FA molecules and warfarin, resulting in reduced binding of the drug (*Chuang et al, 2006*).

Octanoate binds to the indole and benzodiazepine binding region of albumin located within subdomain IIIA. The presence of this FA now produces deleterious effects on the binding of benzodiazepines, prohibiting its binding (*Kragh-Hansen et al, 1991*), thus supporting the view that the distribution of FA is heterogeneous, non-specific, can be shared or overlap with other binding sites for other ligands whether considering MCFAs, saturated, monounsaturated or polyunsaturated LCFAs. An overlap also exists between FA binding site 7 and subdomain IIA, this site on HSA shares 2 aa side chains with FA site 2. Site IIA overlaps with FA sites 3 & 4. FA site 1 acts as a primary site for the haemin ligand, and FA site 5 is a secondary site for propofol and thyroxine (Figure 2.6). Lastly, FA site 6 is a secondary site for ibuprofen and diflunisal. In summary, binding site IIA will bind small, medium and LCFAs. Subdomains IIB, IB & IIIB will bind MCFAs & LCFAs, with subdomains IB & IIIB showing the greatest similarities. Further FA binding sites may be found in IB – IIA & IIB – IIIA, in the inter-domain clefts (*Kragh-Hansen et al, 2001*).

The nomenclature of FAs refers to a general formula of Cm:n where m corresponds to the number of carbon atoms in the methylene tail, and n referring to the number of double bonds. Figure 2.6 shows two examples of FA binding, C18:1, oleic acid that has 18 carbons in the methylene tail with one double bond, and C20:4 which is arachidonic acid having 20 carbons in its methylene tail and four double bonds (*Bhattacharya et al, 2000*).

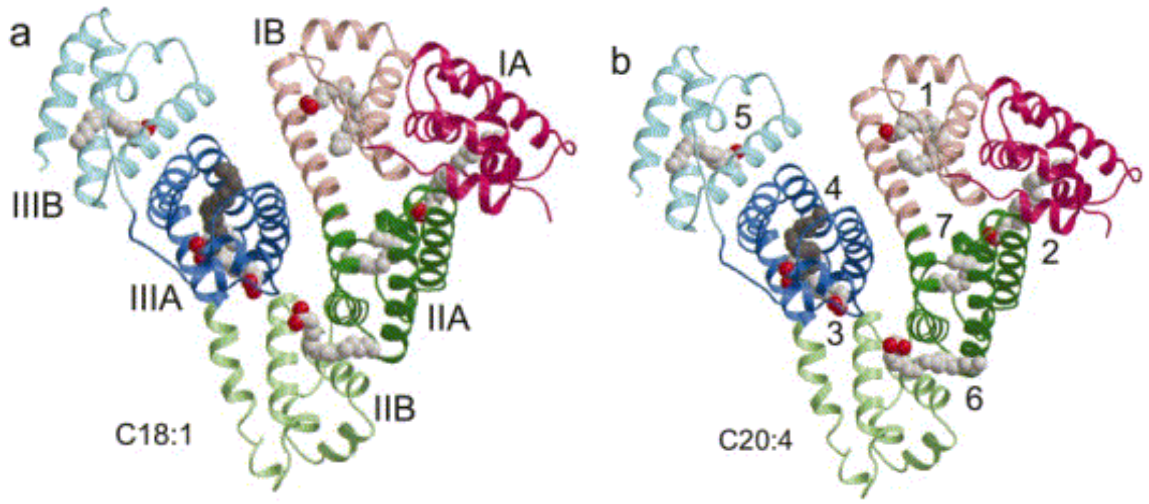

Figure 2.6. Schematic representation of the binding of up to 7 Myr molecules.
(Bhattacharya et al, J of Mol Biol, vol 303, Issue 5, 721 – 732, 2000)

The colour coding for albumin domains with bound Myr is the same as described in Figure 2.3. C18:1 is monounsaturated oleic acid and C20:4 is polyunsaturated arachidonic acid. Binding of the FA for sites 1 to 5 will be similar, if not the same. Numbers 1 to 7 indicates the binding sites for FA.

In accommodating larger FAs some of the binding site/tunnels on HSA adapt to accommodate the larger molecule, thus making the site "flexible;" this is shown in Figure 2.7. (*Curry et al, 2001*). The binding of FAs at sites 2 & 4 are different to that at site 5. The cross sectional dimensions of sites 2 & 4 increase to as much as 1 - 2Å, with the upper part of site 2 wide, while site 4 broadens in two regions (Figure 2.7). Site 2 is said to be the most enclosed FA binding sight in HSA, enclosing the whole FA when bound thus shielding it from solvent effects. Site 2 binding causes a rotation of domain I relative to domain II. Conversely, site 5 is relatively inflexible and remains long and narrow. This analysis was achieved by measuring the deviation of the methylene tail of the FA;

deviations in site 2 & 4 are much more than those observed for the smaller FA (C18:0 & C18:1).

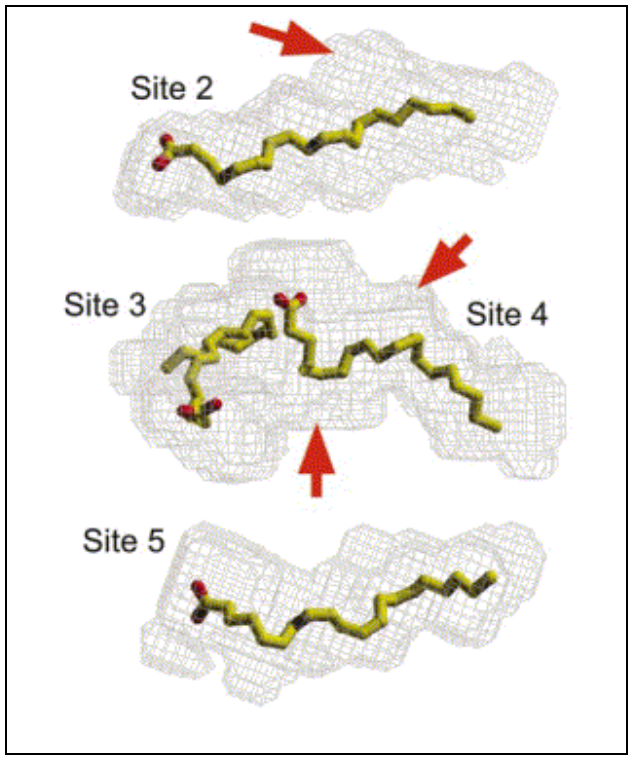

Figure 2.7. Comparison of the binding site for FA site 2, 4 & 5 on HSA for the FA C20:4.
(Carter et al, J Mol Biol, 314, 955 – 960, 2001)

The red arrows indicate the broadening of the tunnel at this site. C20:4 is polyunsaturated arachidonic acid.

The FA binding sites are summarised in Figure 2.8, which shows the location of the FA binding site in the subdomains for each of the 9 binding sites now known. The different lengths of the FA are superimposed, and are shown as coloured ball and stick models in the binding pockets. Of the 7 FA sites previously mentioned two additional sites (site 8 & 9) have now been found located close to the base of the inter-domain crevice between the junction of domains II & III; C10:0 was the FA used to investigate these pockets.

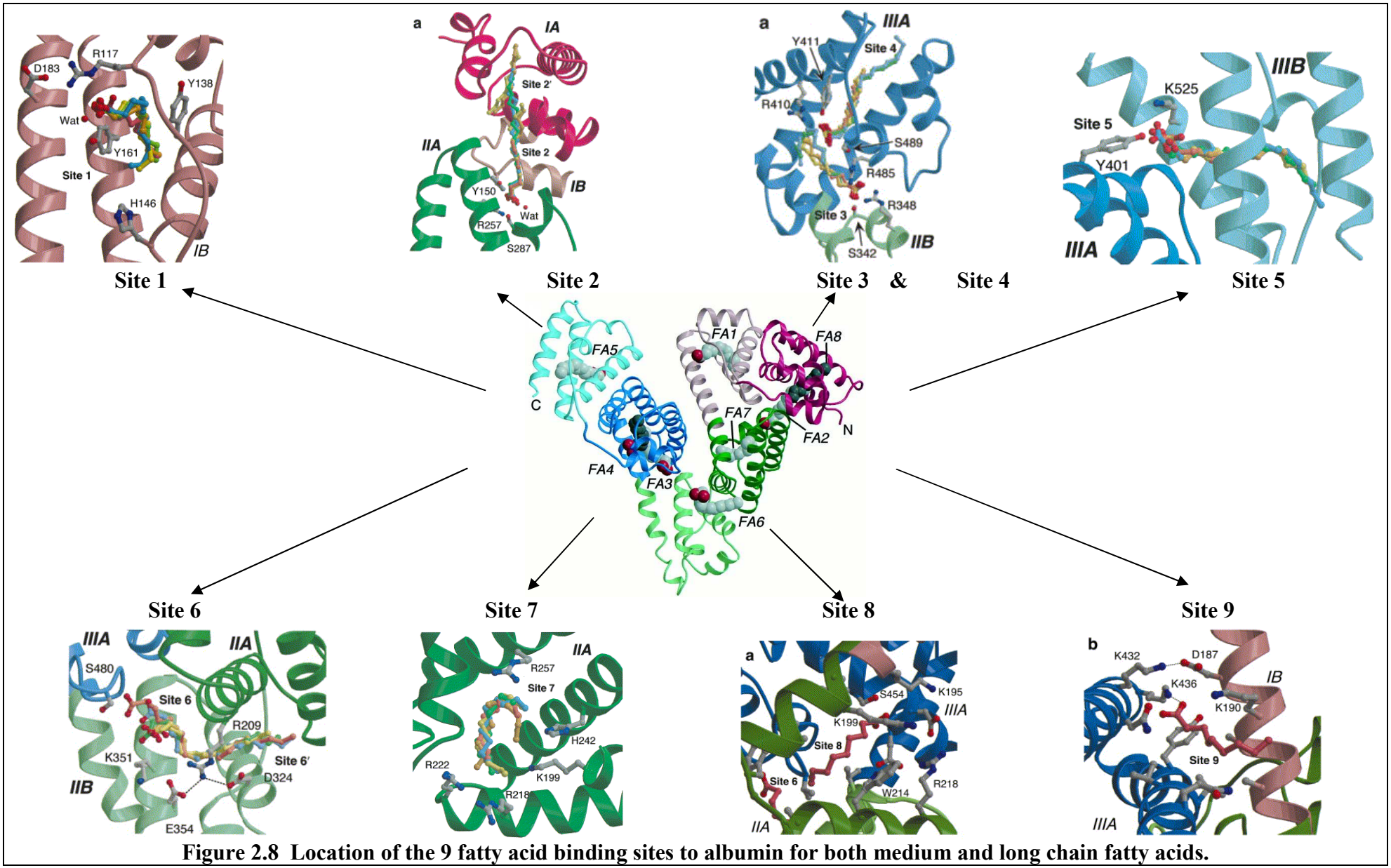

Figure 2.8 Location of the 9 fatty acid binding sites to albumin for both medium and long chain fatty acids.

Considering capric acid, C10:0, which represents a saturated FA, one of the methylene tails that bind to site 6 also assists in forming the hydrophobic end of the site 8 pocket, showing possible cooperative interactions between the two site. At the other end of site 8 there is a ring of polar residues that included Lys 195, Lys 199, Arg 218, Asp 451 and Ser 454, with the formation of an H-bonding of the carboxylate FA to the side chain of Ser 454. Site 8 is located at the base of the crevice between subdomaims IA – IB –IIA on one side and IIB – IIIA – IIIB on the other. Conversely, site 9 lies further up the inter-domain crevice; this site is very exposed with only limited contact of the FA with the protein. A salt-bridge between Glu 187 (in domain I) and Lys 432 (in domain III) across the top of the crevice helps to keep this FA in place, with the interaction of the FA with the side chain of Lys 190. Interaction at site 9 has only been seen for C10:0 because the residues involved in binding at this pocket are so far apart due to the movement of domains I and III as a result of other FA binding, this produces a 1 – 2 Å narrowing of the crevice that exists between these two domains.

A common set of 7 binding sites exists for FA (MCFA & LCFA), with an additional set of 4 sites found for the simple MCFA. Site 7 (IIA) is the primary site for short chain fatty acids (SCFA) but not for LCFA. Esterase activity through Tyr 411 is inhibited by MCFAs up to C10:0. A weaker inhibition is observed by LCFA due to the fact that this is a weak site for LCFA. MCFAs bind preferentially to IIA and IIIA. At least one high affinity site for LCFA is found in domain I, another is found in domain III. There is a great amount of overlap of the binding sites with a commonality in several of the sites. The importance of FA in the crystallographic determination of the structure of albumin has already been stated (*Curry et al, 1998*). The presence of FA in recent drug binding studies by crystallography has made possible the elucidation of more subtle structural determinations. Previously, only Carter & co-workers in 1989 (published in 1992) were able to both grow

and measure meaningful data, albeit under extreme conditions (*Sugio et al, 1999*). There exist only a limited number of specific drug binding sites on albumin known as site I and site II, with site II being the preferential binding site for most drugs (*Sudlow et al, 1975*). There also exist other low affinity sites as well as high affinity sites for the same ligand (*Dröge et al, 1988*). On the binding of a ligand HSA undergoes conformational changes, the most important is the N – B transition. Additional binding sites can be found between the fusion of sites IIA & IIIA, also subdomain IIB is involved in some instances as well.

2.5.iii. Mechanism of Binding to Subdomain IIA (Sudlow site I)

Salicylic acid (SA) and its derivatives are all examples of a special class of ligands that will bind to both IIA and IIIA within albumin. Binding site IIA is formed by six helices that contains two sub-chambers, possibly one of these chambers is for the FA7 site. Ligands that prefer site IIA tend to be bulky hetrocyclic anions with the charge situated centrally within the ligand. Ligands preferentially binding to this site tend to be aromatic. The Sudlow site I binding cavity within albumin is large, flexible and able to accommodate chemically diverse ligands with high affinity. Site IIA is said to contain several individual ligand binding sites that bind independently or can mutually influence each other (*Chuang et al, 2006*). The major pocket is created by the smaller disulphide double loop (h5 & h6) that is found within the interdomain connection (*Frofanov et al, 1997*). The two disulphide bonds in the smaller double loop are thought to experience a change in conformation upon binding, changing from the g – g – g form to the more extended g – g – t and g – t – g conformations, resulting in the relative rotation of the domains. Trp 214 that is located at the bottom half of the h4 helix of IIA, moves from a hydrophobic to a hydrophilic environment. Competitive binding exists at this site (*Kragh-Hansen, 1985*), examples include warfarin that competes with bilirubin but is not displaced by phenol red. The subdomain IIA site is enantio-selective and will bind, for example, the S-isomer of

warfarin 33% more selectively than the R-isomer (a more detailed account is given in Chapter 5); the presence of domain I is thought to be important for the binding activity of this site. Subdomain IIA is affected by the N-B transition, binding warfarin and bilirubin tighter at pH8 and above. Other residues implicated in the functionality of this site are Lys 199 and His 242.

The binding of a ligand such as salicylic acid at subdomain IIA involves the participation of many amino acids. Residues Leu 219, Phe 223, Leu 234, Leu 238, Leu 260, Ala 261, Ile 264, Ile 290, Ala 291 and Glu 292 are all close to the aromatic ring of the carboxyl group of salicylic acid on docking. The carboxylate group itself interacts with Arg 257, Arg 222 and Lys 190 of the protein, His 242 is also thought to be involved when determined by X-ray crystallography (*Carter et al., 1992*). Figure 2.9 illustrates the early crystallographic determination showing just how the ligand is situated in this binding pocket. The binding of 2,3,5-triiodobenzoic acid (TIB) is identical to salicylic acid but the presence of the iodine gives this molecule a handle in that allows easier spectroscopic measurements to detect and measure ligand orientation. TIB was the preferred molecule used in early crystallographic determination. The binding cavity is situated within the double loop created by the disulphide of h5(II) and h6(II) as shown in Figure 1.6.

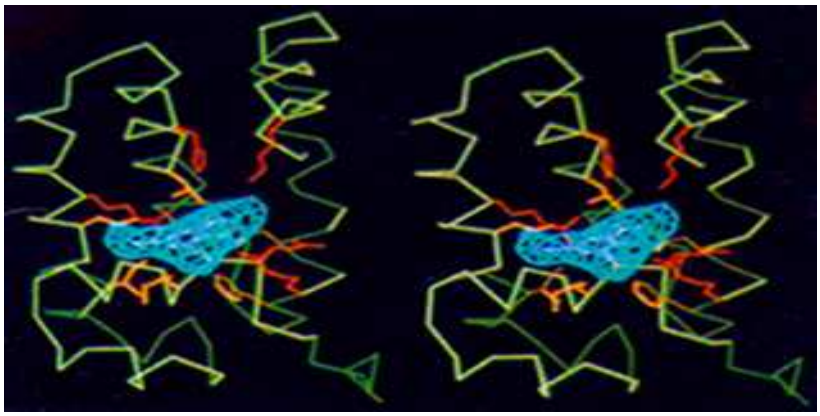

Figure 2.9. Stereo view of subdomain IIA binding 2,3,5-triiodobenzoic acid (TIB)
(Carter et al, Nature, 358, 209 – 215, 1992)

2.5.iv. Important Residues in the Site I Binding Site (Subdomain IIA)

There are common features present within the binding sites of albumin. However, there are specific residues within the binding pocket that if removed, will debilitate, hinder or cease the binding functionality of that pocket. Within subdomain IIA several residues are implicated, for example Lys 199 is the site of esterase activity (*Curry et al., 2001*). HSA possesses enzymatic activity that was first observed in 1951. This activity was seen in both subdomains IIA & IIIA with the activity of IIIA being the more dominant (*Yang et al., 2007*). For example, aspirin acetylates HSA under normal physiological conditions via Lys 199 with the transfer of its acetyl group (see Equation A).

Both aspirin and salicylic acid bind to albumin, both at similar locations. However, the molecular orientations of the ligands on binding are different with aspirin producing a rotation of 30° to accommodate the acetylation, converting Lys 199 to acetyl-lysine (*Yang et al., 2007*). Esterase activity occurs via a two step process, although no direct evidence has been found. The first stage involves the binding of aspirin to site IIA with the acetyl group of aspirin pointing towards Lys 199. The second stage is Lys 199 attacks the acetyl group of aspirin. It should be noted at this stage that the esterase activity of salicylic acid (SA) has a stronger binding activity than that observed for aspirin due to the closer contact of SA.

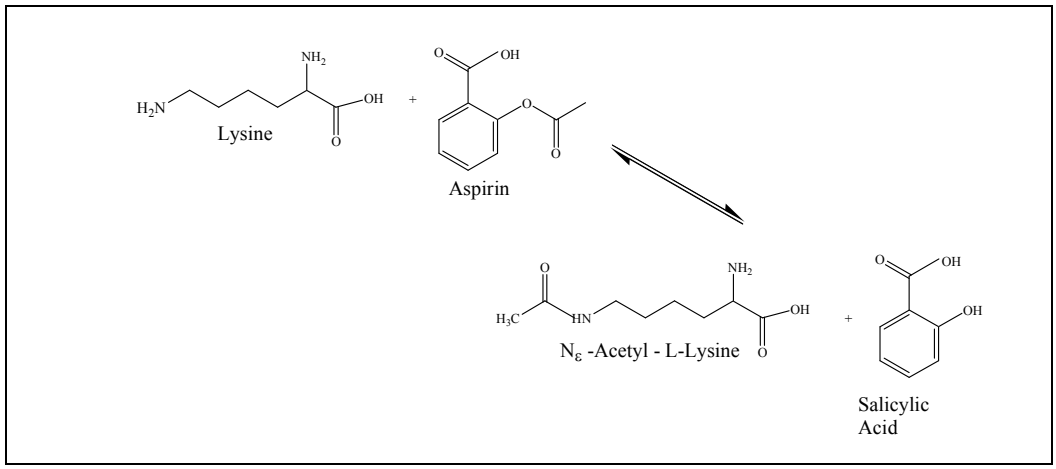

Equation A: Possible mechanism for the acetylation of lysine 199 in albumin using aspirin.

Subdomain IIA presents a large hydrophobic cavity, truncated compared to the cavity of IIIA as a result of the presence of bulkier hydrophobic side chains. The entrance of this binding pocket is surrounded by positively charged residues (K195, K199, R218 & R222), with Lys 199, His 242 and Arg 257 functioning sterically and electrostatically in ligand binding (*Tuan et al., 2006*). A second cluster of positive residues is found at the bottom of the sock shaped pocket (Y150, H242 & R257) that permits simultaneous interaction at the two clusters.

2.5.v. Mechanism of Binding to Subdomain IIIA (Sudlow site II)

Binding site IIIA is a T-shaped hydrophobic pocket with two hydrophilic entrances with a separation of 10Å. The entrance contains residues that interact with the carboxyl groups of the binding ligand. Like site IIA, this pocket is also formed from six helices. However, h3 & h4 form the floor, h1 & h2 form the sides and h5 & h6 form the roof of the internal cavity. The binding pocket of IIIA is smaller and narrower than that of IIA and cannot accommodate the binding of long ligands since it is less flexible than IIA. The binding at this pocket is stereoselective, for example, L-tryptophan binds preferentially to the D-isomer. Within the pocket are two regions of H-bond partners, the first is located across the interface of domains II & III through Ser 342 & Arg 348 in subdomain IIB and Arg 485 in sudomain IIIA. The second region is located at Arg 410, Tyr 411 & Ser 489, all found in IIIA. Within the pocket Arg 410 & Tyr 411 are thought to be the most important residues. Bound FAs occupy tunnels between the helices that are lined with hydrophobic residues. Myr4 interacts with Arg 410 in IIIA and Myr3 interact with Arg 485 in subdomain IIIA and residue 348 in subdomain IIB. The sequence Arg-Tyr*-Thr-Arg has been found to be important for the activity and functionality of this site. It was later found that the active residue Tyr* located at position 411 in the tip of the loop was the important residue. Lys 414 has also been implicated in the activity of this site (*Peters, 1996*). In this

subdomain the binding of salicylic acid and its derivatives have been considered in depth. Pro 384, Leu 387, Ile 388, Phe 395, Leu 407, Leu 430, Val 433, Ala 449 and Leu 453 all interact with the aromatic ring, with influences from the hydrocarbon chains of Arg 485 and Glu 450. Arg 410 interacts with the carboxyl group with influences from the oxygen of Tyr 411, (Figure 2.10.). Typically, TIB was used as the marker ligand to investigate the characteristics of this binding pocket, since like salicylic acid, TIB binds to both site IIA and IIIA in albumin and exhibit similar binding orientations. The binding cavity is situated close to h1(III). One main polar cluster exists at the entrance and on one side of the pocket; the residues involved are Tyr 411, Arg 410, Lys 414 and Ser 489.

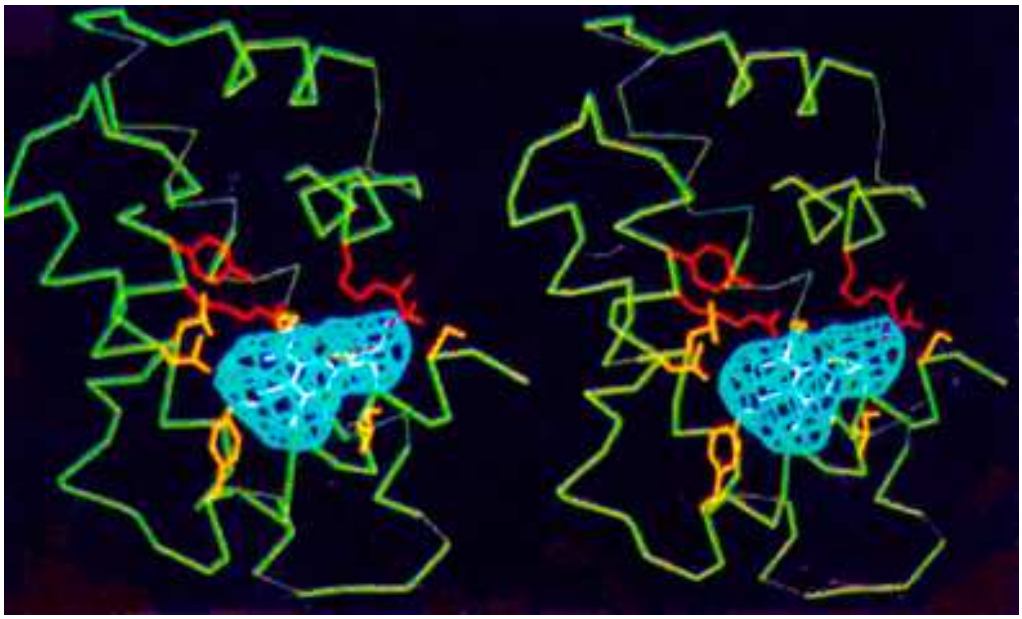

Figure 2.10 Stereo view of subdomain IIIA binding 2,3,5-triiodobenzoic acid (TIB)
(Carter et al, Nature, 358, 209 – 215, 1992)

2.5.vi. Important Residues in the Site II Binding Site

Arg 410 and Tyr 411 project into the middle and overlap with the centre of the site II binding site, and play an integral part in the functionality of this site. The functionality is reliant on the close proximity of the two residues, Tyr 411 being approximately 2.7Å from the nitrogen of Arg 410. Arg 410 interacts with the charged carboxy group on the ligand

through electrostatic interaction between the ligand carboxylate and the guanidine portion of the residue (*Kragh-Hansen et al, 2001*). The aromatic ring of Tyr 411 and the phenolic oxygen both play a key role. Diazepam binds to this site but does not possess a carboxyl group and therefore the two points of contact for Tyr are the important features (refer to Chapter 5 for more detail). Tyr 411 seems to be the vital moiety and key to the binding in this pocket (*Kragh-Hansen et al, 2001*). Also located in the site II binding pocket are two FA binding sites for molecules FA3 & FA4, with the carboxyl of FA4 interacting with Arg 410 & Tyr 411. The combination of the two residues is said to play an important role in "modulating the affinity of HSA for a variety of ligands" (*Kragh-Hansen et al, 2000*). It has also been found that these two residues are highly conserved in a variety of species in evolution (along with Arg 218 in site I).

2.6. Quantification of Ligand Binding

The pharmacokinetics of drug binding to plasma proteins such as albumin is very important as its binding will affect the concentrations of the unbound drug, its distribution in the body and its elimination (*Curry et al, 2001*). Warfarin is an example of a drug that binds to albumin in quantities as much as 99% under normal therapeutic conditions; this gives rise to a small volume of distribution and a low clearance. It is vital to know and understand the binding mechanism of any drug, its chemistry and activity within the body in order to ensure effective and optimum use. The quantification of the binding of a ligand to a protein can be achieved by two different approaches, one is the thermodynamic treatment derived from the stoichiometric equilibrium constant K_i, and the other method is using non-linear mathematical computer fits.

There are many methods and techniques employed to analyse binding, all offer advantages as well as disadvantages. Where macromolecules are concerned there is no definitive

method that can give all the information required. Each method offers only a proportion of the information, thus highlighting the fact that each method has built in inherent problems. Often the structure of the macromolecule is unknown. Therefore, studying binding effects may only add to the confusion. Breaking the macromolecule down into fragments that are more manageable is an act in itself that is problematic. Fractions, often created from the natural breaks that are present within the protein, often referred to as domains if multiple domains are present in the macromolecule, will exhibit characteristics that may or often may not be found in the intact protein itself. Albumin is one such protein that has been systematically studied for binding over the years even when its structure was unknown and not fully characterised. This may explain the diversities in determining just how many binding sites are present.

A prerequisite to understanding binding is to understand the structure of the macromolecule under investigation. Often binding will evoke a structural change to the macromolecule at a local level. However, changes can occur on a more global scale that in turn may affect the functionality of the remaining binding sites. This kind of response is referred to as an allosteric mechanism. The macromolecule can be envisaged as a "molecular transducer" that will respond to, and is somewhat controlled by the modulating effects of a ligand, that can control the molecular shape and response to subsequent ligand binding. In the simplest case, ligand binding involves the stoichiometric binding of a ligand to a specific binding site on a macromolecule.

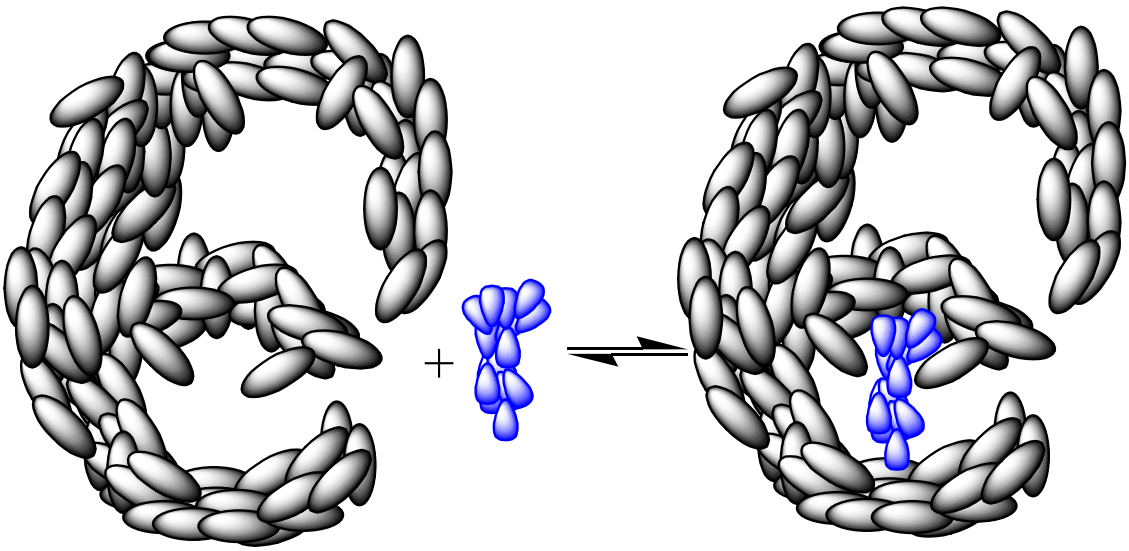

Macromolecule / Protein

HOST

Ligand

GUEST

Primary Binding Site filled first

HOST:GUEST COMPLEX

Addition of second Ligand

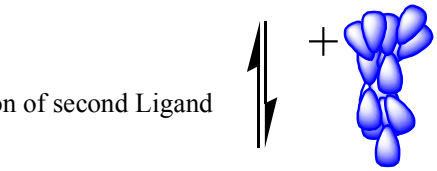

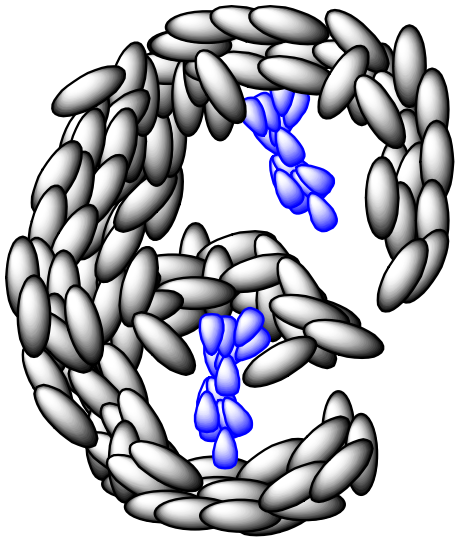

Secondary Binding Site filled, orentation of second binding ligand changed so that it can be accomindated by the protein

HOST:GUEST COMPLEX

If more than one binding site is present for the same ligand, then there is often a dominate site that will always bind preferentially; this is called the primary binding site. Subsequent ligands that bind may have to be modified in some way, such as orientation, in order that they may also be accommodated on the macromolecule. The modifications in the macromolecule on binding of the first ligand may act as a trigger to allow subsequent ligands to bind; equally, it may also act as an inhibitor for further interactions. In this thesis the larger macromolecule (the protein) is considered to be a host (H) which will accepts the binding of a smaller guest molecule (G). The choice of which entity is referred to as the guest and which the host is probably best set by the mathematical treatment. Thus, for example, a small peptide is often referred to as a ligand when it binds to a metal ion. On the other hand, the metal ion is termed the ligand when binding to a protein. In a binding process, the largest species involved is often trivially referred to as the host. In mathematical terms, the species that is being monitored (with a fixed concentration) is best termed the guest, the other molecule the host. In practice, the binding of ligands to proteins is more complicated when considering large multi-binding site proteins. The equilibrium can be described by the expression,

$$\begin{array}{ccccc} [\text{Host}] & + & [\text{Guest}] & \rightleftharpoons & [\text{Host:Guest}] \\ [\text{H}] & + & [\text{G}] & \rightleftharpoons & [\text{HG}] \end{array} \qquad (1)$$

The quantification of this process concerns the concentration of the various species and the solution conditions. The binding constant (or association constant) is defined as:

$$K_a = \frac{[HG]}{[H_f] \,.\, [G_f]} \qquad (2)$$

where $[H_f]$ is the equilibrium concentration of the free host (protein), $[G_f]$ is the equilibrium concentration of the free guest (ligand) and [HG] is the equilibrium concentration of the complex. This is the relatively simple picture for a [1:1] binding to give a [protein:ligand] complex. The picture is further complicated by the effects of other

ligands present and whether the ligands,

i) compete for the same binding site on the protein.
ii) enhance the binding of one, or the other, or both of the ligands present at the same or different binding sites.
iii) mutually reduces the binding to one, or the other, or both of the binding sites if different or at the same binding site if the same.
iv) bind to different sites on the protein;

There are two main algebraic approaches associated with the characterisation of ligand binding. The first approach is based largely on pre-computer mathematical method and is described in detail in books such as that published by Wyman and Gill. The second method is a more pragmatic approach with simpler algebra requiring a more computer-based approach to directly simulate unmodified experimental data. The two approaches overlap, are complementary and will be only briefly reviewed here. The reader is referred to the original texts for a more detailed discussion.

2.6.i. Classical Determination of Binding Constants

2.6.i.(a) 1:1 Macromolecule:Ligand Binding

The ability to investigate binding interactions relays something about the forces of interaction between the two molecules, and the relative stability of the resulting complex. Classically, ligand binding has been quantified following the schemes of Hill (1910), Scatchard (1949), Klotz (1946) and Job (1949). Scatchard originally assumed:

i) Ligands are bound to independent binding sites on the protein.
ii) There exits groups of binding sites with the same binding constant.
iii) The binding of one ligand is unaffected by the binding of another.

In the classical treatment, the binding process is explicitly considered in terms of proteins and ligands. The equilibrium constant is derived from the association of the protein and the ligand. Thus,

$$\begin{array}{ccccc} \text{Protein} & + & \text{Ligand} & \rightleftharpoons & \text{Protein:Ligand} \\ [\text{P}]_{\text{free}} & + & [\text{L}]_{\text{free}} & \rightleftharpoons & [\text{PL}] \end{array} \quad (3)$$

The association constant (K_{ass}) is defined as,

$$K_{ass} = \frac{[PL]}{[P]_{free}\ [L]_{free}} \quad (4)$$

where [PL] is the concentration of the complex, [P] is the free equilibrium concentration of the protein and [L] is the free equilibrium concentration of the ligand. K_{ass} is also abbreviated as K and is related to the dissociation constant (K_d), where $K = 1/K_d$. An important parameter to consider is the number of moles of ligand bound per mole of protein defined by Scatchard as '$\bar{v}$', which is the degree of binding and can be defined as :

$$\bar{v} = \frac{[L]_{bound}}{[P]_{Total}} = \frac{[PL]}{[PL] + [P]_{free}} \quad (5)$$

Substituting equation (4) into (5) gives:

$$\bar{v} = \frac{K\,[L].[P]}{[P] + K\,[L][P]} = \frac{K\,.\,[L]}{1 + K\ [L]} \quad (6)$$

Equation (6) can be rearrange to give the ratio of filled to unfilled sites, thus:

$$\frac{\bar{v}}{1 - \bar{v}} = K.[L] \quad (7)$$

where $(1-\bar{v})$ is the fraction of unoccupied sites. Scatchard multiplies equation (7) by the term $(1-\bar{v})$ / [L] to give:

$$\frac{\bar{v}}{[L]} = K - \left(K.\bar{v}\right) \quad (8)$$

If $\bar{v}$ / $[L]$ (on the ordinate) is plotted against $\bar{v}$ (on the abscissa) a straight line is obtained for a single site binding, with the slope of –K and an intercept of K. The Hill plot takes logs of equation (7) to give:

$$\log \frac{\bar{v}}{1-\bar{v}} = \log K + \log[L] \qquad (9)$$

If $\log \bar{v} / \left(1-\bar{v}\right)$ is plotted against log [L], a straight line is obtained with an intercept of log K. A typical way to plot a binding curve is by plotting $\bar{v}$ against log [L]; this shows a sigmoid relationship. Plotting the equations in different forms brings out the different attributes of the binding relationship, and allows a better understanding of the underlying factors of the mechanism of binding. For example, the Hill plot and the binding curve both give information on the cooperativity of the binding process (see later). Equation (6) can be rearranged to give:

$$\frac{1}{\bar{v}} = \frac{1}{K_{ass}} \cdot \frac{1}{[L]} + 1 \qquad (10)$$

$\bar{v}$ is a measure of the extent of binding and is dependent on the total protein concentration. If there is more than one binding site, then by Scatchard's assessment equation (6) can be expressed in terms of reciprocals where the number of binding sites are taken into consideration:

$$\frac{1}{\bar{v}} = \frac{1}{nK} \cdot \frac{1}{[L]} + \frac{1}{n} \qquad (11)$$

Equation (11) highlights several different plots that can be constructed to investigate the binding characteristics of a specific interaction. A double reciprocal plot of $1/\bar{v}$ against 1/[L] produces a linear regression line with a slope of 1 / nK and an intercept of 1/n with the ordinate axis. This is known as the Klotz plot (*Kragh-Hansen, 1990*).

2.6.i.(b) Multiple Binding Sites on a Protein

A protein can possess multiple binding sites for the same ligand, this is usually seen in proteins that contain multi-domains such as human serum albumin. When a ligand has more than one site that can be occupied on a macromolecule, several possible multi-

binding configurations can exist depending on which site is occupied first. There will be a binding constant, which will be specific to each site. The greater the number of binding sites the greater becomes the complexity of the mathematics required to analyse the experimental data. Thus a two binding site case can be treated simply as a global bound / unbound case, as the first site followed by the second site binding case, or as a multi-equilibrium case with "micro" individual binding constants. This can be best illustrated diagrammatically as shown in Figure 2.11.a.

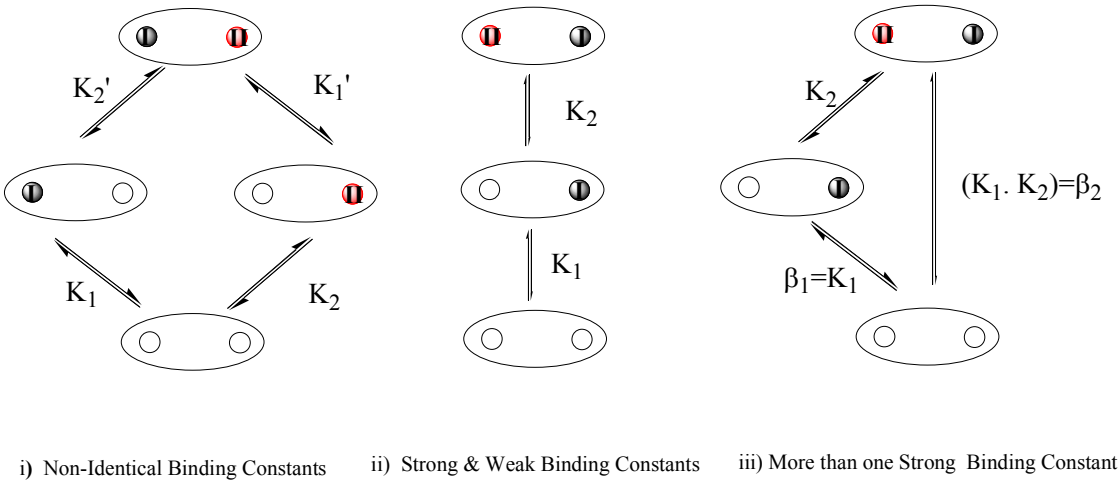

Figure 2.11.a. Schematic Representation of the Binding Sites on a Protein.

As discussed earlier, albumin has many binding sites (*Klotz et al., 1979*). The binding of a ligand to a particular site can depend upon the occupancy of other sites. One binding ligand can induce changes in site accessibility due to stereochemical bulk or protein conformation changes (2^{ry}, 3^{ry} or 4^{ry}) that can affect the binding of another ligand. In the extreme, the binding of one ligand may completely inhibit the binding of subsequent ligands. The location of binding sites within the macromolecule will play a vital role in binding capability, and will control the type, shape and size of the ligand that will be accepted at the site. Therefore, although different multi-binding configurations cannot be discriminated for in terms of binding site constants, they may play an important role in the binding capacity and capability of the macromolecule. In the case of albumin, the situation

is further complicated by the shear numbers of binding sites that could be present as represented in Figure 2.11.b., the possibilities that can exist for three and four binding sites show the complexity of the situation and highlights the problems associated with determining any meaningful binding data.

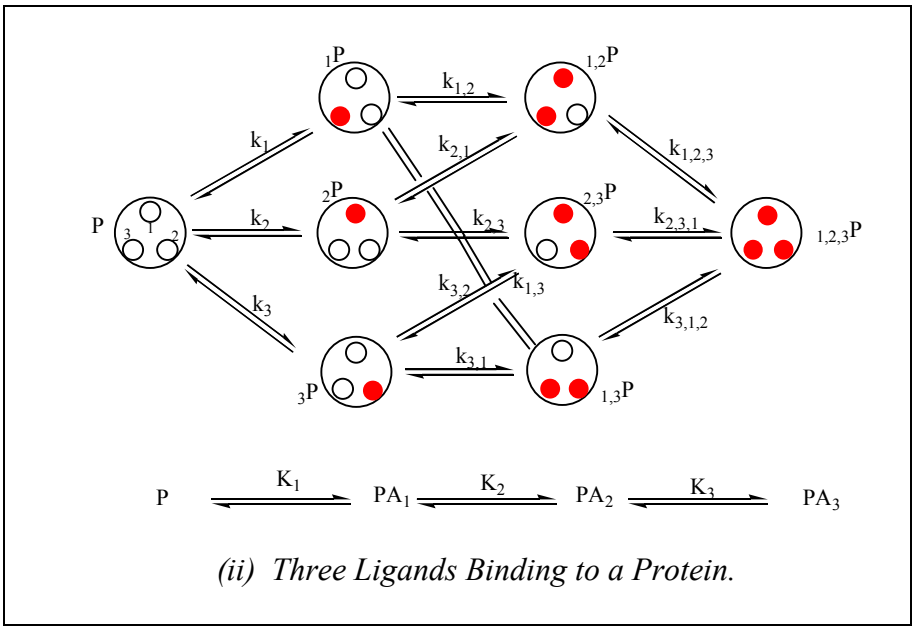

(ii) Three Ligands Binding to a Protein.

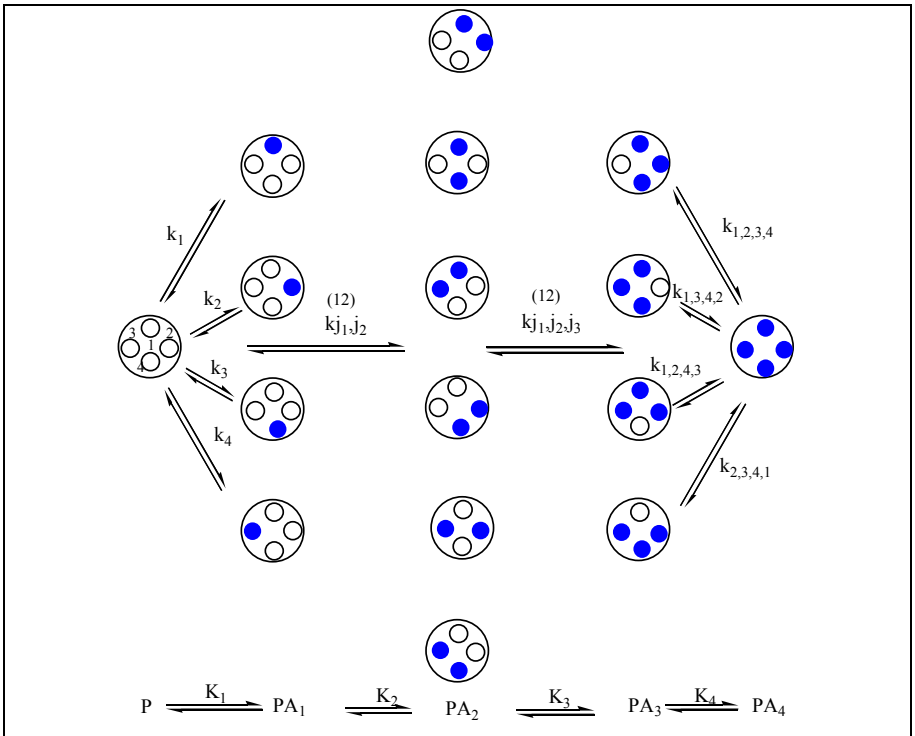

(iii) Four Ligands Binding to a Protein.

Figure 2.11.b. Schematic Representation of the Binding Intermediates.

Binding to a Protein containing One strong Site and One weak Site

For a strong and a weak binding site with values differing by over an order of magnitude, Figure 2.11.a.i. can be reduced to Figure 2.11.a.ii. with $K_1 = K_1'$ and $K_2 = K_2'$. The analysis can be taken as a two step process applying the Scatchard analysis to two concentration regimes.

Two Independent Binding Site Models

A relatively simple approach to demonstrate independent but identical ligand binding is to consider the binding of oxygen to two sites on haemoglobin, according to the solution shown in Figure 2.11.a.iii. There are two possible binding constants associated with this protein K_1 and K_2 where,

$$P + L \rightleftharpoons PL \qquad K_1 = \frac{[PL]}{[P].[L]} \tag{12}$$

$$PL + L \rightleftharpoons PL_2 \qquad K_2 = \frac{[PL_2]}{[PL].[L]} \tag{13}$$

Equations (12) and (13) looks at the individual binding at each binding site. However, the binding can be considered from the prospective of the overall reactions with respect to the un-reacted protein with binding constants now termed β_1 and β_2. The two sets of constants are equated by $K_1 = \beta_1$ and $K_1 K_2 = \beta_2$. Now the reactions can be expressed as:

$$P + L \rightleftharpoons PL \qquad \beta_1 = \frac{[PL]}{[P].[L]} \tag{14}$$

$$P + 2L \rightleftharpoons PL_2 \qquad \beta_2 = \frac{[PL_2]}{[P].[L]^2} \tag{15}$$

The degree of binding is expressed as,

$$\bar{v} = \frac{[PL] + 2[PL_2]}{[P] + [PL] + [PL_2]} \tag{16}$$

Unlike the single site model, there is no simple linear relationship that can express this type of binding; the binding will have to be analysed by non-linear data fitting methods. In terms of the Scatchard or Hill type format, in taking the ratio of sites filled to the sites unoccupied for two sites, the fraction of unoccupied sites is expressed as $\bar{v}/2 - \bar{v}$. The Scatchard equation becomes:

$$\frac{\bar{v}}{2 - \bar{v}} = \frac{K_1 [L] + 2K_1 K_2 [L]^2}{2 + K_1 [L]^2} \tag{17}$$

Therefore, at low concentrations of ligand, $[L] \rightarrow 0$

$$\frac{\bar{v}}{2 - \bar{v}} = \frac{1}{2} K_1 [L] \tag{18}$$

At high concentrations $[L] \rightarrow \infty$

$$\frac{\bar{v}}{2 - \bar{v}} = 2 K_2 [L] \tag{19}$$

The Hill plot (log $\bar{v} / \left(2 - \bar{v}\right)$ against log [L]) will only show linearity at the extreme conditions. There will be two intercepts on the y-axis, one at the lower limit asymptote of log ((1/2) K_1) and the other at the higher limit asymptote of log ($2K_2$). Extensions to this approach with more complex analyses of binding processes are presented in the book by Wyman and Gill.

2.6.i.(c) Cooperativity and its Effects

In some cases of multiple binding sites, the binding at one site can affect the binding at another and visa versa. An affinity increase results in positive cooperativity; a negative cooperativity implies a reduction in binding ability. Cooperativity is measured by comparing the experimental binding curve with the theoretical curve, the theoretical curve constructed from a plot of independent but identical binging sites. Where there are 'n'

identical binding sites each with a binding constant of 'K', then the number of moles of ligand bound per mole of protein is expressed as :

$$\bar{v} = \frac{n\,K\,[L]}{1 + K[L]} \tag{20}$$

Taking the differential of equation (20) will give:

$$\frac{d\,\bar{v}}{d\,[L]} = \frac{n\,K}{\left(1 + K\,[L]\right)} - \frac{n\,K^2\,[L]}{\left(1 + K\,[L]\right)^2} \tag{21}$$

Multiplying equation (21) throughout by [L] gives:

$$\frac{[L]\,d\bar{v}}{d[L]} = \frac{n\,K\,[L]}{\left(1 + K\,[L]\right)} - \frac{n\,K^2\,[L]^2}{\left(1 + K\,[L]\right)^2} \tag{22}$$

In terms of equation (20) then,

$$\frac{d\,\bar{v}}{d\,In[L]} = \bar{v} - \left(\bar{v}\right)^2 / n = \bar{v}\left(1 - \bar{v} / n\right) \tag{23}$$

When $\bar{v} = n / 2$, the maximum slope is observed which is equal to n / 4. Comparisons of binding curves with suspected cooperativity and curves obtained for the equivalent site independent binding will show if cooperativity exists. If the curve showing cooperativity has a slope greater than that obtained for the reference curve then positive cooperativity exists. Assessments of cooperativity are best achieved from Hill plots. Fractional saturation 'θ' can be defined as:

$$\theta = \bar{v} / n \tag{24}$$

Determining the slope of the reference curve in equation (22) in terms of 'θ' gives:

$$\frac{d\,\theta}{d\,In[L]} = \theta\,\left(1 - \theta\right) \tag{25}$$

Therefore, the Hill plot is given by $\ln\left[\theta / \left(1 - \theta\right)\right]$ against ln [L] with a slope 'n_H' of:

$$n_H = \frac{d\,In\left(\theta/\left(1 - \theta\right)\right)}{d\,In[L]} = \frac{d\,In\,\theta}{d\,In[L]} - \frac{d\,In\left(1 - \theta\right)}{d\,In[L]} \tag{26}$$

or

$$n_H = \left(\frac{1}{\theta} + \frac{1}{1 - \theta}\right) \frac{d\,\theta}{d\,In[L]} \tag{27}$$

Therefore, $$n_H = \frac{1}{\theta\,(1 - \theta)} \cdot \frac{d\,\theta}{d\,In[L]} \tag{28}$$

From equation (28), the slope (of the reference curve) of the Hill plot will now be $\left(d\,\theta\,/\,d\,In[L]\right)\,/\,\theta\,(1 - \theta)$, where the slope of the reference curve $\theta\,(1 - \theta)$ is given by equation (25). The Hill plot gives a direct measure of cooperativity at any point along the curve. Thus, if the slopes of both the binding curve and the reference curves are the same then $n_H = 1$ showing no cooperativity.

2.6.i.(d) Competitive Binding of Ligands

A protein that contains a single binding site for two different ligands 'A' and 'B' presents two equilibrium constants as shown:

$$\mathrm{P} + \mathrm{A} \rightleftharpoons [\mathrm{PA}] \qquad k_A = \frac{[PA]}{[P]\,[L]} \tag{29}$$

$$\mathrm{P} + \mathrm{B} \rightleftharpoons [\mathrm{PB}] \qquad k_B = \frac{[PB]}{[P]\,[L]} \tag{30}$$

The degree of binding associated with each ligand is:

$$\overline{v_A} = \frac{[PA]}{[P] + [PA] + [PB]} = \frac{k_A\,[A]}{1 + k_A\,[A] + k_B\,[B]} \tag{31}$$

$$\overline{v_B} = \frac{[PB]}{[P] + [PA] + [PB]} = \frac{k_B\,[B]}{1 + k_A\,[A] + k_B\,[B]} \tag{32}$$

The binding effects of one ligand on the binding ability of the other ligand is called linkage effects. Equations (31) and (32) can be rearranged to give the following relationship:

$$\frac{1}{\overline{v_A}} = \frac{1}{[A]}\left(\frac{1 + k_B\,[B]}{k_A}\right) + 1 \tag{33}$$

If 'B' is present in a large excess, and the conditions are set such that the concentration of free 'B' is equal to the total concentration of 'B', this introduces a small error which is due

to the small absorption of 'B' compared to its large total volume, then equation (33) holds. Plotting 1 / $\overline{v_A}$ against 1 / [A] yields a straight line with an intercept on the y-axis equal to binding without inhibitor. In practice, the concentrations of all three components (Ligands 'A' and 'B' and the protein) are comparable to minimise binding at the second and additional sites (as in the case of albumin that has several binding sites). Under these conditions, a straight line plot is not obtained but a hyperbolic curve. Determination of the binding at the second and subsequent sites is also hard to correct for. As a result of the use of comparable concentrations then:

(1) The concentration of free A and B will have to be determined.

(2) If by plotting 1 / $\overline{v_A}$ against 1 / [A] a straight line is not obtained then competitive binding exists.

The Scatchard analysis converts equation (33) to give,

$$\frac{\overline{v_A}}{[A]} = 1 - v_A \cdot \left(\frac{k_A}{1 + k_B \cdot [B]} \right) \tag{34}$$

Experimental data should include both high and low ligand:protein ratios (i.e. high and low values of $\overline{v_A}$ / $[A]$). Taking the ratios in equations (31) and (32) gives,

$$\frac{\overline{v_A}}{\overline{v_B}} = \frac{k_A\ [A]}{k_B\ [B]} \tag{35}$$

If a plot of $\overline{v_A}$ / $\overline{v_B}$ against [A] / [B] is drawn yielding a straight line graph then the two ligands are competing for the same site. A slope of k_A / k_B (these can be determined by independent experiments) is obtained. However, this plot does not take into consideration the binding at secondary sites, it would be better to plot $\overline{v_A}$ against [A]. It is now possible to construct a theoretical binding curve of 'A' in the presence of a constant concentration of "B'. If competitive binding is assumed at the high affinity binding site, and compared to experimental data, k_A, k_B *and* $[B]$ can be determined from equation (31) where k_A, k_B are

calculated from independent studies of single ligand binding. [B] and $\overline{v_B}$ can be determined by substituting equation (36), which is :

$$[B] = [B]_{Total} - \overline{v_B} \,.\, [P]_{Total} \tag{36}$$

where $[B]_{Total}$ is the total concentration of the second ligand and $[P]_{Total}$ is the total concentration of protein. Substituting into equation (32) to give,

$$K_B [P]_{Total} \overline{v_B^2} - \left(1 + K_B [B]_{Total} + K_A [A] + K_B + [P]_{Total}\right) \overline{v_B} + K_B [B]_{Total} = 0 \tag{37}$$

This quadratic equation has two solutions for $\overline{v_B}$. However, one of the expressions can be dismissed since the solution results in a negative number for [B]. Equation (36) is used to calculate $\overline{v_B}$, equation (37) is used to calculate [B], the expected value of $\overline{v_A}$ is calculated from equation (31) and can be compared to that determined experimentally.

2.6.i.(e) Binding of Two Different Ligands to a Protein

A protein can possess two distinct binding sites for two different ligands, A and B. Several equilibria can be considered:

$$P + A \leftrightarrow PA \qquad k_A = \frac{[PA]}{[P][L]} \tag{38}$$

$$P + B \leftrightarrow PB \qquad k_B = \frac{[PB]}{[P][L]} \tag{39}$$

$$P + A + B \leftrightarrow PAB \qquad K_A K_B = \frac{[PAB]}{[P][A][B]} \tag{40}$$

The degree of binding in each case is therefore,

$$\overline{v_A} = \frac{[PA] + [PAB]}{[P] + [PA] + [PB] + [PAB]} = \frac{K_A [A] + K_A K_B . [A] . [B]}{1 + K_A [A] + K_B [B] + K_A K_B . [A] [B]} \tag{41}$$

$$\overline{v_B} = \frac{[PB] + [PAB]}{[P] + [PA] + [PB] + [PAB]} = \frac{K_B [B] + K_A K_B . [A] [B]}{1 + K_A [A] + K_B [B] + K_A K_B . [A] . [B]} \tag{42}$$

$$\overline{v_{AB}} = \frac{[PAB]}{[P] + [PA] + [PB] + [PAB]} = \frac{K_A \; K_B \,.\, [A].[B]}{1 + K_A\,[A] + K_B\,[B] + K_A \; K_B \,.\, [A].[B]} \qquad (43)$$

2.6.i.(f) Mutually Reduced Ligand Binding

It is possible that the mutual binding of ligands reduces their individual abilities to bind to the protein. This cannot be described by competitive means. The ligands, A and B, bind to different sites on the protein resulting in conformational changes and a reduction in CD signal in the case of CD spectroscopy (*Kragh-Hansen, 1990*). The effect of binding ligand B on the binding of ligand A can be quantified by the expression,

$$X = \frac{K_{BA}}{K_A} = \frac{K_{AB}}{K_B} \qquad (44)$$

where K is the association constants for ligands A and B, K_{BA} is the association constant for the mutual binding of ligand B first with respect to A, K_{AB} is the association constant for the mutual binding of ligand A first with respect to B and X is the coupling constant. There is a mutual relationship between ligand A and B with them being affected to the same degree. The relationship between X on binding characteristics can be summarised in Table 2.4.

X > 1	Cooperative Binding
X = 1	Independent Binding
X < 1	Anti-cooperative Binding
X = 0	Competitive Binding

Table 2.4. The effects of the Coupling Constant on Binding of Ligands to a Protein.

From the procedure described by Kragh-Hansen the value of the coupling constant, X, can be calculated from the following expression (*Kragh-Hansen, 1983*),

$$[P]_{Total} = [P] + [PA] + [BP] + [BPA] \qquad (45)$$

Equation (45) can be transformed to:

$$[P]_{Total} = [P] + K_A [P][A] + K_B [B] [P] + X K_A K_B [A] [B] [P] \quad (46)$$

The concentration of bound ligand A, $[A]_{Bound}$ can be calculated from:

$$[A]_{Boundl} = [A]_{Total} - [A] = K_A [P][A] + X K_A K_B [A] [B] [P] \quad (47)$$

Subtracting equations (46) and (47) gives,

$$[P]_{Total} - [A]_{Bound} = [P] + K_B [B][P] \quad (48)$$

If $[P]_{Total}$, $[A]_{Total}$, [A], K_B and [B] are known, it is possible to calculate [P]. Inserting this value and the known values of K_A and [A] in equation (45) makes it possible to calculate X, which can also be calculated in terms of bound B from equation (46).

2.6.ii. Direct Analysis of Ligand Binding Measurements

In pre-computer days, it was desirable to reduce the mathematics behind an analysis of observed data to a linear "$y = mx + c$" plot. Linear regression leads to values of the intercept (c) and the gradient (m) from which the desired parameter (e.g. Binding constant) can be extracted. Nowadays, computers have better enabled the fitting of non-linear equations using for example the Levenberg–Marquardt procedure to reproduce measurements themselves directly. The latter scheme provides more insight into the measurement process and reasonability of the calculations. Mathematically, the Levenberg–Marquardt method is as valid as the simpler linear regression. However, computer manipulation of data is required.

Using CD spectroscopy as the analytical monitor, in the simplest case of a 1:1 binding complex formation, there are three possible conditions (*Drake, 2001*):

(1) Class 1A: Non-chiral guest / chiral host. Single binding site.
(2) Class 1B: Chiral guest / non-chiral host. Single binding site.
(3) Class 1C: Chiral guest / chiral host. Single binding site.

For the purposes of CD certain criteria have to be fulfilled. The guest must possess an "accessible ordinary electronic absorption" (*Drake, 2001*). Both the guest and the host may possess a CD in the free solution, the host CD being detected at the chosen detection wavelength. Chirality must exist between the associations of the guest/host pairing that is detectable at the designated detection wavelength; this gives rise to four possibilities (*Drake, 2001, and Strat, 1998*). In this thesis, any CD due to a host (albumin) is considered to be unaffected by ligand binding. Accordingly, only classes 1A and 1B are considered explicitly.

Case 1A

Consider the simplest case where there is a 1:1 binding relationship,

Free guest shows no CD signal at guest based detection wavelength.

Free host shows no CD signal at the detection wavelength.

The bound guest (the complex) shows a CD signal at the guest detection wavelength.

If H_T is the total host concentration, G_T is the total guest concentration, at equilibrium the free host concentration (protein) is H_f and the free guest concentration (ligand) is G_f. The complex concentration HG can be determined from the following expression,

$$H_f + G_f \rightleftharpoons HG$$

with $$H_T = H_f + HG \quad (49)$$

and $$G_T = G_f + HG \quad (50)$$

From equations (49) and (50) the association constant 'K_a' can be determined and calculated as,

$$K_a = \frac{HG}{H_f . G_f} \quad (51)$$

The detectable CD signal is produced from the induced signal upon binding of the guest to the host and is detected at the guest detection wavelength, therefore,

$$\Delta A_{calc} = \Delta A_{HG} = l.\ \Delta\varepsilon_{HG}.\ HG \tag{52}$$

where ΔA_{calc} is the calculated differential absorbance, $\Delta\varepsilon_{HG}$ is the differential extinction coefficient of the complex detected at the guest wavelength and *l* is the pathlength. For the purpose of CD, the concentration of the guest (ligand) is kept constant and the host concentration (protein) is varied until the entire guest concentration encounters the host (i.e. excess host). The extent of binding ($\bar{i}$) is the average number of guest molecules bound per molecule of host and can be expressed as,

$$\bar{i} = \frac{G_T - G_f}{H_T} = \frac{[\sum(G\ bound\ to\ H)]}{[\sum(all\ H)]} \tag{53}$$

Equation (53) can be rearrange to give,

$$\bar{i} = \frac{HG}{H_T} = \frac{K.G_f.H_f}{H_f + K.G_f.H_f} = \frac{K.G_f}{1 + K.G_f} \tag{54}$$

$\bar{i}$ is a measure of the extent of binding and is dependent on the total host concentration (note, when H_T is the independent variable, the extent of binding is now given by the expression $\bar{j} = HG / G_t$ and is dependent on the bound guest molecules complex). Equation (53) can be rewritten in terms of the independent ($x = G_f$) and dependent ($y = \bar{i}$) variables to give equation (55).

$$y = \frac{p.x}{q + r.x} \tag{55}$$

p, q and r are constant where p=K, q=1 and r=k. Equation (6) can be expressed in terms of reciprocals to give,

$$\frac{1}{\bar{i}} = \frac{1}{nK}\frac{1}{G_f} + \frac{1}{n} \tag{56}$$

Note this expression is the same as that determined in the classical analysis shown in equation (11). The same graphical plots (Scatchard plot, Hill plot etc.) can be represented here; the quantities H_f, G_f, HG and ε_{HG} are unknown from equations (49), (50), (51) and (52), with H_T and G_T known, these quantities can also be expressed by the following equations:

$$H_f = H_T - HG \tag{57}$$

$$G_f = G_T - HG \tag{58}$$

$$HG = K \,.\, H_f \; G_f \tag{59}$$

Substituting equations (57) and (58) into equation (59) will give two possible expressions for the theoretical differential absorbance:

$$HG_1\ (H_T) = \frac{K.H_T + K.G_T + 1 - \sqrt{(K.H_T + K.G_T + 1)^2 - 4K^2.H_T.G_T}}{2K} \tag{60}$$

$$HG_2\ (H_T) = \frac{K.H_T + K.G_T + 1 + \sqrt{(K.H_T + K.G_T + 1)^2 - 4K^2.H_T.G_T}}{2K} \tag{61}$$

Where HG_1 is the complex formed from the theoretically negative contributions of the quadratic expression, and HG_2 is the complex formed from the theoretically positive contributions of the quadratic expression. Substituting equations (60) and (61) into equation (52) will give:

$$\Delta A_{calc1} = \Delta\varepsilon_{HG}.HG_1 \tag{62}$$

$$\Delta A_{calc2} = \Delta\varepsilon_{HG}.HG_2 \tag{63}$$

Now if equations (60) and (61) are both used in the formulae then two possible expressions for the theoretical CD will be obtained:

$$\Delta A_{calc1}\left(H_T\right) = \Delta\varepsilon_{HG}.\frac{K.H_T + K.G_T + 1 - \sqrt{(K.H_T + K.G_T + 1)^2 - 4K^2.H_T.G_T}}{2K} \tag{64}$$

$$\Delta A_{calc2}\left(H_T\right) = \Delta\varepsilon_{HG}.\frac{K.H_T + K.G_T + 1 + \sqrt{(K.H_T + K.G_T + 1)^2 - 4K^2.H_T.G_T}}{2K} \tag{65}$$

Only $\Delta A_{calc1}(H_T)$ gives the realistic solution. In these and future equations ΔA refers to the CD that would be observed in a 1cm pathlength cuvette. An example of Case 1A binding is represented in the binding of diazepam to HSA. The mathematical function that represents the realistic expression of the experimental data is seen in $\Delta A_{calc1}(H_T)$.

Case 1A'

Free guest shows no CD signal at guest based detection wavelength.

Free host shows a CD signal at detection wavelength.

The bound guest (the complex) shows a CD signal at guest based detection wavelength.

Keeping the concentration of the guest constant while varying the concentration of the host and using the same nomenclature, at equilibrium,

$$H_T = H_f + HG \tag{66}$$

$$G_T = G_f + HG \tag{67}$$

The association constant is given by the expression,

$$K = \frac{HG}{H_f . G_f} \tag{68}$$

Adopting the same principals as for Case 1A, the induced (theoretical) CD signal of the bound guest is given by,

$$\Delta A_{calc} = \Delta A_{HG} + \Delta A_{Hf}$$

$$\Delta A_{calc} = \varepsilon_{HG}.HG + \varepsilon_H.H_f$$

$$\Delta A_{calc} = (\varepsilon_{HG} - \varepsilon_H).HG + \Delta\varepsilon_H.H_T \tag{69}$$

Ideally $\Delta\varepsilon_{HG}$ can be determined directly (experimentally) and represents the molar CD of the complex (HG) detected at the guest detection wavelength; $\Delta\varepsilon_H$ is the molecular CD of the host alone (free). The resulting complex concentration is determined by the same expressions used in the previous case and gives two possible solutions for ΔA_{calc},

$$\Delta A_{calc1} = \left(\varepsilon_{HG} - \varepsilon_{H}\right).HG_1 + \varepsilon_{H}.H_T \tag{70}$$

$$\Delta A_{calc2} = \left(\varepsilon_{HG} + \varepsilon_{H}\right).HG_2 + \varepsilon_{H}.H_T \tag{71}$$

Again $\Delta A_{calc1}\left(H_T\right)$ is the realistic mathematical function that represents the experimental data.

Case 1B

Free guest shows a CD signal at guest based detection wavelength.

Free host shows no CD signal at detection wavelength.

The bound guest (complex) shows a CD signal at guest based detection wavelength.

Under these conditions, the free chiral guest (ligand) is modified on binding will also generates the optical activity. The modified CD associated with the guest is now altered according to equation (65),

$$\Delta A_{calc} = \Delta A_{HG} + \Delta A_{Gf}$$

$$\Delta A_{calc} = \varepsilon_{HG}.HG + \varepsilon_{G}.G_f$$

$$\Delta A_{calc} = \left(\varepsilon_{HG} - \varepsilon_{G}\right).HG + \varepsilon_{G}.G_f \tag{72}$$

Again ε_{HG}, the molar CD of the complex detected at the guest based detection wavelength has to be determined; $\Delta\varepsilon_G$ is known. The complex concentration is determined and the calculation of the theoretical CD gives two possible solutions when equations (61) & (62) are substituted into equation (72) that gives:

$$\Delta A_{calc1} = \left(\varepsilon_{HG} - \varepsilon_{G}\right).\frac{K.H_T + K.G_T + 1 - \sqrt{(K.H_T + K.G_T + 1)^2 - 4K^2.H_T.G_T}}{2K} + \varepsilon_{G}.G_T \tag{73}$$

$$\Delta A_{calc2} = \left(\varepsilon_{HG} - \varepsilon_{G}\right).\frac{K.H_T + K.G_T + 1 + \sqrt{(K.H_T + K.G_T + 1)^2 - 4K^2.H_T.G_T}}{2K} + \varepsilon_{G}.G_T \tag{74}$$

This case is represented by the titration of (+)-S-Ibuprofen binding to cyclodextrin or the binding of Cu^{2+} (a non-chiral host) binding to peptides (acting in this case as the chiral guest).

$\Delta A_{calc1}\left(H_T\right)$ is the realistic solution.

Case 1C

Free guest shows a CD signal at guest base detection wavelength.

Free host shows a CD signal at detection wavelength.

The bound guest (the complex) shows a CD signal at guest detection wavelength.

This is characterised by the existence of both the guest and host having detectable CD signals at the detection wavelength together with the complex. Here the relationship of the bound complex will be given by:

$$\Delta A_{calc} = \Delta A_{HG} + \Delta A_{Gf} + \Delta A_{Hf}$$

$$\Delta A_{calc} = \varepsilon_{HG}.HG + \varepsilon_G.G_f + \varepsilon_H.H_f$$

$$\Delta A_{calc} = \left(\varepsilon_{HG} - \varepsilon_G - \varepsilon_H\right).HG + \varepsilon_G.G_T + \varepsilon_H.H_T \qquad (75)$$

ε_{HG} is unknown and has to be determined with detection based at the guest detection wavelength. The molecular CD of the guest, $\Delta\varepsilon_G$, is known together with the molecular CD of the host alone, $\Delta\varepsilon_H$. Once again, two possible solutions for the theoretical CD are found if equations (61) & (62) are substituted into equation (75):

$$\Delta A_{calc1} = \left(\varepsilon_{HG} - \varepsilon_G - \varepsilon_H\right).HG_1 + \varepsilon_G.G_T + \varepsilon_H.H_T \qquad (76)$$

$$\Delta A_{calc2} = \left(\varepsilon_{HG} - \varepsilon_G - \varepsilon_H\right).HG_2 + \varepsilon_G.G_T + \varepsilon_H.H_T \qquad (77)$$

Where HG_1 is the complex formed from the theoretically negative contributions of the quadratic expression, and HG_2 is the complex formed from the theoretically positive contributions of the quadratic expression. $\Delta A_{calc1}\left(H_T\right)$ is the realistic expression of the experimental data. An example of this case is in the dimerisation processes of chiral molecules where the monomer acts as both the guest and the host.

Although the treatment of the data for all four cases was fitted in terms of CD, this method can be adopted for other techniques. The assignments of the guest and host terms are interchangeable provided that the correct mathematical treatment is conducted. If the experiments were conducted such that the host concentration (protein) is now kept constant and the guest concentration (ligand) varied then the four expressions for ΔA_{calc} would not be affected and would remain the same.

When fitting the expressions, two unknown parameters exists which are the molar CD of the bound complex ($\Delta \varepsilon_{HG}$) that is associated with the bound complex and the equilibrium constant (K). $\Delta \varepsilon_{HG}$ can be determined from the limiting value of ΔA_{obs} (ΔA_{lim}), obtained by titrating a fixed guest (ligand) concentration to a variable concentration of host. From this 'K' can be determined using CD. Values of 'K' that are detectable by this method are in the region of 10^3 to 10^6 M^{-1}. There is some ambiguity that may exist in CD where there is an overlap of the guest and host signals, this usually occurs for wavelengths less than 290nm and for this reason studies below this wavelength should be avoided or investigated under very defined conditions. An example of this case can be seen in Cu^{++} binding to a peptide. Cu^{++} absorbs at 600 – 800nm, however to monitor the titration at this wavelength large quantities of copper and peptide will be required and the transitions are weak. In order to overcome this problem the titration is conducted at a wavelength of around 230nm which will require much smaller quantities. At this wavelength there is a reversal of roles in that the Cu^{++} is treated as the host keeping its concentration variable while the peptide is treated as the guest at fixed concentration. Although the spectral changes at this wavelength are complex in terms of the CD, only the guest (peptide) and the complex (Cu^{++}/peptide) will have a CD in this region, all else will be invisible as in the case of IB.

2.6.ii.(a) Binding of Ligands to Two Sites on a Protein

When dealing with proteins there is always the possibility that more than one binding site exists for the same ligand (e.g. aspirin). If there are two binding sites present then these can be classified in the following way,

Class 2A: Non-chiral guest / Chiral host – two binding sites.

Class 2B: Chiral guest / Non-chiral host – two binding sites.

Class 2C: Chiral guest / Chiral host – two binding sites.

Four possible cases can be highlighted in terms of analysing the data, these are:

Case IIA: - Free guest shows no CD signal at guest base detection wavelength.
- Free host shows no CD at the detection wavelength.
- The bound guest (complex) shows a CD at the guest detection wavelength.

Case IIA': - Free guest shows no CD signal at guest based detection wavelength.
- Free host shows a CD signal at the detection wavelength.
- The bound guest (complex) shows a CD signal at the guest based detection wavelength.

Case IIB: - Free guest shows a CD at the guest based detection wavelength.
- Free host shows no CD signal at the detection wavelength.
- The bound guest (complex) shows a CD signal at the guest based detection wavelength.

Case IIC: - Free guest shows a CD at the guest based detection wavelength.
- Free host shows a CD signal at the detection wavelength.
- The bound guest (complex) shows a CD signal at the guest based detection wavelength.

Case IIA

Adopting the same format by keeping the guest concentration fixed and varying the host concentration (protein), as the host is added the guest will see two possible binding sites that it can bind to (site 1 or 2). There will be an association constant associated with both sites, and if one site binds more strongly, then there will be four possible association constants, K_{1s}, K_{1w}, K_{2s} and K_{2w}.

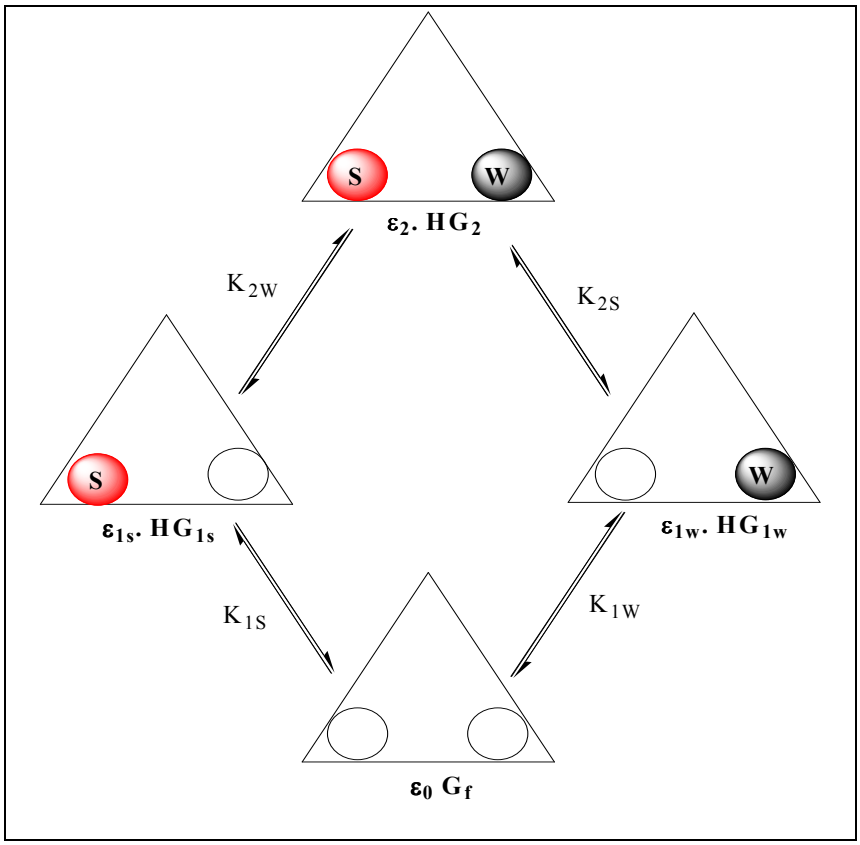

Figure 2.12. Schematic Representation of the Binding of a Ligand to Two possible Sites.

Where K_{1s} is the binding constant for the guest at the first binding site (1), with 's' denoting the strong site. K_{1w} is the binding of the guest to the second site (2) with site (1) being vacant, 'w' denoting the weak interaction. K_{2s} represent the binding of the guest to the second site (2) with site (1) occupied. K_{2w} is the binding of the first site (1) with site (2) filled (Figure 2.12). Three assumptions are made. The first is that there are two binding sites which are independent. Further, the guest is in the form of an un-associated monomer.

The last assumption is that there is independent binding at the two sites where $K_{1s} = K_{2s}$ and $K_{1w} = K_{2w}$. If we define the following quantities as:

H_T = the total concentration of the Host.

G_T = the total concentration of the Guest.

H_f = the concentration of the free (unbound) Host.

G_f = the concentration of the free (unbound) Guest.

HG_{1s} = the concentration of the first complex – binding constant K_{1s}.

HG_{1w} = the concentration of the second complex – binding constant K_{1w}.

HG_{2w} = the concentration of the third complex – binding constant K_{2w}.

HG_{2s} = the concentration of the forth complex – binding constant K_{2s}.

Thus, binding can be represented as:

$$H + G \xleftrightarrow{K_{1s}} HG_{1s}$$

$$H + G \xleftrightarrow{K_{1w}} HG_{1w}$$

$$HG_{1s} + G \xleftrightarrow{K_{2w}} HG_{2w}$$

$$HG_{1w} + G \xleftrightarrow{K_{2s}} HG_{2s}$$

The binding constants can be given by:

$$K_{1s} = \frac{HG_{1s}}{H_f.G_f} \tag{78}$$

$$K_{1w} = \frac{HG_{1w}}{H_f.G_f} \tag{79}$$

$$K_{2w} = \frac{HG_{2w}}{HG_{1s}.G_f} = \frac{HG_{2w}}{K_{1s}.H_f.G_f^2} \tag{80}$$

$$K_{2s} = \frac{HG_{2s}}{HG_{1w}.G_f} = \frac{HG_{2s}}{K_{1w}.H_f.G_f^2} \tag{81}$$

Binding is dependent upon two unknown concentrations, H_f and G_f that refers to the free Host and Guest concentrations respectively, and are given by the expressions:

$$H_T = H_f + HG_{1s} + HG_{1w} + HG_{2w} + HG_{2S}$$

$$G_T = G_f + HG_{1s} + HG_{1w} + 2HG_{2w} + 2HG_{2S} \tag{82}$$

Substitution of the complex concentration as defined in equations (78) to (81) into equation (82) gives equation (83).

Where,

$$\begin{aligned} H_T &= H_f + K_{1s}.H_f.G_f + K_{1w}.H_f.G_f + K_{1s}.K_{2w}.H_f.G_f^2 + K_{1w}.K_{2s}.H_f.G_f^2 \\ G_T &= G_f + K_{1s}.H_f.G_f + K_{1w}.H_f.G_f + 2.K_{1s}.K_{2w}.H_f.G_f^2 + 2.K_{1w}.K_{2s}.H_f.G_f^2 \end{aligned} \tag{83}$$

And

$$\begin{aligned} H_f.\left(1 + K_{1s}.G_f + K_{1w}.G_f + K_{1s}.K_{2w}.G_f^2 + K_{1w}.K_{2s}.G_f^2\right) - H_T &= 0 \\ G_f^2.\left(2 + K_{1s}K_{2w}.H_f + 2.K_{1w}.K_{2s}.H_f\right) + G_f.\left(1 + K_{1s}.H_f + K_{1w}.H_f\right) - G_T &= 0 \end{aligned} \tag{84}$$

By defining additional functions where,

$$C_1 = K_{1s}.K_{2w} + K_{1w}.K_{2w} \tag{85}$$

$$C_2(H_T) = (2.H_T - G_T).C_1 + K_{1s}K_{1w} \tag{86}$$

$$C_3(H_T) = K_{1s}K_{1w}.(H_T - G_T) + 1 \tag{87}$$

And,

$$E_1(H_T) = \frac{1}{6}.\frac{C_3(H_T)}{C_1^2}.C_2(H_T) + \frac{1}{2}.\frac{G_T}{C_1} - \frac{1}{27}.\frac{C_2(H_T)^3}{C_1^3} \tag{88}$$

$$E_2(H_T) = \frac{1}{18}.\sqrt{4.C_3(H_T)^3 - C_3(H_T)^2.C_2(H_T)^2 + 18.C_3(H_T).C_2(H_T).C_1.G_T + 27.G_T^2.C_1^2 - 4.G_T.C_2(H_T)^3}.\frac{\sqrt{3}}{C_1^2} \tag{89}$$

$$E_3(H_T) = \left[E_1(H_T) + E_2(H_T)\right]^{\frac{1}{3}} \tag{90}$$

$$E_4(H_T) = \frac{1}{3}.\frac{C_3(H_T)}{C_1} - \frac{1}{9}.\frac{C_2(H_T)^2}{C_1^2} \tag{91}$$

From equation (84), the free Guest and Host concentration can be determined respectively.

$$G_f\left(H_T\right)=E_3\left(H_T\right)-\frac{E_4\left(H_T\right)}{E_3\left(H_T\right)}-\frac{C_2\left(H_T\right)}{3.C_1} \tag{92}$$

$$H_f\left(H_T\right)=\frac{H_T}{1+K_{1s}.G_f\left(H_T\right)+K_{1w}.G_f\left(H_T\right)+K_{1s}.K_{2w}.G_f\left(H_T\right)^2+K_{1w}.K_{2s}\ .G_f\left(H_T\right)^2} \tag{93}$$

The induced CD signal (theoretical) that is derived from the bound guest is,

$$\Delta A_{calc} = \Delta A_{1s} + \Delta A_{1w} + \Delta A_{2s} + \Delta A_{2w} \tag{94}$$

where ΔA_{1s} is the CD associated with the [1:1] complex of the guest bound to the strong site. ΔA_{1w} is the CD associated with the [1:1] complex of the guest with the weak site. ΔA_{2s} is the CD of the [2:1] complex of the guest with the strong site, the weak site is filled, and ΔA_{2w} is the CD of the [2:1] complex of the guest with the weak site, the strong filled.

Expression (94) can be rewritten to give,

$$\Delta A_{calc}=\varepsilon_{1s}\ .HG_{1s}+\varepsilon_{1w}\ .HG_{1w}+\varepsilon_{2w}\ .HG_{2w}+\varepsilon_{2s}\ .HG_{2s} \tag{95}$$

Equation (84) can now be written to incorporate the expressions of equation (78) – (81) to give,

$$\Delta A_{calc}=\varepsilon_{1s}.K_{1s}.H_f.G_f+\varepsilon_{1w}\ .K_{1w}.H_f.G_f+\varepsilon_2\ .K_{2w}.K_{1s}\,H_f.G_f^2+\varepsilon_2\ .K_{2s}.K_{1w}H_f.G_f^2 \tag{96}$$

Where,

ε_{1s} = Molecular CD of the 1:1 Guest:Host complex formed to the strong site (strong binding constant).

ε_{1w} = Molecular CD of the 1:1 Guest:Host complex to the weaker sites (weaker binding constant).

ε_2 = Molecular CD of 2:1 Guest:Host complex with the binding of the Guest to both binding sites of the Host.

A better representation of the theoretical CD signal is shown in equation (97),

$$\Delta A_{calc}(H_T) =$$

$$H_T.G_f(H_T).\frac{\varepsilon_{1s}.K_{1s} + \Delta\varepsilon_{1w}.K_{1w} + G_f(H_T).\ \varepsilon_2\ K_{1s}\ K_{2w} + G_f\left(H_T\right)\ \varepsilon_2\ K_{1w}\ K_{2s}}{1+G_f\left(H_T\right).C_2\left(H_T\right)-2\,G_f\left(H_T\right)C_1.H_T+G_f.\left(H_T\right).C_1.G_T + C_1.G_f.\left(H_T\right)^2} \quad (97)$$

Case IIA':

- Free guest shows no CD signal at the guest based detection wavelength.
- Free host shows a CD signal at the detection wavelength.
- The bound guest (complex) shows a CD signal at guest based detection wavelength.

On binding of the Guest to the Host, an induced CD signal is observed at the detection wavelength and is defined as:

$$\Delta A_{calc} = \Delta A_{1s} + \Delta A_{1w} + \Delta A_{2s} + \Delta A_{2w} + \Delta A_{H_f} \quad (98)$$

ΔA_{1s} is the CD of the [1:1] complex of the guest binding to the strong host binding site.

ΔA_{1w} is the CD of the [1:1] complex of the guest binding to the weak site.

ΔA_{2s} is the CD of the [2:1] complex formed from the guest binding to the strong site, the weak site is occupied.

ΔA_{2w} is the CD of the [2:1] complex of the guest binding to the weak site, the strong site is occupied

ΔA_{H_f} the CD of the free host.

Equation (98) can be rewritten in terms of the extinction coefficients and concentrations to give:

$$\Delta A_{calc} = \varepsilon_{1s}\ .\ HG_{1s} + \varepsilon_{1w}.HG_{1w} + \varepsilon_{2w}\ .\ HG_{2w} + \varepsilon_{2s}.HG_{2s} + \varepsilon_H.H_f \quad (99)$$

Where,

$\Delta\varepsilon_{1s}$ is the molar CD of the first complex with the stronger binding constant at the guest based detection wavelength (has to be determined).

$\Delta\varepsilon_{1w}$ is the molar CD of the second complex with the weaker binding constant at the guest based detection wavelength (has to be determined).

$\Delta\varepsilon_{2}$ is the molar CD of the third complex (both sites filled) at the guest detection wavelength (has to be determined).

$\Delta\varepsilon_{H}$ is the molecular CD of the free Host (its value known).

Now equation (95) becomes,

$$\Delta A_{calc} = \varepsilon_{1s}.HG_{1S} + \varepsilon_{1w}.HG_{1w} + \varepsilon_{2w}.HG_{2w} + \varepsilon_{2s}.HG_{2S} + \varepsilon_{H}.H_{f} \qquad (100)$$

The determination of the free Host H_f is given by equation (93). The theoretical CD can be calculated from the substitution of the concentrations in expression (96) to give:

$$A_{calc} = H_T.G_f(H_T).\frac{\varepsilon_{1s}.K_{1s} + \varepsilon_{1w}.K_{1w} + G_f(H_T).\varepsilon_2.K_{1s}.K_{2w} + G_f(H_T).\varepsilon_2.K_{1w}.K_{2s}}{1 + G_f(H_T).C_2(H_T) - 2.G_f(H_T).C_1.H_T + G_f(H_T).C_1 G_T + C_1 G_f(H_T)^2} + \varepsilon_H.\frac{H_T}{1 + K_{1S}.G_f(H_T) + K_{1W}.G_f(H_T) + K_{1s} K_{2w} G_f(H_T)^2 + K_{1w} K_{2s} G_f(H_T)^2} \qquad (101)$$

Case IIB

- Free guest shows a CD at the guest based detection wavelength.
- Free host shows no CD signal at the detection wavelength.
- The bound guest (complex) shows a CD signal at guest based detection wavelength.

The calculated CD of the complex will give an expression of:

$$\Delta A_{calc} = \Delta A_{1s} + \Delta A_{1w} + \Delta A_{2s} + \Delta A_{2w} + \Delta A_{G_f} \qquad (102)$$

where ΔA_{G_f} is the CD of the free Guest at the Guest detection wavelength. Thus, the molecular CD(ε_G) of the Guest only (its value known) will be given by the revised expression of equation (102) that becomes:

$$\Delta A_{calc} = \varepsilon_{1s} \,.\, HG_{1s} + \varepsilon_{1w} . HG_{1w} + \varepsilon_{2s} \,.\, HG_{2s} + \varepsilon_{2w} . HG_{2w} + \varepsilon_G . G_f \qquad (103)$$

Therefore, G_f will be determined by the expression derived in equation (92) that gave,

$$G_f(H_T) = E_3(H_T) - \frac{E_4(H_T)}{E_3(H_T)} - \frac{C_2(H_T)}{3.C_1} \qquad (92)$$

The calculated CD will now be expressed as:

$$\Delta A_{calc}(H_T) = H_T . G_f(H_T) \frac{\varepsilon_{1s} . K_{1s} + \varepsilon_{1w} . K_{1w} + G_f(H_T) . \varepsilon_2 . K_{1s} . K_{2w} + G_f(H_T) . \varepsilon_2 . K_{1w} . K_{2s}}{1 + G_f(H_T) . C_2(H_T) - 2 . G_f(H_T) . C_1 . H_T + G_f(H_T) . C_1 G_T + C_1 \, G_f(H_T)^2} + \varepsilon_G . \left[E_3(H_T) - \frac{E_4(H_T)}{E_3(H_T)} - \frac{C_2(H_T)}{3.C_1} \right] \qquad (104)$$

Case IIC:

- Free guest shows a CD at the guest based detection wavelength.
- Free host shows a CD signal at the detection wavelength
- The bound guest (complex) shows a CD signal guest based detection wavelength.

Considering the bound complex then the calculated CD will be given by:

$$\Delta A_{calc} = \Delta A_{1s} + \Delta A_{1w} + \Delta A_{2s} + \Delta A_{2w} + \Delta A_{G_f} + \Delta A_{H_f} \qquad (105)$$

where ΔA_{G_f} is the CD of the free Guest detected at the Guest based detection wavelength. ΔA_{H_f} is the CD detected for the free Host. If $\Delta\varepsilon_G$ and $\Delta\varepsilon_H$ are the molecular CD's of the free Guest only and the Host only respectively and are both known, then the calculated CD now becomes:

$$\Delta A_{calc} = \varepsilon_{1s} \,.\, HG_{1s} + \varepsilon_{1w} . HG_{1w} + \varepsilon_{2w} \,.\, HG_{2w} + \varepsilon_{2s} . HG_{2s} + \varepsilon_G . G_f + \varepsilon_H . H_f \qquad (106)$$

The free Host and Guest concentrations can be derived from equations (93) & (92) respectively.

2.6.ii.(b) Cooperativity of Binding Sites

Positive and negative cooperativity can exist, the former bringing about an enhancement in the observed binding and the latter leading to an decrease. A Host with 'y' binding sites, all exhibiting independent binding activity will, on interaction with the Guest, bind 'x' molecules to give a binding constant K_{1x} where :

K_{1x} = K . (Number of empty sites on $HG_{(x-1)}$ / (Number of occupied sites on HG_x)

$$K_{1x} = \frac{y-(x-1)}{x} \,.\, K = \frac{y-x+1}{x} \,.\, K \qquad (107)$$

where K is the binding constant at each site. Therefore at the $(x+1)^{th}$ site :

$$K_{1(x+1)} = \frac{y-(x+1-1)}{x+1} \,.\, K = \frac{y-x}{x+1} \,.\, K \qquad (108)$$

Taking the ratio of equation (107) to (108) gives :

$$\frac{K_{1(x+1)}}{K_{1x}} = \frac{(y-1)\,.\,x}{(x+1)\,.\,(y-x+1)} \qquad (109)$$

Positive cooperativity exists when the ratio calculated in equation (109) i.e. $\left(\frac{K_{1(x+1)}}{K_{1x}}\right)$ is greater than the calculated value of $\frac{(y-x)\,.\,x}{(x+1)\,.\,(y-x+1)}$. Negative cooperativity is the reverse situation of positive cooperativity in that the ratio is less than the calculated value. In the situation of non-cooperativity both the ratio and the calculated value are the same.

When two binding sites are present, with one site binding strongly and the other weakly, then according to equations (78) and (79) the overall binding constant in the first instance will be :

$$K_{11} = K_{1s} + K_{1w} \tag{110}$$

with $$HG = HG_{1s} + HG_{1w} \tag{111}$$

The binding constants associated with the second site as expressed in equations (80) and (81) will now give an overall expression of:

$$HG_2 = HG_{2s} + HG_{2w} \tag{112}$$

Substituting equations (73) and (74) in equation (112) gives :

$$HG_2 = (K_{2w} \,.\, K_{1s} + K_{2s} \,.\, K_{1w}) \,.\, H_f \,.\, G_f^2 \tag{113}$$

Also the substitution of equations (64) and (65) in equation (91) will give:

$$HG = (K_{1s} + K_{1w}) \,.\, H_f \,.\, G_f \tag{114}$$

Using equations (93) and (94) binding at the second site can be represented as:

$$K_{12} = \frac{K_{2w} \,.\, K_{1s} + K_{2s} \,.\, K_{1w}}{K_{1s} + K_{1w}} \tag{115}$$

Therefore, cooperativity can now be defined as:

$$\frac{K_{12}}{K_{11}} = \frac{K_{2w} \,.\, K_{1s} + K_{2s} \,.\, K_{1w}}{\left(K_{1s} + K_{1w}\right)^2} \tag{116}$$

All binding constants can be obtained from fitting routines.

2.6.ii.(c) Competitive Binding of Two different Guest to a Single Host Site

When two different types of guest molecules exist in solution (Guest A and Guest B) with a host containing one binding site for both guests, there will exist competition at that binding site. The degree of binding for each guest molecule will be dependent upon the binding constants of each, the guest molecule with the highest binding constant will bind in preference to the other molecule so will form the largest amount of complex. However, there will exist a dynamic equilibrium between all the molecules in proportion to their binding constants given by:

$$H_f + G_{fA} + G_{fB} \rightleftarrows HG_A + HG_B \quad (117)$$

Where H_f is the concentration of the free host, G_{fA} is the concentration of the free guest A, G_{fB} is the concentration of the free guest B, HG_A is the concentration of the complex between the host and guest A and HG_B is the concentration of the complex between the host and guest B. In terms of the total host concentration H_T :

$$H_T = H_f + HG_A + HG_B \quad (118)$$

And $$G_{TA} = G_{fA} + HG_A \quad (119)$$

$$G_{TB} = G_{fB} + HG_B \quad (120)$$

Where G_{TA} and G_{TB} are the total concentrations of guest A and B respectively. The binding constant (K_A and K_B) for each complex will be:

$$K_A = \frac{HG_A}{H_f \,.\, G_{fA}} \quad (121)$$

$$K_B = \frac{HG_B}{H_f \,.\, G_{fB}} \quad (122)$$

In this equilibrium there will be five unknowns: H_f, G_{fA}, G_{fB}, K_A and K_B. If the concentrations of both guest molecules are kept constant with a varying concentration of total host, then the concentration of total guest A, total guest B and the total host concentrations can be determined experimentally. For both species the amount of free guest will be:

$$G_{fA} = \frac{G_{TA}}{1 + K_A . H_f (H_T)} \quad (123)$$

$$G_{fB} = \frac{G_{TB}}{1 + K_B . H_f (H_T)} \quad (124)$$

In terms of the amount of complex formed for both ligands the following expressions will apply:

$$HG_A\left(H_T\right) = K_A.H_f\left(H_T\right)\frac{G_{TA}}{1 + K_A.H_f\left(H_T\right)} \quad (125)$$

$$HG_B\left(H_T\right) = K_B.H_f\left(H_T\right)\frac{G_{TB}}{1 + K_B.H_f\left(H_T\right)} \quad (126)$$

The resulting mixture will contain five species all contributing to the final CD signal at the detection wavelength, these are the free Guests, free Host, and that due to the bound complexes formed from the two ligands. The observed CD will be given by:

$$\Delta A_{calc} = \Delta A_{HG_A} + \Delta A_{HG_B} + \Delta A_{G_{fA}} + \Delta A_{G_{fB}} + \Delta A_{H_f} \quad (127)$$

Therefore:

$$\Delta A_{calc}\left(H_T\right) = \Delta\varepsilon_{HG_A}.HG_A\left(H_T\right) + \Delta\varepsilon_{HG_B}.HG_B\left(H_T\right) + \Delta\varepsilon_{G_A}.G_{f_A}\left(H_T\right) + \Delta\varepsilon_{G_B}.G_{f_B}\left(H_T\right) + \Delta\varepsilon_H.H_f\left(H_T\right) \quad (128)$$

The equilibrium constant for both of the complexes has to be calculated separately from independent experiments.

CHAPTER 3

CHAPTER 3: Spectroscopy

3.1. Introduction

In the wave theory, light is considered as an oscillating electric field. Associated with any electric field, there is a transverse magnetic field Figure 3.0.

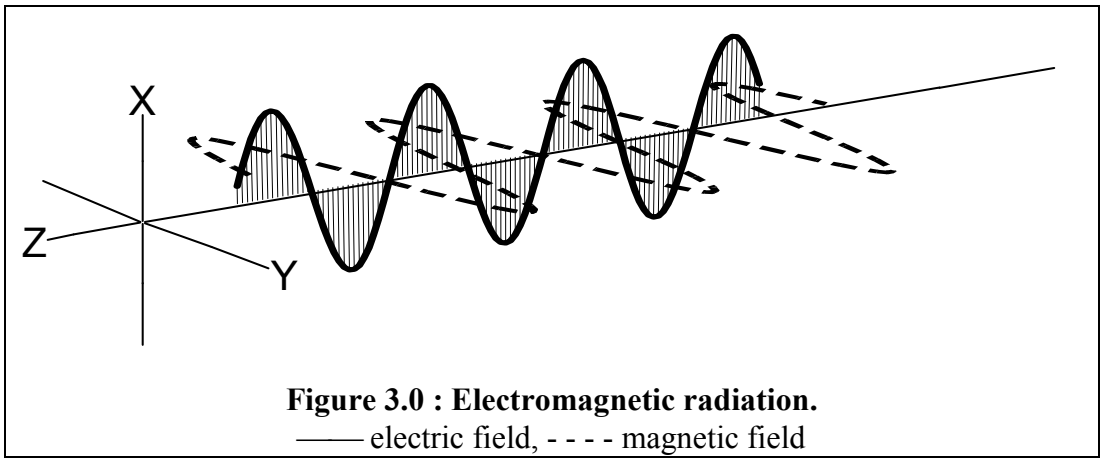

Figure 3.0 : Electromagnetic radiation.
—— electric field, - - - - magnetic field

Oscillating electric and magnetic fields are consequences of each other. As interactions are with molecules usually involving charged particles (eg electrons), only the electric field is explicitly considered. The electric field is illustrated in Figure 3 2. along with the 5 main properties of a light beam.

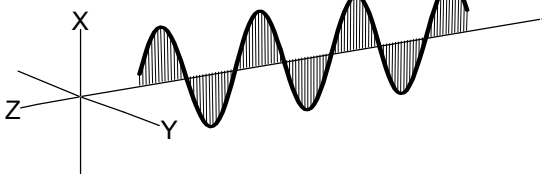

1.	Wavelength	Energy, (E=hc/λ)
2.	Intensity	Extinction coefficient, (A=ε.c.l)
3.	Velocity	Refractive index, (n=c/ν)
4.	Polarisation	Circular, elliptical, linear
5.	Propagation direction	Light scattering, reflection, emission

Figure 3.1 : The oscillating electric field of light and its properties.

3.1.i. The wavelength and energy of light

According to the Planck equation, the energy associated with a light beam is given by :

$$E = h\,\nu = \frac{h\,c}{\lambda} \qquad (1)$$

where E represents the energy, *h* is Planck's constant, ν is the frequency of the absorbed

radiation, c is the velocity and λ is the wavelength of light . Equation (1) indicates that the shorter wavelengths give rise to higher energy and vice versa, longer wavelengths possess less energy. This thesis is concerned with UV light (180-400nm) and visible light (400-750nm), which has enough energy to excite electrons albeit at the same time associated vibration and rotational motions are also excited, to give a spectroscopic features width. Nevertheless, only loosely held electrons are excited in this wavelength range. Such electrons are found in localised regions of a molecule called the chromophore.

3.1.ii. The absorption of light

The ability to absorb light is quantified in Beer's law for a sample of thickness "*l*",

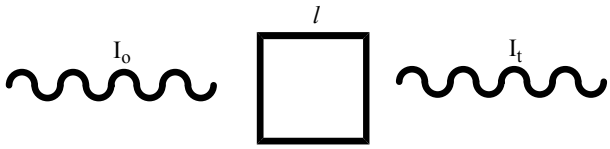

The relationship between the incident beam I_o and the transmitted beam I_t is defined as the absorbance,

$$A = \log\left(\frac{I_o}{I_t}\right) \tag{2}$$

Beer's law relates absorbance to concentration and pathlength in an expression shown as,

$$A = \varepsilon . c . l \tag{3}$$

where, c is the concentration in moles/litre and *l* is the pathlength in centimetres. The extinction coefficient "ε" is effectively a proportionality constant that quantifies how strongly a particular transition will absorb light. The larger the value of ε the greater will be the probability of absorption. Even if light of the right wavelength (energy) is available it may or may not be strongly absorbed if ε is not of the right order of magnitude (*Drake, 1994*). Table 3.1 gives values for the extinction coefficients. The conditions for absorption are quite specific in that, for an allowed absorption ε has to be at least equal to or greater than 10,000 and the electric dipole moments must be greater than zero, since $D = \mu^2$, where

D represents the dipole strength and is the area under an absorption curve. When the value of $\mu = 0$, then ε is very small, of the order of 100, and the transition will be forbidden. It is important to note that it is the electric dipole moment that will determine the value of the extinction coefficient that will in turn indicates whether absorptions are forbidden or allowed (Dr. *A. F. Drake, unpublished*).

Extinction Coefficient 'ε'	Absorption 'A'
<10	Very weak absorption
100 - 1000	Weak absorption (Forbidden)
≈10,000	Strong absorption (Allowed)
≈50,000	Very strong absorption (Allowed)
Table 3.1. Conditions in ε for absorption.	

3.2. Characteristic Electronic transitions in Organic Molecules

As light is absorbed, a charge displacement ensues that produces a transition electric dipole moment "μ". If a molecule contains a single C=C double bond then the resulting electronic charge displacement will produce a π-π* transition at ~200 nm. If more than one double bond exists within the molecule as in the case of conjugated organic molecules, conjugation will lead to electron delocalisation and the electronic transition will be shifted to lower energy (longer wavelengths). In molecules that contain less than a conjugation of 8 double bond, the solutions appear colourless to the human eye as absorption takes place in the UV region. Successive addition of a double bond after 8 produces a shift in the absorption wavelength, appearing yellow at first and changing through to red as the conjugation increases.

Organic molecules containing isolated double bonds produce π - π* transitions, absorbing at wavelengths between 180 - 195nm. Cyclic organic compounds such as benzene, purine etc. have delocalized π-electrons that can be excited more easily to the π* state. This is also

true for linear polyenes such as carotene which absorbs in the visible region of the spectrum. The carbonyl groups (C=O) gives an n - π* transition at approximately 300nm (Figure 3.2.), shifted to approximately 210nm in esters and carboxylic acids (*Drake, 1994*). Amides produce an n - π* transition around 200nm and a π - π* transition at 190nm. The presence of transition metals ensures that there are electrons in d-orbital available for excitation. The d-electrons produce weak absorptions in the visible region giving rise to bright colours.

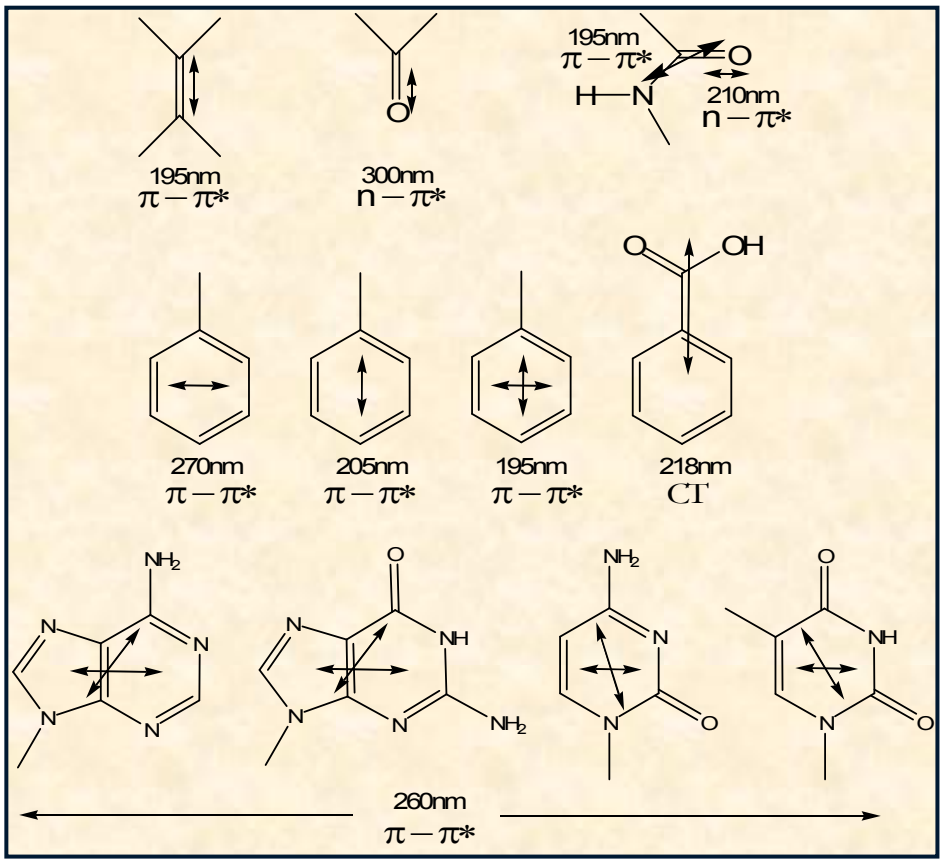

Figure 3.2. The electric dipole moment transitions.
(Dr. A. F. Drake (unpublished presentation))

3.3. Optical Activity and the Generation of Circularly Polarised Light

Optical activity can be defined as the differential interaction of left and right handed circularly polarised light with a chiral molecule. Optical Rotation is the differential velocity (refractive index) whereas Circular Dichroism (CD) is the differential absorption of the two hands of circularly polarised light (*Cotton 1882)*).

3.3.i. Optical Rotation

Linearly polarised light can be considered to be the resultant of two circular components (one left handed and the other right handed circularly polarised). (Figure 3.3.).

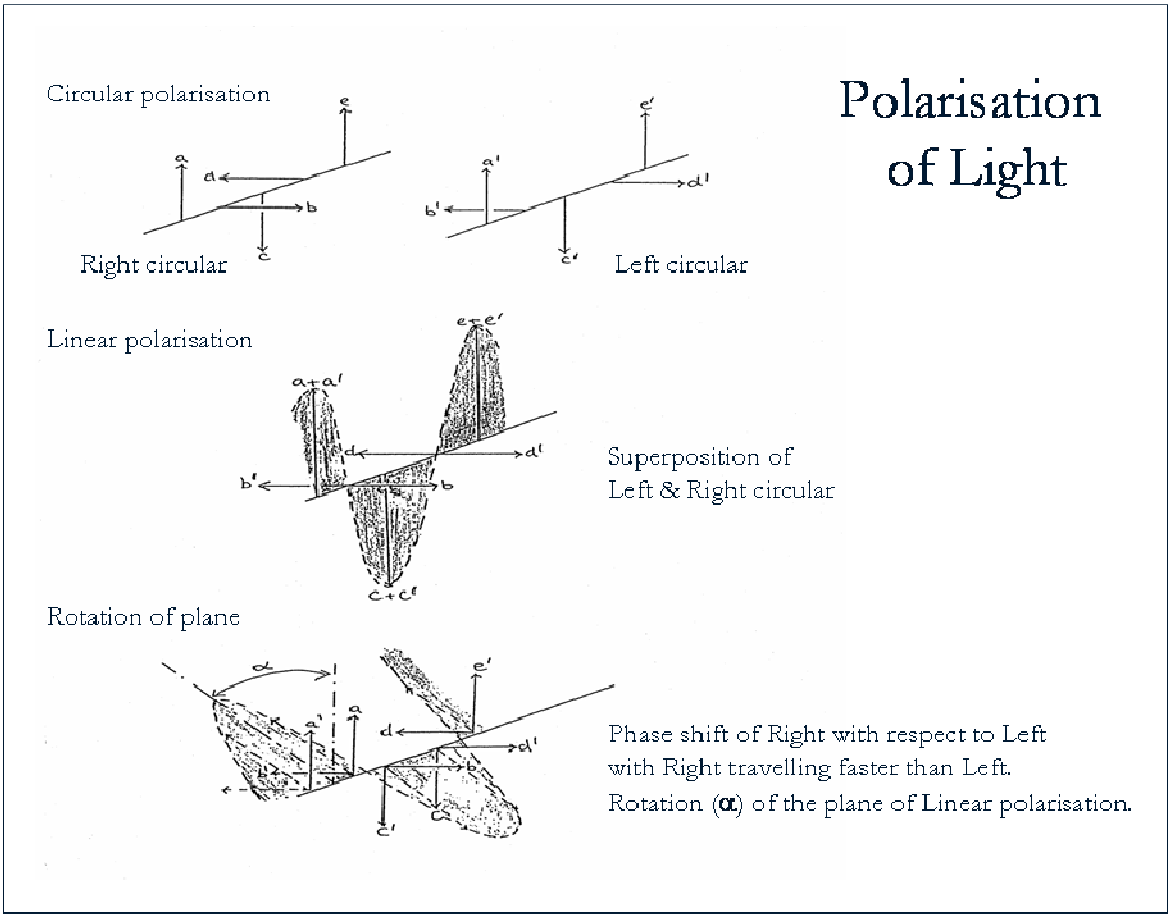

Figure 3.3. : The rotation of the plane of linearly polarised light.
(Slide courtesy of Dr Alex F Drake)

When linearly polarised light passes through an optically active medium, the two circular components travel with different speeds (refractive indices); the result is a rotation of the plane of the incident linearly polarised light (*Drake, unpublished,*). If the right circular component (RCPL) travels faster then the left circular component (LCPL), the result is a clockwise rotation of the plane of linear polarisation. The reverse is true if LCPL travels faster giving an anticlockwise rotation of the plane of linear polarisation.

The observed rotation (α_{obs}) of the plane of the linearly polarised light is called optical rotation and is given by the expression:

$$\alpha = \left(\frac{4\pi l}{\lambda} \right) \left[n_L - n_R \right] \tag{4}$$

l is the pathlength, λ is the wavelength, n_L and n_R represents the refractive indices for left and right circularly polarised light . The specific rotation [α] is now defined to take into consideration the concentration (c) in g/dl of the sample and the pathlength (l) of the cell in decimetres, therefore:

$$\left[\alpha\right]_\lambda = 100 \cdot \alpha_{obs,\lambda} / c \cdot l \tag{5}$$

The molecular rotation (Φ_λ) takes into consideration the molecular weight of the sample (MW) where,

$$\Phi_\lambda = \left[\alpha\right]_\lambda . MW / 100 \tag{6}$$

In a region of absorption, the two circular components will travel with differential speeds and be absorbed to different extents. The emergent beam is now becomes elliptically polarised. The angle and orientation of the major axis of the elliptical light beam indicates the sign and magnitude of the optical rotation. The ellipticity (major axis intensity/minor axis intensity) is a measure of circular dichroism.

3.3.ii. Circular Dichroism (CD)

CD is the differential absorption (ΔA) of left and right circularly polarised light, which is defined with reference to the Beer-Lamber law as :

$$\Delta A = \left(A_L - A_R \right) = \left(\varepsilon_L - \varepsilon_R \right) \cdot c \cdot l = \Delta\varepsilon \cdot c \cdot l \tag{7}$$

The values of ΔA is very small with an order of magnitude between 0.00001 – 0.01. In the early days before 1960, ΔA was too small to be measured directly. Instead CD was measured as the ellipticity ("θ") induced in an incident linearly polarised light beam. The ellipticity unit unfortunately still remains historically; however, it is possible to interconvert molar ellipticity and molar circular dichroism with the relationship:

$$\theta = 32982\ \Delta A \tag{8}$$

The Molar Ellipticity [Θ], measured in degrees cm^2 $dmol^{-1}$, is defined as:

$$[\Theta] = 3298.2 \ \Delta\varepsilon \qquad (9)$$

This relationship shown at equation (9) originates from the derivation of the ellipticity of polarisation that takes into consideration the tangential angle of the electric field vectors of the left and right circular polarised light, shown in equation (10) and represented diagrammatically in Figure 3.3.b.,

$$\tan\theta = \frac{E_R - E_L}{E_R + E_L} \qquad (10)$$

where E_R and E_L are the electric field vectors of right and left circularly polarised light respectively.

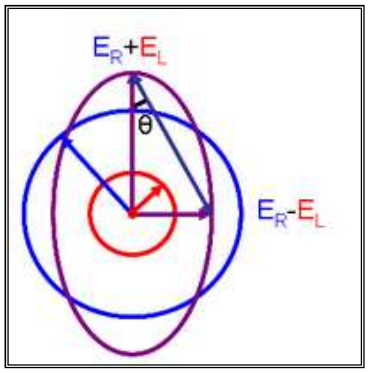

Figure 3.3.b. The formation of elliptical polarised light (**violet**) constituted from the unequal distribution of right (**blue**) and left (**red**) circular polarised light. (http://en.wikipedia.org/wiki/Circular_dichroism)

When $E_R = E_L$, then $\theta = 0$ and the resulting light is linearly polarised. If either of the components of E_R or E_L is equal to zero, then this means that there is complete absorption of light of one of the components in one direction, thus, $\theta = 45°$ and the light is circularly polarised. CD can only be measured in the region of the absorption, i.e. ΔA and Δε; optical rotation (α), that is $n_L - n_R$, can be detected throughout the entire electromagnetic spectrum. A CD spectrum contains relatively few individual components; ORD at a given wavelength is the resultant of contributions from all transitions in the molecule, assignment and explanation of spectral bands becomes far more complicated. CD is now the preferred analytical technique used to study chirality and molecular conformation (*Dr A. F. Drake, unpublished)*.

3.4. Circular Dichroism and Chromophore Classes

If a chiral molecule preferentially interacts with left CPL, then $A_L > A_R$ and the resulting CD will be positive; preferential absorption of right CPL gives $A_R > A_L$ and the resultant CD will be negative. If a sample exhibits optical activity a helical displacement of charge will ensue resulting in the rotational strength "R" that is defined as the area under the CD band. For any electronic transition, the rotational strength (R) is defined by the area under the CD band as :

$$R = \mathrm{Im}\{\mu . m\} \tag{11}$$

where μ and m are the collinear transition electric and magnetic dipole moments of the spectroscopic transition. The Im (imaginary) part is taken as angular moment (magnetic moment) is imaginary in quantum mechanics. The ensuing helical displacement of charge (being either clockwise or anticlockwise) will be dependent on mutual orientations of μ and m (Figure 3.4.).

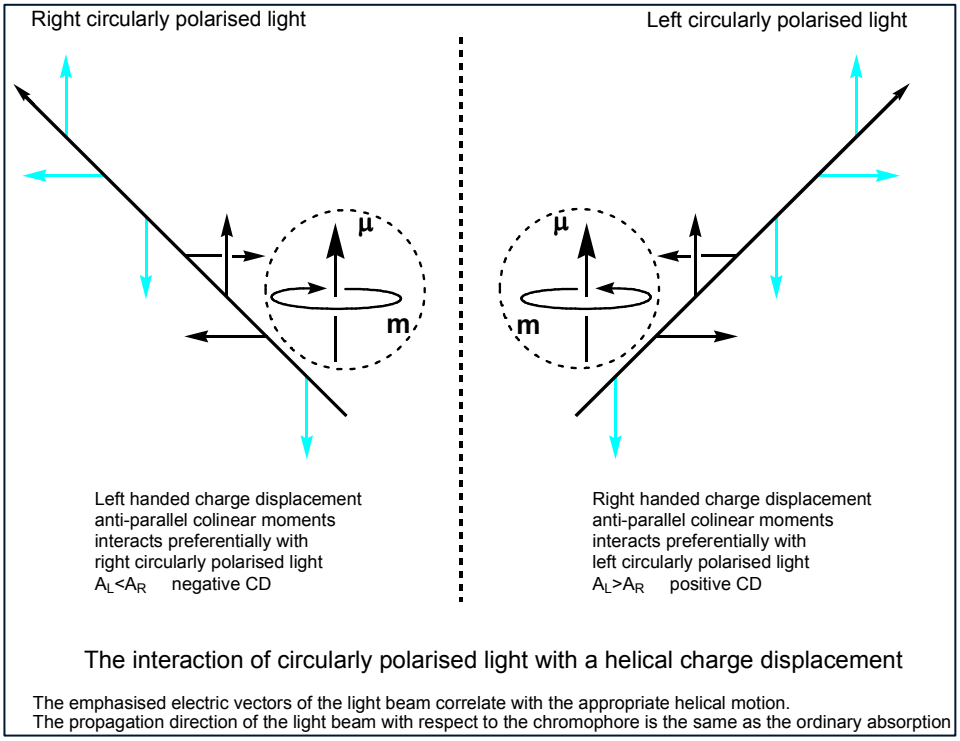

Figure 3.4. Helical charge displacement during an electronic transition.
(A. F. Drake, 2001)

Only if the chromophore itself is chiral do electronic transitions have collinear electric and magnetic transition dipole moments. To explain circular dichroism, chiral molecules are divided into four classes : inherently dissymmetric, coupled oscillators (exciton coupling), symmetric isolated chromophore in a dissymmetric environment and vibronic effects.

Inherently Dissymmetric Chromophore	Coupled Oscillator (Exciton Coupling)	Symetric Isolated Chromophore in Dissymmetric Environment	**Vibronic Effects**
Hexahelicine 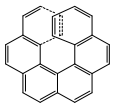	Bases in Nucleic acids 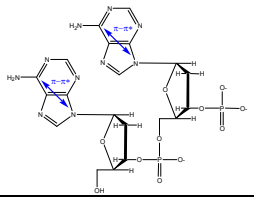	Ketones 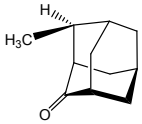	Dimethylallene 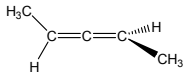
Twistene 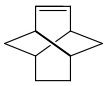	Amides in proteins 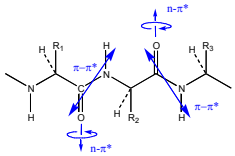	Amino acids 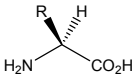	
Disulphide 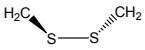	Diaryls 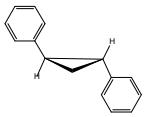	S-ibuprofen 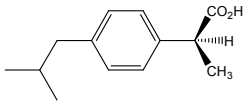	
Class 1 ($\mu \neq 0, m \neq 0$)	Class 2 ($\mu \neq 0, m = 0$)	Class 3 ($\mu \neq 0, m = 0$) ($\mu = 0, m \neq 0$)	Class 4 ($\mu = 0, m = 0$)

Figure 3.5. Classes of chromophores.
(A. F. Drake, 2001)

3.4.i. Class 1: Inherently Dissymmetric

In this situation the chromophore itself is chiral, and therefore will produce transitions that will posses an electric dipole moment together with a collinear magnetic dipole moment.

3.4.ii. Class 2: Coupled Oscillator (Exciton Coupling)

When two or more non-conjugative chromophore are present within the molecule in close

proximity the resultant effect is more complicated, in that not only the individual chromophores have to be considered, but their effect with respect to each other. The induced effect of the chromophores interaction is called exciton coupling. Both CD and UV can measure multiple chromophores yielding meaningful stereochemical information about the exciton coupling and alignment (*Dr A. F. Drake, unpublished)*. The transition electric dipole of one chromophore can interact with transition electric dipoles in other chromophores. Exciton splitting results from the chromophore interaction with maximum effects seen when the excitation energies are similar. The CD bands are opposite in sign for exciton splitting and are often seen under a broad featureless single absorption band. (*Lightner et al, 2000*).

The generation of both UV and CD exciton spectra are as a result of the intrinsic electronic spectral properties of the chromophore together with their relative distance in relation to each other, and their orientation. The ensuing electronic transition of the chromophore is a result of induced electronic dipole-dipole coupling, where for two chromophores represented by either "X" and "Y", either X=Y as in the case of identical chromophores, or $X \neq Y$ for non-identical chromophores. Only one of the chromophores needs to be explicitly excited. The electronic dipole transition of the excited chromophore will interact with the second chromophore resulting in the delocalisation of the excitation (also referred to as the exciton), distributing that excitation over the two (or more) chromophores producing exciton splitting (*Lightner et al, 2000*). This is an important class of which proteins and DNA are members.

Exciton splitting produces distinct absorption bands in the UV spectrum, a single broad UV band is observed for allowed excitation transitions. The UV absorption from the exciton splitting will produce a corresponding CD spectrum that corresponds to the orientations of the dipoles, showing characteristic positive and negative cotton effects. The

greatest CD and UV changes are seen when the excitation energies are similar. There are three extreme orientations of the chromophores as shown in Figure 3.6. depicting the alignment of the dipoles, these are as follows, in-line, oblique and parallel. The possible orientations will have defined spectral optical splits in the UV that may or may not generate CD spectra. For dipoles in-line, a red shift is produced in the UV, this is due to the fact that only lower energy excitations will be allowed. For stacked chromophores, these give a blue shift in the UV band due to the fact that only higher energy excitons will be allowed. Both are limiting cases as no CD will be found as there is no chirality associated with their alignment. In the case of oblique alignments, both the higher and lower exciton transitions are allowed. The resultant UV will be the summation of the contributors, and may be seen as split or un-split which will be governed by the level of energy. The CD will be generated as a result of overlapping positive and negative Cotton effects (*Lightner et al, 2000*).

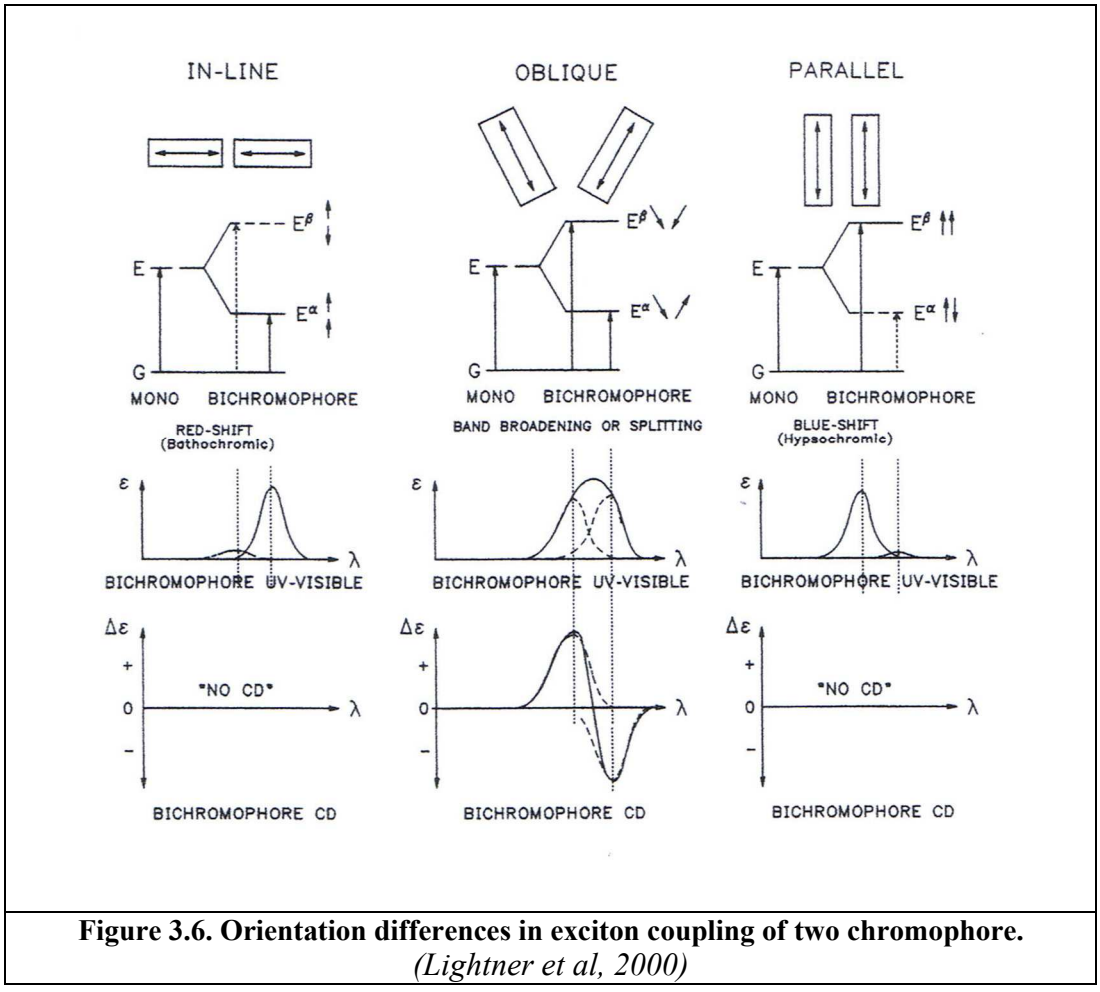

Figure 3.6. Orientation differences in exciton coupling of two chromophore. *(Lightner et al, 2000)*

The condition where exciton coupling is in the oblique position will only generate CD spectra. Within the oblique position there are two possible exciton orientations that are energy dependent. Configuration I is where the electric transition dipole moments are aligned in a head to tail arrangement (↑↓). In this configuration a right handed helical displacement of charge results at low energy that will give rise to positive CD spectra at longer wavelength (Figure 3.7.). Conversely, configuration II results from the electric transition dipole moment aligned in a head to head arrangement. Here there is a left handed helical displacement of charge at high energy resulting in negative CD spectra (Dr. *A. F. Drake, 2001)*.

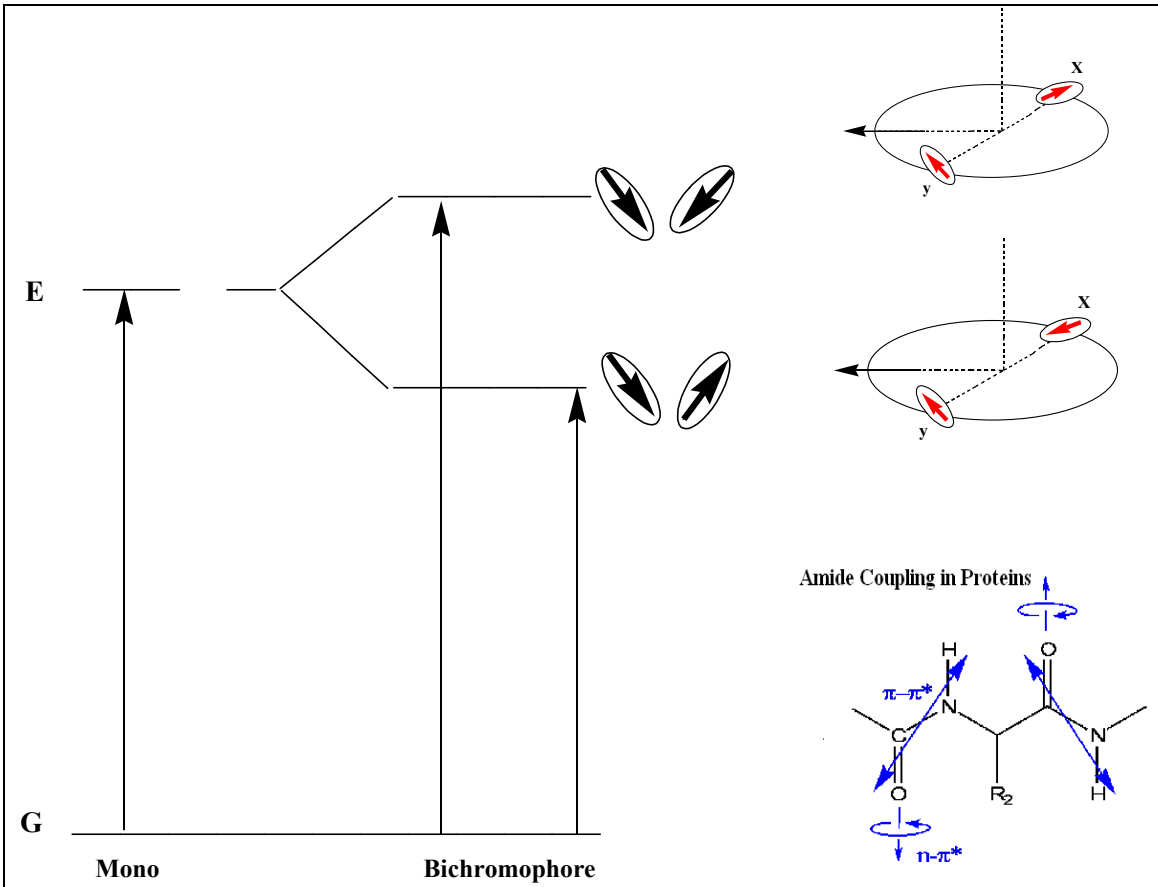

Figure 3.7. Exciton coupling of bichromophores in the oblique position.
(Modified from A. F. Drake (unpublished))

3.4.iii. Class 3: Symmetric Isolated Chromophore in a Dissymmetric Environment

This situation relates to a transitions in a chromophore that inherently have either one of the transition moments, or neither of them. CD spectra will only be generated if the chromophore is located in a dissymmetric environment. A ketones is an example of a chromophore in this category that produces an n-π* transition, this will produce a transition magnetic dipole moment but will not produce the collinear electric dipole moment or visa versa. ε is very small. Induced CD certainly falls into this class.

3.4.iv. Class 4: Vibronic Effects

This effect occurs when the chromophore becomes distorted due to non-symmetric vibrational components. Dimethylallene is an example of this class of chromophore where the CD will be the result of the chiral distortion of the allene chromophore (Dr. *A. F. Drake, 2001)*.

3.5. The Application of Circular Dichroism Spectroscopy (CD)

CD spectroscopy is a specialised form of UV spectroscopy in that a differential absorption occurs, but instead of plane polarised light being used as in UV spectroscopy, the differential absorption of circular polarised light is determined. When both forms of circular polarised light interacts with an optically active sample, for absorption to take place there will need to be a helical charge displacement of the ground state electrons of the chromosphere to the energetically allowed excite state, the interaction being the result of either LCPL or RCPL. The resulting electronic displacement in the chromophore is either left handed or right handed and is as a result of both a translational and rotational motion, clockwise or anticlockwise. CD spectroscopy is very intuitive in being able to detect and monitor conformational changes in macromolecules such as peptides and

proteins, monitoring any environmental changes experienced by chiral or induced chirality in molecules. Being able to use CD in such a diverse manner utilises its inherent characteristics that has seen the use of CD spectroscopy expand at such a rate in the last 50 years, that now CD has become mainstream with most institutions having access to an instrument.

The secondary structure of proteins and peptides can be analysed by CD spectroscopy. This technique requires small quantities of sample, a big advantage over other techniques that require a lot more sample than may be available, or may prove too expensive to produce. Quantities of between 0.3 - 0.5mg/ml are required to produce an adequate sample yielding meaningful CD data. CD spectroscopy is relatively fast with high sensitivity. It can be used to study and monitor many structural changes within the protein, changes such as denaturation studies, binding and displacement studies, solvent changes, the effect of changing pH, temperature effects both high and low and kinetic studies are but a few examples. CD is a good tool for classifying and characterising proteins and peptides before more detailed work is carried out such as x-ray crystallography and NMR studies. The CD spectrometer monitors the changing absorption of chiral molecules such as proteins with changing wavelength. When considering large proteins, using CD spectroscopy for the initial investigation can be a significant tool in identifying secondary structure that is relatively quick, a clear advantage over more conventional methods. Several structural conformations have been identified by CD that give a characteristic profile, these are the α-helix, β-sheet, β-turn, left handed helix (P_{II}) and the irregular structure (Figure 3.8), these structures will be discussed in more detail later.

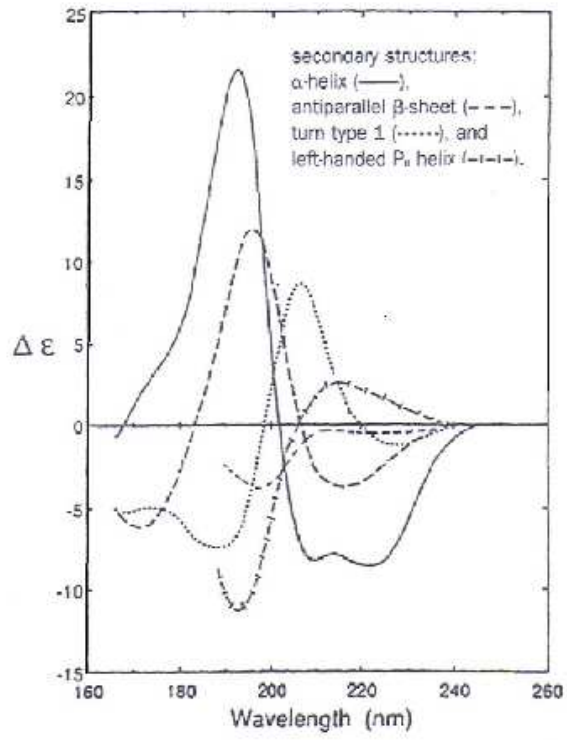

Figure 3.8. Structural contributions of secondary structure components of proteins by CD. *(Drake et al, 1994)*

CD has the ability to asses the folded state of proteins (containing 40 residues or more), or peptide (containing 39 residues or less), and has the ability to investigate and monitor multi-domain proteins and its various unfolded intermediates. A critical number of residues have been determined to produce the functionality of a domain and this has been determined to be between 40 – 50 residues. Domains in themselves can be considered as structured folded "self-stabilising" entities in that although they form an integral part of the protein, they themselves are units that possess both defined secondary and tertiary structures specific for a particular function. Within the domain regions are unstructured sequences that will exists creating loops of varying length, this allows specific regions of structure within the domain to be brought together allowing the generation of ordered regions, thus creating binding pockets, tunnels or sites that create the active site of the protein. Several domains can exist within a protein that may be structurally similar;

however, the primary structure of the domains may be different. CD has the capability to detect and monitor such regions within the peptide/protein.

3.5.i. Secondary Structure Conformation of the α-Helix

One of the most commonly found structures in proteins and peptides is the α-helix. The CD of the α-helix is derived from two main transitions, the n-π* and π-π* transitions that are associated with the amide backbone (Figure 3.9.). There is a negative CD peak at 220nm produced from the n-π* transition of the protein. A second negative peak is located at 208nm and a third maximum, a positive found at 192nm, the latter two peaks are the result of interacting π-π* neighbouring transitions. Since the structure of proteins and peptides are more complex involving more than one structural component, the effects of the other structures, if present, will dilute the overall contribution of the helix conformation. This principle is true for all the other structures.

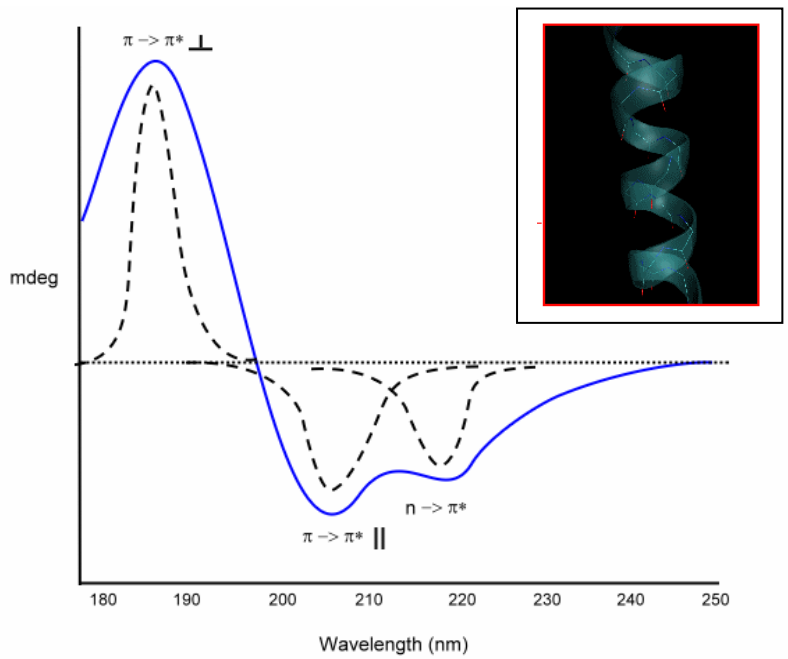

Figure 3.9. CD spectrum of an α-helix showing the electronic contributions.
(*www.proteinchemist.com/cd/cdspec.html*)

Exciton coupling of π→π* transitions that lead to two contributions :
i) a positive (π→π*) at 192nm perpendicular to the molecular helix
ii) a negative (π→π*) at 209nm parallel to the molecular helix
iii) a third contribution is a negative, red-shifted to 222nm.

3.5.ii. Secondary Structure Conformation of the β-Pleated Sheets

β- structure can be formed from both parallel and anti-parallel strands that can vary in both width and length in contrast to an α-helix that can only varies in length (*Woody et al, 1994*). The profile of the CD spectra for the β-sheet is seen in Figure 3.10. The CD profile of the β-sheet is characterised by a negative maximum at 216nm produced from the n-π* transition, and a positive maximum of similar size found at 195nm formed from the π-π* transition. The variation in the CD spectra of the β-sheet varies readily with solvent and chain length.

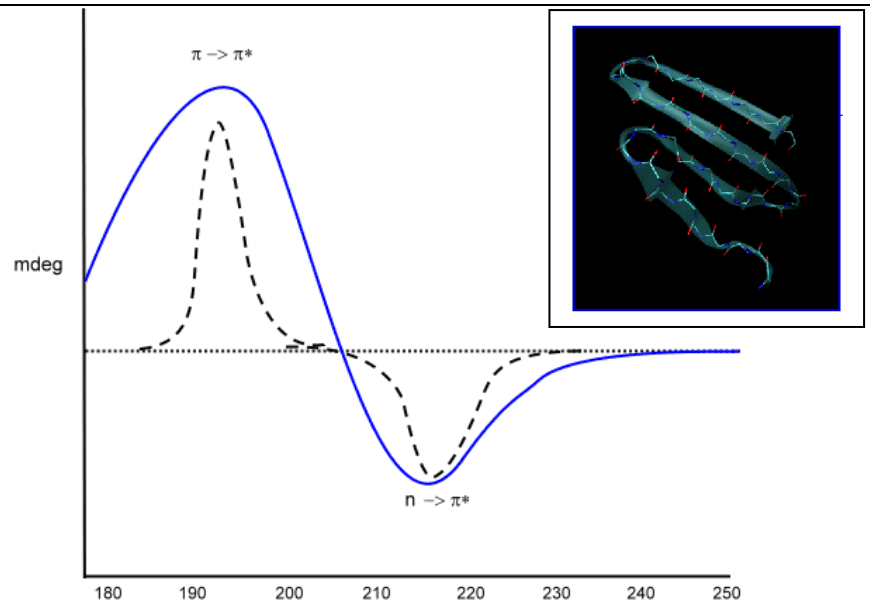

Figure 3.10. CD spectrum of a β sheet showing the electronic contributions.
(*www.proteinchemist.com/cd/cdspec.html*)

Two contributions, a negative at 218nm (n→π*) & a positive at 196nm (π →π*)

3.5.iii. Secondary Structure Conformation of the β-Turns

The CD generated for this type of structure is weak with a negative peak around 225nm due to the n-π* transition, a strong positive maximum at 200nm due to the π-π* transition and a strong negative maximum found around 185nm. The spectrum of the β-turn is red shifted by between 5-10nm from that of the spectrum produced by the β- sheet (Figure 3.8.).

3.3.iv. Secondary Structure Conformation of the Left –handed P_2 Helix

The left-handed P_2 helix is a specific type of structure that is only found in peptides (not proteins) with limited chain length. The CD is characterised by a positive absorption located at around 218nm and a strong negative absorption at approximately 190nm (Figure 3.11).

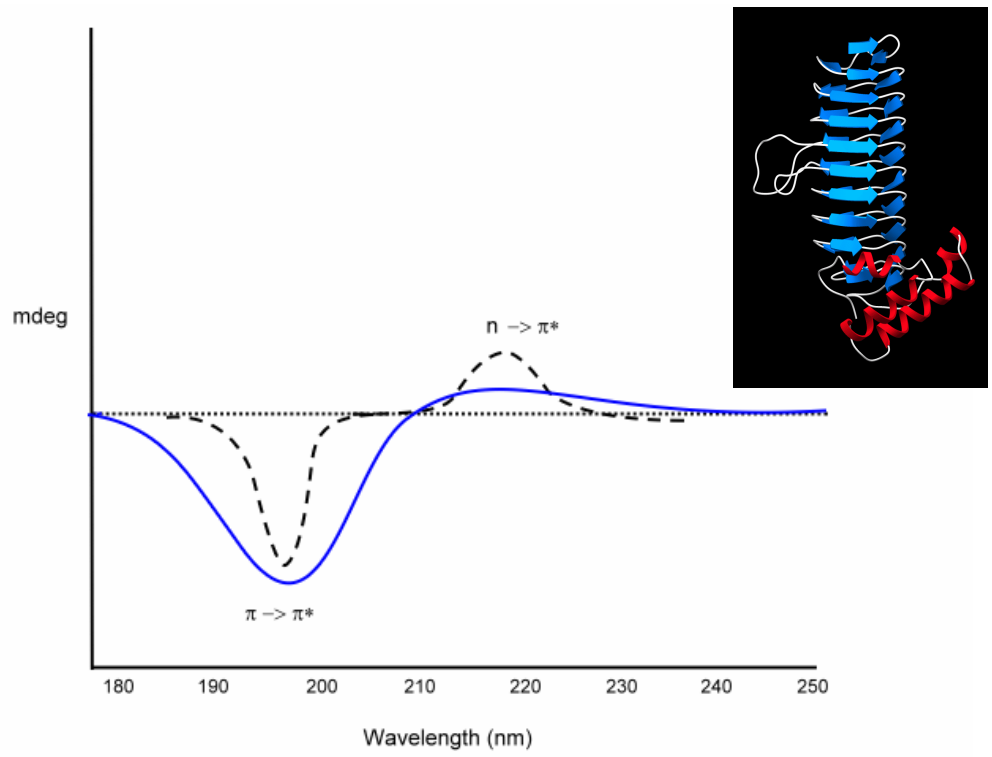

Figure 3.11. CD of a left –handed P_{II} helix showing the electronic contributions.
(*www.proteinchemist.com/cd/cdspec.html*)
Two contributions,
A positive at 212nm (n→π*), RCPL, left handed charge displacement, $A_R > A_L$
A negative at 195nm (π →π*), LCPL, right handed charge displacement, $A_L > A_R$

3.5.v. Secondary Structure Conformation of the Irregular Structure

The CD of the irregular structure is characterised by a weak negative absorption located at around 220nm and a stronger negative peak located at around 200nm. Peptides and proteins that fall in this category are shown to possess none of the other structural components mentioned previously (Figure 3.8.).

3.5.vi. Aromatic Side Chains and Disulphides

Proteins that contain an aromatic group (Trp, Tyr and Phe) show in both the UV and the CD spectra weak transitions, absorbing around 260nm (Tyr and Trp ~280nm) with an ^1L_b band that is electronically electric dipole forbidden (Figure 3.12.). Tyr absorption is detected at 280nm with two other additional vibronic bands detected at 285nm and 290nm. The high symmetry of the molecule results in a small extinction coefficient and also makes it the least responsive to environmental changes. Phe tend to be masked by stronger absorbing groups such as tyrosine (Tyr) and tryptophan (Trp). Absorptions are also seen at 215nm and 180nm due to the ^1L_a and B bands.

Changing the pH of the Tyr environment to between pH9 and pH10 results in a red shift to 295nm produced from the ^1L_b band in the near UV CD band; Trp produces the most complex absorption and CD spectra in the near UV region (Figure 3.12.). Two distinct regions of detection are observed, the first lying between 250 - 300nm produced from the ^1L_b and ^1L_a bands, and although the absorption of the ^1L_b band is weak its fine structure is well developed thus easily distinguished from the other aromatics. The second absorption is detected at between 287 - 292nm, and although stronger in terms of energy produced from the ^1L_a band, its fine structure is practically non-existent. The ^1L_a band is more sensitive to environmental changes.

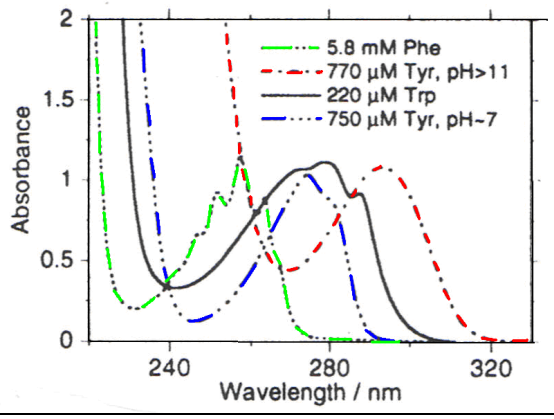

Figure 3.12. The UV spectra of the aromatics (Phe, Tyr and Trp).
Note: pH shown is the pH of the solutions containing the amino acid residues

There exist within the disulphide two n-σ* transitions in the near UV region of the spectrum, these are weak when measuring the UV, but the CD can be relatively strong. The dihedral angle in disulphides is very important as disulphides can be left handed or right handed, normally around ±90° and will give an absorption maximum between 250 - 260nm. As the angle changes and moves away from the 90° position a split in the absorption is detected, one maximum moves to longer wavelength and the other moves towards the shorter wavelength region giving rise to a CD signal with opposing signs. The fine structure observed in the CD for Trp is now lacking in the disulphides, sometimes a tail is seen which extends past 300nm.

3.5.vii. Near UV CD Spectra and Extrinsic Chromophores

The predominant features detected in this region are due to Phe, Try, Trp and disulphide contributions, these are relatively weak when compared to that detected for the secondary structure in the far UV CD region (wavelength ranging between 260 - 185nm). The working range of the near UV CD region is between 340 - 240nm, but it is possible to study a wider wavelength range working as far out as 700 - 340nm. This is important when studying ligand binding if a suitable chromophore is chosen such that its absorption falls within this working range. There are some molecules that although they possess a strong absorption are achiral and do not possess a CD signal, examples of these are dyes such as phenol red and bromocresol blue. However, when such ligands are added to a strongly chiral molecule such as proteins, an induced CD signal is obtained in the region of the absorbing ligand. An extrinsic chromophore is produced due to the presence of the chiral molecule (protein) that can now be measured and monitored. The sign and magnitude of the induced CD signal is purely the result of the protein/ligand interaction.

3.5.viii. The Ultra-violet / Visible Absorption Spectrometer

Absorption spectrometers determine and measure the intensity of light at different wavelengths. There are four main components:

i) Light of the appropriate wavelength can be generated using a tungsten - halogen lamp (350 - 1000nm), and a deuterium lamp is also used (200 - 400nm). Nowadays, DC xenon (Xe) lamps are used in CD and pulse Xe lamps are now being used in UV/Vis.

ii) A monochromator that selects the measurement wavelength situated between the lamp and the sample housing.

iii) A sample compartment, where the sample is placed during measurements.

iv) A light detector, in the form of a photomultiplier or silicon diode.

Penetration into the UV, particularly towards and below 200nm is limited by three factors. The first is that there is interference by the absorption of oxygen in air that is very strong and causes major interference artefacts. Far UV light (<200nm) induces the conversion of O_2 to ozone (O_3) which is corrosive and will attack the components of the spectrometer, ozone absorbing at 254nm. Secondly, there is a problem of reduced transmittance of optical components below 200nm producing interference when measuring spectra, this effect can only be reduced at great expense (*Donney et al, 1993*). The last factor that has to be considered is the effects of solvent absorption that is particularly strong below 200nm, this effect cannot be eliminated but can be reduced if the appropriate solvent is selected, as some solvents are more transparent than others, or by a reduction in optical pathlength of the measurement cell.

3.5.ix. Circular Dichroism Instrumentation

The CD spectrometer used in this thesis is illustrated in Figure 3.13.

Figure 3.13. The JASCO J720 Spectrophotometer.
(A. F. Drake, 2001)

The light source in the form of a xenon lamp (this lamps covers the whole spectral region of the UV/Vis range) delivers a focused, stable high intensity beam to provide a constant output. The beam passes first through a monochromator that transforms it into monochromatic light and polarizes it linearly; this then enters the photoelastic modulator. The modulator (in the Jasco design) uses a Piezo device that works at a fixed frequency of 50kHz and is designed to create sinusoidal waves. The modulator is responsible for creating the LCPL and RCPL by introducing a phase lag 'δ' coursed from the "periodic variation in the polarization" of the impinging light beam (*Drake, 1994*). The emergent beam passes through all ellipticities from left circular, elliptical, unchanged linear, elliptical through finally to right circular, all created at a fixed wavelength and constant intensity giving I_O. If a chiral sample is now placed in the sample compartment and scanned through all ellipticities at each wavelength throughout the region where the sample is optically active, some of the ellipticities will be differentially absorbed creating a CD spectrum. Now, a change in intensity is detected that shows wavelength specificity and is represented by I_X. and is the intensity detected from the modulator at a specific wavelength that can be due to either absorption of left or right CPL. Therefore,

$$\Delta A = \log(I_o / I_x) = \log(I_o/I_L) - \log(I_o/I_R) \quad (12)$$

then,

$$\Delta A = (A_L - A_R) = (I_R - I_L) / (I_R \ I_L) = V_{AC} / V_{DC} \quad (13)$$

V_{DC} is the voltage detected when an absorbing optically inactive sample is put into the sample compartment; its output is constant but very small. Likewise is V_{AC} that is detected as a result of the differential absorption of the optically active sample. Both V_{AC} and V_{DC} are amplified by the photomultiplier by the same amount, such that the difference between them is conserved and is proportional to ΔA over the entire wavelength region measured and for all conditions. V_{DC} is a measure of the light intensity and is also a measure of the ordinary absorption (*Drake, 1994*) measured on a separate output channel (HT voltage) used to indicate the performance of the sample under those conditions set.

CHAPTER 4

CHAPTER 4: Spectroscopic Characterisation of Human Serum Albumin

4.1. Introduction

The size of albumin has made its study by NMR difficult, and has enabled only the assignment of <100 residues out of 585. Crystallographic studies have also been problematic. It has been relatively easy to produce crystals of HSA, but the quality has been poor, yielding little to no high resolution diffraction patterns until fairly recently. Only a few scientists have been able to achieve meaningful data by x-ray, the earliest group to produce outstanding results was Carter and co-workers (*Carter et al, 1990*). More recently there has been a plethora of information resulting from crystallographic studies most notably from Curry and co-workers (*Curry et al, 1998 & 2006)* who have shown the importance of fatty acids in the crystal formation of albumin and the effect it has on the binding ability and activity of the molecule. Others including Muravskya and co-workers, Chuang and co-workers and Sugio and co-workers are but an important few that have contributed greatly to this field (*Muravskya et al, 2004; Chuang et al, 2006; Sugio et al, 1999*).

Using CD spectroscopy, different samples of albumin have been characterised by observing spectroscopic changes in two regions, the near UV region (340 - 240nm) and the far UV region (260 - 185nm). Each region is indicative of specific changes that may occur within the protein; the near UV characterises changes that occur within the environment of the aromatic residues and disulphides, and the far UV region represents changes that occur in the secondary structure or the backbone region of the protein. Recombinant human serum albumin (rHSA) was the preferred protein used throughout most of this thesis. However, in order to ensure that changes observed were not as a result of the methods employed in obtaining the protein, the characterisation of rHSA was compared with several types of albumin including native and defatted albumin (nHSA & dHSA

respectively) for structural integrity and binding abilities. Wherever possible, all three types of protein were investigated and compared. Some experiments were also conducted on the glycosylated form of nHSA referred to as L27 HSA (only a small amount of this sample was available so experimentation was restricted). Two fractions of albumin corresponding to domain I and domain I+II, were also investigated and characterised. All six samples were investigated for pH and temperature changes.

Secondary structure analysis for all the samples of albumin were made and used to investigate structural changes in the presence of chemical and structural perturbations. All secondary structure predictions were calculated using the protocol formulated by K. M. Malik (*Malik, Thesis, 1997*). Principal component regression (PCR) was the algorithm used, the form of the CD spectra of proteins under analysis being similar to that of the CD spectra in the calibration data set.

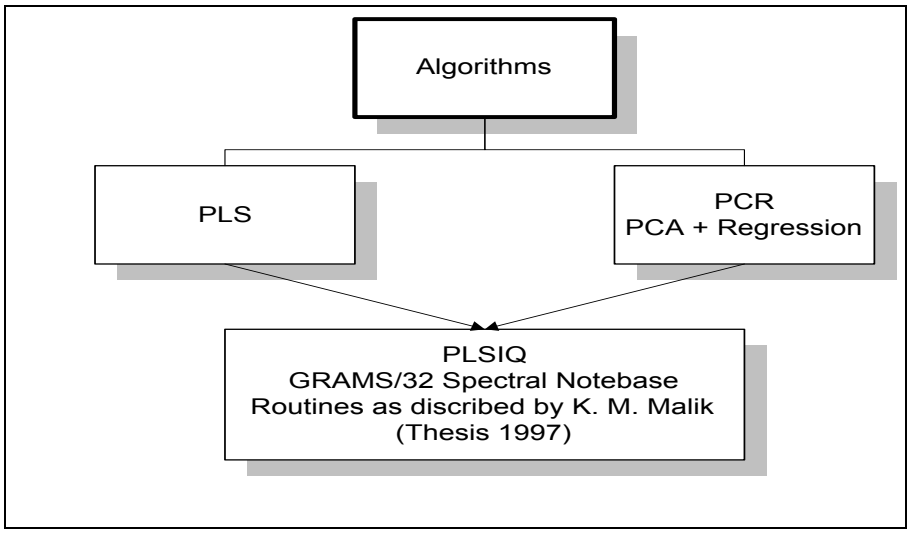

Figure 4.0. Schematic representation of principal component regression

4.2 Experimental Procedures

4.2.i. Procedures for pH Investigation

pH studies were conducted in the presence and absence of a buffer, the buffer of choice was Britton Robinson buffer (B/R) chosen for its buffering range of pH2 to pH12. When

freshly prepared B/R attains approximately a pH2; albumin was dissolved at pH2 and the titration conducted measuring the UV and CD spectra at regular pH increments. In the absence of a buffer, albumin samples were dissolved in distilled water and divided into two equal portions. One of the samples was used to investigate increasing pH using 0.1M and 1M sodium hydroxide as the pH adjusting solutions, and the other sample was investigated for low pH adjustments made with 0.1M and 1M hydrochloric acid. The volumes of both acid and alkali required to adjust the pH were minute in comparison to the total sample volume of albumin used to conduct the experiment, the adjustments were made using a calibrated 10µl or 20µl Gilson pipette. Therefore the dilution factor was considered to be minimal if not negligible.

4.2.ii. pH Titration Data Fitting

When conducting a pH titration the data can be fitted using the Mathcad 8 Professional computer programme adapted by Dr A. Drake (unpublished) for an equilibrium equation where :

$$[B] + [H^+] = [BH]^+ \qquad (a)$$

Then,

$$K_a = \frac{[BH]^+}{[B].[H]^+} \qquad (b)$$

Also,

$$\Delta A_{obs} = \Delta A_B + \Delta A_{BH} \qquad (c)$$

where ΔA_{obs} represents the observed changes in absorbance, ΔA_B is the changes in absorbance associated with the base and ΔA_{BH}. Combining equation (b) with equation (c) will give the CD expression given by the expression:

$$\Delta\varepsilon_{obs}(pH) = \frac{\Delta\varepsilon_B . K_a . \Delta\varepsilon_{BH} . 10^{-pH}}{1 + (K_a . 10^{-pH})} \qquad (d)$$

where $\Delta\varepsilon_{obs}(pH)$ is the theoretical CD value observed at a given pH, $\Delta\varepsilon_B$ is the molar CD at the base limit and $\Delta\varepsilon_{BH}$ is the molar CD at the acid limit. This equation can be

extended to incorporate more than one K_a.

4.2.iii. Procedures for Temperature Analysis

Temperature studies were conducted by a variety of methods. The simplest temperature investigation was conducted with the sample being heated by increasing increments from room temperature to 95^{o}C in the spectrometer, heated by a brass cell holder block connected to a thermostatically controlled water bath. The CD was measured in both wavelength regions (340 – 240nm & 260 – 185nm) at regular temperature intervals with the heated sample being allowed to equilibrate at the desired temperature before measuring both the CD and the sample's true temperature that was measured via a thermocouple in direct contact with the sample solution in the cell. The second method of temperature investigation involved sequential heating, then quenching the albumin sample back to room temperature. Albumin was heated to a predetermined temperature in the spectrometer, allowed to equilibrate and then scanned in both regions recording the temperature of the sample at the time of scanning. The sample was then allowed to cool to room temperature where the two regions were scanned again. The heated sample was then further heated to a higher predetermined temperature and the process of scanning, cooling and re-scanning repeated until the sample had been heated to the highest temperature setting.

The third method of temperature analysis was to investigate the effects of temperature using incubated samples of HSA that were pre-heated in the absence of a ligand but in the presence of a buffer. A large sample volume of albumin of known concentration was heated in a water bath to a predetermined temperature, at equilibrium an aliquot of the heated sample was removed and cooled to room temperature (RT), the rest of the albumin solution remained in the water bath. The temperature of the bath was then increased and the sample was allowed to equilibrate at the higher temperature before removing and

cooling a further aliquot. This process was repeated for temperature ranging from RT to 95^{o}C with the exact temperature of the sample removed recorded. Each heated sample removed was cooled down to RT before measuring both the UV and CD spectroscopy. All the measured samples were compared for possible structural changes and differences.

The final method of temperature analysis was to investigate the effects of temperature by CD at fixed wavelength, monitoring the unfolding of the protein as a direct response to heating. The spectrometer was adjusted to monitor at fixed wavelength with respect to time. This process was conducted in two ways. The first method was to allow the spectrometer to start recording at fixed wavelength at RT; a stopwatch was then started simultaneously with the start of the scan. The circulating water bath was adjusted to its maximum temperature (97°C) and using the thermocouple placed in direct contact with the sample in the cell, the temperature of the sample was recorded at regular temperature increments, whilst recording the time when the temperature was measured. The unfolding of the protein would typically take approximately 40 minutes from start to completion. This method was quite rapid and once the protein started to unfold, there was no way of stopping or allowing the sample to equilibrate at the temperature before measuring.

To compensate for such rapid and unpredictable unfolding, the method for this type of heating cycle was modified by adjusting the heating rate by discrete manual incremental adjustments to the water bath to allow for a more controlled heating rate. Although this meant that the running time for scanning had considerably increased (approximately 3 hours), this method allowed for more discrete temperature increases, a more controlled heating rate that allowed for a period of time for the sample to equilibrate before recording both the time and temperature at which the scan was taken. By this method the spectrometer was set to monitor at a fixed wavelength but using a longer time period for scanning. The spectrometer was started simultaneously with the stopwatch with the water

bath set to RT. The water bath was then manually adjusted to 50°C (the temperature below the point at which HSA showed any signs of denaturation), allowed to equilibrate, and both the time and temperature recorded. The water bath was then increased by a predetermined amount and once again allowed to equilibrate before recording the time and temperature at equilibrium, in this way the temperature, with reference to time, could be used to determine the changes in CD. This process was repeated for temperatures up to 97°C.

4.2.iv. Calculations for Temperature Fit

The experimental data obtained from the temperature studies was also fitted using the Mathcad 8 Professional programme adapted by Dr A. Drake (unpublished) adapted to fit the modified Van't Hoff equation. Here,

$$\frac{d\ \log K}{d\,T} = \frac{H_{vH}}{R.T} \tag{1}$$

Integrating equation (1) and substituting for K gives:

$$\Delta\varepsilon_{obs}(T) = \frac{\Delta\varepsilon_u.\exp\left(-\frac{k}{T}+\frac{k}{T_m}\right)+\Delta\varepsilon_1}{1+\exp\left(-\frac{k}{T}+\frac{k}{T_m}\right)} \tag{2}$$

Where T is the measured absolute temperature, T_m is the melting temperature or transition midpoint, $\Delta\varepsilon_{obs}(T)$ is the calibrated molar CD value at a given temperature; $\Delta\varepsilon_1$ is the molar CD observed for the lower temperature state and $\Delta\varepsilon_u$ is the molar CD observed for the upper temperature state. A theoretical curve is generated of $\Delta\varepsilon_{obs}(T)$ against T for given values of k and T_m. Similar to pH data fitting there is the provision to fit more than one transition, this is indicated in equation (3),

$$\Delta\varepsilon_{obs}(T) = \frac{\Delta\varepsilon_{u1}.\exp\left(-\frac{k_1}{T}+\frac{k_1}{T_{m1}}\right)+\Delta\varepsilon_{11}}{1+\exp\left(-\frac{k_1}{T}+\frac{k_1}{T_{m1}}\right)} + \frac{\Delta\varepsilon_{u2}.\exp\left(-\frac{k_2}{T}+\frac{k_2}{T_{m2}}\right)+\Delta\varepsilon_{11}}{1+\exp\left(-\frac{k_2}{T}+\frac{k_2}{T_{m2}}\right)} \tag{3}$$

where subscript 1 and 2 denotes the first and second transitions. Independent melting

processes are assumed here.

4.2.v. Recombinant Human Serum Albumin Production (rHSA)

Delta Biotechnology Ltd based in Nottingham has pioneered recombinant albumin production. In 1986 Delta, together with BASF, were able to express rHSA from cultured yeast on a large scale (*Hinchcliffe et al., 1986 & Quirk et al., 1989*). The drive towards recombinant products has been governed partly in responses to viral contamination, but also because of the worldwide demands on albumin with rHSA currently under clinical trials. Native human albumin is prepared by fractionation of plasma from blood donors and used as a therapeutic agent to restore and maintain blood volume. Albumin is also used as a stabilizing agent in vaccine formulations and as a medium for various imaging procedures such as X-rays. The production of human albumin each year is in the hundreds of tons but because of the possible potential of viral transmissions of diseases such as HIV and hepatitis, the drive to recombinant products is prevalent. The production of the recombinant product involves neither human nor animal-based raw materials. Therefore, the recombinant product is much safer, as the genetically engineered protein is expressed by yeast cells with virtually zero risk of viral contamination, high purity giving a product that is structurally equivalent to HSA (*Schindel et al, 2003*).

cDNA from human liver cells are used to express the appropriate mRNA. The plasmid is transferred to yeast cells using standard molecular biological techniques. rHSA is secreted in the culture by the yeast in quantities of the order of 40 - 55mg/ml of mature albumin. With rHSA production by this method, 3% of the product is fragmented forming both known and unknown fragments. Small amounts of prepro and proalbumin have also been detected. The protein is then lyophilised and would normally contain between 3 - 5% water; this value could rise to as much as 15% if stored in a humid environment. The Food and Drug Administration (FDA) require caprylate and N - acetyl - DL tryptophanate to be

added as part of the pasteurisation process, around 0.08mM/g of each are required to attain the specifications laid down by the FDA. Experiments using rHSA were undertaken after all additives were removed. Additives have been shown to interfere with the binding of some ligands used in this project.

4.2.vi. Purification of Human Serum Albumin

A prerequisite to the requirement of the purification of HSA is to preheat the protein to 60°C for ten hours to destroy any possible viral contamination. Caprylate (a (MCFA) and/or N- acetyl - DL tryptophanate are added prior to the heat treatment to protect the protein, stabilizing it against any adverse heating effect. However, the amount of stabilizer present can sometimes affect the ability of the protein to bind some ligands (*Peters, 1996*). With this in mind, albumin was dialysed against water to remove small ligands including salts. All samples were dialysed, lyophilized and stored in the refrigerator until used. Dialysis only removed small ligands and proved ineffective against stabilizers where denaturation conditions were required. To remove MCFA and LCFA, the purification protocol using activated charcoal as described by Chen and co-workers was employed (*Chen et al., 1967*). Samples were dialysed and lyophilized and stored as described above. Albumin treated by charcoal is referred to as defatted albumin (dHSA).

4.2.vii. Materials

All HSA samples with the exception of L27 HSA were supplied courtesy of Delta Biotechnology (Nottingham, UK). L27 HSA was supplied courtesy of a personal gift to Dr. A. F. Drake. Concentrations of the protein ranged between 0.3 to 0.6mg/ml were dissolved in either phosphate buffer (P/B) (supplied by BDH, UK), Britton Robinson buffer (B/R) (comprising of citric acid 21.01g/l, sodium citrate 29.41g/l and

diethanolamide 21.02g/l), also supplied by BDH, UK, analytical grade (B/R having a buffering range between pH2-pH12) or distilled water.

4.2.viii. Absorption Spectroscopy (UV)

UV spectra for all samples were measured using an Aviv 17DS spectrophotometer or a Varian 2390 spectrophotometer with a spectral bandwidth of 0.2nm, scanning at a rate of 60nm/min at intervals of 0.2nm. A 1cm pathlength cell was used in the wavelength region between 340nm to 240nm. For regions below 260nm either a 0.02 or an 0.05cm cell was used. All samples were measured at room temperature. Some of the binding experiments involved the filtering of small volumes of samples through micro-filters, this yielded volumes of 200µl or less. To cope with such small volumes specially designed cuvettes were used to allow the UV to be determined. Examples of such cuvettes are shown in Figure 4.1.a.

To ensure continuity throughout measurements, the same cuvettes were used to measure both the UV and the CD for the sample in the specified region with the exception of the small volume samples that used the specifically designed cuvettes shown in Figure 4.1.a., specifically designed for the UV spectrometer only with a pathlength of 1cm. In addition to the use of a specially designed cuvette, the space in the cell was not entirely filled with the solution of the sample, the cell was masked and positioned in the spectrometer to ensure maximum throughput of light passed through the sample only. This ensured that the spectrometer light beam was targeted and concentrated through the sample only, so that the maximum use of the light beam was used.

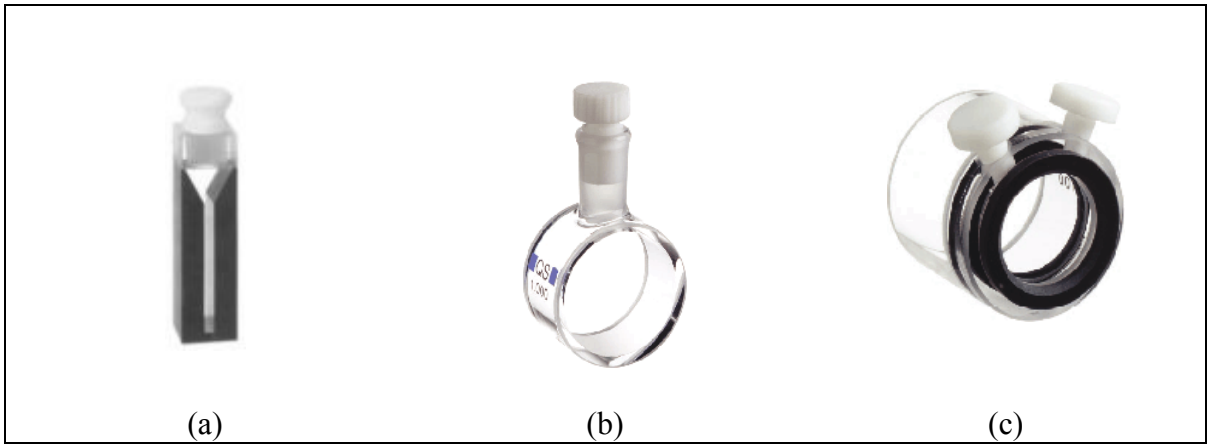

(a) (b) (c)

Figure 4.1. A selection of cells used to measure UV and CD spectra.

(a) 1cm Micro cell with black walls and Teflon stopper used for small volumes (0.2ml).
(b) 1cm Cylindrical cell used when the volume of the sample is not a restriction (2.8ml).
(c) 0.05cm Cylindrical cell used when volume of sample is a limiting factor (0.28ml).

4.2.ix. Circular Dichroism Spectroscopy (CD)

Two CD instruments were used to measure the spectra, either the JASCO J600 spectropolarimeter or the JASCO J720 spectropolarimeter with conditions of slit bandwidth of 1-2nm, a scan speed of 10nm/min at a time constant of 4sec with the data acquisition every 0.2nm. All instruments were calibrated to ensure consistent and accurate results; this meant that the spectra from both instruments could be compared without fear of any erroneous or unspecified errors affecting the results. Three cells were used depending on the wavelength region investigated, between 340-240nm (near UV CD region) a 1cm cuvette was used. For the wavelength region of 240-185nm (far UV CD region) either a 0.02cm or a 0.05cm cuvette was used. The data was corrected for concentration and pathlength per mean residue to determine the extinction coefficient $\Delta\varepsilon$ per residue enabling samples of different molecular weights to be compared (Drake, 1994).

4.3. pH Characterisation of Albumin

Albumin will inherently exhibit a pH of between pH 6.8 – pH7 when dissolved in water (concentration of 6.02 x 10^{-6}M); a role utilised when buffering and maintaining the pH of the blood. Albumin is quite resistant to small changes in pH (*Kragh-Hansen, 1990*). The CD spectra of the different forms of albumin were first determined and compared for structural differences; the results are show in Figure 4.2. The magnitude and characteristics of nHSA, dHSA and rHSA were essentially the same. The presence of a small amounts of fatty acid or the effects of recombinant preparation did not affect neither the secondary nor the tertiary environment significantly, yielding spectra of similar magnitude and form in both wavelength regions investigated.

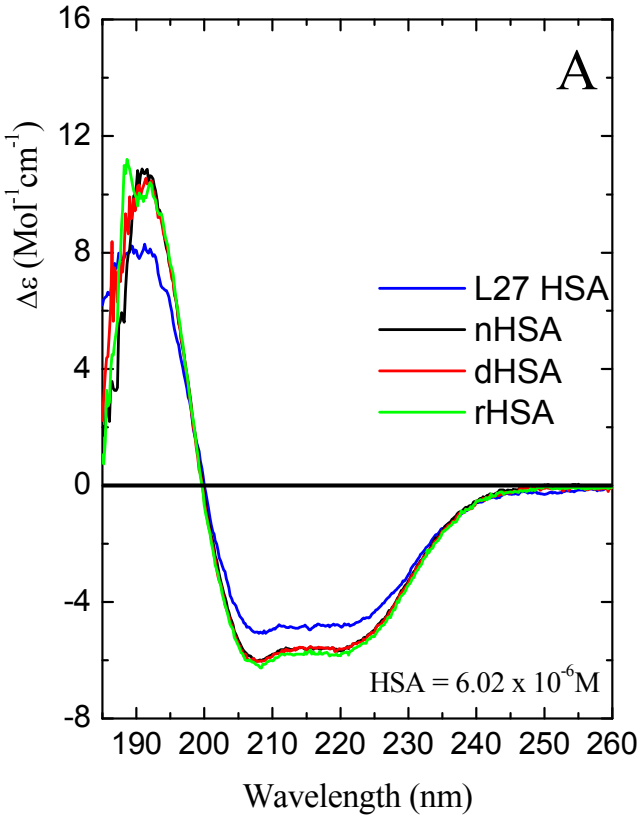

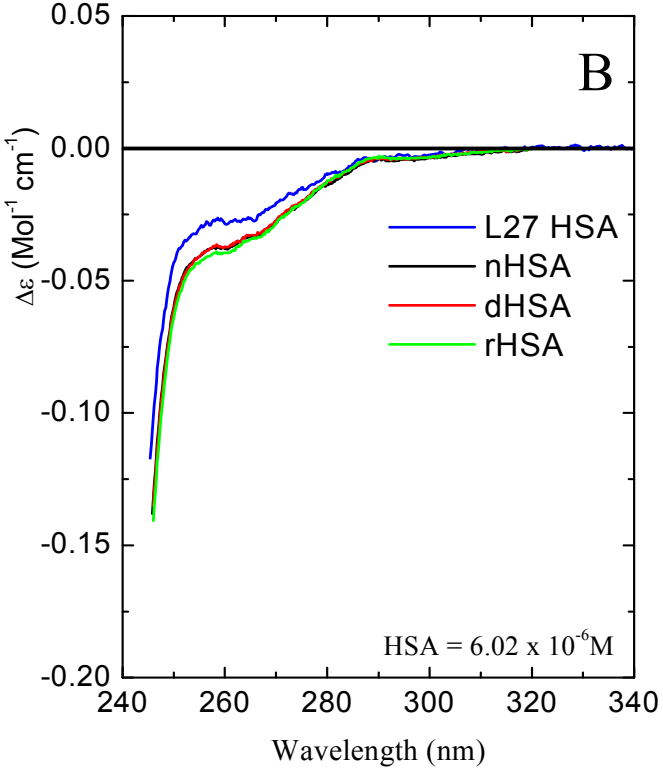

Figure 4.2. Spectroscopic characterisation of the different forms of HSA.

A. Far UV CD region in 10mM P/B, pH7.2, 0.05cm
B. Near UV CD region in 10mM P/B, pH7.2, 1cm cell

The CD spectra shows a protein rich in α-helix content (52% calculated by PCR) and a small amount of β-sheet (16%), the remainder (32%) was found to be irregular structure. Crystallographic studies found albumin to contain 67% helix, 23% extended chain and ~10% exists as turns. The values of the secondary structural components calculated by PCR were much lower for helical composition than that obtained by X-ray crystallographic studies even though both methods showed a rich helical content. As a first approximation and with the lack of meaningful crystallographic data PCR gives a good initial indication on structural analysis and a first approximation of the structural composition of the protein/peptide under investigation. In view of this PCR was used as a tool to investigate changes in structural forms rather than absolute values. The use of PCR will highlight trends and changes in structural composition when chemical and/or physical perturbations are applied. The near UV CD region reveals a protein whose aromatics are buried deep within the protein, shielded and protected from any environmental perturbations.

The glycosylated sample L-27 HSA (6.02×10^{-6}M) showed structural changes in both regions of the spectrum with the loss in both secondary structure and tertiary environment; the reductions were calculated to be a 5% reduction in α-helical content with an 8% reduction in β-sheet and an associated increase in irregular structure of 12.5% (Figure 4.2). Glycosylation occurring at the ∈-amino group of lysine 525 within albumin (*Shaklai et al, 1984*), and clearly the affects of the presence of a sugar molecule has a marked effect on the way in which the protein folds and the overall interaction of the three domains with respect to each other. It is clear that the presence of sugar will also have chemical implications on the glycosylated protein such as the way in which it might interact and bind to other molecules, drug interaction and perhaps the biochemistry of the whole molecule could be compromised. All these factors need careful consideration and are beyond the scope of this thesis due to the lack of glycosylated material. Some preliminary investigations were undertaken however, and this will give some indication of the effect glycosylation has on the characteristics of the protein.

One of the essential characteristics of albumin is that the structural changes experienced with changing pH are completely reversible. Figure 4.3. shows the results of the response of nHSA with changing pH. CD spectroscopy was sensitive enough to detect subtle changes in both the secondary and tertiary environment of the protein, with the greatest loss in structural content found at the extreme pH regions that were detected at pH 4.0 and below and above pH 10.0, relative stability was attained between the extremes conditions. Subtle changes were detected between pH 5 to pH 3 (Figure 4.3.c. & d.). A residual amount of structure always remained in the core of the protein showing that some of the core hydrophobic structures remained shielded from the surrounding solvent environment. Plotting at fixed wavelength revealed similar trends throughout the entire albumin series of samples studied. In the near UV CD region the aromatic contributions were exposed in the extreme pH regions, but remained sufficiently buried not to pose a significant problem for the integrity of the protein's tertiary structure. Figure 4.4. shows the fixed wavelength plots of the other HSA samples studied revealing similar trends throughout.

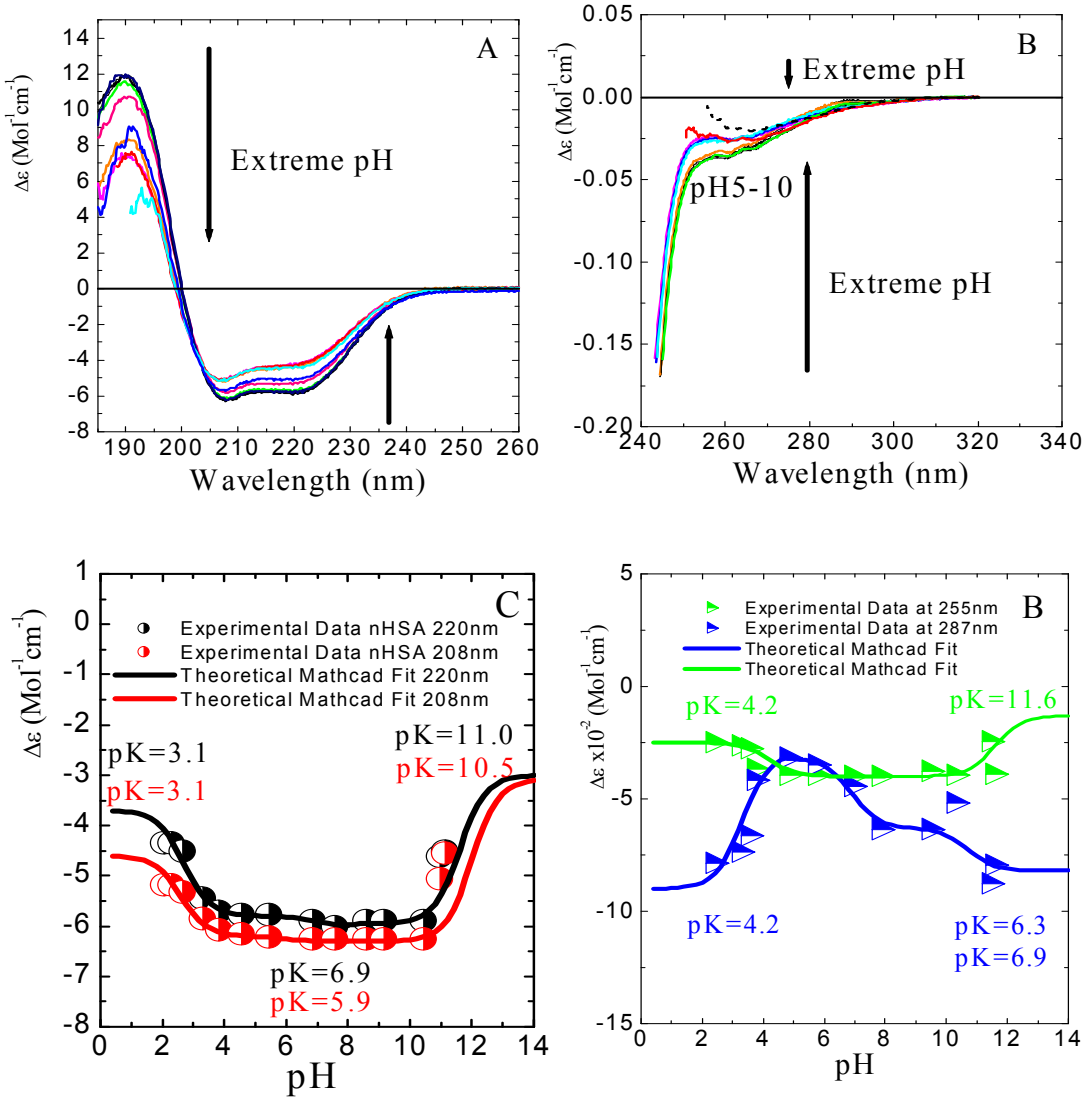

Figure 4.3. pH titration of nHSA in water in both the far and near UV CD regions

A. Far UV CD spectra of the pH titration in H_2O, 6.02×10^{-6}M, 0.05cm cell
B. Near UV CD spectra of the pH titration , 3.00×10^{-5}M (2.0mg/ml), in H_2O, 1cm cell
C. Fixed wavelength plot of the pH titration in the far UV CD region
D. Fixed wavelength plot of pH titration in the near UV CD region

Interestingly, the fixed wavelength plot in that aromatic region at 255nm behaves similarly to the changes measured in the secondary structure region. Only the measurements detected at 287nm in the aromatic region showed the greatest susceptibility to changing pH, suggesting that throughout the entire pH region studied the aromatic residues vulnerability or susceptibility to their environment was exposed.

Superimposing all three whole HSA samples reveals that all the albumin samples behaved in a very similar fashion in response to pH changes (Figure 4.5.). The subtle changes detected were not significant enough to show any real or measurable differences that would indicate any structural or preparation differences between the samples.

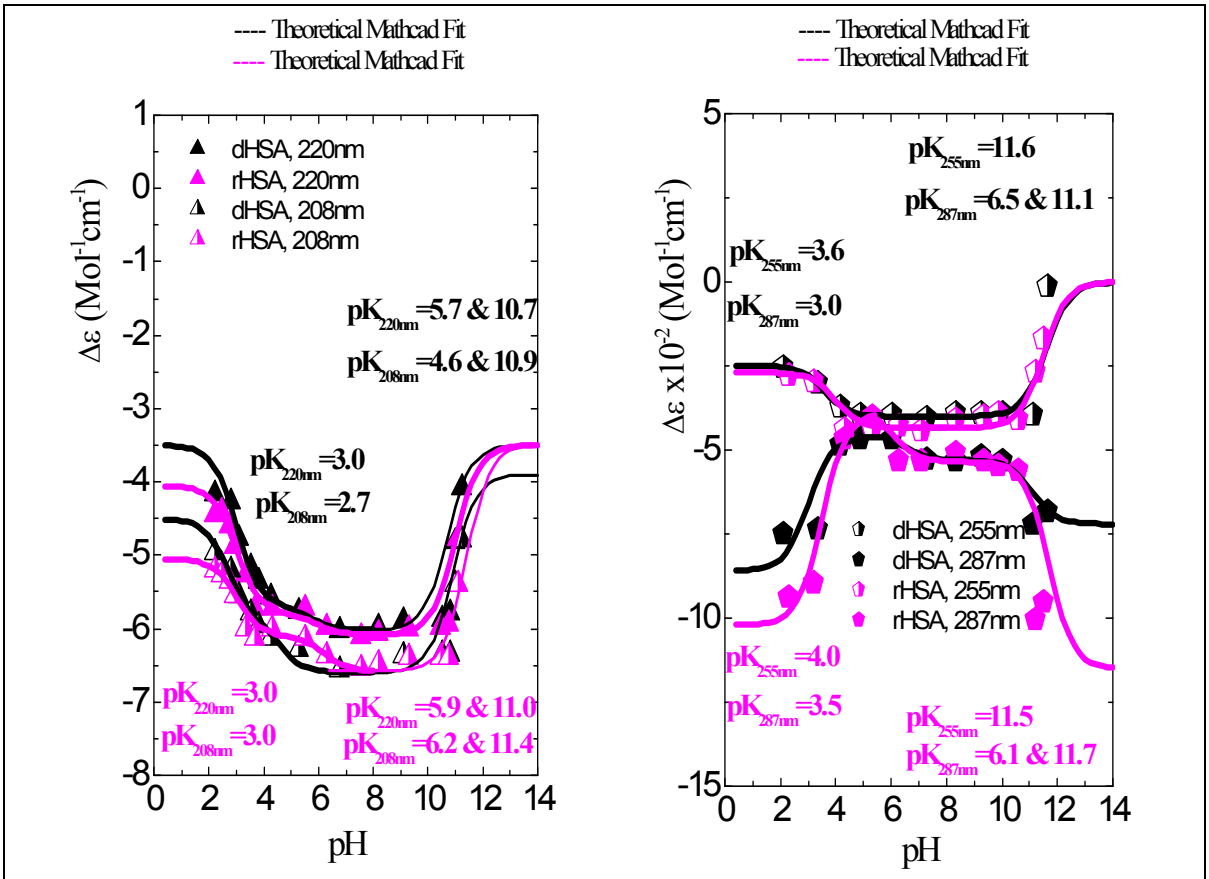

Figure 4.4. Fixed wavelength plots of recombinant and defatted HSA – pH titration.

Fixed wavelength plot of HSA in H2O, 6.02x10^{-6}M, 0.05cm, far UV CD plot
Fixed wavelength plot of HSA in H2O, 6.02x10^{-6}M, 1cm, near UV CD plot

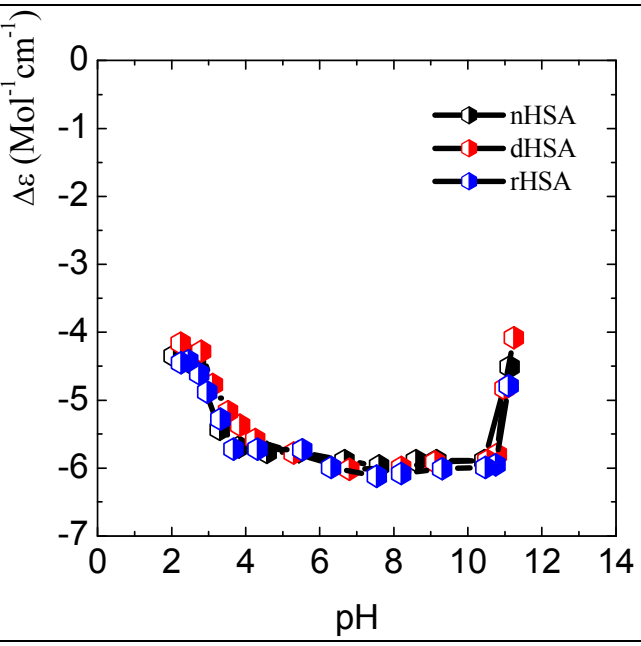

Figure 4.5. Superposition of the fixed wavelength plot of all the whole albumin samples.

Fixed wavelength plot of the pH titration of the three types of HSA, 4.51×10^{-6}M in H_2O at 220nm, 0.05cm

One of the first characteristic that was revealed by the pH titration was that when the data was fitted with Mathcad, three transitions were observed in the secondary structure region for wavelengths 208nm and 220nm. However, in the tertiary wavelength region, depending on which wavelength was viewed, either two or three transitions were observed as shown in Table 4.0. The first transition for all the samples studied gave a pK in the region of 3.0, with nHSA and dHSA showing the greatest similarities. The second transition at wavelength 208nm showed the greatest diversity with dHSA showing the lowest value for pK. All the transitions at 220nm revealed close similarities.

HSA Samples 4.51 x 10^{-6} M	**pK at 208nm Backbone**			**pK at 220nm Backbone**			**pK at 255nm Aromatic**		**pK at 287nm Aromatic**		
Transitions in pH Titration	**1st**	**2nd**	**3rd**	**1st**	**2nd**	**3rd**	**1st**	**2nd**	**1st**	**2nd**	**3rd**
nHSA	2.6	5.9	10.5	2.7	5.9	11.6	4.2	11.6	4.2	6.3	10.7
dHSA	2.7	4.6	10.9	3.0	5.7	10.7	3.6	11.6	3.0	6.5	11.1
rHSA	3.0	6.2	11.4	3.0	5.9	11.0	4.0	11.5	3.5	6.1	11.7

Table 4.0. Characterisation of the pH Transitions of all the HSA samples studied.

In the aromatic region of the spectrum only two transitions were observed at 255nm, but three transitions were detected at 287nm, this was reflective of the changing environment of the aromatic residues. It was clear that the two wavelength reflected different changes with the first transitions of each wavelength showing greatest diversity for all the HSA samples studied. Later on in this chapter pH studies of nHSA in the presence of small ions were conducted and compared with nHSA in the absence of ions. The changing environment in the presence of small ions on the protein will be compared and more fully studied.

Briton Robinson buffer (B/R) is a universal buffer with a wide buffering capacity and was chosen to investigate changing pH for this very reason. When the pH titration was repeated in the presence of B/R buffer the results revealed a transition at neutral pH different from that obtained when the titration was conducted in water (Figure 4.6.). B/R buffer, when freshly prepared attains a low pH value (~2.5) and the samples were prepared at this pH and titrated to higher values within the working range of the buffer (pH2-12). Between the pH regions of pH4 - pH8 a dramatic decrease in elipicity was observed in all three samples to varying degrees as shown (Figure 4.6.). Since B/R buffer contains a cocktail of boric acid, acetic acid and o-phosphoric acid, it was evident that one or a combination of several of the constituents in the buffer interacted with the protein resulting in the secondary structural changes observed. The effect in rHSA with the buffer was not as pronounced as that seen in the other samples indicating a certain degree of resilience; this may be as a result of the way in which the recombinant protein was produced. The effects of fatty acids also helped to protect the protein in some manner, resulting in a less dramatic effect on the protein in response to changing pH environments. In this way, the presence of fatty acids showed to have a stabilising effect on the protein, supporting the fact that in nature albumin contains naturally occurring bound fatty acids may act in this way. The greatest effect was detected at 208nm, and although the similar effects were seen at 220nm they

were not as pronounced. Maybe by dissolving the protein at such a low pH produced some kind of pH shock that provoked the protein into behaving in this manner. It is clear from the previous pH studies that there is a transition that occurs between pH6 and pH7, it is during this range that further interactions with ions take place. In any event, what was certain was that this buffer could not be used in further work with albumin due to its interactions at physiological pH.

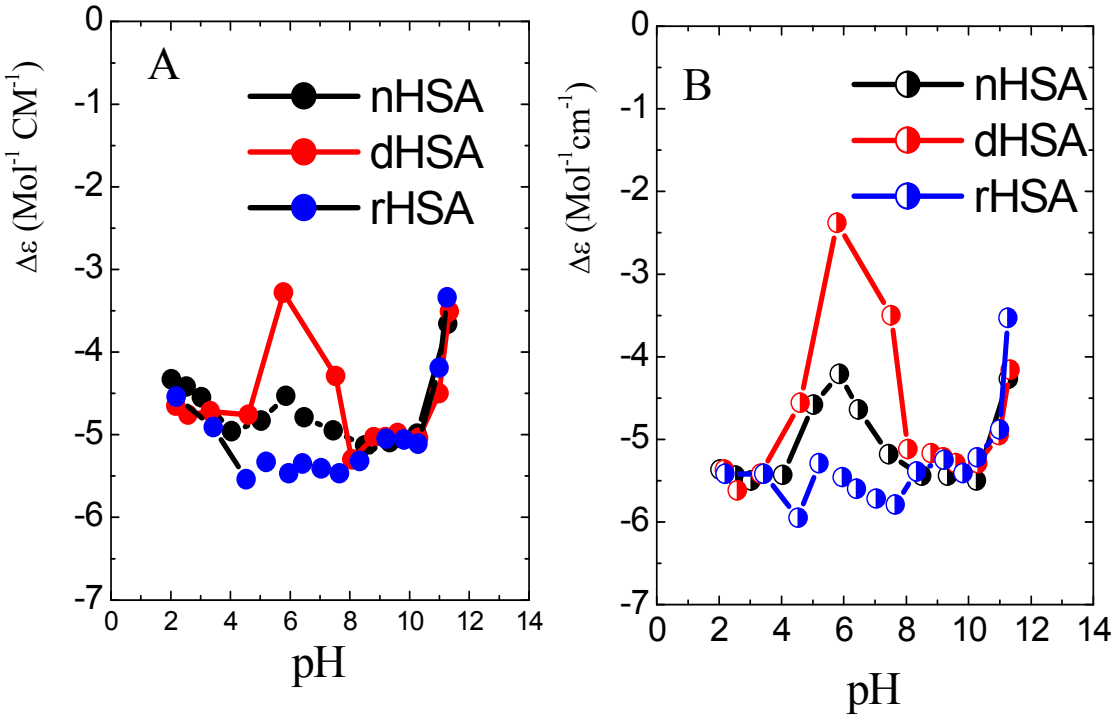

Figure 4.6. :Fixed wavelength plots of the three forms of HSA, 6.02x10^{-6} M in B/R buffer, 0.05cm; A = $\Delta\varepsilon_{220}$ versus pH and B = $\Delta\varepsilon_{208}$ versus pH.

4.3.i Conclusion of pH Studies

One can conclude from the initial investigation of pH that by monitoring the CD at different wavelengths different information can be extracted. If was possible to isolate and detect all the known transitional forms of albumin under pH considerations. The two regions as monitored by CD reflects the different transitions with the backbone susceptible to revealing the extended, neutral and aged forms of the protein, and the aromatic region,

namely at wavelength 255nm being the only wavelength able to detect the fast form of the protein. It is possible that at wavelength 287nm the fast form was also detected, however, the results from Table 4.0 were not as conclusive as for wavelength 255nm. Both wavelengths regions of the aromatic regions revealed the aged form with only wavelength 287nm detecting the neutral transition.

Initials studies by CD concurs with the findings of other techniques in that it is possible to study the different transformation forms of albumin by the use of pH, provided that the correct wavelength region is selected and monitored. None of the protein samples studied, however, could detect the basic form under pH considerations, this eluded the studies and in all forms relative stability was observed in the region (basic form isolated at pH8). There was notably a transition that underlies the neutral region that was isolated by CD studies and that was the transition that was detected between pH6 – pH6.5, highlighted profoundly when Briton Robinson buffer was used. The most pronounced effect was observed in dHSA, possible giving an indication of the lack of fatty acids present within the sample and the important role they play protecting the conformational forms of HSA under neutral conditions. The view is further supported by the results found in nHSA that appeared to be more resilient against that type of perturbation, thus producing a more diminished effect. rHSA proved to be the most resilient hardly being affected by the buffer , this could be as a result of the mode of synthesis.

4.4. Temperature Characterisation of Albumin by Circular Dichroism

One of the attributes of albumin is its ability to withstand heating to temperatures not exceeding 60ºC without deleterious effects, its size together with its secondary and tertiary structures shield the vital hydrophobic core structural components thus maintaining the integrity of the protein. The reversible changes that occur is thought to be due to the separation of domain I and domain II at these temperatures (*Rezaei-Tavirani et al, 2006*),

the unfolding was thought to be due to the presence of an unfolded intermediate as shown in Scheme 1. Under the unfolding process of Scheme 1 domain II is said to unfold first.

Native $\rightleftharpoons$ Unfolded Reversible $\rightleftharpoons$ Unfolded Irreversible **Scheme 1**

Studies have also shown that albumin's binding ability has not been compromised at these temperatures, and indeed heating albumin to 57ºC has become incorporated as part of the purification process in albumin preparations. Initial stability studies have shown once albumin had been heated to temperatures exceeding 57ºC the structural alterations that result remain fixed in the protein, with little to no recovery on cooling once temperatures above 60˚C is exceeded. Any recovery in structure was lost once the protein was reheated to the original temperature. For temperatures not exceeding 70ºC, the irreversible changes that occur is thought to be due to the irreversible unfolding of domain II (*Rezaei-Tavirani et al, 2006*). For temperatures exceeding 70 ºC produces the irreversible unfolding of domain I (*Flora et al, 1998*). Watzel and co-workers did not believe the unfolding of albumin occurred in such a simplistic picture, but believed that the unfolding occurred as a multistate process according to Scheme 2 (*Watzel et al, 1980*).

Native $\rightleftharpoons$ Extended Form $\rightleftharpoons$ Intermediate Form $\rightleftharpoons$ Unfolded Form **Scheme 2**

This can be rewritten as,

N $\rightleftharpoons$ E $\rightleftharpoons$ I $\rightleftharpoons$ U **Scheme 3**

Where E represents the separation of domains I & II, I represents the intermediate transition where domain II unfolds and domain I remains intact, and U represents the partly unfolded state where both domain I & II are both in the unfolded state, domain III is said to remain intact with no unfolding (*Shaklai et al, 1984*). There is a general loss of helix that is unrecoverable (*Walleyik, K., 1973*), with Cys 34, a free SH group located in a pocket, forming disulphides with other domains, assisting in intermolecular cooperation that allows some of the protein to retain its structure (*Flora et al, 1998*).

Differential Calorimetry Spectroscopy (DCS) studies have revealed two peaks for the unfolding of HSA, that of a major and minor peak. The minor peak was detected at 65 ºC, attributed to the reversible changes; the major peak was attributed to the irreversible changes that were detected at 70 ºC (*Saboury et al, 2003*). Deconvoluting shows the minor peak to possibly be constructed of three transitions that can be broken down and represented in Table 4.1, and are suspected to be due to the links between the domains (*Sugio et al, 1999*). The last transition that occurs at 42 ºC is also the maximum fever temperature in the body at pathological conditions. The presence of FA as that found in nHSA only produces two transitions when studied by DSC (*Farruggia et al, 2001*).

Sub-Transitions	ΔH, kJmol^{-1}	T_m, ºC	T_m, K
I	248	27	300
II	260	35	308
III	333	42	315

Table 4.1. DSC results showing the transitions of the minor peak of HSA.
(Rezoei-Tavirani et al, J of Biochem & Mol Biol, Vol 39, No. 5, 530 – 536, 2006)

4.4.i. Variable Temperature Wavelength Scans by CD Spectroscopy

Intact Protein Samples

All of the HSA samples studied showed similar trends. The effect of heating albumin was studied by two methods, at variable and at fixed wavelengths. Initial investigations involved the heating of HSA to a predetermined temperature, once at equilibrium the corresponding far UV CD spectra was measured within the wavelength regions of 260nm to 185nm (this is referred to as a variable wavelength scan), and its secondary structure was calculated. The temperature was increased by a suitable increment, once heated to the designated temperature the sample was allowed to equilibrate and its corresponding far UV CD measured. The same sample was scanned between temperatures of 20°C and 97°C, measuring at suitable temperature increments; this was referred to as the first temperature

cycle as the sample was heated through the whole temperature range once. The heated sample was then cooled to room temperature and reheated through a second temperature cycle to determine whether any further denaturation could be induced (known as the second temperature cycle). The CD spectra, melting curves together with secondary structural changes were plotted and the results are shown in Figures 4.7 to 4.10.

When considering the secondary structural changes, trends rather than absolute values were monitored and studied. All the HSA samples behaved in a similar manner to heat denaturation with the unfolding of the protein and the loss of α-helix. However, the β-sheet content and the irregular structure seemed to mirror each other, following parallel paths with the increase in content of both structural forms as a result of temperature increases. This was also true of the glycosylated form (L27-HSA) even though its initial content in terms of structure was different, the loss in α-helix was distributed evenly between the β-sheet and the irregular structure content.

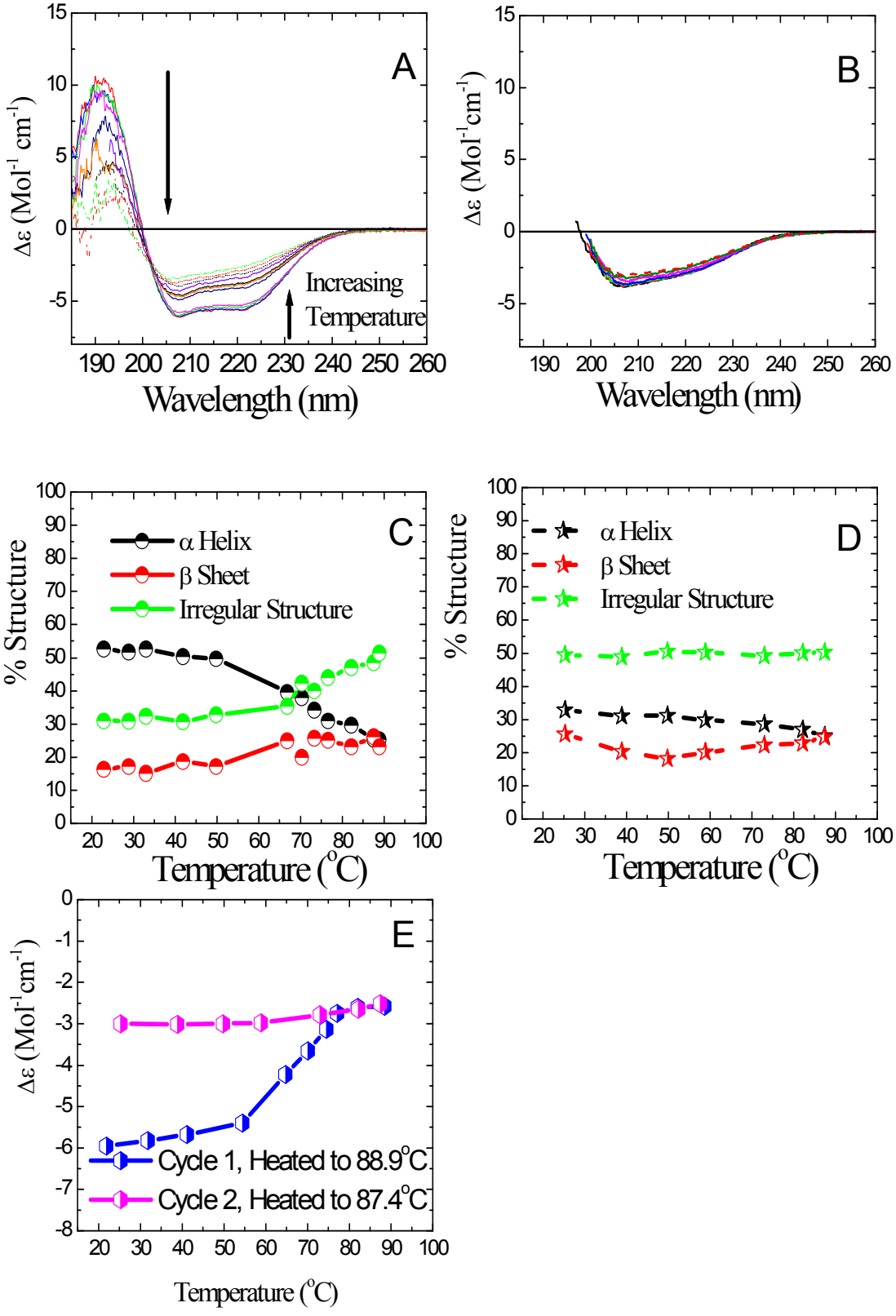

Figure 4.7. Heat denaturation studies of nHSA in 10mM P/B

A= Temperature cycle of nHSA ,6.02×10^{-6}M, P/B, pH7.2, 0.05cm.
B= Second temperature cycle in P/B.
C= Secondary structural changes in the first denaturation cycle.
D= Secondary structural changes in the second denaturation cycle.
E= Fixed wavelength plot heated through two temperature cycles.

The melting of HSA was not a single smooth isotherm as was expected, but seemed to show intermediate transitions indicative of domain or inter-domain unfolding; this was most prevalent in rHSA and L27-HSA as shown in the fixed wavelength plots of Figures 4.9. and 4.11. Like DSC, CD analysis revealed more than one transition on heating albumin with the consistent lost of a proportion of its helical content, even in the reversible section below 60°C. It was not possible to determine the exact number of transitions only that several (approximately 3 transitions) were found throughout the entire melting curve. The other albumin samples did display similar effects but the transitions were more subtle and not as well defined. The effects of these inter-molecular transitions were reproducible, and in order to isolate and characterise them more fully heat denaturation studies were monitored at fixed wavelengths. By monitoring at fixed wavelength and varying the rate of heating to incorporate much more discrete temperature increments, it may be possible to isolate and determine the intermediate transitions more precisely. As with the variable temperature scans, a second temperature denaturation cycle was also studied at fixed wavelengths in order to elucidate further possible changes in the denatured sample.

The investigations highlighted a core of protein structure that could not be perturbed even when the sample was boiled and/or reheated. There was a further loss in structure but this was minimal. The transitions seen in both temperature cycles were discriminate in terms of T_m values (the mid-point in the transition temperature) and values of K. The results were determined using a fitting routine in the Mathcad software package (Mathsoft plc), with the algorithm formulated especially to incorporate CD data (developed by T Bui, Thesis 1998). The results are summarised in Table 4.2. and the fitted overlaid data are shown in Figure 4.10 for both temperature cycles. From the Mathcad fit it was evident that the first temperature cycle contained on average three transitions whereas the second cycle contains two, this was true for all the intact HSA samples studied.

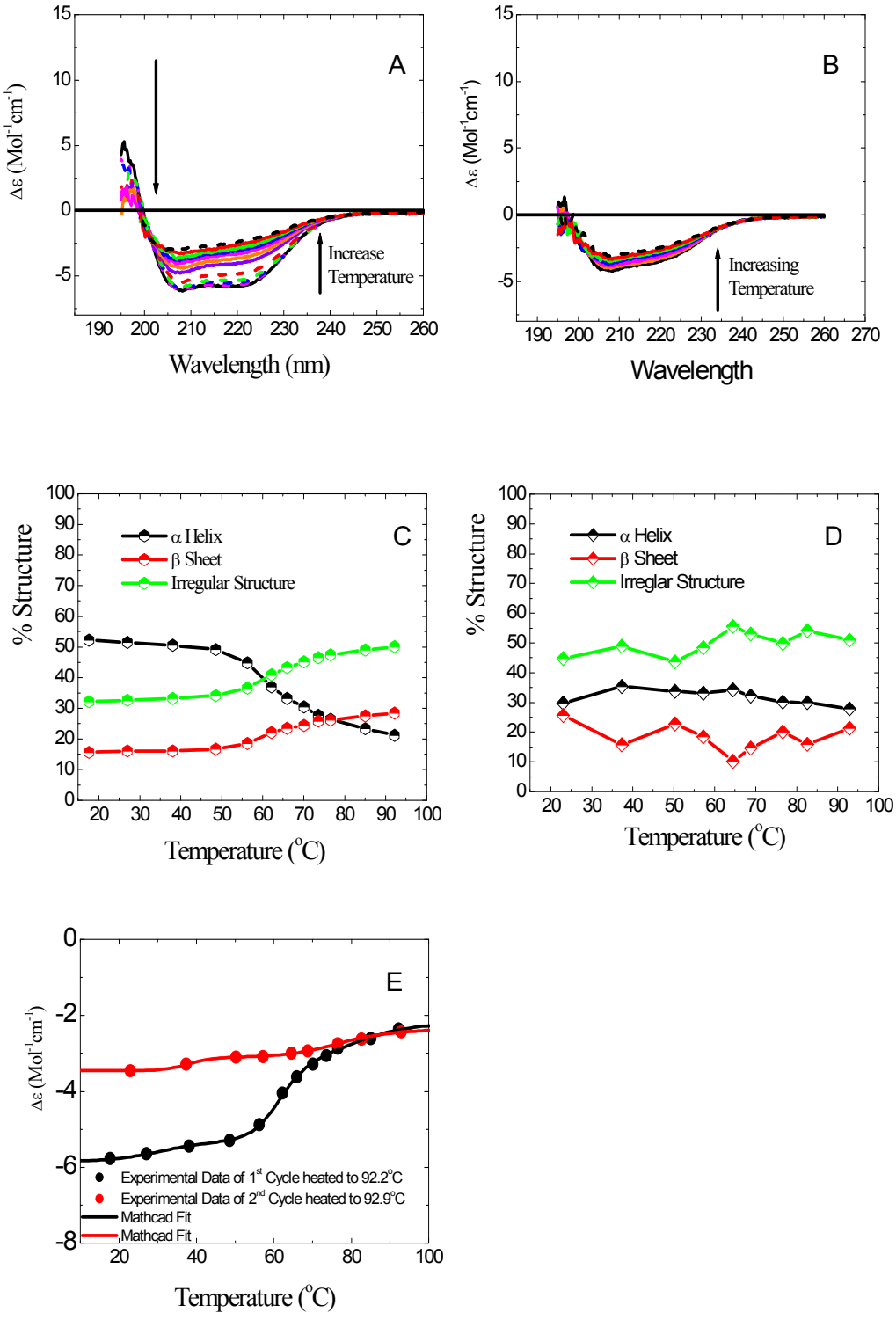

Figure 4.8. Heat denaturation studies of dHSA in 10mM P/B.

A= Temperature cycle of dHSA, 6.02×10^{-6}M, P/B, pH7.2, 0.05cm
B= Second temperature cycle in P/B.
C= Secondary structural changes in the first denaturation cycle.
D= Secondary structural changes in the second denaturation cycle.
E= Fixed wavelength plot heated through two temperature cycles.

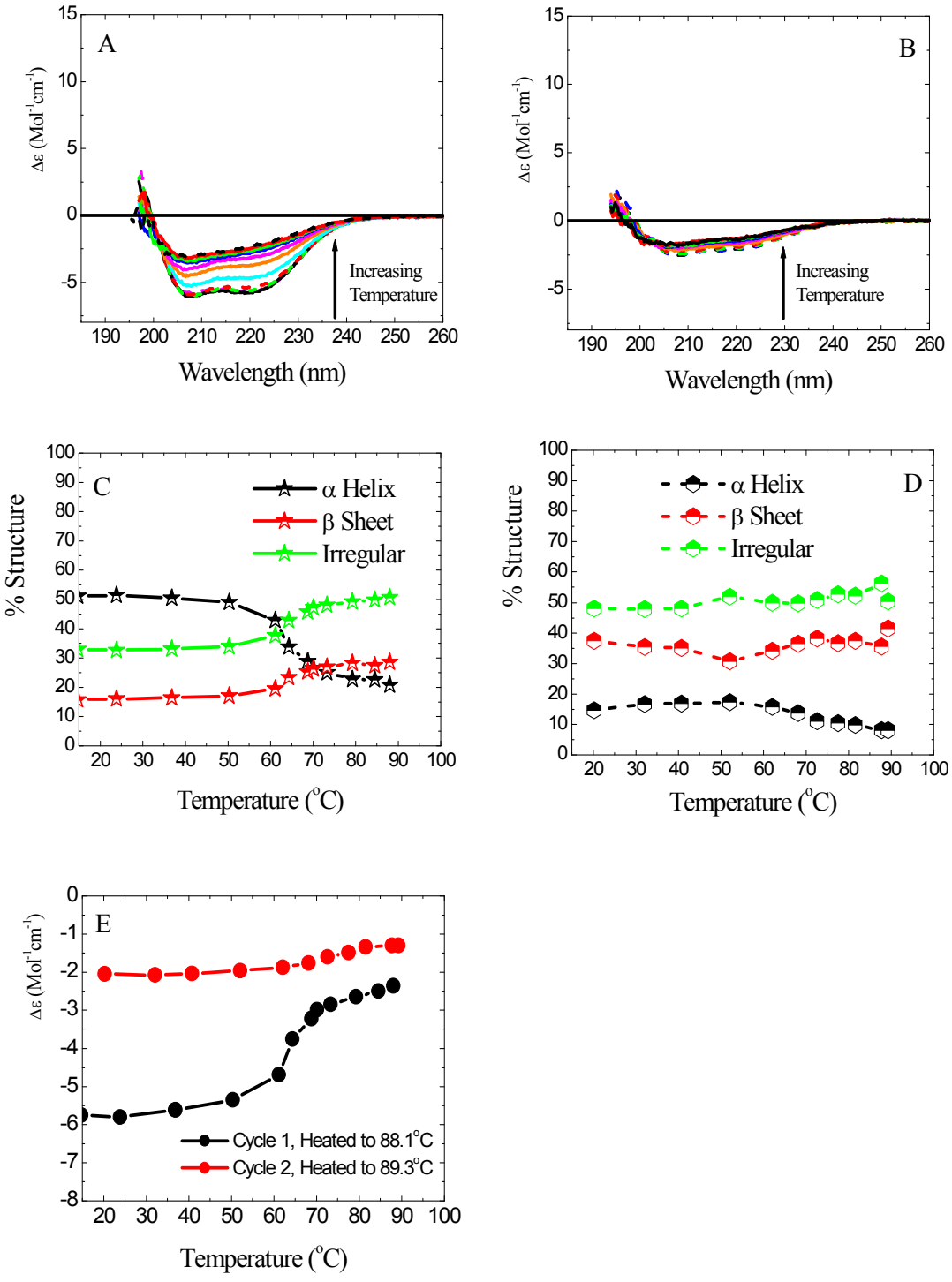

Figure 4.9. Heat denaturation studies of rHSA in 10mM P/B.

A= Temperature cycle,6.02x10^{-6}M, P/B, pH7.2, 0.05cm
B= Second temperature cycle in P/B.
C= Secondary structural changes in the first denaturation cycle.
D= Secondary structural changes in the second denaturation cycle.
E= Fixed wavelength plot heated through two temperature cycles.

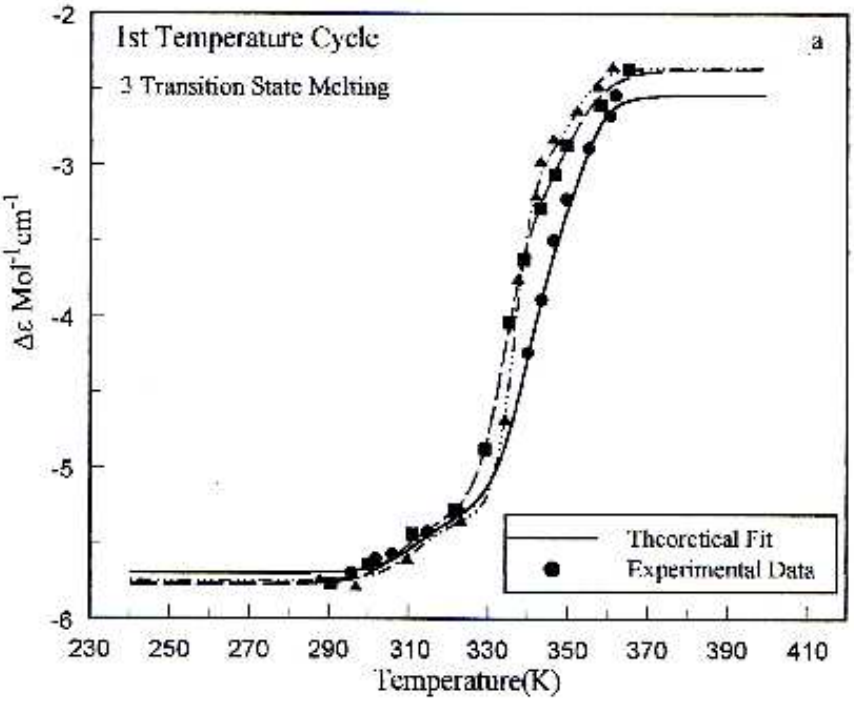

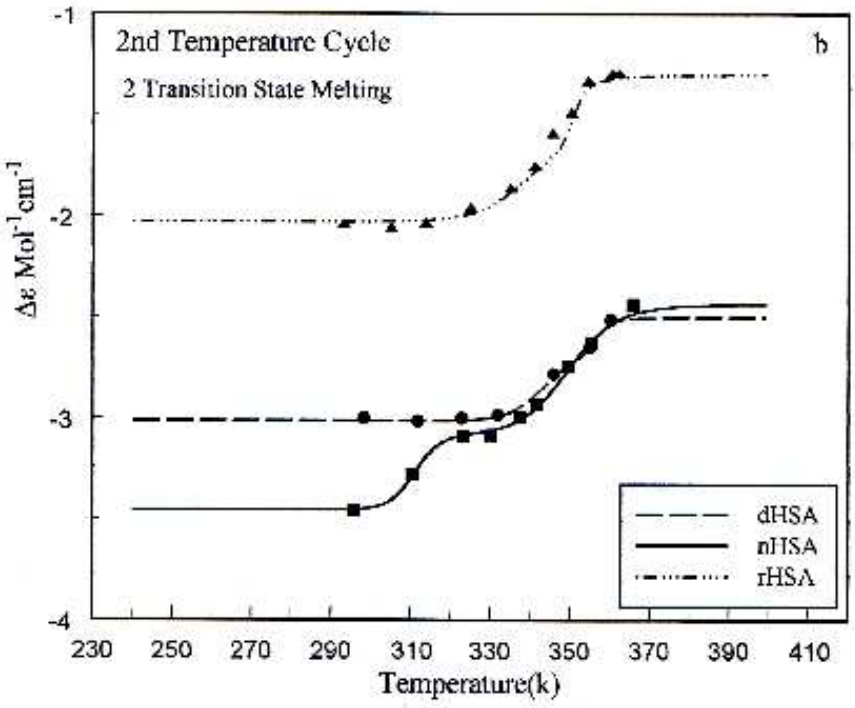

Figure 4.10. Superposition of the three forms of albumin using the Mathcad fit

a = The first temperature cycle revealed that the melting curves of dHSA and rHSA showed similar melting profiles, while that for nHSA highlighted a slightly higher T_m.

b = The second cycle reflected greater similarities between nHSA and dHSA with rHSA being the exception. On cooling, dHSA showed some signs of recovery which allowed it to follow a similar path to nHSA. All samples at concentration 6.02×10^{-6}M.

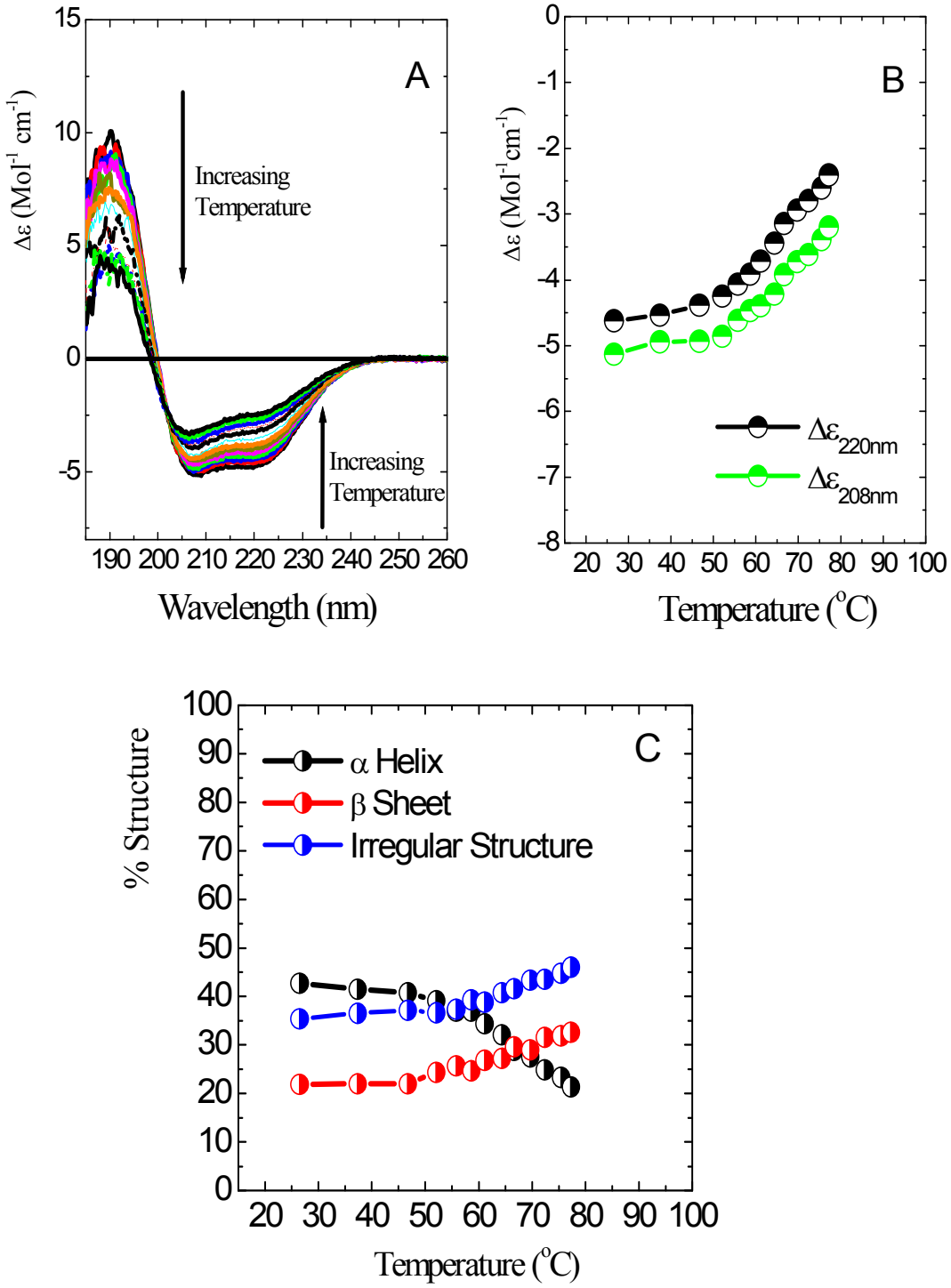

Figure 4.11. Heat denaturation studies of L27-HSA in 10mM P/B.

A= CD spectra of the heat denaturation of L27-HSA ,6.02x10^{-6}M, P/B, pH7.2, 0.05cm
B= Fixed wavelength plot of L27-HSA.
C= Secondary structural changes caused by heat denaturation.

Using the Mathcad fits, the T_m and K values were determined for each of the whole albumin samples and Table 4.2. was constructed for comparison of the first and second temperature cycles.

Intermediate States of		**1st Cycle**			**2nd Cycle**	
		1st	2nd	3rd	4th	5th
nHSA	T_m (K)	310.0	340.0	355.0	343.0	357.0
	$Kx10^{-3}$	18	25	40	25	90
dHSA	T_m (K)	304.0	334.5	353.0	311.0	350.0
	$Kx10^{-3}$	18	31	40	30	18
rHSA	T_m (K)	313.0	336.5	352.0	334.0	348.0
	$Kx10^{-3}$	18	45	40	35	16
L27-HSA	T_m (K)	329.5	336.5	347.0	-	-
	$Kx10^{-3}$	12	35	60	-	-

Table 4.2. Melting temperatures and the equilibrium constant of the different forms of HSA for two temperature cycles.

Table 4.2. highlights that for the various forms of HSA, three main intermediate transitional states were isolated for the various whole forms of albumin, with similar equilibrium constants for the first and third transitional intermediates observed with the exception of L27-HSA. However, the T_m was noticeably lower for dHSA than for nHSA and rHSA, with L27-HSA showing no similarities to the other forms. Both the K values and the T_m for the second intermediate transitional state showed no similarities in all of the forms studied, no general trends were observed, each sample behaving slightly differently. It should be noted that the DSC results listed for nHSA in Table 4.1. gave different results to that observed by the CD analysis, with at least two transitions observed in DSC occurring at much lower T_m temperatures than the CD. This suggests that the two techniques may be observing different structural changes, as will be shown later the fixed wavelength measurements isolates approximately seven potential intermediate transitions, showing that the DSC could have isolated temperature transitions not found by the variable wavelength scans. The exception to the general rule observed was that found for L27-HSA

that seemed to give a much higher value for T_m and a much lower K value for the first transition. The third transition was equally as diverse revealing a much lower T_m and a much higher K value for this transition. One would expect the folding of the protein to be somewhat different in L27-HSA in order to accommodate the presence of the additional sugar molecule. However, one would expect this change to be small. Indeed the CD analysis revealed a 5% loss on helical content and an 8% loss of β-sheet content. In binding the sugar, the folding geometry has changed sufficiently to alter the melting profile, and although three melting transitions are observed, their values are all different from any of the other three whole albumin samples studied.

Although the second transitions for the first temperature cycle were energetically higher than that of the first, they showed diversity between the different forms of albumin that made it difficult to generalise or summarise. Considering the values of K for the first temperature cycle, two distinct groups emerged, the intermediate transition state 1 and the intermediate transition state 3. No obvious trends however were observed for the values of T_m, all samples of albumin studied showed differing results with no general trends observed. For the last transition in the first temperature cycle nHSA, dHSA and rHSA showed exactly the same values for K, with L27-HSA proving once again to be the exception, melting at a much lower temperature;

The second temperature cycle highlighted the existence of two further transitional intermediate states with no correlation between the different forms. All samples showed a small degree of initial recovery in some structure on cooling after the first temperature cycle, shown as an increase in magnitude in the CD spectra suggesting some sort of internal reorganisation (see Table 4.3.). This however was transient, once heating recommenced, this recovery was soon lost and further denaturation resulted even though this was minimal. Figures 4.7.d. to 4.9.d. showed that the main conformational change

observed occurred within the β-sheet and irregular structures, with the α-helix content remained relatively constant. It appears that the α-helix content of the protein was mostly affected during the first denaturation cycle with the subsequent increase in the other two structural components. The reverse was true for the second temperature cycle where the helical content was relatively unaffected.

Protein	Structure	Initial Content (%)	% Structure after 1st Temp Cycle	% Recovery (after heating)	% Structure after 2nd Temp Cycle
nHSA	α-Helix	52.7	25.4	26.9	25.0
	β-Sheet	16.3	23.1	31.6	24.7
	Irregular	31.0	51.5	41.4	50.3
dHSA	α-Helix	52.2	21.1	29.8	27.8
	β-Sheet	15.6	28.5	25.6	21.3
	Irregular	32.2	50.4	44.7	51.0
rHSA	α-Helix	51.2	20.8	14.6	8.1
	β-Sheet	15.8	28.6	37.4	41.5
	Irregular	33.0	50.6	48.0	50.4
L27-HSA	α-Helix	42.7	21.3		
	β-Sheet	21.9	32.6		
	Irregular	35.4	46.0		
Domain 1	α-Helix	32.6	20.7		
	β-Sheet	27.7	29.6		
	Irregular	39.7	49.7		
Domain 1+2	α-Helix	39.1	21.4		
	β-Sheet	24.3	29.5		
	Irregular	36.6	49.1		

Table 4.3. Secondary structure changes observed during the heating cycles.

From the CD studies, it is hard at this present time to show what the inter-transitional states truly represent. It is clear that HSA undergoes some structural rearrangement and unfolding with the unfolding of domain II that is said to occur preferentially first, followed by domain I. Domain III is said to remain unaffected and intact throughout the whole heating process, and although this fact cannot be either confirmed or disproved, this theory will be investigated at a later stage in this thesis when preheated samples of the whole protein will be tested for binding ability using specific marker ligands known to bind to specific sites

HSA Fractions

Small amounts of the domain fractions, namely domain I and domains I + II, were made available for select experiments, and were used to determine whether the intermolecular transitions observed in the intact samples were as a result of domain or subdomain deformation (domain fractions were also used in some drug binding studies as will be seen later). Initial investigations revealed a high amount of irregular structure relative to the whole fragments, with a high amount of β-sheet at the expense of the α-helix. This may be as a result of the way the fragments were generated, in that it is recognised that the production of some domain fractions might not fold in the recognised conformation as in the intact sample. Heating the fractions produced changes similar to those observed for the intact protein with the loss of helical structure as demonstrated in Figures 4.12.a. and 4.13.a., with the isolation of intermolecular transitions found previously in the whole samples. The high amount of irregular structure was prevalent when the fixed wavelength plots were constructed with the % helix noticeably lower. Unlike the whole protein, the domain fraction's β-sheet content and irregular structure did not seem to follow the parallel paths as shown previously, but the generation of β-sheet seem to decline with the increase of temperature, with a more rapid formation of irregular structure. The crossover between the helical and the β-sheet content occurred at a much lower temperature in the domain fractions than in the intact protein, occurring around 60°C as opposed to around 70 - 73°C for the intact proteins. nHSA gave the highest crossover value of around 87°C, maybe as a result of its FA content. Interestingly, L27-HSA produced a crossover at around 65°C, midway between the domain fractions and the intact samples; this must be a result of the presence of sugar within the molecule and the way the sugar molecules impacts upon the folding of the molecule.

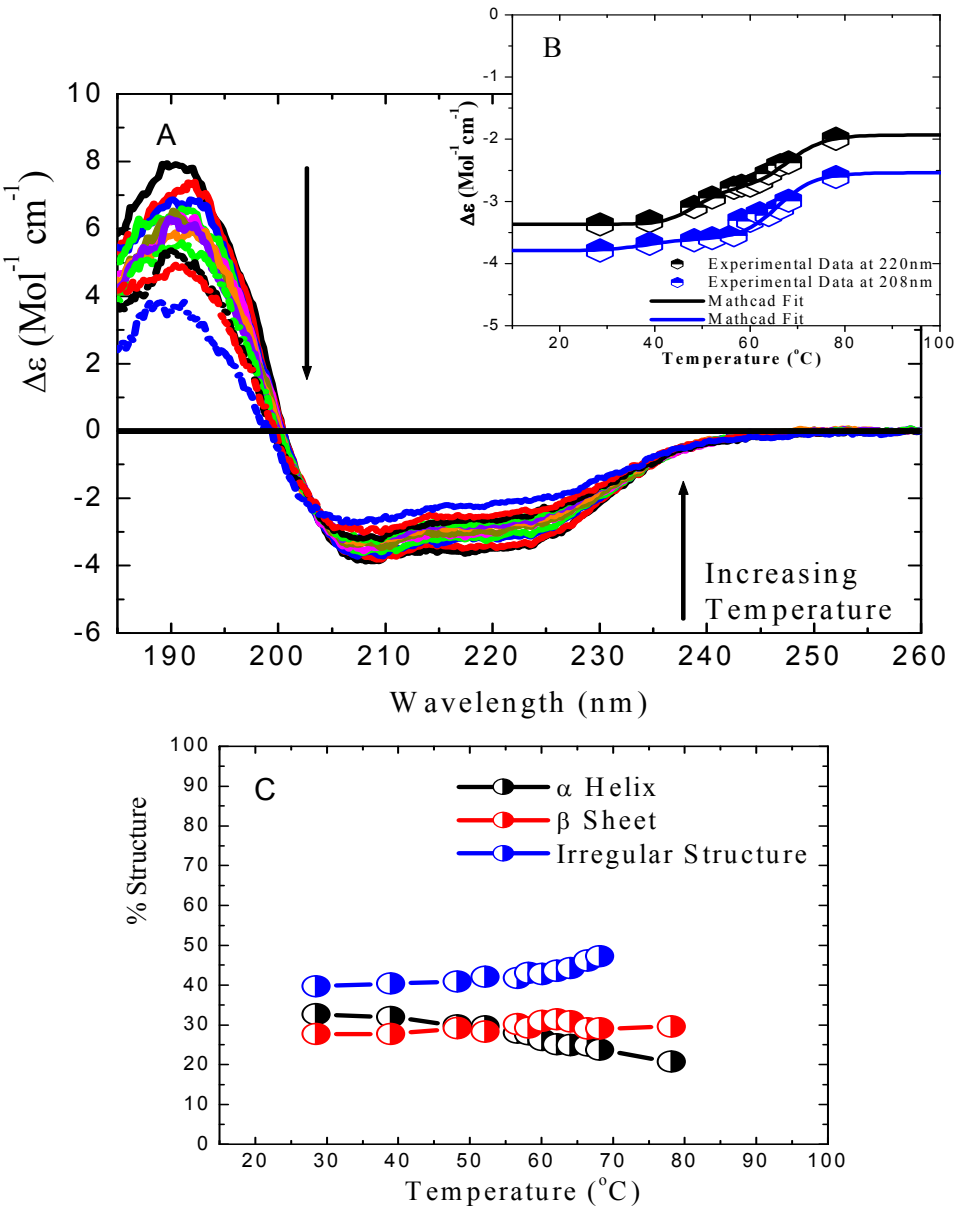

Figure 4.12. Heat denaturation studies of Domain I in 10mM phosphate buffer.

A. CD spectra of the heat denaturation, 1.53×10^{-5}M in 10mM P/B, pH7.2, 0.05cm
B. Fixed wavelength plot of the heat denaturation at 220nm and 208nm.
C. Secondary structural changes caused by the heat denaturation cycle.

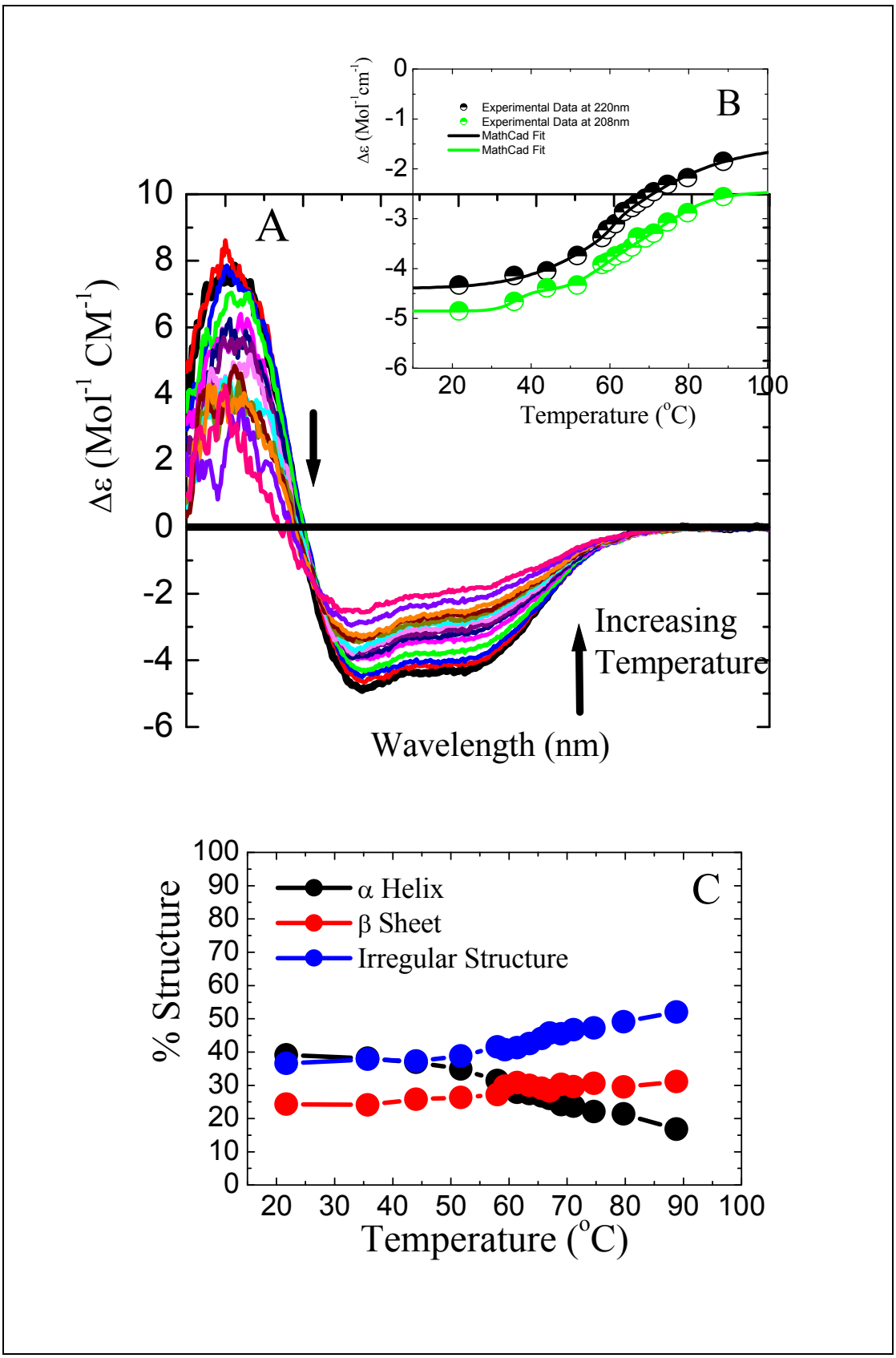

Figure 4.13. Heat denaturation studies of Domain I+II in 10mM phosphate buffer.

A. CD spectra of the heat denaturation, 1.32×10^{-5}M in 10mM P/B, pH7.2, 0.05cm
B. Fixed wavelength plot of the heat denaturation at 220nm and 208nm.
C. Secondary structural changes caused by the heat denaturation cycle

HSA has three equally sized domains similar in structure, therefore it is conceivable to expect domain I to have 1/3 of the structural content of whole HSA and domain I + II to have approximately 2/3 of the intact structural content. Experimental analysis of the fractions has found domain 1 to contain more than 2/3 of the total helical content, and a β-sheet content much higher than that found in the whole protein. One must consider that by producing fractions the mechanism of folding may be compromised resulting in the end product not being a true representation of that fraction if present in the intact sample. Secondary and tertiary structural constraints are not only affected by the primary sequence but also by the size of the protein as a whole, various interactions that may have been present previously may no longer exist. Table 4.4. shows the percentage structure of rHSA compared to the domain fractions that were derived from rHSA and introduced a structural factor which should adjust the percentage to allow for size. The factor was derived from the multiplication of the percentage structure and the number of residues present. The table shows that even taking into consideration the number of residues present in each fraction, the changes observed were more than can be explained by a multiplying factor. The folding of the fractions appears to have altered as a direct result of their preparation.

Protein	Number of Residues	Structure	Initial Content (%)	Structural Factor ($x10^4$)	Structure after 1st Temp Cycle (%)	Structural Factor ($x10^4$) after Heat Cycle
rHSA		α-Helix	51.2	3.0	20.8	1.2
	585	β-Sheet	15.8	0.9	28.6	1.7
		Irregular	33.0	1.9	50.6	3.0
Domain 1		α-Helix	32.6	0.6	20.7	0.4
	195	β-Sheet	27.7	0.5	29.6	0.6
		Irregular	39.7	0.8	49.7	1.0
Domain 1+2		α-Helix	39.1	1.5	21.4	0.8
	390	β-Sheet	24.3	0.9	29.5	1.2
		Irregular	36.6	1.4	49.1	1.9

Table 4.4. Percentage comparison of rHSA with the Domain fractions.

The structural content determination was based on the Principal Component Regression with the algorithm based on the CD spectra comparison from the protein calibration data set.

Heating the samples through the first temperature cycle reflected more consistently with expectations in terms of secondary structural content for the intact samples. Domain I contained one third of the helical content of the intact, and domain I + II containing two thirds, the other structural content also follow suit. Table 4.5. shows the thermodynamic properties of the domain fractions after the first denaturation cycle with reference to rHSA as comparison. Domain I + II exhibited three transitions in the first denaturation cycle, whereas domain 1 only possessed two. All of the intact samples of HSA studied gave a value for their first transition enthalpy of 18 x 10^3kJmol^{-1}, neither of the fractions reflected this (compare Table 4.1. and 4.5.). The T_m of the fractions were also non reflective of the whole protein giving much higher values, only L27-HSA gave a similar value to the fractions, much higher than the other three intact proteins.

Intermediate States of Transition		**1st Heat Denaturation Cycle**		
		1st	2nd	3rd
rHSA	T_m (K)	309.0	334.0	351.0
	Kx10^3	18	30	25
Domain 1	T_m (K)	311.5	339.0	-
	Kx10^3	23	30	-
Domain 1+2	T_m (K)	324.0	333.0	347.0
	Kx10^3	10	80	9

Table 4.5. Properties of the Domain fractions

The 2nd intermediate transitional state revealed that although the values of K varied vastly with the domain fractions giving a much higher value in the case of domain I + II, and much lower value for domain I, the T_m's were similar. The 3rd intermediate transitional reveals once again the similarities in domain I + II to the intact protein, the absence of this transition in domain 1 may prove to be the significant factor to differentiate the ligand binding abilities between the two domain fractions (see Chapter 5). It is worth noting that values for the second intermediate transition between domain I and rHSA supports the theory that domain II unfolds first, leaving domain II relatively intact.

4.4.ii Fixed Wavelength Measurements by CD Spectroscopy

The unfolding of a protein can be monitored at a fixed wavelength with respect to time/temperature. The CD spectrometer was set to monitor HSA unfolding at 220nm, one of the negative maxima, to determine whether the small intermediate transitional state observed previously during the variable wavelength scans could be isolated, highlighted and characterised. The spectrometer was initially set to record over a fixed period of 30 minutes for all of the HSA samples used, including the domain fractions; all the results are shown in Figure 4.14. as an overlay so that all samples cold be compared under the same conditions. Once again, the transitions highlighted in the full scans were evident in the fixed wavelength scans, showing the same triple transitional states when the data was corrected and put through the Mathcad package (Figure 4.14.b.).

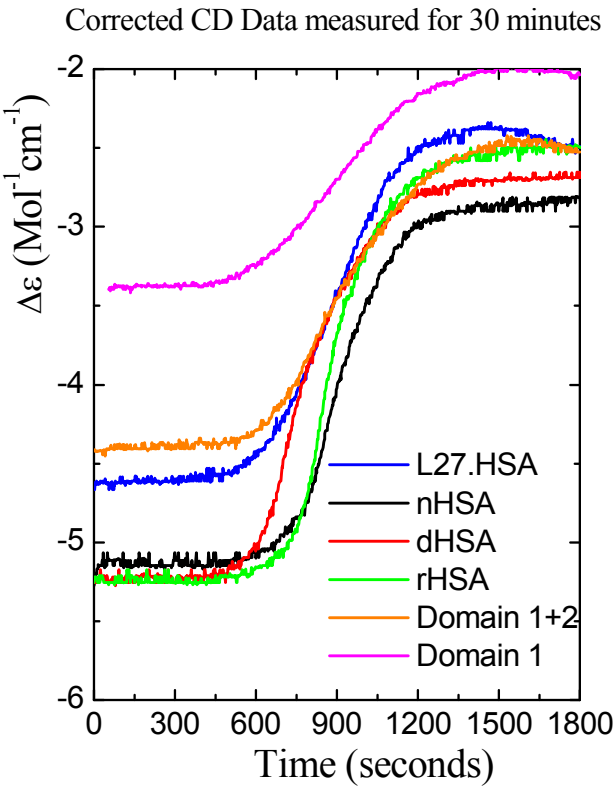

Figure 4.14.a. Superposition of the corrected data for the fixed wavelength plots of HSA.

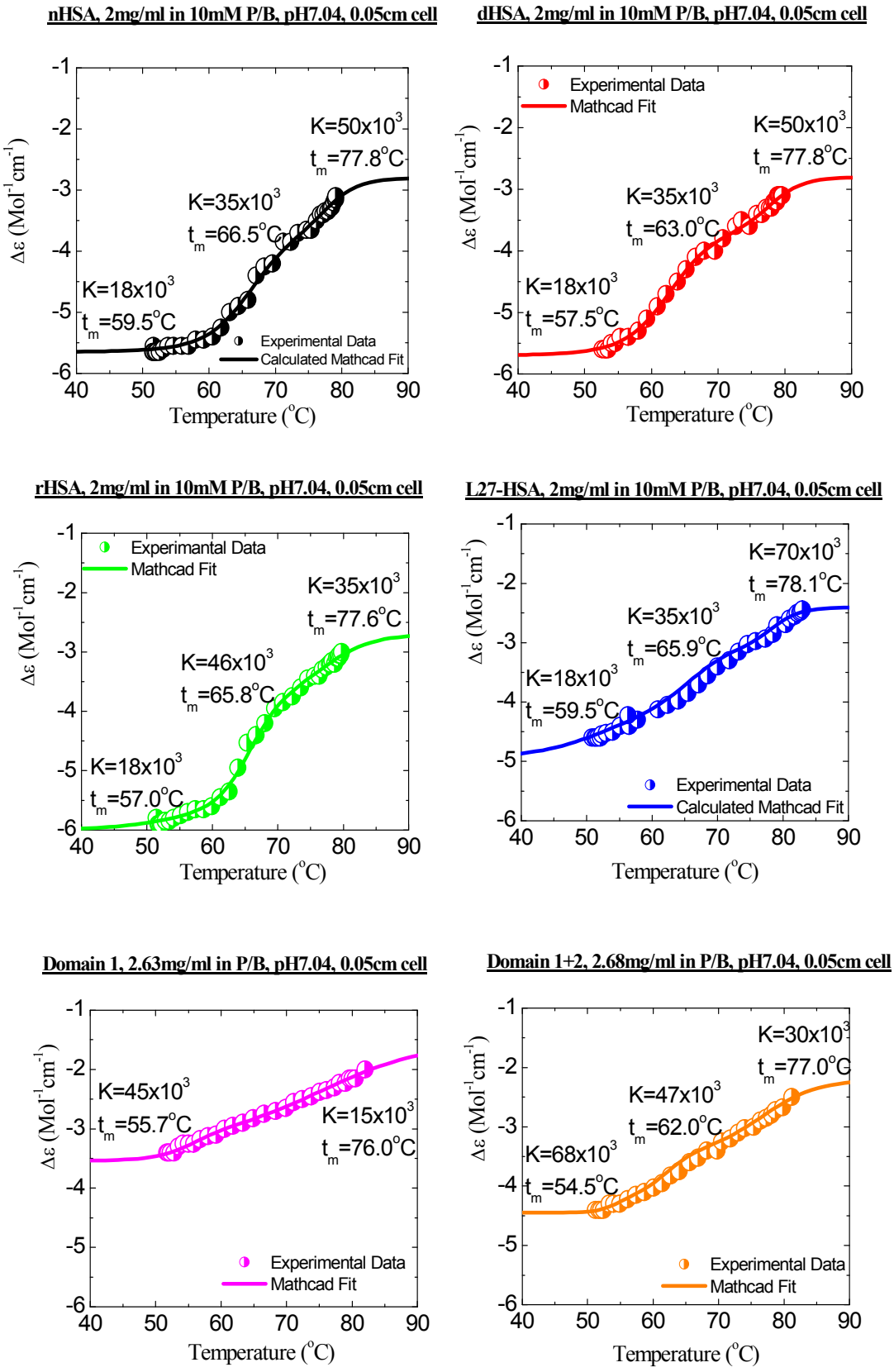

Figure 4.14.b. Mathcad fits of the fixed wavelength plots for the 30 minute scans, corrected for temperature, of the different forms of HSA.

Calculating the first derivatives for the melting curve of the intact samples of albumin for nHSA, dHSA and rHSA (data not shown) isolated between 7-10 peaks that may relate to the interstate transitional states. In order to try to characterise these transitions fully, scans were repeated and measured over a longer period of time, increasing the temperature by single degree increments, this was done to locate the exact position of the transitions. However, instead of clarifying the situation, the single degree increments reduced the clarity of the transitions, no further information could be extracted or gained. The Mathcad fits revealed three main transitions for the whole proteins and for the domain I + II fraction in line with the results previously determined, and for domain I, two intermediate transitional states were found. All results were consistent with that determined by the wavelength scans in terms of intermediate transitions, however, the values determined for t_m and K were different (Table 4.6.).

Intermediate States of Transitions		1st Temperature Cycle		
		1st	2nd	3rd
nHSA	T_m (K)	332.5	339.5	350.8
	$Kx10^3$	18	35	50
dHSA	T_m (K)	330.5	336.0	350.8
	$Kx10^3$	18	35	50
rHSA	T_m (K)	330.0	338.8	350.6
	$Kx10^3$	18	46	35
L27-HSA	T_m (K)	332.5	338.9	351.1
	$Kx10^3$	18	35	70
Domain I	T_m (K)	328.7	349.0	
	$Kx10^3$	45	15	
Domain I + II	T_m (K)	327.5	335.0	350.0
	$Kx10^3$	68	47	30

Table 4.6. Mathcad fit of the fixed wavelength scans for the unfolding of the albumin samples.

The first intermediate transition gave a value of K=18 x 10^3 for all intact samples, even for L27 HSA, somewhat agreeing with the results of the variable wavelength scans, except for L27 HSA that was found to have K=12 x 10^3. With respect to the domain fractions, the

values of K were much higher than those detected for the variable scans with a possible discrepancy of 22 x 10^3 & 58 x 10^3 for domain I and domain I + II respectively. These results for the domain fractions seem questionable, however, when you consider that for the intact samples gave values of K that were identical, perhaps the two techniques may not be monitoring the same transitions; this will be investigated further when pre-heated samples are considered. Considering the T_m values for all the samples, the values were found to also be considerable higher by as much as 22K for the intact samples and 16K for the factions. The disparity in the second and third intermediate transitions were not as dramatic and proved to be more consistent with those determined previously.

4.4.iii CD Analysis of Pre-Heated HSA Samples

The effects of pre-heating HSA was investigated in one of two ways. The first method involved pre-heating a stock solution of HSA of known concentration in a thermostatically controlled water bath of known temperature (e.g. 50^{o}C). Once the desired temperature was reached within the sample, an aliquot was removed and cooled to room temperature. The temperature of the bath was increased (e.g. 58^{o}C) and another aliquot was removed after equilibrium was attained and maintained within the sample. This process was repeated until a selection of samples were acquired, each heated to different but predetermined temperatures from the same stock solution and all cooled to room temperature and can be referred to as the pre-incubated samples. The pre-incubated samples were then measured with the CD spectrometer, heating each sample from RT to 90^{o}C monitoring at fixed wavelength (λ in nm). The results are shown in Figure 4.15.; HSA seems to follow a specific melting profile referred to as the primary melting curve as shown for the data determined for the pre-incubated sample heated to 50^{o}C, the melting profile is shown in Figure 4.15. All the pre-incubated samples joined the primary melting curve at a designated position determined by the temperature to which the sample was incubated, each joining the primary melting curve at the exact temperature to which it was incubated

at. Since all the incubated samples were cooled to room temperature, as seen previously some recovery was obtained on cooling but this was minimal. Once heated, any residual gain in structure was soon lost; the melting curves seem to follow parallel paths until the incubated temperature was achieved. Heating HSA to temperatures not exceeding 60^{o}C had little effect on the structural integrity of the protein thus affirming that heat treatment process of albumin.

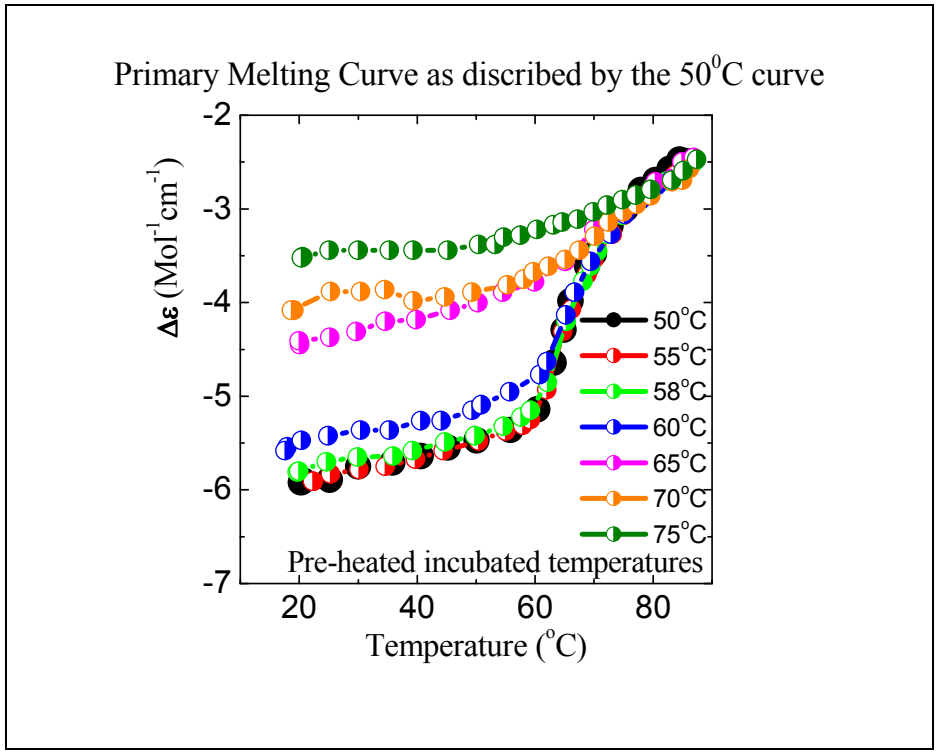

Figure 4.15. Melting curves of the incubated samples of rHSA, 6.02x10^{-6}M in 10mM P/B, 0.05cm cell.

A second thermal method was employed that involved the use of a single stock solution of protein that was heated through a series of small temperature cycles; a stock solution of HSA (concentration 0.4mg/ml in 10mM P/B) was made up to ensure all samples used in this experiment derives from the same stock solution. A sample was taken and places into the CD spectrometer, the water-bath was set to a known temperature (50˚C) and allowed to heat. As the bath heated the spectrometer was initiated and the unfolding of the protein monitored at fixed wavelength until the designated temperature was reached, and the complete melting for that temperature had been achieved. Once at equilibrium further

measurements were recorded, then the thermostat on the water bath was reduced to room temperature and the sample was allowed to cool, monitoring its cooling curve by CD in the process. When the sample had reached room temperature the thermostat was adjusted to the maximum temperature (95˚C) and the sample monitored for its complete unfolding. This process was repeated, each time choosing a higher designated temperature and monitoring its melting curve, cooling curve and then complete unfolding curve for each temperature increment chosen, producing cycling heating curves for temperatures up to 75^{o}C. The results are displayed in Figure 4.16. and Table 4.7.

Like the pre-incubated samples, rHSA followed a designated and well-defined primary melting curve. Both the pre-incubated samples and the heated samples, at the same designated temperature, followed exactly the same melting curve which was characterised by that temperature. The length of time to which the samples were heated played no significance to the end results and was not a determining factor, i.e. no time dependence. The unfolding of the protein was instantaneous, producing consistent, yet reproducible degrees of unfolded intermediates characteristic to that temperature (Figure 4.14.). Like the variable wavelength scans, little/no denaturation was detected for temperatures below 58^{o}C. However, for temperatures exceeding 60˚C, varying degrees of denaturation were detected that were characterised by the temperature to which they were heated. It was possible to determine the degree of denaturation samply by the profile of the CD spectra and by the secondary structural content at that temperature. No matter how the sample was heated HSA always rejoined the primary melting curve and followed the same profile of unfolding when heating resumed. The criterion that affected HSA was the specific temperature, only this determined the degree of unfolding.

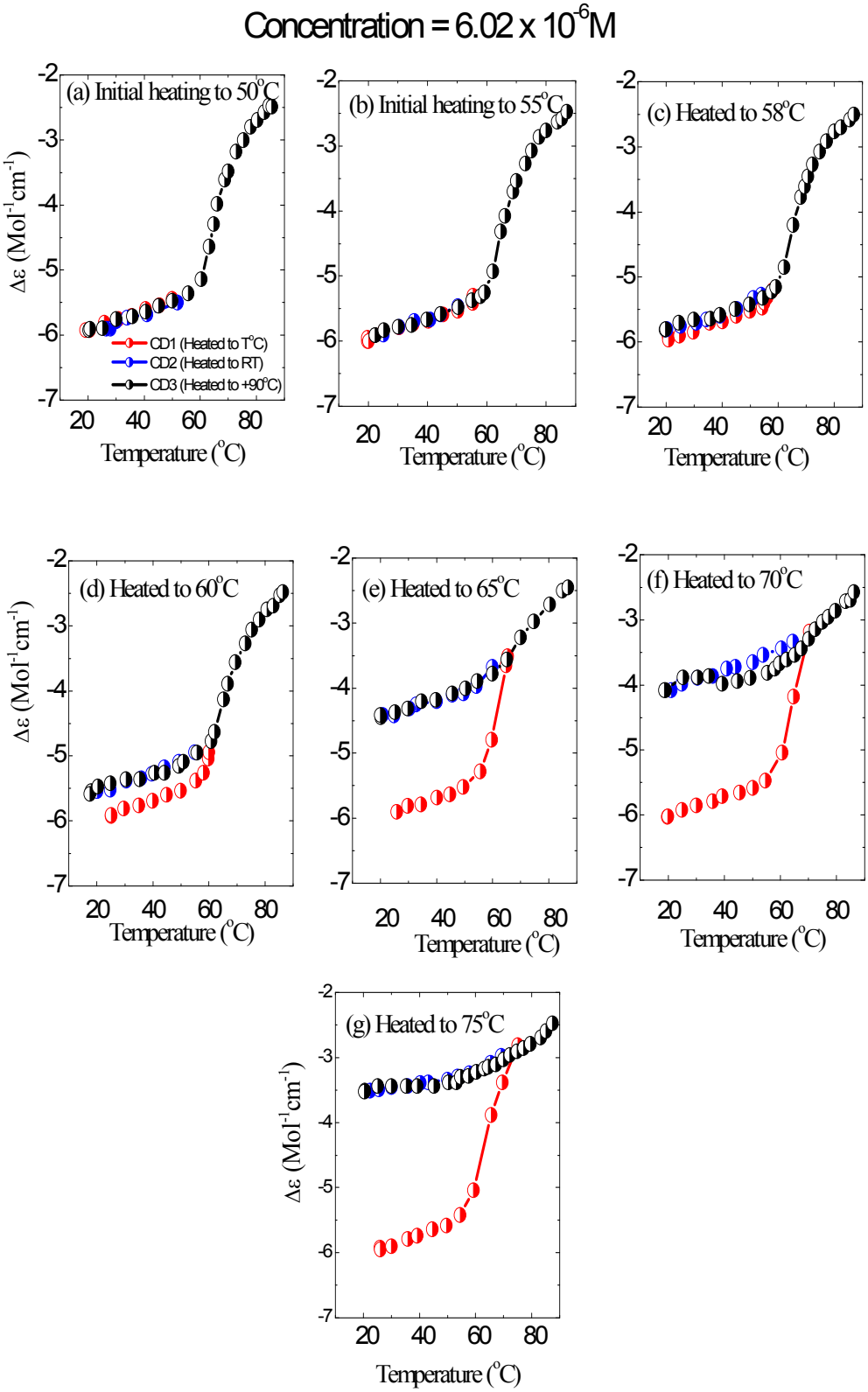

Figure 4.16. Melting profiles of rHSA showing the primary melting curve. Heating Curve → Cooling Curve → Melting Curve

It is clear from Figure 4.16. that there is a definite and well define melting profile that albumin will follow when heated. Regardless of what temperature to which the protein is heated and cooled down to RT, once heating recommences, the protein will rejoin the melting profile at the point at which it was previously heated to and unfolds/melts along the preferred melting curve. As shown in Figure 4.16.(c)., no visible effects of heating is seen within the protein until a temperature of 58˚C is achieved, then small changes are observed attributed to the domains and/or inter-domain separation. Heating to 60˚C gives bigger visible effects on the protein, but from previous measurements, although there appears to be some sort of loss in structural integrity, this is due to the residues between the domains, the domains themselves remain intact at this temperature. For temperatures greater than 60˚C, there is a sequential and reproducible loss is structure that is define by the temperature to which the protein is heated, the loss in structure by this stage is permanent with little to no recovery in structural integrity. It is clear from these results that the degree of denaturation can be defined by the temperature to which the protein is heated. Analysis of the data from Figure 4.16. is presented in Table 4.7.

Initial Heating	**Property**	**Heating Transition**			**Melting Transition**		
		1st	**2nd**	**3rd**	**1st**	**2nd**	**3rd**
328K (50˚C)	T_m K x 10^3				315.0 18.0	338.0 45.0	350.0 30.0
328K (55˚C)	T_m K x 10^3	**321.0** **5.0**			315.0 18.0	338.0 45.0	350.0 30.0
328K (58˚C)	T_m K x 10^3	**321.0** **5.0**			315.0 18.0	338.0 45.0	350.0 30.0
328K (60˚C)	T_m K x 10^3	**316.0** **10.0**	**333.3** **45.5**		305.0 10.0	337.5 37.0	351.5 30.0
328K (65˚C)	T_m K x 10^3	**316.6** **10.0**	**334.5** **45.0**		313.7 10.0	346.0 15.0	
328K (70˚C)	T_m K x 10^3	**320.0** **10.0**	**339.0** **35.0**		345.5 14.0		
328K (75˚C)	T_m K x 10^3	**320.0** **10.0**	**339.0** **28.0**		353.0 10.0		

Table 4.7. Properties of the transitions of the temperature processes of Figure 4.14.

Table 4.7. reveals the physical measurements of the melting curves for all the temperatures studied. At 55˚C a small melting transition is revealed at 321K of $5x10^3$. When the sample was heated to 58˚C the same transition observed at 55˚C was observed at 58˚C. The turning point seems to appear around 60˚C where two possible transitions were observed in the melting curve. Cooling the 60˚C sample and then reheating thought the whole temperature range to maximum temperature highlighted a further three possible transitions, the lowest occurring at 305K (32.0C) in the melting. For the 65˚C melting cycle, two transitions were isolated in the melting curve and two in the heating curve. For the higher melting cycles, two transitions were observed in the heating and one transition found in the melting curves. The table reveals that HSA can be characterise by temperature and proves that it is possible to isolate HSA's intermediate, unfolded and partially unfolded transitional states.

4.5. Small Ion Interaction with Albumin

Albumin contains a large number of ionisable residues; 116 have acidic groups with 98 carboxyl residues and 18 phenolic-OH. There are also 100 basic residues consisting of 60 amino (lysine), 16 imidazolyl (histidine) and 24 guanidyl groups (arginine) (*Bordbar et al, 2004*). This is important when you consider that HSA provides 80% of the osmotic pressure within the body, of which 30% is attributed to the physical presence of albumin itself, the other 50% is attributed to the presence of cations such as sodium and potassium that associate with the negative charge of albumin (*RezaeiTavirani et al, 2006*). Albumin makes up about 55% of the total protein concentration in the blood. When studying the physical attributes of the protein with binding, depending on the physical technique used, different dynamic and structural information will be obtained that will be dependent on the technique (*Lucas et al, 2006*). At pH7 a net charge distribution of -9 across domain I and the N-terminal is found, with a charge of -8 across domain II and +2 across domain III and

the C-terminal. From this, it can be seen that a net negative charge exists across domains I & II (Figure 4.17.).

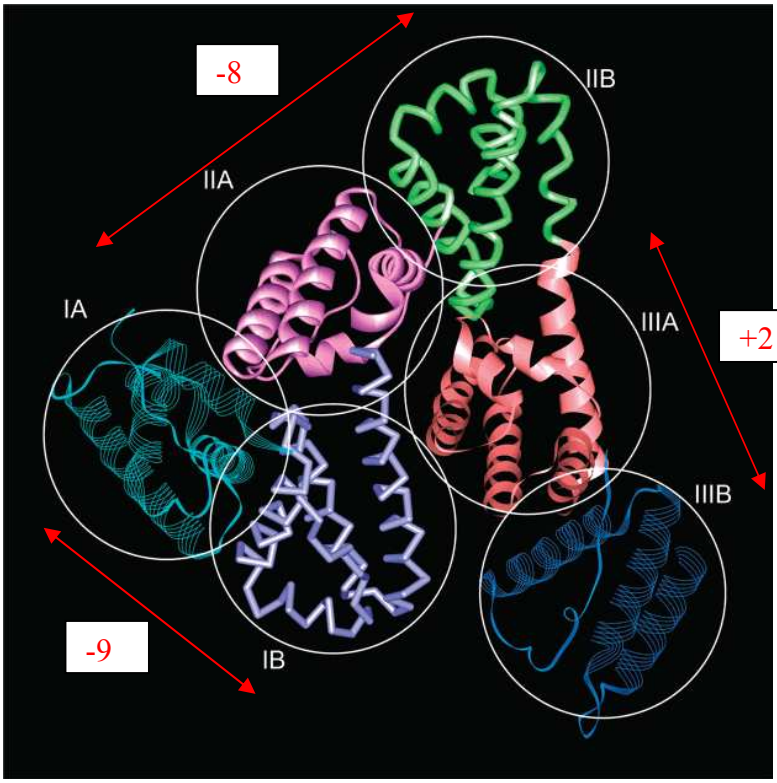

Figure 4.17. Schematic representation of HSA showing the domain regions of overlap.
(Modified from Reference: J. Phys. Chem. B ***2008,*** *112, 4884-4891)*

The diagram shows the influences that each domain has with respect to the other, and the points of inter-domain contact. The charge distribution is also shown in red.

The interaction of HSA with small ions can have a profound effect both on its tertiary structure and binding capability. An example of the effect of ion binding is seen in the interaction of calcium chloride ions (0.002M) in the presence of 0.16M sodium chloride (*Foster et al*, *1974*), warfarin is found to have reduced binding capability in this environment. Medium and long chain fatty acids are also known to have a marked effect on the binding ability of the protein, reducing its interaction with some ligand and in some cases prohibiting it completely (diazepam is known to be inhibited by the presence of ligands); all these ions are known to exist in the blood. Several ions were investigated for

their structural effects on HSA when bound in varying molar concentrations. The ions considered are shown in Table 4.8.

Ion Studied	Concentration	Concentration	Protein	Experiment
Sodium Citrate			nHSA	Concentration Studies
Sodium Sulphate	200mM	1M	nHSA	pH Titration
Sodium Chloride	200mM	1M	rHSA, nHSA	pH Titration
Sodium Acetate	-	1M	nHSA	pH Titration

Table 4.8. Study of small ion interaction with albumin.

Two concentrations were studied, the pH titration determined and comparisons made in both the near and far UV CD regions, these results are shown in Figures 4.16. to 4. 20.; sodium citrate is found in the blood with a concentration of around 0.1mM. It has been reported that citrates have a marked effect on HSA and its binding ability so concentrations of 10^{-1}M to 10^{-5}M were investigated both in the near and far CD UV regions. No changes in both of these regions were detected, if sodium citrate were to have an effect, there were no changes seen in either of the secondary and tertiary structural regions (no changes in extinction coefficient).

4.5.i. Results of Small Ion Interaction with HSA

Considering the ions mentioned in Table 4.8., the binding of ions to HSA was monitored for structural changes over the pH range between 1 and 14 in the far UV CD region. Two concentrations were chosen and their results were compared with the results obtained from nHSA in the absence of any ligands and reported earlier in this chapter (see Figure 4.2.). All the results of the ionic interactions are shown in Figures 4.18. to 4.22.

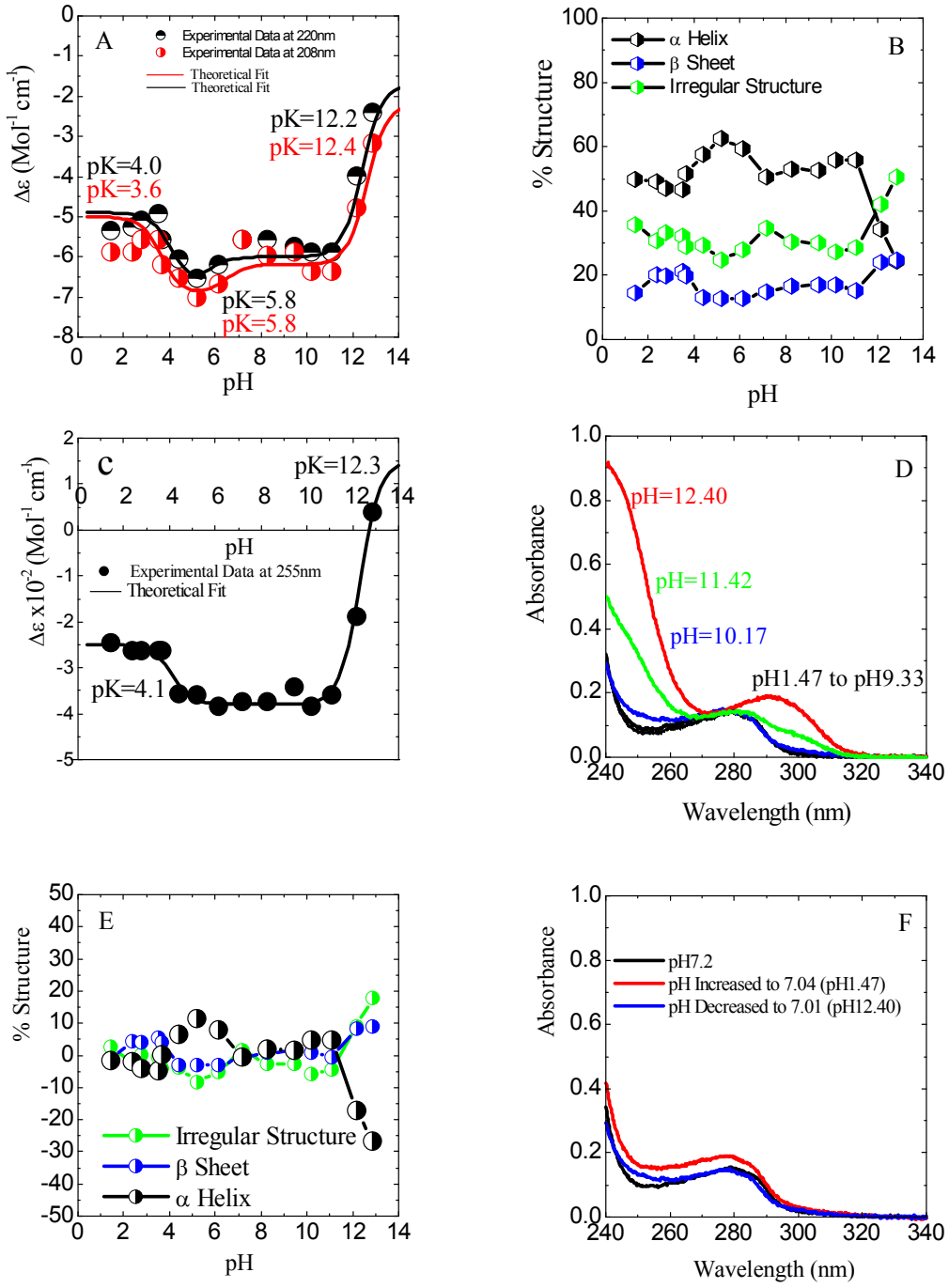

Figure 4.18. Characterisation of nHSA in the presence of 200mM NaCl.

A. pH Titration of nHSA, 4.51x10^{-6}M in 200mM NaCl, 0.02cm cell
B. pH Titration showing the % Structural Changes
C. Near UV CD of nHSA, 4.51x10^{-6}M in 200mM NaCl,1cm cell
D. Absorption Spectra of 4.51x10^{-6}M of nHSA in 200mM NaCl, 1cm cell
E. Differential Structural Changes of nHSA in the presence of 200mM Nacl
F. Absorption Spectra of nHSA after readjustment of pH, 1cm cell

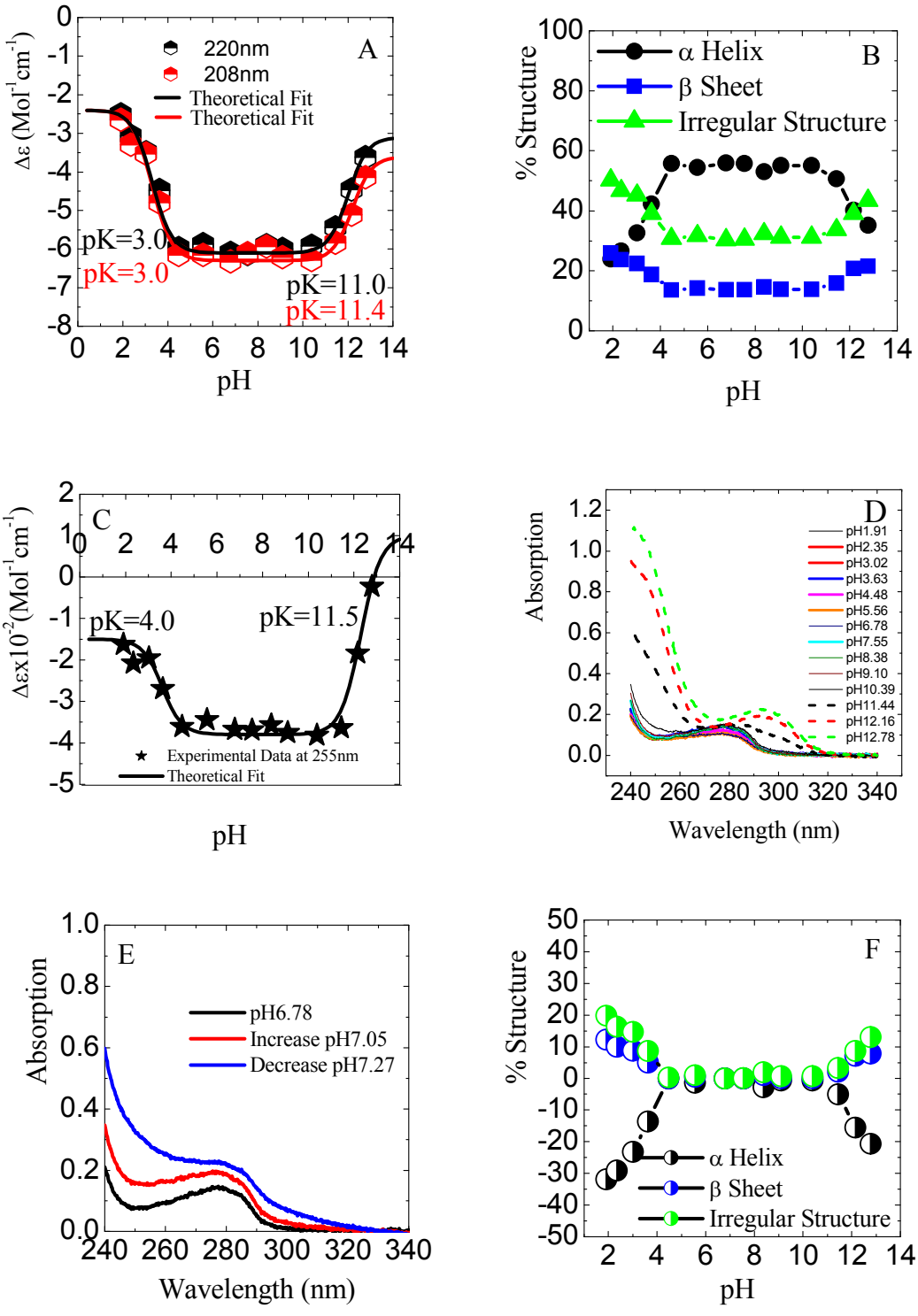

Figure 4.19. Characterisation of nHSA in the presence of 1M NaCl.

A. pH Titration of nHSA, 4.51x10^{-6}M in 1M NaCl, 0.02cm cell
B. pH Titration showing the % Structural Changes
C. Near UV CD of nHSA, 4.51x10^{-6}M in 1M NaCl,1cm cell
D. Absorption Spectra of 4.51x10^{-6}M of nHSA in 1M NaCl, 1cm cell
E. Absorption Spectra of nHSA after readjustment of pH, 1cm cell
F. Differential Structural Changes of nHSA in the presence of 1M NaCl

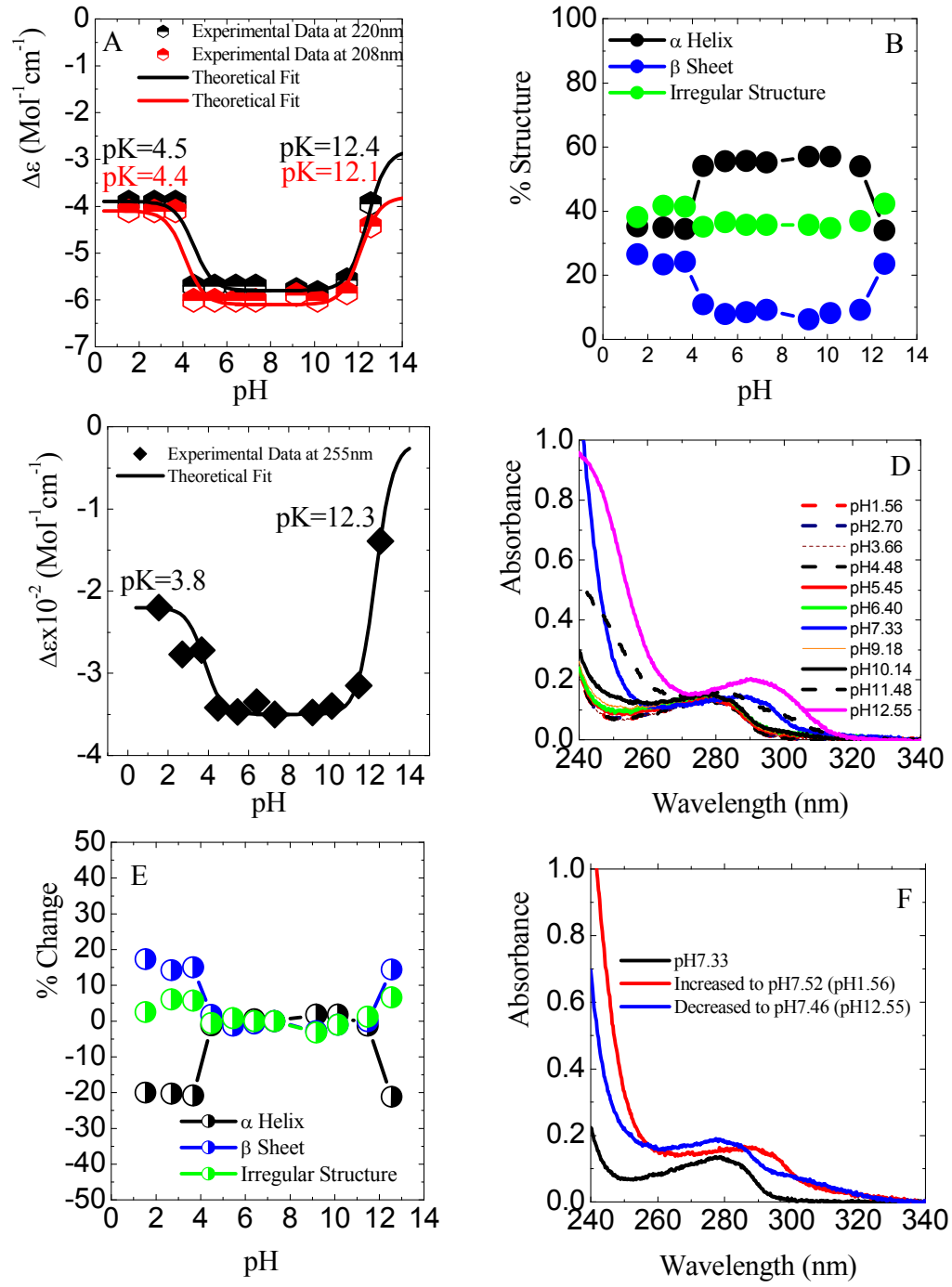

Figure 4.20. Characterisation of nHSA in the presence of 200mM Na_2SO_4.

A. pH Titration of nHSA, 4.51x10^{-6}M in 200mM Na_2SO_4, 0.02cm cell
B. pH Titration showing the % Structural Changes
C. Near UV CD of nHSA, 4.51x10^{-6}M in 200mM Na_2SO_4,1cm cell
D. Absorption Spectra of 4.51x10^{-6}M of nHSA in 200mM Na_2SO_4, 1cm cell
E. Differential Structural Changes of nHSA in the presence of 200mM Na_2SO_4
F. Absorption Spectra of nHSA after readjustment of pH, 1cm cell

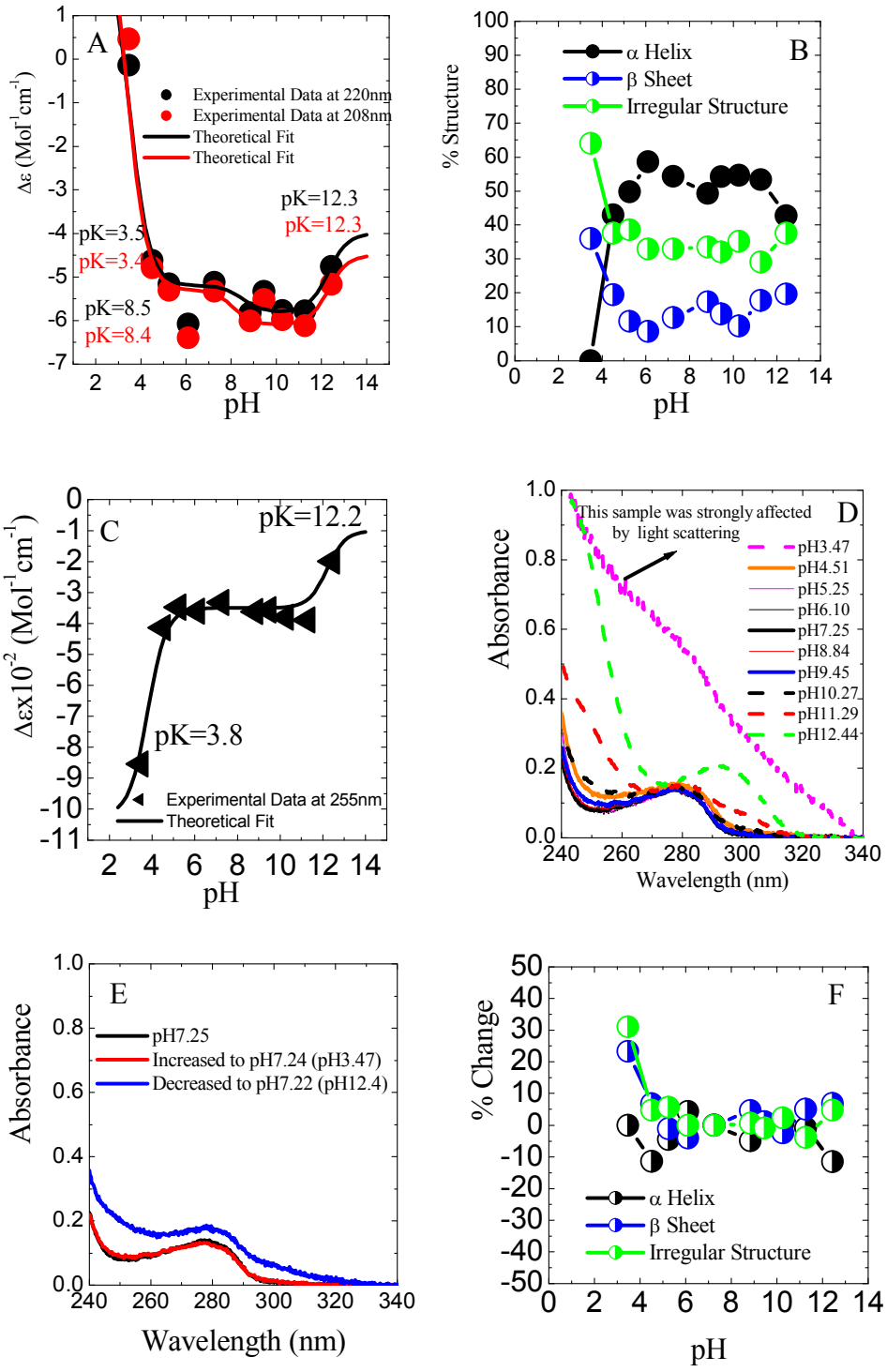

Figure 4.21. Characterisation of nHSA in the presence of 1M $NaSO_4$.

A. pH Titration of nHSA, $4.51x10^{-6}$M in 1M Na_2SO_4, 0.02cm cell
B. pH Titration showing the % Structural Changes
C. Near UV CD of nHSA, $4.51x10^{-6}$M in 1M Na_2SO_4,1cm cell
D. Absorption Spectra of $4.51x10^{-6}$M of nHSA in 1M Na_2SO_4, 1cm cell
E. Absorption Spectra of nHSA after readjustment of pH, 1cm cell
F. Differential Structural Changes of nHSA in the presence of 1M Na_2SO_4

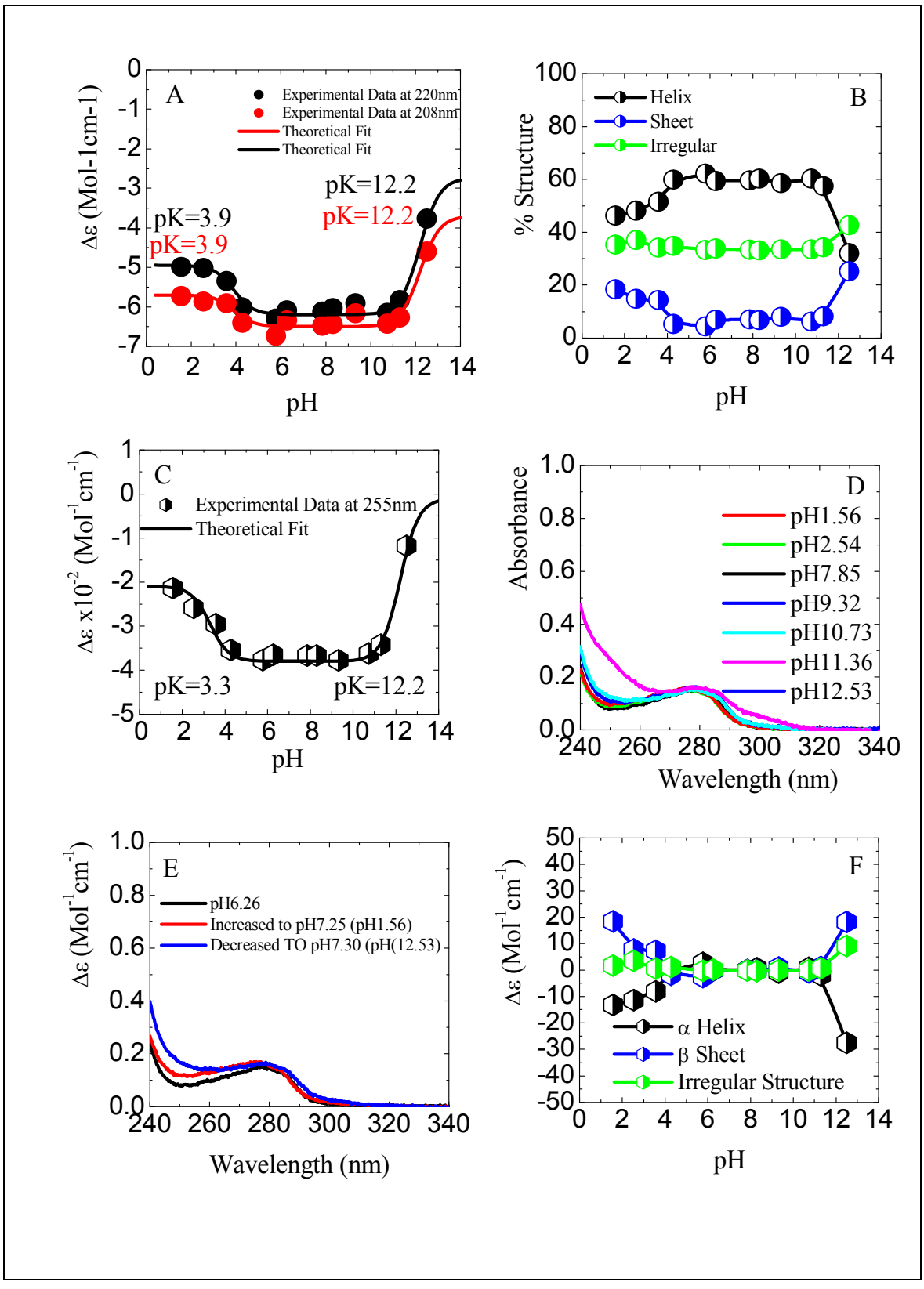

Figure 4.22. Characterisation of nHSA in the presence of 1M CH_3COONa.

A. pH Titration of nHSA, $4.51x10^{-6}$M in 1M CH_3COONa, 0.02cm cell
B. pH Titration showing the % Structural Changes
C. Near UV CD of nHSA, $4.51x10^{-6}$M in 1M CH_3COONa, 1cm cell
D. Absorption Spectra of $4.51x10^{-6}$M nHSA in 1M CH_3COONa, 1cm cell
E. Absorption Spectra of nHSA after readjustment of pH, 1cm cell
F. Differential Structural Changes of nHSA in the presence of 1M CH_3COONa

HSA Samples 4.51×10^{-6} **M**	**pK at 208nm Backbone Region**				**pK at 220nm Backbone Region**				**pK at 255nm Aromatic Residues**			
Transitions in pH Titration	**1st**	**2nd**	**3rd**	**4th**	**1st**	**2nd**	**3rd**	**4th**	**1st**	**2nd**	**3rd**	**4th**
nHSA	**2.6**	**5.9**	**10.5**		**2.7**	**5.9**	**11.6**		**4.2**	**11.6**		
dHSA	2.7	4.6	10.9		3.0	5.7	10.7		3.6	11.6		
rHSA	3.0	6.2	11.4		3.0	5.9	11.0		4.0	11.5		
nHSA in 200mM NaCL	3.8	5.8	12.4		4.0	5.8	12.2		4.1	12.3		
nHSA in 1M NaCL	3.0	-	11.4		3.0	-	11.0		4.0	11.5		
nHSA in 200mM Na_2SO_4	4.4	-	12.1		4.5	-	12.4		3.8	12.3		
nHSA in 1M Na_2SO_4	3.4	8.4	12.3		3.5	8.5	12.3		3.8	12.2		
nHSA in 1M CH_3COONa	3.9	-	12.2		3.9	-	12.2		3.3	12.2		
	Secondary Structure								**Tertiary Structure**			

Table 4.9. Comparative pH Studies of the different forms of HSA in different ionic environments.

It is evident that the presence of ions can have a profound effect on the properties of albumin and the way in which it behaves in changing environments as shown in Table 4.9. With the exceptions of 200mM NaCl and 1M Na_2SO_4, all the ions studied have eliminated the second transition in both wavelengths studied in the secondary structure region, only two out of the potential three transitions previously observed were detected. In the aromatic region, of the wavelengths monitored, the two transitions that were detected previously still remained. Considering the secondary structural region first at 208nm, the addition of ions increased the first transition from pK= 2.6 to values in excess of pK = 3.0, with the highest value observed for 200mM Na_2SO_4 attaining a value for the pK = 4.4. As previously stated the second transition only exists for the 200mM NaCl and the 1M Na_2SO_4 samples with values of pK = 6.4 and 8.4 respectively. It was the second transition found in the 1M Na_2SO_4 sample that was proven to be distinctly different from that found in the native sample, and was found to be 2.5 units higher than that found for the native. The albumin structure was perturbed sufficiently enough to eliminate the second transition. The third transition proved equally diverse with 1M NaCl producing a pK value of almost 1 unit higher that that of the native. The other ions produced values nearly 2 units greater than the native. When considering the transitions at 220nm the values proved equally as diverse and reflected the same or similar trend as that detected at 208nm. In the tertiary wavelength region the protein was monitored at 255nm. With the two transitions observed the first transition produced a general lowering of the pK detected. The second transition generally increased. It is evident that the presences of ions could have a profound influence on the structural properties of albumin, and this would suggest that it could have an influence on the way ligands could potentially bind.

When considering the differential structural changes in the presence of ions, for 200mM NaCl, an increase in structure was detected between pH4 and pH6 with an increase in α-helical content only as shown in Figure 4.16.b. The relative amounts of β-sheet remained

constant but there was a corresponding change in irregular structure at the same point indicating that the increase in helix was as a direct result of a decrease in irregular structure, the protein became more structured. Figure 4.16.e. highlighted this mutual change corresponding to the F-form of the protein conformation. Outside the pH range of 4 to 10 were seen the biggest changes and variations from that seen in the native, and this was true for all the ions investigated.

When nHSA was dissolved in 1M NaCl no unexpected changes were observed as shown in Figure 4.19. Relative stability was attained between pH4 and pH10, with only the high pH region showing changes in the UV spectra plot (see Figure 4.19.d.). Albumin in the presence of 1M NaCl meant that the pH changes in both regions exhibited irreversible changes. The greatest changes shown were under alkali conditions with the UV highlighting the greatest amount of light scattering, this was indicative of aggregation. There was some aggregation observed under acidic conditions, however, the amount was not as significant.

The presence of 200mM Na_2SO_4 did not affect the nature of nHSA in the middle region of the pH range (p5H to pH10) but did affect the protein in the extreme regions; this was not uncharacteristic of the protein. However, UV changes in both the low and high pH regions were seen (Figure 4.20.d.), with the reversibility to pH of the protein greatly compromised, shown in Figure 4.20.f.; the effect of 1M Na_2SO_4 gave detectable changes over the entire pH range with the greatest changes observed in the low pH region. At pH3.47, the sample became turbid suggesting aggregation and was greatly affected by light scattering as shown in Figure 4.21.d., no further measurements were possible. Secondary structure analysis revealed that one of the biggest changes, other than at pH3.47, was observed at around pH6 with an increase in α-helix, this was compensated by a corresponding decrease in β-sheet. Another significant change was seen around pH9 with a decrease in helix and an increase

in β-sheet. At this concentration of Na_2SO_4 only the reversibility at high pH was compromised; the affect of 1M CH_3COONa did not seem to have any untoward effects on the protein conformation behaving as was expected (Figure 4.22), only between pH4 and pH6 were slight changes detected. Since no significant effects were seen at 1M equivalent of CH_3COONa, measurements at a lower concentration were unnecessary.

4.6. Denaturantion Studies using Guarnidinium Hydrochloride and Urea

The complexity of the albumin molecule and its binding ability has made it a topic of much investigation. Albumin's metabolic pathway and the mechanism of its ability to unfold on binding have still not been fully characterised, especially in terms of its partially unfolded intermediates. Because of albumin's multi-domain properties make it even more complicated to study by denaturation studies, as each domain/subdomain may be able to act independently of each other, folding and unfolding independently to each other domains. The interdomain helices may also play a vital and/or independent role affecting the overall conformation seen (*Muzammil et al, 2000*). Certain chemical can be used to induce partial unfolding in proteins by causing varying degrees of denaturation. Guanidinium Hydrochloride (GuHCl) and urea (U) are two such chemicals whose rate of denaturation of the protein is concentration dependant. GuHCl is considered to be the stronger denaturant by destabilizing the electrostatic interactions of the protein, binding to the protein via the peptide bond. Small amounts of these chemicals have been shown to increase the binding of some ligands as a result of opening the protein sufficient enough to either expose the binding site or make it more assessable, this usually occurs at low concentrations of the denaturant. Many studies have been conducted with denaturants and albumin, but little is known about the exact mode or nature of the mechanism resulting from the actions of the denaturant. It is believed that the two denaturants work in different ways on the protein and can involve the generation of intermediates. Indeed conflicting

information has been published when the same denaturant has been investigated by different scientists (*Flora et al, 1998*).

For concentrations of less that 1M GuHCl local changes within domain II are said to take place, but for concentrations between 1M – 6M global changes occur that affect the whole molecule, initially with the separation of domains I & II, then followed by the unfolding of domain II. The chemical unfolding of the protein can be shown in the following scheme,

$$N \underset{}{\overset{Step1}{\rightleftharpoons}} E \underset{}{\overset{Step2}{\rightleftharpoons}} I \underset{}{\overset{Step3}{\rightleftharpoons}} U \qquad \textbf{Multiple Step Transitions}$$

where N is the native protein, E is the extended protein, I represent the intermediate state where domain II is unfolded but domain I remain intact, and U is the unfolded state. The use of urea in denaturation experiments have shown that urea works differently to GuHCl in that only one transition occurs,

$$N \underset{}{\overset{Step1}{\rightleftharpoons}} U* \qquad \textbf{Single Step Transition}$$

where N is the native protein but U* represents the partially unfolded intermediate. Urea is said to only affect domain II leaving domain I intact (*González-Jiménez et al, 2002*).

Two denaturants were used in this investigation; urea and GuHCl were added separately to rHSA (0.4mg/ml) in the concentration range of 0.1 to 10M equivalent of the denaturants. Both urea and GuHCl encourage unfolding in the protein, the degree of unfolding was dependent upon the concentration of denaturants present and the type of denaturant used. Two distinct sets of results were obtained: urea exhibited minimal effects for concentrations up to 2M equivalent, above this concentration the protein unfolded in approximately two stages. Conversely GuHCl affected the protein at a lower concentration of 1M equivalent, inducing a much sharper change also unfolding the protein in two stages as shown in Figure 4.21.

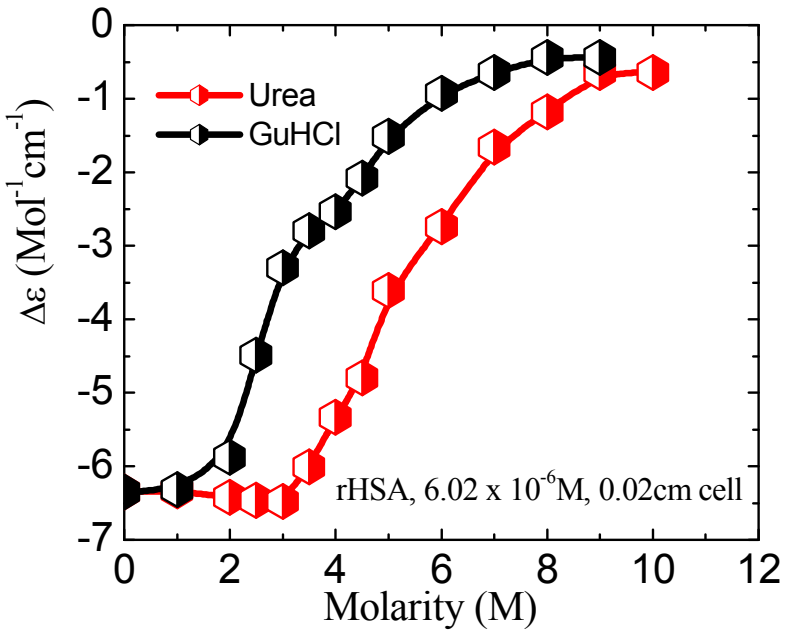

Figure 4.23. Denaturation studies of rHSA at 220nm.

Like with heat denaturation, chemical denaturants unfolds the protein in multi-stages, unfolding specific areas within the protein that could correspond to changes within the domains or subdomains. The denaturation effects in urea required more than 3M equivalent to induce any response, this denaturant only produced one transition that could be detected by CD analysis. Conversely, GuHCl produced two defined transitions that could be detected by CD thus reinforcing the theory of intermediate transitions produced as a result of chemical denaturation. Once the protein begins unfolding due to the presence of the denaturant, the path of the two denaturants followed distinct routes that seemed to be dependent on the denaturant used. The amount of detectable unfolded intermediates was approximately four, less that that found by heat denaturation. There exists the possibility of using one of these denaturants to induce partial unfolding.

4.7. Conclusion

HSA was found to be quite a robust protein withstanding heat denaturation for temperatures up to 58°C and pH changes between pH4 to pH10. Albumin's ability to show such restraint may explain its versatility as a blood protein and a scavenger, mopping up any excess ligands found in the blood. Temperature studies highlighted the conformational stability of the unfolded intermediates; it was shown that by heating the protein to a predetermined temperature, HSA would unfold by a specific, reproducible and measurable amount that could be determined. The behaviour of albumin to heat denaturation enabled the melting curve to act like a fingerprint for the partially unfolded intermediate state. Each state of denaturation could be exactly fitted to the general melting profile curve determined when the protein was heated from room temperature to 95˚C. On cooling the sample, little to no recovery was evident. However, the heated intermediate would, upon reheating, re-enter the melting curve at the point of exit; there was a residual core structure for albumin that could not be denatured (suggested to be domain III), calculated to be approximately 25% helix, 25% irregular structure and 50% β-sheet. Heating the sample through a second cycle had little effect on the protein and on the residual unperturbed core that remained from the first temperature cycle.

pH had a similar effects to that of the temperature studies in that it promoted specific conformational changes within the protein that were specific to that pH and reproducible, and like that of the temperature studies, the pH studies proved just as distinctive. However, unlike heating, the pH changes were totally reversible once physiological conditions were restored. Five possible intermediate states were highlighted that reflected the conformational states of albumin while possibly binding or off-loading, and may also reflect the possible conformational states that revealed the movement of amino acids to accommodate potential ligand binding. pH studies have highlighted their potential use in

the isolation and identification of intermediate state. Further work will be undertaken in this thesis using the pH unfolded intermediates on the affects of ligand binding with a view to elucidate or evaluate the characterisation of HSA.

The use of small ions as inhibitors in binding studies revealed significant structural changes in the secondary region, with the elimination of the second transition seen in the pH titration in three of the five samples studied. The modification in the secondary structure of albumin was as a direct result of the binding of the ions with all the pK's increasing in the secondary regions. The pK's in the tertiary region remained remarkably unaffected, proving that the ions only affect the secondary structure of the protein and may be used in the body as a way of affecting or controlling the binding activity of albumin. CD studies showed no significant changes with respect to secondary structure with exceptions of 200mM NaCl and 1M Na_2 SO_4 that gave increased helical content in the pH range between pH4 to pH6, this was at the expense of the β–sheet. It can be stated that although ions may have a significant effect on the binding abilities of other ligands to albumin, the structural changes as determined by CD spectroscopy were found to be subtle, and in some cases almost insignificant. However, as determined by the pK's, marked effects were detected in their absolute values.

4.8 Discussion

The nature of albumin and its response toward heat, pH, denaturants and small ion interactions meant that any one of these could be used to investigate the binding of ligands such as drugs with the view to locate binding sites. Both physical and chemical perturbations of albumin causes partially unfolded intermediates that could reflect the unfolding of domains or even subdomains. If this is true it would be possible to use these intermediates and bind known ligands with known binding site locations to determine if the binding at the specified site had been affected or altered by such perturbations. pH would appear to be the most obvious choice as these effects are reversible and therefore pose the least risk to the protein, also there are five known conformational states already highlighted. Binding at a specific pH would represent binding at a given conformational state; this would allow the characterisation of that conformation and thus the site, domain and/or subdomain.

Pre-incubated samples of albumin would be an alternative way to investigate ligand binding. It has been demonstrated that pre-heating albumin causes partial unfolding of the protein. Therefore, the use of marker ligands of known binding location would make it possible to determine which site on albumin was affected at a specific temperature. Thus it would make it possible to use pre-incubated samples of albumin to determine possible binding location of new and novel drugs whose binding location to albumin had not been characterised. With this in mind the effect of binding of two classes of ligand was investigated by pH, chemical denaturation and temperature, using the characterisations of the protein as determined in this chapter. The ligands were chosen because of their known specifications with the view to isolate and characterise by CD spectroscopy the binding sites of ligands to HSA.

CHAPTER 5

CHAPTER 5: Small Ligand Interaction

5.0. Introduction

The multifaceted role of human serum albumin towards the binding of ligands has enabled it to adopt one of the most pivotal roles in plasma binding within the body. Albumin serves to regulate the levels of certain drugs and metabolites and shows little specificity. The binding affinities of the different ligands may vary but is of the same order of magnitude as the specific interaction of the drug/metabolite and its specific protein (*Spencer, 1970*). Albumin acts as a depot, inactivating potential toxins by transporting them to sites where they can be disposed of safely. Drug pharmacokinetics all hinge on their interactions with HSA, that is there absorption, distribution, metabolism and excretion. Of the four pharmacokinetics properties, distribution is the property affected by HSA (*Yang et al, 2007*). Bound drugs are protected from rapid catabolism, acting as a reservoir and replacing the free drug levels as the drug is consumed, thus maintaining the therapeutic levels and prolonging the duration of the drug (*Ascoli et al, 1995*). If binding is very strong or weak to HSA then the distribution of the drug will be poor, which would mean that the dose given would have to be increased, thus could lead to stronger side effects being seen. HSA increases the solubility of hydrophobic drugs in plasma and modulates their delivery, revealing the dominant role of HSA in drug dispersion (*Hu et al, 2005*).

Albumin's structure is especially suited for its role to bind numerous ligands, found by X-ray crystallography to contain salt bridges and hydrophobic interactions between IA, IB & IIA on one side, and IIB, IIIA and IIIB on the other side. The salt bridge between Arg 218 and Asp 451 is 3.65Å, and if broken causes thermal instability that causes Trp 214 to move into a more hydrophobic environment. Trp 214 is also thought to be responsible for holding the two halves of HSA together (*Carter et al, 1994*). Another important consideration is the effects that each domain has on the binding abilities of the molecule. One important discovery in the functionality of the Sudlow site I, is its dependence on its

interaction with domain I (Figure 5.1.), and if this linkage is broken then the binding of warfarin is dramatically affected (*Perry et al, 2006*).

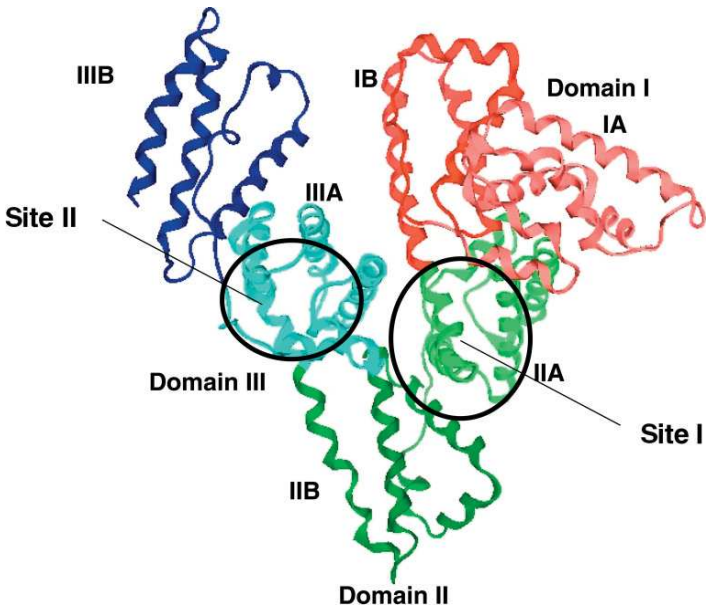

Figure 5.1. Crystal structure of the two main binding sites of HSA.

(Chuang et al, Chirality, 18, 159–166, 2006)

Although extensively studied, the binding of ligands to albumin has been ambiguous in the determination of the number of binding sites this protein contains until recently, with the new generation of crystal structures that have long been waited for (*Muravskya et al, 2004; Chuang et al, 2006; Sugio et al, 1999., Zhu et al., 2008*). Albumin was previously thought to contain numerous sites, but more recent studies have shown there to be only a few select sites (*Sjödin et al., 1976 & Feske et al., 1981, Zhu et al., 2008*). There are two main non equivalent sites found and initially formalized by Sudlow (*Sudlow et al., 1976*), the first site is referred to as "site I", located in domain IIA, thought to be an elongated sock-shaped pocket, binding the site-specific drug warfarin (Warf). The second site known as "site II" is located within domain IIIA and is thought to be a T-shaped hydrophobic pocket with two

hydrophobic entrances with a separation of 10Å (Figure 5.1.). There is an asymmetric distribution of hydrophobic and hydrophilic residues within the pocket of site II, with the cavity lined with hydrophobic residues and the surface lined with polar residues making it hydrophilic (*Peyrin et al 1999*). Site II is said to be similar to site I in that they are both comprised of 6 helices, however, site II is a hydrophobic cavity with distinct polar regions and is smaller than that of site I; Site II bind diazepam as one of its marker ligands (refer to Chapter 2 on Ligand Binding).

Site I was previously thought to bind acidic, bulky hetrocyclic molecules containing enol groups that possess a negative charge centralised within the molecule. Located close to this site are MCFA & LCFA binding sites that have been shown to affect the binding of some ligands to this site, causing a reduction or an enhancement of binding by both competitive and/or allosteric effects (*Kragh-Hansen, 1990*). The binding of warfarin has been shown to be enhanced by the presence of fatty acids producing a 2-3 fold reduction in binding in their absence. Site I is thought to contain several overlapping binding sites, this can be seen by the close proximity of the fatty acids binding sites to the main binding cavity (*Kragh-Hansen, 2002*). Ligands of diverse chemical structure bind to this region as this site is not as discerning as site II, examples include dicarboxylic acids and/or bulky heterocyclic molecules with a central negative charge. Site I is a large hydrophobic cavity formed from the hydrophobic side chains of the protein with 7 openings. The cavity is 17% hydrophilic and 83% hydrophobic with a surface area of 2236.1 $Å^2$ and a solvent accessibility volume of 788.6$Å^3$ (*Perry et al, 2006*). The entrance to the pocket is surrounded by positively charged residues, with the pocket being more truncated than that found in site II due to the presence of bulkier hydrophobic side chains (*Chuang et al 2006*). Lys-199, His-242 and Arg-257 function sterically and electrostatically in ligand binding. The helix h1 within site I (IIA) is displaced outwards, thus producing a hydrophobic surface towards the cavity.

Site I is said to be 'flexible', accommodating all the chemically diverse ligands which are bound in high affinity. Site I is said to contain several individual ligand binding sites that bind independently or can mutually influence each other, an example is HSA-Myr-Warf. Positive contributions within the binding pocket are derived from Trp 214 and Arg 218, negative contributions come from residues Lys 199 and His 242, all situated within the 6 helices that construct the warfarin binding pocket (*Chuang et al 2006*). Another example of stereoselectivity is found in tryptophan where L-tryptophan binding 100x more than D-isomer. Binding sites are found in the interdomain cleft between subdomain IA and IIA which includes Trp 214. LCFA are thought to control the binding of HSA by competitive and allosteric mechanisms which mainly involves domain 1, this may be a possible explanation as to why limited ligand binding sites are found in domain I.

The properties of site II (in domain IIIA) are different to those of site I in that, the entrance of the pocket contains residues that interact with carboxylates from the binding ligand. Within the pocket of site II are two regions of hydrogen bond partners, the first is located across the interface of domains II & III through Ser 342 and Arg 348 in subdomain IIB and Arg 485 in IIIA. The second region is located at Arg 410, Tyr 411 and Ser 489 all found in subdomain IIIA. Within this pocket Arg 410 and Tyr 411 are thought to be the most important residues, although Arg 410 is not thought to be important in diazepam (Diaz) binding (*Chuang et al 2006*). The site II binding pocket is said to be 'less flexible' than site I, therefore less accommodating and is smaller and narrower than that of Site I with a ligand length constraint. Binding at this pocket is influenced by stereoselectivity, an example is shown in L-tryptophan (*Chuang et al, 2006*). The reverse effect has been seen for site II where diazepam binding is restricted or inhibited in the presence of FA. The revised consensus is thought to be that binding to this site is by hydrophobic and electrostatic interaction, with the hydrophobic force providing the strongest effect.

Tryptophan seem to offer an important contribution within this area, its modification affecting the binding of some ligands including warfarin (*Ellis et al., 1991 & Schreiber et al., 1978*), but has been shown not to affect ligands such as phenyl butazone and azapropazone (*Newman et al., 1990 & Pende et al., 1991*). Site II binding is thought to show great specificity, and is shown not to be affected by short chain fatty acids (SCFA) of chain length $C_1 - C_5$, but are affected by MCFA and LCFA of chain length $C_6 - C_{12}$ and $C_{11} - C_{18}$ respectively. This pocket seems to have a critical length for ligands that it can and will except, determined to be around 14.7Å. Binding to this site is complicated and seems to be affected by many parameters, properties and characteristics such as hydrophobicity, chain length and charge of the ligand are all important determinants (diazepam having a chain length of 11.6 Å). The hydrophobic cleft of this site has an approximate depth of 12-16A and a width of 6-8 Å, with at least one cationic group located near the surface of albumin that inhibits ligands carrying positive charges. The main forces for binding at this pocket are the hydrophobic interactions. Carboxyl groups are also thought to be required for effective binding to this site (*Maruyama et al, 1993*).

There are many drugs that exhibit chirality, a property whose importance was established as far back as 1886 when Pasteur observed the differences in the chiral salt of tartaric acid. Two optically active isomers (enantiomers) were found that rotated the plane of polarization, the “natural form” that rotated the light to the right so called dextrorotatory (d or + enantiomer), and the other form that rotated the light by the same amount but in the opposite direction, rotating the light to the left or levorotatory (l or - enantiomer) (*Williams, 1991*). Mason and others have served to reinforce this concept, establishing the fundamental rules that elucidate chirality as we know it today (*Mason, 1988 & 1989*). Enantiomers have in the main identical physical characteristics; optically activity is a means of distinguishing them. Therefore, CD spectroscopy with its chiral discrimination

has the ability to measure the optical activity of different chiral forms and determine absolute values, a fact utilized throughout this thesis when considering drugs and cocktails of drugs. A further fact to consider in the pharmacology of drugs is that the active drug in plasma is the unbound or free drug. Absorption of the drug occurs in the intestine by passive means. When the drug is administered orally, lipophilicity is paramount. Albumin is thought to exhibit enantioselectivity showing chiral discrimination, in these circumstances the equilibrium constants for both enantiomers (K_R & K_S) have to be considered. Nonsteroidal anti-inflammatory drugs (NSAID) are found to bind stereoselectively to HSA, the degree of separation is dependent on the drug. Some drugs, however, are not stereoselective and the enenatiomers are found to bind to the protein equally. Another fact that has to be considered is that isomers are metabolised by two different enzyme systems and to produce two different rates of metabolic clearance (*Chuang et al, 2006*). The two enantiomers may interact differently with either the protein or receptor site, thus this will affect their distribution and effect.

Albumin also possesses enzymic properties that were first observed as far back as 1951. This enzymic activity is located within site III, with Trp 411 and histidine being the active residue responsible for esterase activity. Arg 410 has also been implicated in esterase activity (*Yang et al, 2007*). Esterase activity has also been seen in site IIA but to a lesser degree. Here acetylsalicylic acid is converted to salicylic acid by hydrolysis with Lys 199 being implicated as the active residue, since during the hydrolysis of aspirin the acetyl group is transferred to Lys 199 forming acetyllysine. The crystal structure has revealed that although both aspirin and salicylic acid bind to HSA via Lys 199, their acetyllysine orientations were quite different with salicylic acid rotated approximately 30˚ to accommodate acetylation in IIA (*Yang et al, 2007*). The nucleophilic substitution of Lys

199 is facilitated by the protonated of Lys 195 which is also a necessary step. Lys 199 is found to have an unusually low pK_a of 8 (*Kragh-Hansen et al, 2002*).

This chapter endeavours to give a better understanding of the binding characteristics and specifications of the two main binding sites of HSA, and to determine whether any other binding locations can be detected and determined. Also considered are the effects of major and minor perturbations within the protein and its response to binding. Lastly the affects of multiple ligands with there possible displacements are also investigated. It is clear that the complexity of albumin and it dominant feature within the blood make it an intriguing protein to monitor, and by virtue of its complexity, has meant that much of albumin's intimate binding sites are still elusive. It is intended that this study will add to the clarity and elucidation of albumin's most intimate details.

5.1 Benzodiazepine Binding

Benzodiazapine and its derivatives are widely used in the medical treatment of depression and other mental disorders; its structure is represented in Figure 5.2.

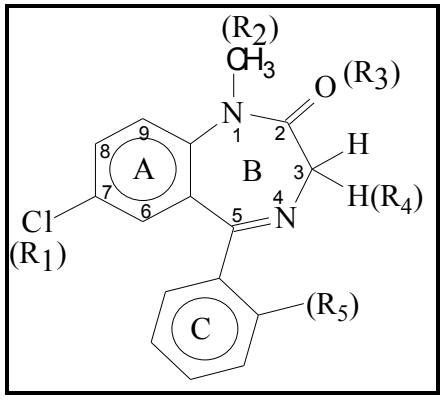

Figure 5.2. Structure of benzodiazepine, the derivatives are obtained by substitution of different functional groups in positions R_1 - R_5.

Diazepam (Diaz), a derivative of benzodiazepine, is referred to as a characteristic marker ligand for site II binding (subdomain IIIA) as shown in Figure 5.3. The opening to this site

is between 8 – 10 Å and lies between two helices. The distributions of hydrophobic and hydrophilic residues have been determined to be asymmetric (*Peyrin et al, 1999*). Subdomain IIIA is the site on albumin that has been determined to be the major ligand binding site, found to be potentially the first site that is targeted. However, its binding characteristics are very specific and is very receptive to enantiomeric selectivity as will be shown later with the type of conformer preferentially selected to bind at this site. The presence of FA equally have dramatic effects on site IIIA pocket's binding ability (*Curry et al, 2001*). Within the binding pocket helices h3 & h4 form the floor of the pocket, h1 & h2 form the sides of the pocket, and h5 & h6 for the roof of the internal cavity (*Kragh-Hensen et al, 2001*). When diazepam binds to HSA there is an expansion of the binding pocket to accommodate the incoming ligand. However, its expansion is not as great as that of subdomain IIA that has been shown to be a more flexible binding pocket.

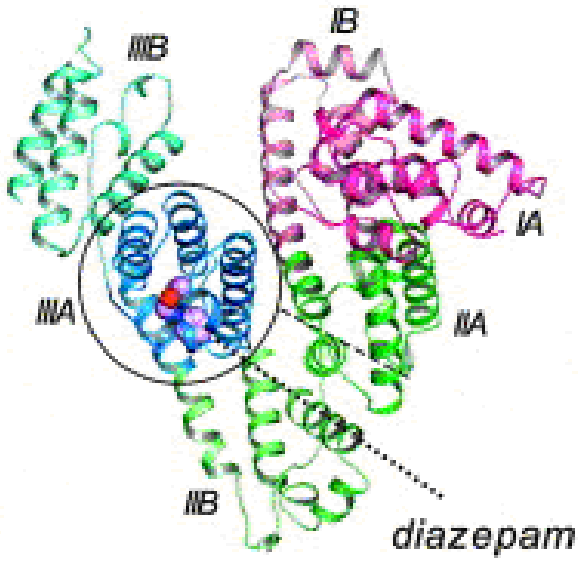

Figure 5.3. X-ray crystral structure of diazepam binding to subdomain IIIA on HSA.

(Curry et al, J.of Mol Biol, vol 353, Iss 1, 38-52, 2005)

The binding is in the absence of FA and in accordance with the findings of Carter and He in 1992. The protein is colour coded to reflect the domains and subdomains. The diazepam molecule is represented as the space filling molecule circled.

When FA binds to site IIIA, then the bound FA forms tunnels between the helices that are lined with hydrophobic residues. Two FA sites are found for Myr3 & Myr4 in this binding location. The carboxylate of Myr3 interacting with Arg 410 while for Myr4 the interaction is between Arg 485 in IIIA and Arg 348 in IIB. The binding activities of IIIA has been closely linked to residues Tyr 411 & Arg 410 with these residues being shown to project into the middle of the pocket, and are in close proximity to each other with approximately a 2.7Å separation (Figure 5.4.). Tyr 411 is thought to play a pivotal role in the functionality of the site, its substitution been shown to affect binding (ketoprofen), accept in the case of diazepam that is unaffected (*Kragh-Hensen et al, 2000, Chuang et al, 1999, Matsushita et al, 1997*).

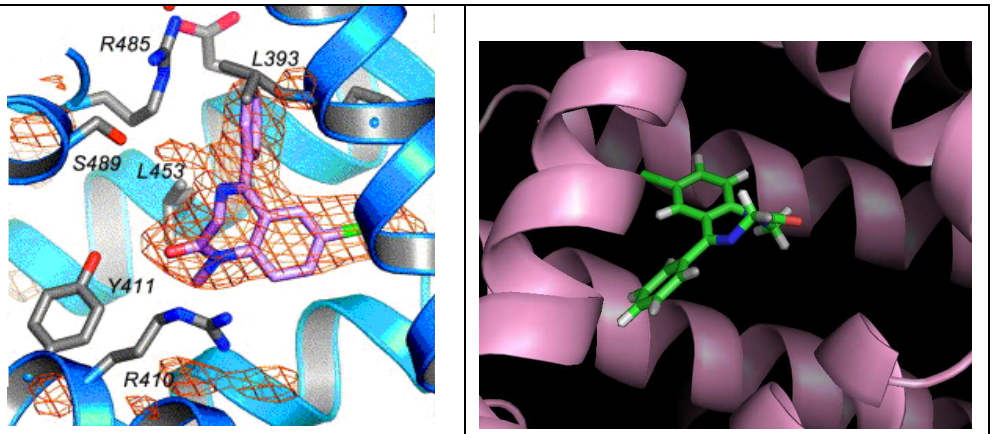

(A) (B)

Figure 5.4. Inside the pocket of IIIA showing diazepam docking.

(Curry et al, J.of Mol Biol, vol 353, Iss 1, 38-52, 2005 & Quantum Pharmaceuticals)

Albumin revealing its closest residues in contact with diazepam that show it to be a hydrophobic cavity with the main polar patch centred around Y 411 as shown in (A). Crystal structure of diazepam shown in a different orientation to that shown in (B).

Three distinct elements have been identified for binding activity at this site,

a. Guanidino moiety of Arg 410 that interacts with COO- group (except in the case of diazepam that does not contain such a group).

b. The phenolic oxygen of Tyr 411.

c. The aromatic ring of Tyr 411 interacts with the aromatic ring of the ligand.

Binding to site IIIA offers dimensional constraints, as this pocket is smaller and narrower than that of its counterpart at site IIA (Figure 5.5.). This site is said to be less 'flexible' since sterioselectivity is key. Unlike IIA, the binding of FA does not cause an expansion within the binding cavity of IIIA. With the higher binding constant of FA calculated to be around $K_a = 10^7\ M^{-1}$, and even taking into consideration that it is the FA's secondary binding site within this area, the FA will inhibit the binding of diazepam, competing for the same site due to its higher affinity. There are also allosteric inhibition constraints of the pocket to be considered as well as cascade effects when diazepam binds. The allosteric constraints occur where diazepam is inhibited by the primary binding of FA to HSA, constricting its binding to site II. Cascade effects are seen when free FA's displace toxins from site II, the toxin is then free to compete with diazepam competitively inhibiting its binding (*Mitsuyoshi et al, 2008*). All in all diazepam binding is affected by allosteric inhibition, competitive and cascade effects (Figure 5.6.).

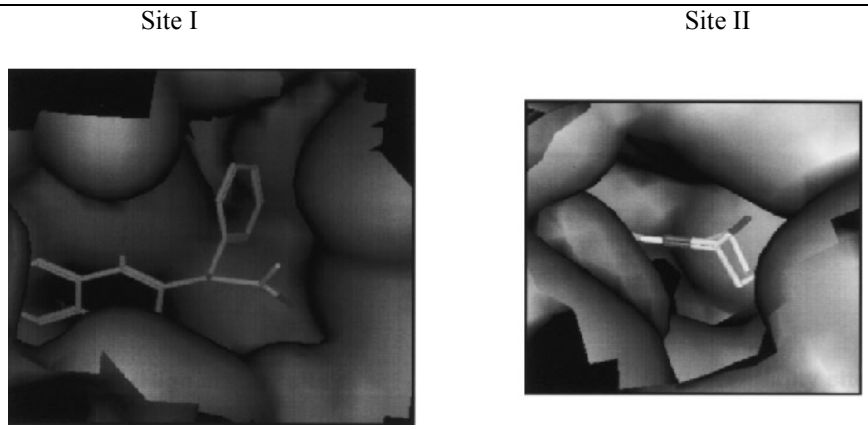

Figure 5.5. Simulation of the binding sites of HSA estimated using MOE based on crystallographic analysis.
(Chuang et al, Chirality, 18, 159-166, 2006)

Site I shows the warfarin molecule bound in the pocket, while site II shows the diazepam in situate. Diagrams indicate relative size differences between the two pockets and accessibility. Comparatively, there is a vast difference in size between the two pockets and a difference in accessibility. Clearly site II reveals the site constraints that may account for the type of ligand bound at that site.

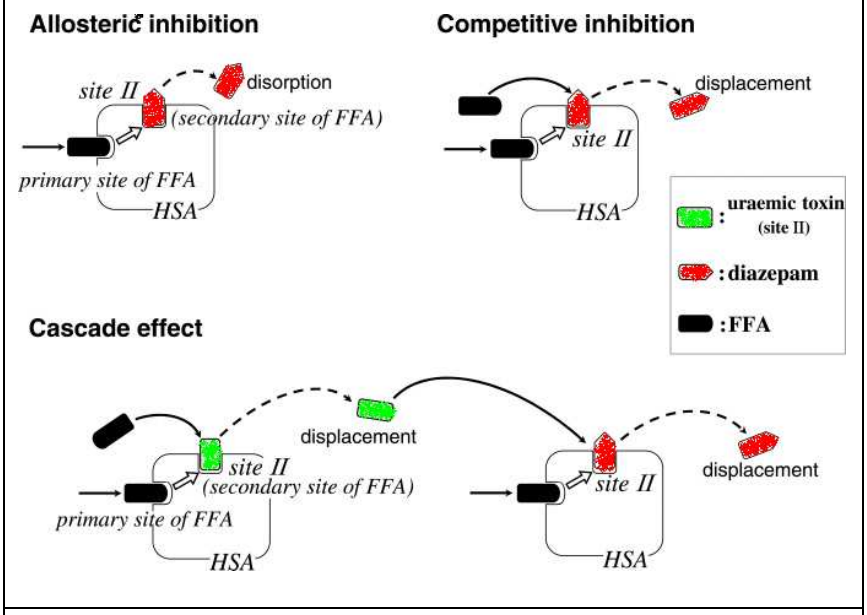

Figure 5.6. Schematic representation of allosteric, competitive and cascade effects.
(Chuang et al, Chirality, 18, 159-166, 2006)

Studies using gel filtration have shown that the binding of benzodiazepines to albumin is mainly restricted to one site (*Muller et al, 1973 & 1974*), and is stereospecific (*Muller et al, 1975*). Diazepam has a K_A of 18 x $10^{-4}M^{-1}$ for the main binding site, however, two weaker sites with lower equilibrium constants have been suggested which by their nature will be low affinity binding sites (*Sjödin et al, 1976*). At a pH = 3.3 the nitrogen at position 4 becomes protonated, with a pK_A = 4.5 it forms benzodiazepoxide, which can be ascribed to the formation of an amidinium structure shown in Figure 5.7., and results in a blue shift observed in CD spectroscopic measurements; there are many derivatives of benzodiazepine, all showing subtle changes in their CD profile. By substituting different substituents in the different aromatic rings (Figure 5.2.) show changes spectroscopically. Substitution in the B-ring results in strong changes in the Cotton effects seen at the positive peak at 262nm, this can be attributed to the influence of $-N_1=C<$ group. Derivatisation at N_1 enhances the positive CD peak. Derivatisation at C_2 has little / no effect on the CD spectra, this is also true for the substitution at position C7 in the A - ring

and substitution of the C - ring. If the number of oxygen atoms is increased at positions C_2 and C_3, the negative CD peak at 300nm increases in magnitude. In terms of energy levels, there is a strong $\pi \rightarrow \pi^*$ transition between the substituted A and C - rings, with a somewhat weaker transition of $n \rightarrow \pi^*$ from the N and O atoms, masked by the $\pi \rightarrow \pi^*$ transition between 300nm.

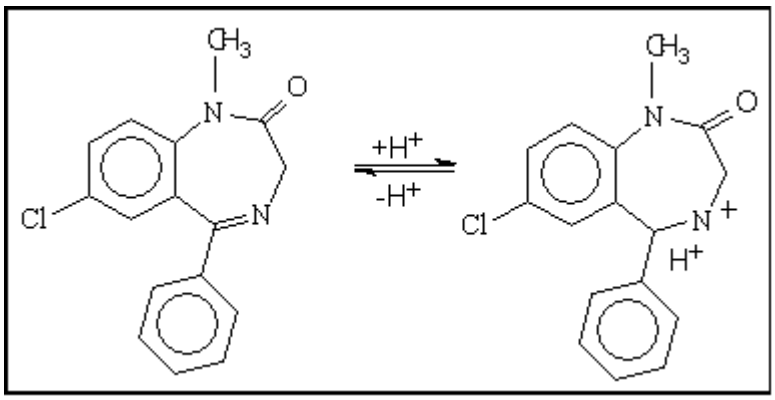

Figure 5.7. Structure of amidinium ion.

The observed CD spectra attributed to binding is due to "intrinsic" (natural optical activity) and/or "induced" or "extrinsic" optical activity (due to the environment of the chromophore). The intrinsic optical activity may be due to conformational changes around the chromophore side chains (Trp, Tyr, Phe and Cys), or they might arise from the asymmetric benzodiazepine molecule itself. NMR studies have shown the B - rings not to be planer, but most probably have the boat conformation. This was also supported by X - ray crystallographic studies (*Carter et al, 1989*), the structures are represented in Figure 5.8. It is the steric interactions within the benzodiazepine (R-) & (S-) enantiomers that restrict the conformers to either the P- or M- conformation. Due to the high enantiomeric selectivity that is present in the central nervous system preferential selectivity of the (S-) enantiomer is favoured by the receptor site, diazepam will adapt the M-conformation in binding to the site (Fitos et al, 2007).

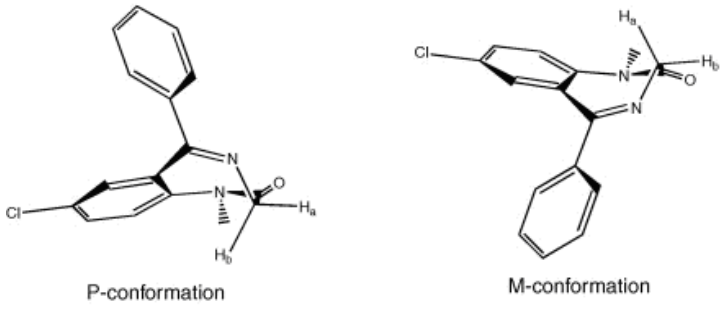

Figure 5.8. The chiral conformers of diazepam.

(Fitos et al, Bioorganic & Medicinal Chemistry, 15, 4857-4862, 2007)

NMR studies conclude that the two isomers are in dynamic equilibrium, with the half-life for both isomer being much less than one second at 23°C. The coalescence temperature for chlordiazepoxide is 41°C, with a half-life at this temperature estimated at 0.019 sec. If binding is stereospecific, one isomer will bind in preference to the other, the mixture will no longer be racemic and will result in intrinsic optical activity. The stereospecific effects will in turn change the optical activity of the albumin binding site of that drug. The induced optical activity will be due to perturbations in the chromophore when bound to HSA. Intrinsic optical activity is very weak in comparison and therefore these effects can be ignored.

5.2. Warfarin Binding

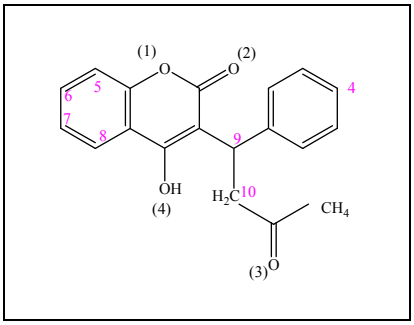

Figure 5.9. Schematic representation of warfarin.

Warfarin is an oral anticoagulant administered as a racemic mixture, sequestered by HSA such that 99% of the drug is found bound under normal therapeutic conditions, this leaves low levels for active distribution (*Curry et al, 2001*). On binding to HSA, warfarin binds to subdomain IIA (Figure 5.10.), and is one of the few ligands that show enhanced binding to

albumin in the presence of FA. On binding, warfarin displaces FA7 that binds within the same domain, but it is FA2 located between subdomain IA & IIA that is in close proximity to the warfarin binding site that plays a pivotal role. When bound, FA2 causes a displacement of subdomain IB resulting in the rotation of helices h2 & h3, thus moving the side chain of Tyr 150 previously within the pocket, to a position outside of the pocket to bind by hydrogen bonding with the carboxylate group of FA2. Arg 257 also rotates and hydrogen bonds.

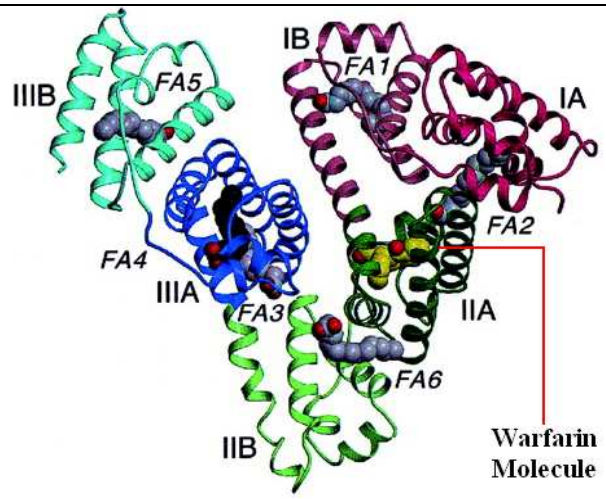

Figure 5.10. An overview as determined by X-ray crystal structure of HSA:Myr:Waf.

(Curry et al, J. Biol Chem, vol 276, iss 25, 22804-22809, 2001)
Domain I, II & III are colour coded as red, green and blue respectively with light and dark shadings representing the subdomains. The FA molecules are shown as space filled molecules (grey is the carbon molecules and red represents the oxygen molecules). Warfarin is shown in yellow depicting the carbon atoms.

The binding pocket found at IIA comprises of three sub chambers that are arranged in a 'sock like' formation, the chambers offering specific points of interaction for the ligand. There are seven openings to this pocket, 17% of the pocket is hydrophilic and 83% is hydrophobic with a surface area of 2234.1Å. There are a large number of basic residues within the binding cavity (*Perry et al, 2006*). Warfarin, being a relatively small molecule interacting with two of the potential three sub chambers available (Figure 5.11.), leaving

one sub chamber, or side pocket as it is also referred to, free for further possible ligand interaction, this side pocket is defined by residues Leu 219, Arg-222, Phe-223, Leu-234, Ile-264, Leu-257, and Ile-290. The interaction of warf:HSA is found to be hydrophobic with specific electrostatic interaction. The benzyl moiety interacts with residues Phe 211, Trp 214, Leu 219 & Leu 232, with aliphatic contacts from residues Arg 218 & His 242. It is particularly the interaction with Trp 214 that has been shown to be of particular importance, as substituting this residue results in reduced binding observed in warfarin.

The coumarin moiety resides in the main sub chamber that is found furthest from the entrance of the binding pocket, this site also occupied by other site I ligands such as 2,3,5-triiodobenzoic acid (TIB). Further hydrophobic interactions also include Val 241 found on the right hand side of the pocket and Arg 222 with electrostatic interaction offered by two of the three oxygen molecules from warfarin. Hydrogen bonding is found between the forth oxygen atom on warfarin with the side chain of His 242 and also to bound water molecules. However, it is the interaction of the oxygen molecules at position two, three and four that are the major considerations that fix the orientation of the bound warfarin.

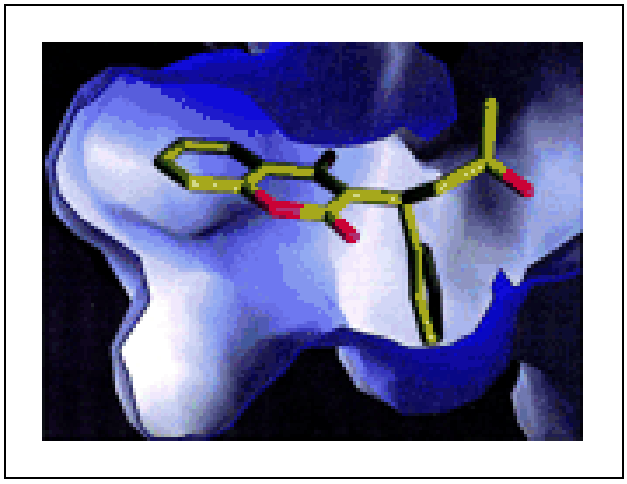

Figure 5.11. Side view of the binding pocket of subdomain IIA showing the sub-chambers.

(Curry et al, J. Biol Chem, vol 276, iss 25, 22804-22809, 2001)

The view of the pocket is rotated 180˚ about the vertical axis from the view of whole warf:HSA:Myr complex shown in Figure 5.10. The pocket is coloured to show the electrostatic potential with the blue depicting the basic patches.

5.2.i. Metabolism of Warfarin

Warfarin is used in the treatment in the prevention of thrombosis, embolisms and other disorders by decreasing blood coagulation. Warfarin works by inhibiting vitamin K epoxide reductase activity for vitamin K dependent clotting factors II, VII, IX & X, as well as regulatory factor proteins (*Costas Loannides, 2008*). The phenoxide group of warfarin has a pK_a 5.0, at pH7 warfarin exists as the anion (w^-) seen in Figure 5.12. (*Perry et al, 2006*).

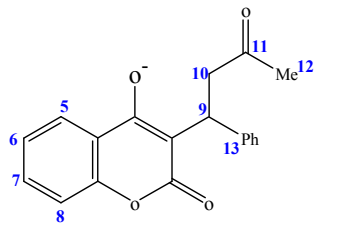

(W^-)

Figure 5.12. Warfarin anion.

The warfarin carboxylate is stabilised by Arg 218, Arg 222 & Lys 195. Two amino acid clusters exist within the binding pocket, the first is Lys 195, Lys 199 & Arg 222 located at the opening. The second cluster consisting of Tyr 150, His 242 & Arg 257 is located in the floor of the pocket. Warfarin is found to interact with the second cluster. Ligands with two anions also bind to this site and interact with both clusters. The main residues are thought to be Lys 199 & Arg 222 in cluster 1 and His 242 in cluster 2 that are thought to be of importance (*Perry et al, 2006*).

Although HSA shows little enantiomeric selectivity at this site the S(-) isomer of warfarin is between 3 - 6 times more potent, and is eliminated more rapidly than the R (+) - isomer (*Banfield et al, 1983*). It is thought that tryptophan is essential for warfarin binding (*Fehske et al, 1981*), and is thought to bind to site IIA of albumin (Sudlow site I). There have been some suggestions that there may be a second binding site for warfarin binding; when warfarin binds to HSA, the induced optical activity of the enantiomer can be

superimposed upon the intrinsic optical activity of the drug. The enantiomers of warfarin vary considerably in their intrinsic activities, but differ only slightly in their affinity to HSA, the S (-) isomer being bound only slightly stronger than the R (+) isomer. The induced optical activity of the R (+) and racemic warfarin appear qualitatively similar, and is represented in Figure 5.13. Studies involving warfarin and structurally related drugs have shown that parameters other than affinities have to be considered, warfarin/HSA binding is not a good model for studying drug transport-receptor interactions (*Brown et al, 1976*).

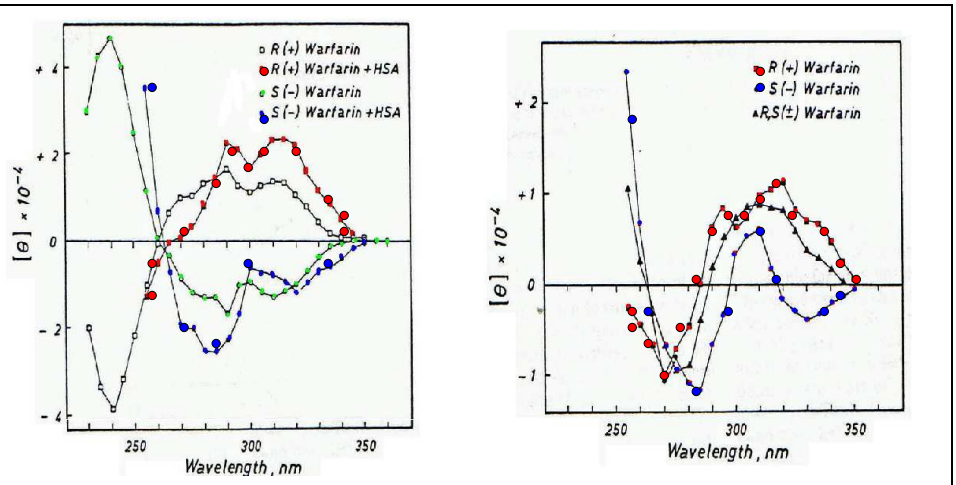

Figure 5.13.a. CD spectra of the S (-), R (+) and racemic warfarin bound to HSA.
(Brown et al, Molecular Pharmacology, 13, 70-79, 1976)

The CD spectrum of HSA has been subtracted from the enantiomers or waerfarin: HSA & racemic warfarin: HSA spectrums only (i.e. observing the induced CD of bound warfarin).

Both the R (+) and S (-) enatiomers bind in very similar conformations to HSA in what is termed an "open conformation," enabling the coumarin groups to rotate or flip 180˚ about the C1-C13 bond resulting in almost superimposable conformations (*Curry et al, 2001*, *Chuang et al, 2006*). The acetonyl group that stems from the chiral carbon of warfarin lies at the mouth of the pocket, and it is this that depicts the differences between the two enantiomers (Figure 5.13.). When bound, both enatiomers exhibit almost identical contacts to the aa within the binding cavity, and it is this that accounts for the lack of stereospecificity of warfarin with HSA (*Curry et al, 2001*).

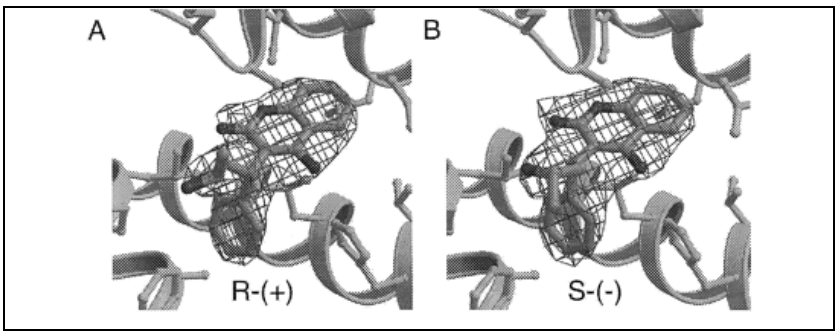

Figure 5.13.b. Electron density map showing the bound enantiomers of warfarin to HSA:Myr.

(Curry et al, J. Biol Chem, vol 276, iss 25, 22804-22809, 2001)

The metabolites of warfarin are 6- and 7-hydroxy warfarin, and RS and SS-warfarin alcohols which are represented in Figure 5.14., the former metabolites undergo reduction forming the two diastereoisomeric alcohols. The 7-hydroxy warfarin is one of the most important by-product of S–warfarin; the isomers of warfarin show different anticoagulant activities and metabolism and should be considered as two separate drugs, they are also dose and concentration dependent (*Aoki et al, 1973*). The metabolites of the enantiomer of warfarin are excreted in different ways, the S-enantiomer undergoes hydroxylation at the aromatic coumarin ring at position 7 and is eliminated in the bile, and a small amount of the diastereoisomeric alcohol is formed. The R-enantiomer is reduced to the RS alcohol and is excreted in urine; a small amount of 7-hydroxy warfarin is also formed. Both enantiomers produce the same amount of 6-hydroxywarfarin.

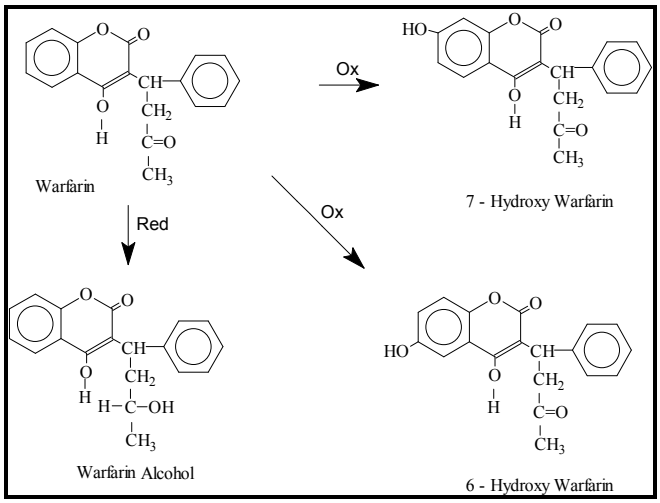

Figure 5.14. The metabolites of warfarin.

There is much speculation about an alternative binding site for warfarin, and indeed speculation of there being a second site located close to myristate bound in close proximity to subdomain IB has been suggested (*Curry et al, 2001, Dockal et al, 2000 & Perry et al, 2006*), the same site that is speculated to accommodate TIB. The binding constant has been suggested to be approximately $0.12 \pm 0.15 \times 10^{-3}$ M^{-1}. Experimental data shows the c-terminal of domain I to be important for the functionality of site II and that the combination of domain I & II was sufficient to bring about the binding of warfarin; domain III was found to be of little importance to warfarin binding (*Dockal et al, 2000*). Although site IB has been found capable of accommodating the coumarin moiety, no space has been found that can accommodate the rest of the drug molecule. Therefore, for this reason this location has been ignored. No other site has been determined for this drug.

The presence of FA as previously stated has a significant effect on the binding of warfarin, its presence has been shown to increase warfarin binding. FA are known to cause great conformational changes in HSA resulting the rotation of domain I and domain III relative to domain II (*Simad et al, 2006, Curry et al, 2001*). The presence of 3Mol of FA per mole of HSA produces a 3 fold increase in binding of warfarin, with concentrations exceeding that value producing reduced binding of warfarin. Since there are FA binding sites in close proximity to the warfarin binding site, then at high concentrations of FA will result in competition between the warfarin molecule and the FA molecules. It has been determined that FA site 7 overlaps with site IIA and shares two aa side chain with FA site 2 (*Simad et al, 2006*). Without the binding of FA2 the side chain of Tyr 150 lies within the binding pocket, binding of the FA displaces Tyr 150 by binding it to the carboxylate group of the FA, displacing domain IB by rotating helices h2 & h3 (*Curry et al 2001*).

After the N-B transition, ligands are bound with a different affinity to that of the N-form. Possible interactions between the two sites have been suggested by allosteric interaction in

HSA, these allosteric effects have neither still not been qualified nor the dynamics between the two sites. It is speculated that the point of interaction between the two domains (IB & IIA) is said to be for the purpose of communication (*Kreigh-Hanson, 1999*), with the greatest sensitivity of HSA observed in the N-conformation. It is thought that the transition to the N-B transition changes from a heart shaped molecule to an ellipsoid.

5.3. Derivatives of Salicylic Acid

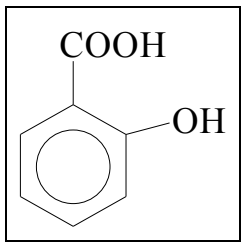

Figure 5.15. Schematic representation of salicylic acid.

Derivatives of salicylic acid drug also belong to the family of drugs called nonsteroidal anti-inflammatory drug (NSAID), widely used throughout the world because of their therapeutic properties for treating a wide range of symptoms. Aspirin, the acetylated form of Salicylic acid (SA) is taken orally for a wide variety of conditions; it has analgesic, anti-inflammatory and antipyretic properties, and can be used to inhibit the biosynthesis of prostaglandins. Aspirin increases bleeding time by decreasing platelet adhesion, and can also be used for pain relief and for acute and chronic inflammatory disorder, e.g. rheumatoid arthritis. Aspirin was the simplest of the drugs considered; nevertheless its importance in drug therapy is resounding. Salicylic acid's small size and ability to bind to more than one site makes it an ideal tool for multi-binding ligand investigations. Appropriate conditions are chosen such that the preferred high affinity site is occupied, this would allow the second site to be probed.

The pioneering work of Carter and He in 1992 in their determination of the first high resolution X-ray crystal structures of albumin highlighted the classic binding sites first

determined by Sudlow. The findings proved the limited binding was seen in mainly subdomains IIA & IIIA. However, this has been found not to be the whole story since the diffraction patterns were determined from defatted albumin crystals when the importance of FA was not quite realised at that time. Although Carter and He recognised that albumin was a carrier of FA, more recent work has determined that albumin's primary function is in the transport of FA, and it is these molecules that have been found to control the tertiary structure of albumin (*Curry et al, 2001*, *Chuang et al, 2006, Muravskya et al, 2004, Bhattacharya et al, 2000, Kragh-Hansen et al, 2000 & Yang et al., 2007*). It is for this reason that albumin is referred to as 'flexible' as it is the presence of FA that has been shown to alter the size and shape of the binding pockets and the molecule as a whole (Figure 5.16.). Bound FA means that for SA bind to subdomains IB & IIA, with subdomain IIA now being the dominant site, the X-ray crystal structure of bound SA is shown in Figure 5.17.

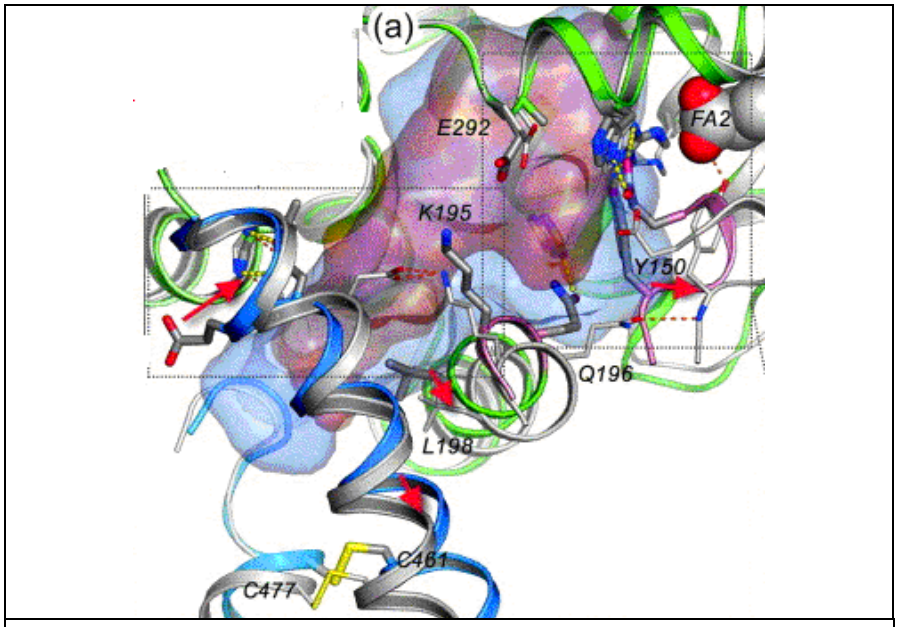

Figure 5.16. Conformational changes that are associated with site I in the presence of FA.
(Curry et al, J.of Mol Biol, vol 353, Iss 1, 38-52, 2005)

The superposition of binding site I in the absence of Myr is shown in light brown, and in the presence of Myr is shown in light blue which shows an expansion of the binding pocket. The red arrows indicate the direction of movement of the pocket. Also shown are the relevant residues associated with the functionality of the pocket, FA2 is shown in the top right hand corner.

Another way in which FA can affect the tertiary structure of albumin is that its presence or absence will affect the specific binding sites of known marker ligands, in particular salicylic acids and its derivatives and warfarin (for a more detailed account on FA binding to HSA refer to Chapter 2). The number of FA molecules bound to albumin is also a determining factor, the presence of five Myr molecules will mean that domain II does not have any FA molecules bound in this region, whereas with seven Myr molecules bound to HSA reveals that FA7 binds to subdomain IIA (*Zhu et al, 2008*).

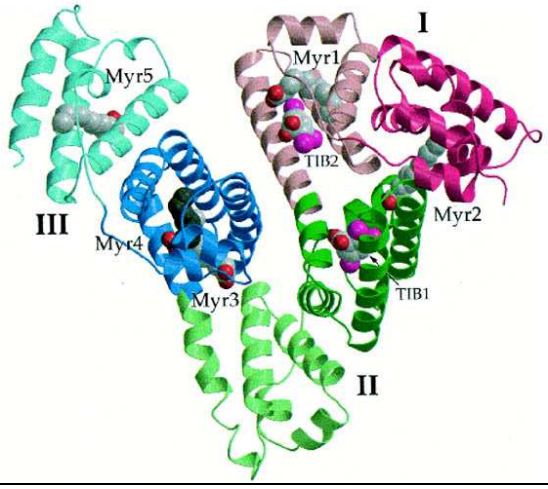

Figure 5.17. X-ray crystal structure of Myr:HSA:TIB.
(Curry et al , Nature Structural Biology, 5, 827-835, 1998)

5 Myr molecules bound to 1 HSA molecule with 2 TIB in situ bound to subdomains IIA & IB. The presence of bound Myr has changed the dominant binding site of TIB from subdomain IIIA to IIA and the secondary site from IIA to IB.

Table 5.1. represents the points of contact of the ligands with albumin showing the residues within the binding cavity together with the protein side chain interaction.

Ligand	Binding location	Ligands to carboxylate[1]	Residues lining cavity wall
Myr1	IB	**IB:** R117[2] (2.9)	**IB:** R117, P118, M123, F134, Y138, L139, I142, F157, A158, Y161, F165, L182
Myr2	IA-IB-IIA	**IB:** Y150 (2.8) **IIA:** R257 (3.1) S287 (2.4)	**IA:** V7, R10, L14, F19, L22, L66 **IB:** A151, P152 **IIA:** L250, L251, A254, A258, L283, L284
Myr3	IIIA	**IIB:** S342[2] (2.9) R348 (2.6) **IIIA:** R485 (3.1)	**IIB:** V344, L345 **IIIA:** P384, L387, I388, F403, L430, V433, N439, M446, A449, E450, L453, R485
Myr4	IIIA	**IIIA:** R410 (3.0) Y411 (2.8) S489 (2.9)	**IIIA:** Y411, V415, V418, T422, L423, V426, L430, L453, L457, L460, V473, R485, F488, L491
Myr5	IIIB	**IIIA:** Y401 (3.4) **IIIB:** K525 (2.6)	**IIIB:** F502, F507, F509, K525, A528, L529, L532, V547, M548, F551, L575, V576, S579, L583
TIB1	IIA	**IIA:** K199 (3.2) H242 (2.8)	**IIA:** L219, F223, L234, L238, V241, L260, A261, I264, I290, A291
TIB2	IB	**IB:** H146 (3.0)	**IB:** I142, F149,L154, F157, Y161, R186, G189, K190

Table 5.1. Ligand-binding residues in HSA.
(Curry et al , Nature Structural Biology, 5, 827-835, 1998)
Table shows the distance of closest approach of a protein side chain atom to one of the carboxylates oxygens in Å.

The absence of FA as determined by Carter and He produce two specific binding sites for 2,3,5-triiodobenzoic acid (TIB), a derivative of salicylic acids with the dominant and primary site located in subdomain IIIA, the second site was located in subdomain IIA (*Carter et al, 1992)*. However, in the presence of FA, albumin experiences conformational changes that result in changes in the specific binding site for salicylic acid. The FA myrastate (Myr) binding to HSA has been shown to cause a rotation of domains I & III relative to domain II (*Zhu et al, 2008*). Now the dominant binding site is found in subdomain IIA with the second site located in IB that also binds Myr 1 with the two ligands in close contact (*Curry et al, 1998*), a site not renowned for its binding ability but has been shown to have increasing prominence as warfarin has also been shown to bind to this site (*Zhu et al, 2008*). The relocation of TIB to sundomain IB is thought to be due to the fact that Myr 3 & Myr 4 both bind to sbdomain IIIA and TIB is incapable of displacing the FA's from their sites, therefore relocates to the low affinity site. This phenomena exhibited by TIB has been shown to exist in other drugs such as the binding of arsenic where two types of protein binding was shown, strong affinity binding to a small number of sites or weak affinity binding to a large number of sites, the site is dictated by the concentration of the ligand (*Uddin et al, 2004*). With seven Myr molecules bound, Myr 7 is found to bind very weakly to IIA with the result that most drugs will displace it on binding, warfarin is found to cause displacement of this FA (*Petitpas et al, 2001, Yang et al, 2007*). However, some drugs such as AZT are not capable of displacing Myr 7 but coexist; displacement is governed by ligand affinity.

Three derivatives were considered, salicylic acid (SA), 5-iodosalicylic acid (5ISA) and 3,5-diiodosalicylic acid (DIS) for their binding properties to albumin and their relative stabilities. The derivatives increased in size by a controlled and known amount, this enabled the theory on ligand size (a possible important parameter in site IIA binding) to be

investigated. The effect of binding derivatives would highlight whether one or both on the binding pockets are affected, this together with changes in the environment such as pH and temperature, should aid to give a better understanding and characterisation of the binding pockets of HSA.

5.4. Multiple Ligand Binding

Multi binding of ligands to albumin is dependent upon the affinity constant (K_f) of each ligand. The ligand with the greatest value of K_f will bind in preference to the others provided that they bind to the same site on the protein, the assumption being that both ligands will compete. However, if the ligands bind to different sites competitive binding is no longer a consideration, provided that one ligand does not alter or change the binding site of the other ligand; Table 5.2. gives some general information on the binding characteristics of some of the drugs studied. The use of ligands with known binding sites meant that it was possible to investigate and characterise drug and other ligands of unknown binding information based on the response and effect on known marker ligands. The presence of two or more strongly binding ligands produce competition at the binding site resulting in a higher concentration of free (unbound) drug, and a greater biological activity of both drugs then if the drugs were present individually (*Perrin et al, 1973).*

Ligand	K_a (in the absence of protein) (M^{-1})	n (no protein)	pK_a (no protein)
Salicylic Acid	2.80×10^{-4}	2.2	3.0
Warfarin	21.0×10^{-4}	1.2	5.1
Diazepam	18.0×10^{-4}	1.0	3.3
Tryptophan	1.10×10^{-4}	0.9	-

Table 5.2. The properties of some ligands investigated.

With the relatively new X-ray crystallographic determination of the sub-chambers in site IIA, it has been found possible for each of the sub-chambers to bind independently making it possible for three ligands to bind and exist within the same pocket.

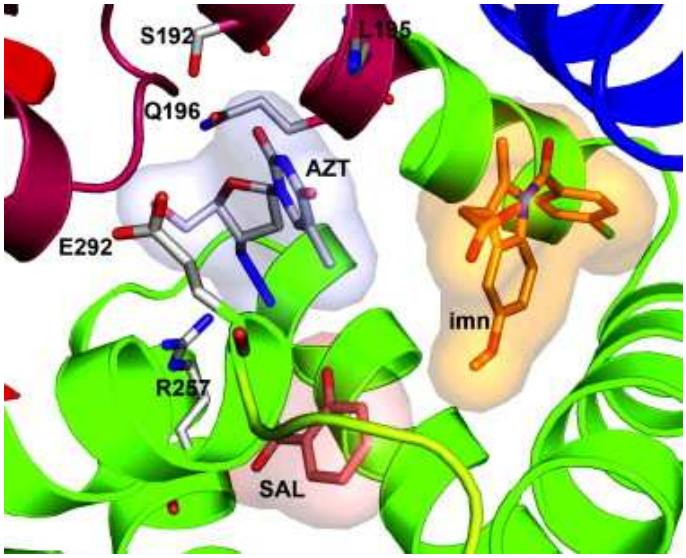

Figure 5.18. The binding of three independent ligands in the sub-chambers of IIA.
(Zue et al, J. of Structural Biol, Vol 162, Iss 1, 40-49, 2008)

AZT is bound in one chamber and is represented in pale blue, indomethacin (Imn) is bound in another chamber and indicated as pale orange, and finally salicylic acid (Sal) is shown as pale red.

5.4.i. Diazepam : Warfarin Interaction with Albumin

Warfarin binds to site IIA on HSA, while diazepam binds to site IIIA, therefore one would not expect these two ligands to compete but to coexist. Experiments such as equilibrium dialysis and fluorescence have shown that the binding of warfarin was not compromised in the presence of a constant amount of diazepam. What is surprising is that the binding of diazepam is somehow enhanced by the presence of warfarin (*Kragh-Hansen, 1985*); independent binding of the two ligands exists, but there appears to be some sort of coopertivity established when both drugs are present.

5.4.ii. Warfarin : Salicylate Interaction with Albumin

Salicylate binds to domain IIA and IIIA on HSA in the absence of FA. It is therefore expected to see some sort of competitive interaction between salicylates and warfarin when both are present. Warfarin, in the presence of salicylate exhibits diminished binding, this is

also true for salicylate in the presence of warfarin. There is a mutual decrease in binding of one drug with respect to the other. From Table 5.2., it would be expected that because of the large difference in K_a between the two drugs with warfarin exhibiting a very much greater K_a than salicylates, warfarin would displace salicylates from its preferred site, that of site IIA if warfarin was added as the antagonist. Conversely, if the situation was reversed with salicylates now added as the antagonist, it would be expected for SA to bind to site IIIA only leaving site IIA occupied by warfarin, the stronger binding ligand.

5.5 Experimental

5.5.i. Materials

All the samples of albumin and the domain fractions were donated courtesy of Dr John Woodrow (Delta Biotechnology, Nottingham, UK). Purification was conducted by either dialysis using tubing with a molecular weight cut-off of 10,000 supplied by Delta Biotechnology, or by column chromatography. In the case of dialysis, the tubing was pre-treated in a warm solution of 0.05% EDTA and 2% sodium bicarbonate (both at analytical grade supplied by BDH) and made up in distilled water, done to clean and degrease the tubing. The alternative method was to use column chromatography using Sephadex G 25m (PD-10) columns, (Code Number-17-0851-01, Lot Number SA 15390, supplied by Pharmacia). All samples of albumin were freeze-dried and stored in the refrigerator until use.

The sample of warfarin used throughout this thesis was purchased from Sigma, UK, (Reference Number A-2250, Lot 16F0026). The diazepam (BN:811009, RO 5-2807) was a gift from Roche Products Ltd, Welwyn Garden City (Hertfordshire). SA, 5ISA and DIS were bought from Aldrich chemicals (UK). Both urea and GuHCl were purchased from

Fluka Biochemika (UK), 99.99% purity. L-tryptophan and all the buffers used were bought from BDH (UK), analar grade to ensure the highest chemical and optical purity.

5.5.ii. Procedure

Binding studies were conducted using a fixed concentration of the drug (concentration of 1M equivalent) to varying concentrations of albumin, all made up in 10mM P/B. Samples of albumin was made up at 2x the required final concentration, with the drug concentration made up at 2 molar equivalent. These were referred to as the protein and drug stock solutions respectively. From the drug stock solution (2M≡), 500µl aliquot were measured using a calibrated Gilson pipettes and put into a series of containers. Into each container was placed a known aliquot from the albumin stock, and the remainder of the volume was made up with P/B so that the total volume added of the two components (P/D & albumin stock) was 500µl. This formed the titration series, each container containing 1M equivalent of the drug on final dilution but varying concentrations of albumin, all made up in P/B. Both CD and UV spectroscopy measurements were obtained of the titration series; for a few experiments the experimental conditions were reversed by now keeping the concentration of albumin fixed at 1M equivalent, the concentration of the drug was varied and compared with the other experimental data to see if there were any variations in the results of the titration curves; the final titration was conducted where a [1:1] molar equivalent of the drug and protein was titration with a 1M equivalent of drug, this ensured that the concentration of drug in the container remained fixed but the molar ratio equivalent varied as the addition of drug diluted the albumin concentration.

pH measurements was conducted on a 3ml sample of the ligand:protein complex solution, diluted to the required P/D ratio in distilled water. The complex solution was divided into two equal portions, one for investigations at low pH and the other for high pH

investigations. Using either 0.1M, 1M or 10M sodium hydroxide or hydrochloric acid (as pH adjusters), the pH was adjusted to the required value and the UV and CD were measured. The use of a range of pH adjusters meant that the volumes added would be small thus minimising dilution effects, the consequences of this meant that dilution factors did not have to be considered as they were within the realms of experimental error. At the end of the titration, both at low and high pH adjustments, the samples were readjusted to physiological conditions, and rechecked by UV and CD to determine if the adjustments at the extreme conditions were reversible.

Finally temperature studies were conducted by three methods; the first method was to take a stock solution of albumin at 2x the required concentration and placed it into a water bath. The temperature of the water bath increased to a pre-determined temperature and the stock sample heated, once at equilibrium the temperature measured and a 500µl aliquot sample removed and cooled to RT. The water bath thermostat was then increased and the sample allowed equilibrate, once established a new 500µl sample was removed, cooled and stored for further investigation. This process was repeated until a series of preheated samples from RT to 90°C were obtained, each time 500µl aliquot was removed. Once all the samples were collected, to each was added 500µl of the 2 molar equivalent stock solution of the drug under investigation producing a [1:1] molar equivalent of protein:drug (P/D) sample. The samples were mixed and measured by UV and CD between the range of 600nm – 240nm.

A second method investigated the unfolding of a solution of the complex at known P/D ratio. The sample under investigation was put into a cuvette and placed into the thermostatically controlled holder in the CD spectrometer. A thermocouple was placed through the lid of the cuvette, immersed in the solution held in the neck of the cuvette. This allowed a more accurate determination of the solution's actual temperature of the

complex as a direct measurement was determined. The temperature of the water bath controlling the cell holder was adjusted to a required value, allowed to equilibrate, the temperature in the cuvette was recorded and the CD measured between 600nm – 240nm. The process of increasing the temperature by regular increments and recording the CD was repeated until the complete unfolding of the P/D complex was achieved and binding lost.

The third method used to study heat denaturation was to investigate the systematic heating and quenching of a simple of the complex through temperatures cycling ranging from RT to 90°C. A sample of the complex was taken of known P/D ratio and placed into the thermostatically controlled CD spectrometer and the CD recorded. The temperature was increased, recorded, and the CD determined after a period of equilibration. The sample was allowed to cool down to RT and a further scan measured. The cooled sample was then reheated to a higher temperature, increased by a predetermined amount, allowed to equilibrate and once again recording its temperature and CD spectra. The sample was cooled to RT, its CD determined and the whole cycling process of heating and quenching repeated for temperatures up to 90°C, all data was compared.

Some samples of the complex was studied after microcentrification. This involved the samples being filtered through a filter contained in an eppindorf tube while being centrifuged at a speed of 1500rpm for approximately 10 minutes, or until enough filtrate was collected that could be measured by UV. The amount of filtrate collected was only small, approximately 100µl, therefore a specially designed cell adapted by Dr A. F. Drake (Kings College London, and made by Helma, UK) was used to record the UV spectra.

5.6. Results of Warfarin Studies

5.6.i. Warfarin Binding

The binding of warfarin was one of the first drugs to be considered as it binds to a single site on albumin (site IIA). The titration of a fixed concentration of the drug to varying concentrations of albumin was adopted and can be shown in Figure 5.19. It should be noted that the CD spectra of the racemic solution of warfarin was complicated by the apparent production of small but detectible CD signal produced by the racemic drug. It was expected that the racemic mix of the drug should produce a CD spectrum of zero through all wavelength regions in the absence of the protein. However, what was found was that the racemic mixture produced a CD maximum that corresponded to the absorbance maxima detected in the UV spectra. The binding of the racemic drug induced CD spectra that were characteristic of the association between the specific drug and the protein and can be used as a handle to monitor changes. The CD also reflected the environment of the drug while bound, and will produce a spectra characteristic to the product with distinct positive and/or negative maxima. Figure 5.19.a. highlights the apparent small positive CD detected found for the racemic warfarin in the absence of protein, shown to be a broad positive maximum expanding the wavelength range of 350 – 290nm; the consequence of the wasrfarin only CD was that it produced an offset when the fixed wavelength plot was plotted as shown in Figure 5.19.b. To normalise, the warfarin CD was subtracted from the data so that the results now pass through zero, this did not affect the overall trend observed merely the point of origin.

The UV absorption of the warfarin titration is shown in Figure 5.19.c. and is found to have a maximum centred at 310nm with a shoulder around 290nm, further absorptions were detected at shorter wavelength but these overlapped with the very strong absorption associated with the protein backbone, making then very difficult to monitor.

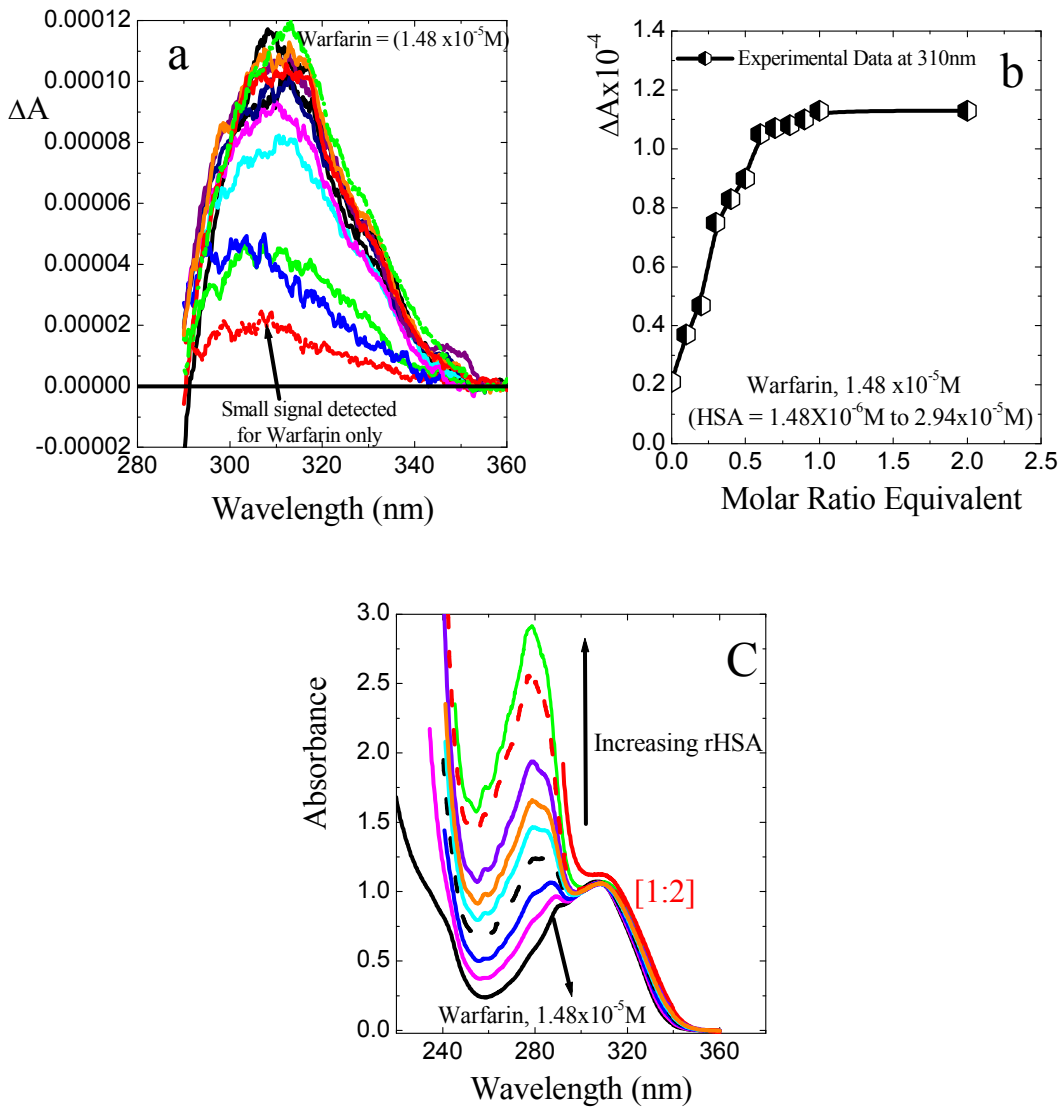

Figure 5.19. Titration of a fixed concentration of Warfarin to rHSA, 5cm cell.

a. The binding of Warfarin to rHSA for ratios between 1:0.1 to 1:2 in P/B, pH7.2, 5cm
b. Fixed wavelength plot of warfarin binding to rHSA, P/B.
c. UV Absorption Spectra of Warfarin:rHSA [1:0.1] to [1:2] equivalent, P/B, pH7.2, 5cm cell

The CD of bound warfarin to albumin was found to contain a positive maximum at 310nm with a shoulder detected at 335nm, the samples were measured in a 5cm cell to compensate for its weak Cotton effects in the CD spectrum. The binding constant determined for this experiment was found to give $K_a = 5 \times 10^{-6} M^{-1}$.

The conditions were altered to the warfarin binding titration such that a larger wavelength region was monitored with a view to monitor the large negative maximum detected at 275nm, overlapping the backbone region and are shown in Figure 5.20. The fixed wavelength plots confirm a one to one drug to protein (D/P) relationship.

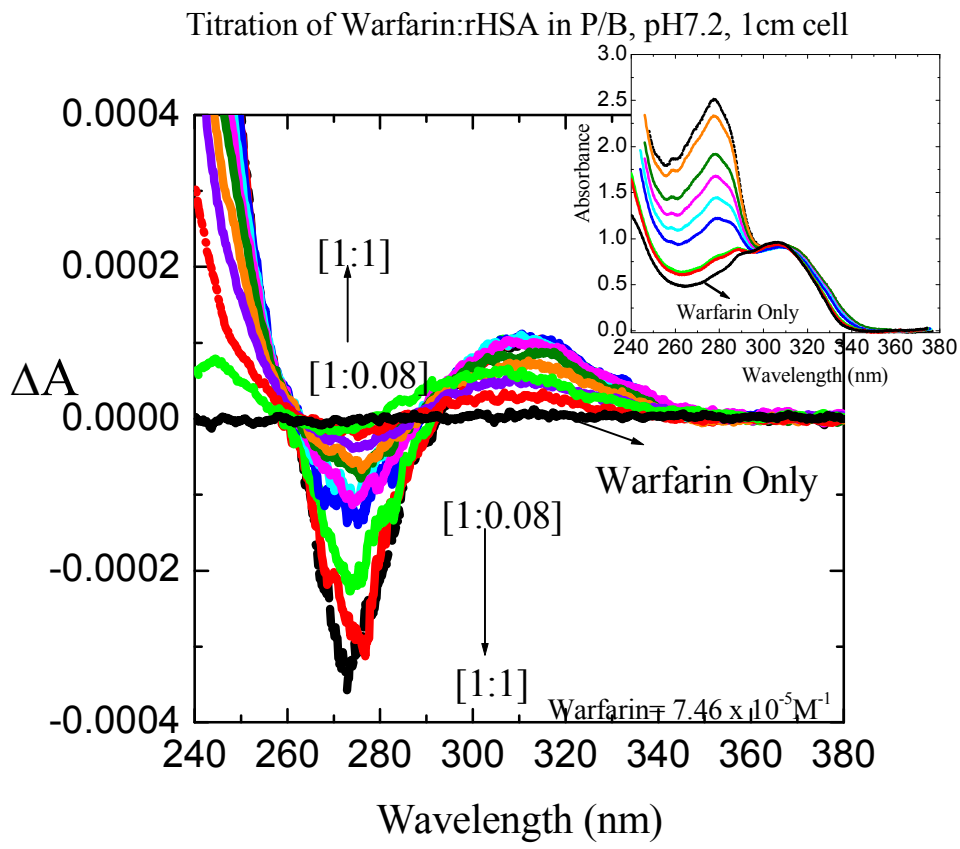

Figure 5.20. Titration of a fixed concentration of Warfarin to rHSA, 1cm cell.

Under the conditions studied in the 1cm cell, the binding constants determined by the fixed wavelength plot revealed for wavelengths 335nm & 312nm values of K_a 5 x $10^{-6}M^{-1}$ (Figure 5.21.). It was reassuring to find that the titration in both the 1cm and 5cm cell gave identical K_a values. However, at the wavelength 275nm which lies directly under the protein backbone, a transition was detected that did not reflect the changes seen at the other

wavelengths. There appeared to be two transitions evident with the second transition not quite obtaining completion for a P/D ratio of [1:1].

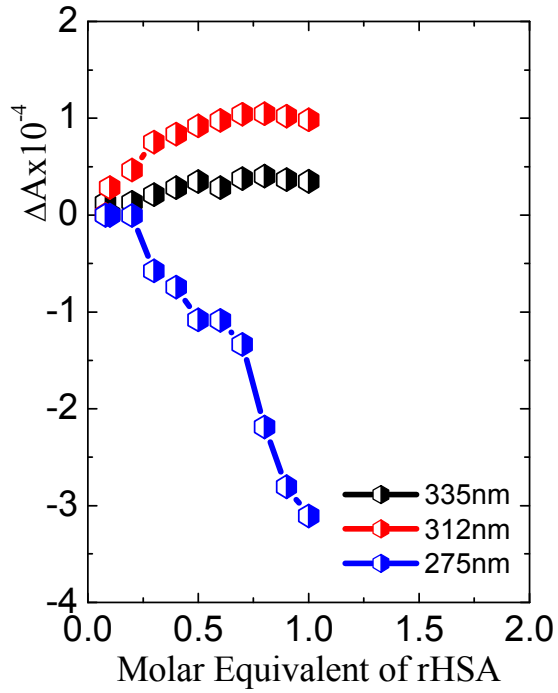

Figure 5.21. Fixed wavelength plot of the titration of a fixed concentration of Warfarin (7.46 x 10^{-5}M) to rHSA, P/B, 1cm cell.

5.6.ii. Warfarin pH Studies.

The P/D ratio of a [1:1] molar ratio equivalent solution of warfarin/rHSA was investigated with changing pH for the three wavelength regions highlighted previously (335nm, 312nm & 275nm). The pH transformations observed in rHSA revealed complex transitions in response to changing pH, with the result that rHSA, on binding to warfarin, produced transitions that overlapped the aromatic region of the protein alone (Figure 5.22.). Depending on the wavelength investigated, either two or three transitions were observed. At 255nm two transitions were seen, and at 287nm three transitions were observed, the results are shown in Table 5.3.

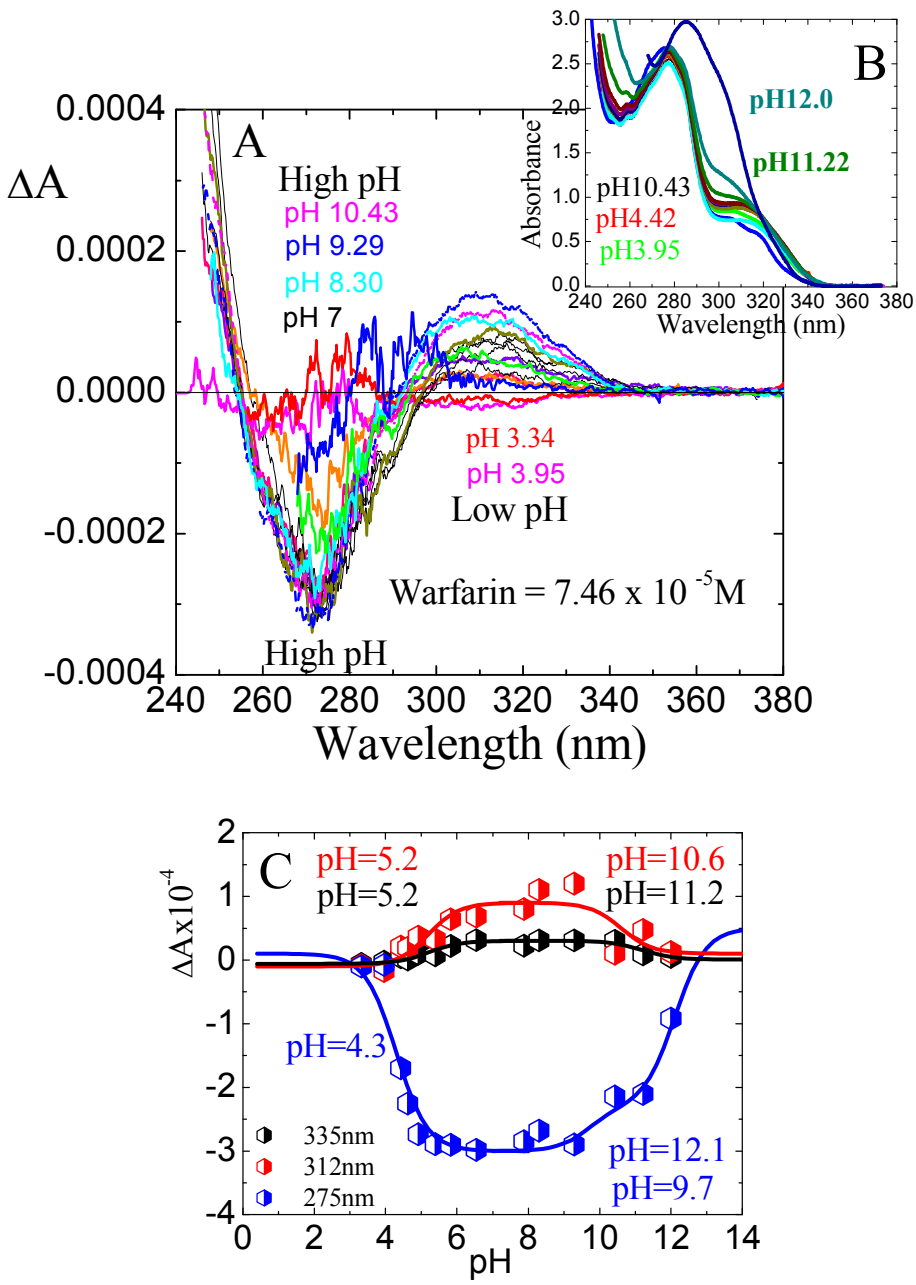

Figure 5.22. pH Titration of a [1:1] molar equivalent of warfarin:rHSA.

A. CD Spectra of the pH titration of warfarin:rHSA, [1:1] in H_2O, 1cm cell.
B. UV Spectra of the pH titration.
C. Fixed wavelength plot of the pH titration of warfarin:rHSA, [1:1] molar equivalent, 1cm cell

The pH titration revealed that the association of the drug to the protein only existed when the pH was not in the extreme regions of the range; otherwise binding was lost once the protein was in the extended form or in the aged form.

pK at 255nm Aromatic for rHSA only		pK at 287nm Aromatic for rHSA only			pK at 312nm Warfarin:rHSA		pK at 335nm Warfarin:rHSA		pK at 275nm Warfarin		
1st	2nd	1st	2nd	3rd	1st	2nd	1st	2nd	1st	2nd	3rd
4.0	11.5	3.5	6.1	11.7	5.2	10.6	5.2	11.2	4.3	9.7	12.1

Table 5.3. pK values of the transitions of Warf:rHSA complex of ratio [1:1].

Comparisons of the pK values between bound warfarin to albumin and albumin only revealed that although tree transitions were seen they were not necessarily in the same region. Once again it was the transitions at wavelength 275nm that highlight the multiple steps involving an intermediate transition with a pK 9.7, not seen in the aromatic residues of the protein nor in the secondary structure of the backbone (refer to Table 4.0 in Chapter 4). The first transition observed at wavelengths 312nm & 335nm reflected the second transition detected in the backbone of the protein only, suggesting that it could be possible changes in the secondary structure of albumin that affected subdomain IIA at this pH. At wavelength 275nm the changes monitored here possibly reflect the changes in the aromatics residues of the protein, occurring at a lower pK value, but not as low as the first transition in the backbone region of the protein that occurred around pK 3.0 and below.

The final pH experiment conducted in this series was to microcentrifuge all the pH adjusted samples of the 1 molar equivalent Warf:rHSA complex to see if it was possible to determine the free unbound drug , the results are shown in Figure 5.23. The experiment highlighted four regions of transition with pK's of 4.1, 5.4, 7.1 & 8.6. For a [1:1] molar ratio equivalent solution of the complex two pH regions were isolated where maximum binding of the drug to the protein was seen, and that was at pH5.4 & pH8.6. Surprisingly,

the highest quantity of free warfarin was found at pH7 with approximately 75% of the drug bound and 25% free. Conversely, at pH 4,8 and at pH 8 were found the highest amounts of bound drug with only trace amounts being found unbound in solution.

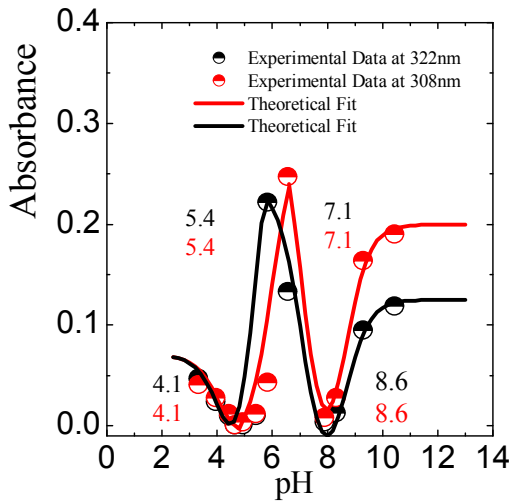

Figure 5.23. Microcentrifuged samples of the pH titration of a [1:1] molar ratio equivalent of Warf:rHSA, 1cm cell.

The filtration through micro-eppingdorf filter tubes proved in this instance to be an effective way in determining the amount of free drug presents, highlighting the conformational stability of albumin in response to pH and in the presence of a drug.

5.6.iii. Warfarin Temperature Studies.

The binding pocket of albumin to warfarin was investigated further with the response of the complex to temperature. On heating the warfarin complex revealed a continuous and increased dissociation of the drug with increasing temperature, with the loss of binding that appeared to occur in one transition as shown in Figure 5.24.a.. The dissociation of the drug was initiated by the onset of heating, occurring at temperatures where albumin in isolation has been shown to have no significant denaturation effects (i.e. below 60˚C). The possible

movement and separation of domain I & II exposes IIA to such a degree that the pocket moves closer to the surface of the molecule, making it more accessible to local environmental changes. Heating causes further exposure and denaturation of the site producing greater deleterious effects. For temperatures exceeding 70°C the binding of warfarin was totally lost, supporting the theory that domain II becomes totally denatured at these temperatures. The transition temperature for the Warf:rHSA complex was found to be 46˚C, and showed the relative instability of the complex towards heating, but was higher than the first t_m detected for rHSA which was found to be at 40˚C. The value of K=10 x 10^{-3} and was found to be lower than that for rHSA alone.

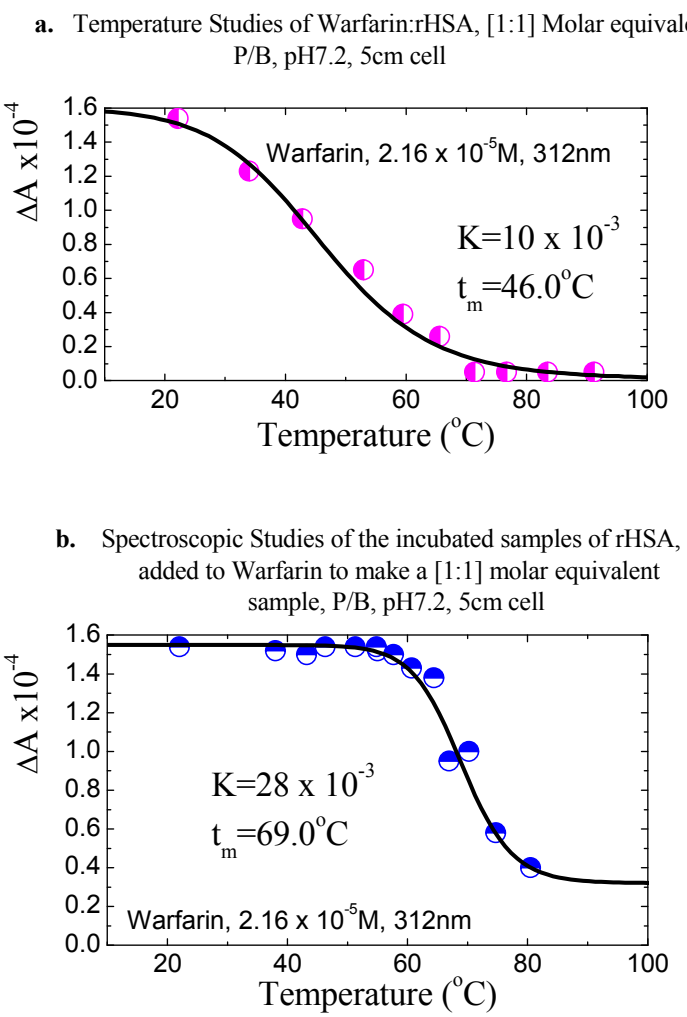

Figure 5.24. Temperature studies of warfarin:rHSA complex.

Preheating the albumin samples prior to binding reflected the conformational changes that resulted within albumin and revealed that functionality of binding site IIA after heat was applied. As expected preheating albumin to 60°C revealed no instability of the binding site, the drug was still fully bound to the protein at this point. For temperatures between 60 - 65°C revealed a slight loss of binding (Figure 5.24.b.). For the temperatures of 65°C – 75°C binding of warfarin was dramatically affected with a cascade in the loss of the drug. The pre-incubated temperature studies highlighted the true loss in binding of warfarin occurring at temperatures exceeding 63°C that reflected the denaturation temperature of albumin only. Once albumin was denatured, binding was rapidly lost supporting that fact that site IIA was rapidly exposed on heating and de-shielded from domain I. The t_m was determined to be 69.0˚C and the value for $K = 28 \times 10^{-3}$ determined for the binding pocket of IIA, lower than that determined for the second transition in rHSA only that was found to be $K = 45 \times 10^{-3}$. From the results it would appear that subdomain IIA denatures between the first and second transition of albumin, supporting the fact of the fragility of IIA.

Cycling the temperature between heating and quenching, measuring at each temperature change the CD spectra of the heated and quenched samples reflected the culmination of the previous two heating methods studied and is shown in Figure 5.24. The sequential heating and subsequent quenching of a [1:1] molar ratio equivalent of the complex of warf: rHSA is represented in Figure 5.25., and reflected the intolerance to direct heating of the complex. However, quenching the sample highlighted some re-association of the drug, re-establishing the complex but never to the same degree as that detected before heating (or that that was found for the pre-incubated samples heated to 60°C). The greatest loss in binding was observed between 60°C - 75°C with the establishing of two transitions for

both heating and quenching. The results of the last temperature cycling experiment revealed the combination of the previous two experiments that detected the fragility of the binding of warfarin in the presence of heat (Figure 5.25.) with a transition observed at RT, this was supported in the results of the quenching curve that showed the loss of immediate binding once heated. Both the second transition of the heating curve and the first transition of the quenching curve gave very similar values for t_m, and the same value for K. The second transition for the quenching curve showed the decomposition of IIA.

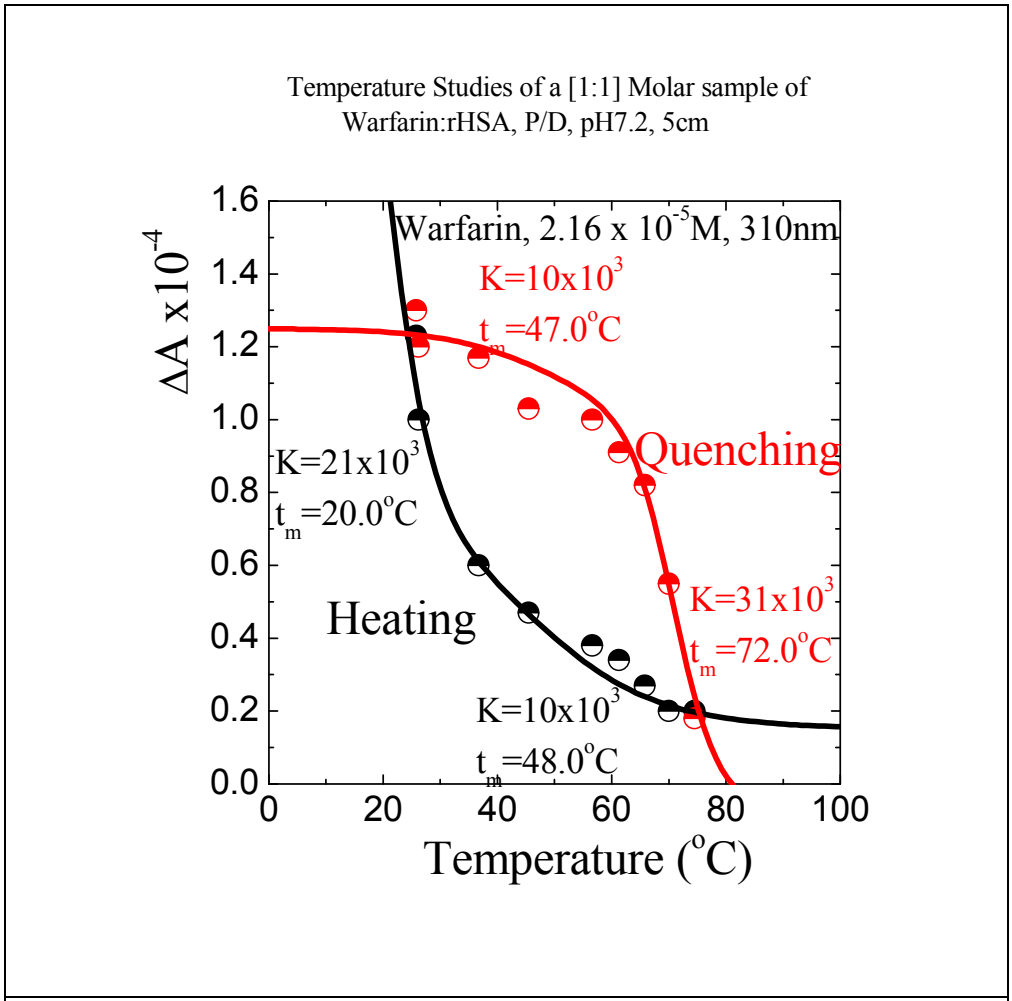

Figure 5.25. Heating and quenching studies of warfarin:rHSA.

The [1:1] warfarin:rHSA heated samples were spun in a microcentrifuge in special eppingdorfs containing micro-filters, this allowed only the free drug solution to pass through. Figure 5.26.a. shows the results of the filtrate obtained after spinning and revealed that there was always an association of the drug to the protein even at high temperatures,

albeit very small. The fixed wavelength plot (Figure 5.26.b.) suggests a gradual loss in binding up to a temperature of 60°C. By 63°C an extensive loss in binding is seen with the continued loss reaching a maximum by 76°C.

a. Microcentrifuged samples of the temperature investigation of a [1:1] molar sample of warfarin:rHSA, P/B, pH7.2, 1cm

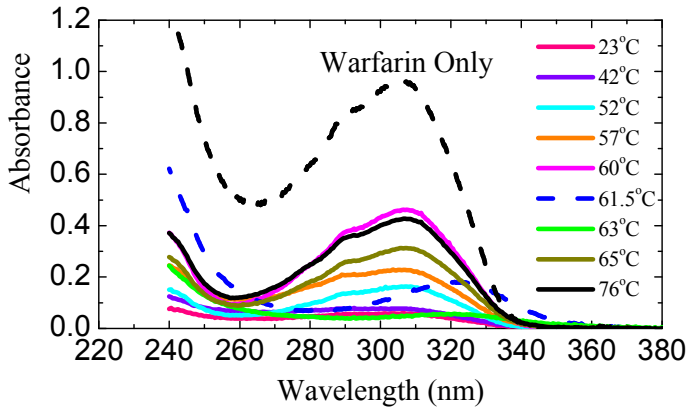

b. Fixed wavelength plot of the heat denaturation of a [1:1] molar equivalent of warfarin:rHSA in P/B, 1cm. (Samples have been microcentrifuged)

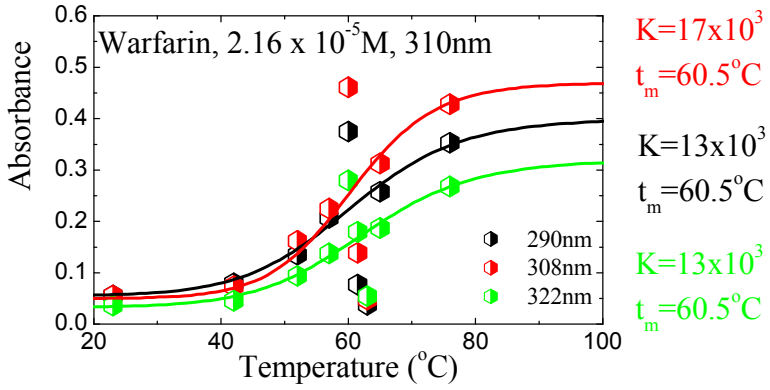

Figure 5.26. Microcentrifuged samples of the temperature study of Warfarin:rHSA

5.6.iv. Denaturation Studies of the Warfarin Complex

Denaturation studies were carried out using urea and GuHCl, the results are shown in Figure 5.27. The addition of small quantities of GuHCl (0.2M) causes an inversion of the positive CD maxima, producing a negative maximum of equal magnitude and position i.e.

a mirror image (Figure 5.27.a.), and seems to be indicative of the S-enantiomer of warfarin binding. The negative maximum appears to be unchanged and suggests that binding for the other enantiomer may be preferred (note, the addition of any denaturants will have its own associated absorption in addition to those of the drug and protein, this makes it difficult to scan to shorter wavelengths). Subsequent additions of GuHCL resulted in the eventual reduction and then loss of the drug binding. The fixed wavelength plot in Figure 5.27.b. reflects the flip and subsequent loss in binding with total loss achieved by 4M; the use of GuHCL may be a way of enantiomeric selectivity, selecting one of the enatiomers from the racemic mixture of warfarin. GuHCL produced a two step deformation curve with the generation of an intermediate product that showed relative stability.

The effect of urea, however, was not as dramatic for the initial additions as was seen for GuHCL. The addition of 1M urea produced an initial loss in binding of 22.2% at wavelength 312nm, that then appeared to stabilize for subsequent additions up to 2.8M ratio equivalent of urea. The main loss in binding occurred between 2.8-3M ratio equivalent as shown in Figure 5.27.c. & d. The loss in binding was quite specific with the initial loss then the subsequent stabilization of the complex between 1M and 2.8M equivalent. It appeared that urea exhibits a threshold producing an all or nothing binding situation,

Microcentrifugation of the denatured samples showed the loss of drug binding. The results obtained in the GuHCL revealed the sequential loss in binding of warfarin that reflected the increase absorption detected due to the increased displacement of free drug found in the filtrate. The transition appears to be a two state process with an intermediate state observed between 2M – 4M (Figure 5.27.f.). What is evident is that although complete loss of binding appears to occur at 4M, the micro-centrifugated samples revealed that only 60% of the amount of displaced free drug was measured. Only after 8M of GuHCL was added did

the micro-centrifuged samples show complete displacement of the bound drug. A similar effect was also seen in the micro-centrifuged samples of the urea samples, where it was expected to see maximum displacement of the drug at 3M, but this was not complete until 8M of urea was added (Figure 5.27.e).

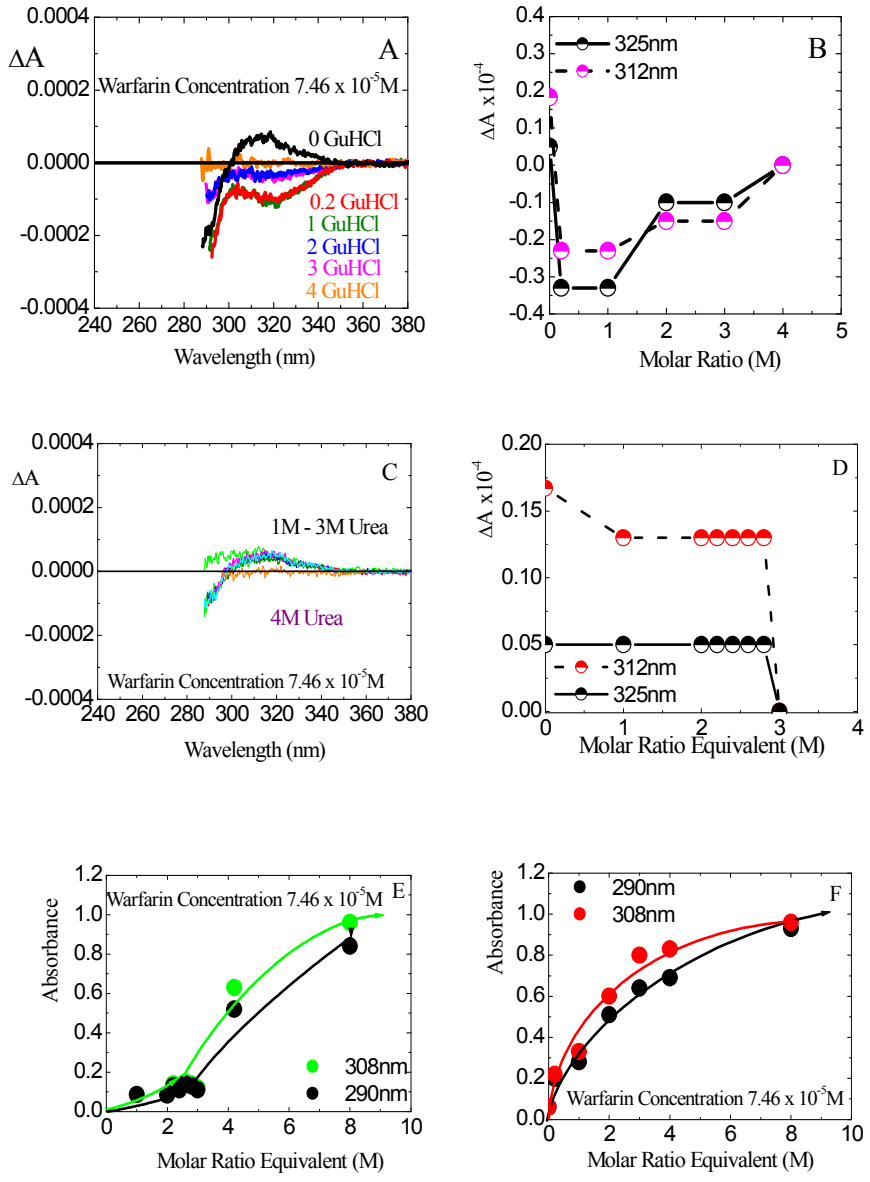

Figure 5.27. Denaturation of a [1:1] molar ratio equivalent of warf:rHSA.

A Titration of a [1:1] molar warfarin:rHSA in H_2O with increasing GuHCl, 1cm cell
B Titration of GuHCl with a [1:1] molar ratio equivalent of Warfarin:rHSA in H_2O, 1cm
C Titration of a [1:1] molar ratio of warfarin:rHSA in H_2O with increasing urea concentration, 1cm
D Titration of urea with a [1:1] molar ratio of warfarin:rHSA in H_2O, 1cm
E Micro-centtrifuged samples of a [1:1] molar ratio warfarin:rHSA in varying amounts of urea, 1cm
F Micro-centtrifuged Samples warfarin:rHSA in varying concentrations of GuHCl, 1cm cell

5.7. Result of Diazepam Studies

5.7.i. Diazepam Binding

The binding of diazepam was the second drug to be considered, and as previously stated has its predominant binding site located within domain IIIA. To determine whether the relationship between diazepam and albumin was [1:1], a titration was conducted at fixed concentration of the drug to a molar equivalent excess of albumin. To ensure consistency throughout all the forms of albumin (nHSA, dHSA and rHSA), the titration was performed in all and was found to have no significant difference. Figure 5.28. shows the results of one such titration that contains a CD profile with a negative peak located at 320nm, and two positive maxima at 286nm and 260nm. A well-defined and established isosbestic point was located at 298nm indicative of a two state system state in equilibrium, as shown in Figure 5.28.a. The absorption spectra of the complex was dominated by albumin absorption, thus limited the effective wavelength range that could be scanned (see Figure 5.28.b.).

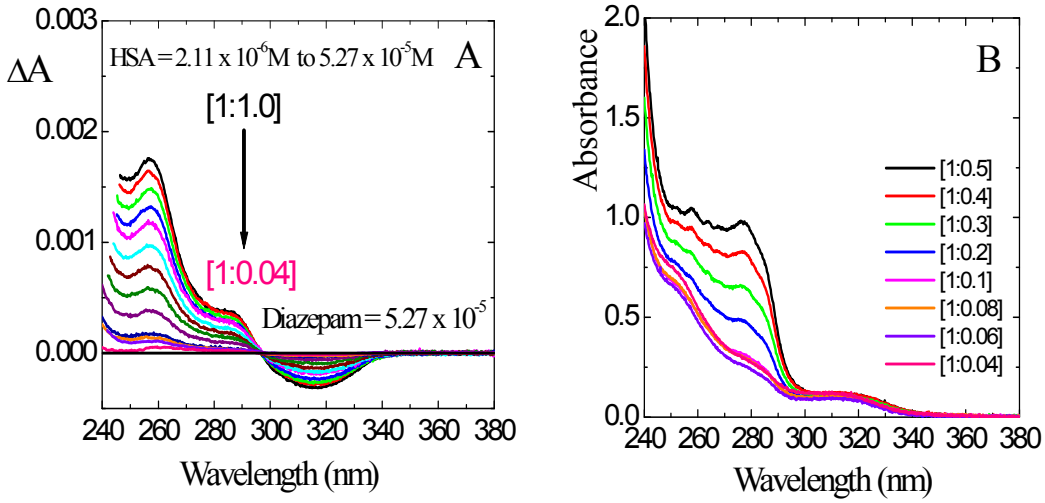

Figure 5.28. CD and UV spectra of the titration of diazepam and HSA.

A Titration of a fixed concentration of diazepam to rHSA in 10mM P/B, pH7.2, 1cm cell
B Absorption spectra of the titration of diazepam with rHSA in 10mM P/B, pH7.2, 1cm

Mathematically fitting the data derived from the titration (Mathcad software) produced a [1:1] relationship with a very strong binding constant, $K_a = 8 \times 10^7$, this is shown in Figure 5.28.c.

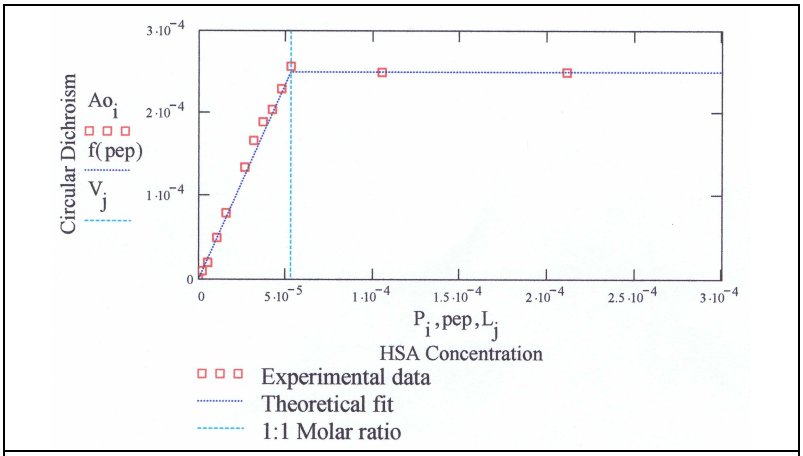

Figure 5.28.c. Mathcad fit of the titration of Diaz:rHSA
Diaz = 5.27 x 10^{-5}M

Filtering the titrated samples of the Diaz:rHSA complex to determine the free drug revealed that the samples with the lowest D/P ratio gave the largest amount of detectable free drug as would be expected (Figure 5.29.). Even though complete binding was achieved by [1:1] molar ratio equivalent, the fixed wavelength plot highlighted a continued loss in free drug up to a ratio of [1:2]. The continued loss in absorption between the [1:1] and [1:2] was significant, highlighting the fact that binding continued.

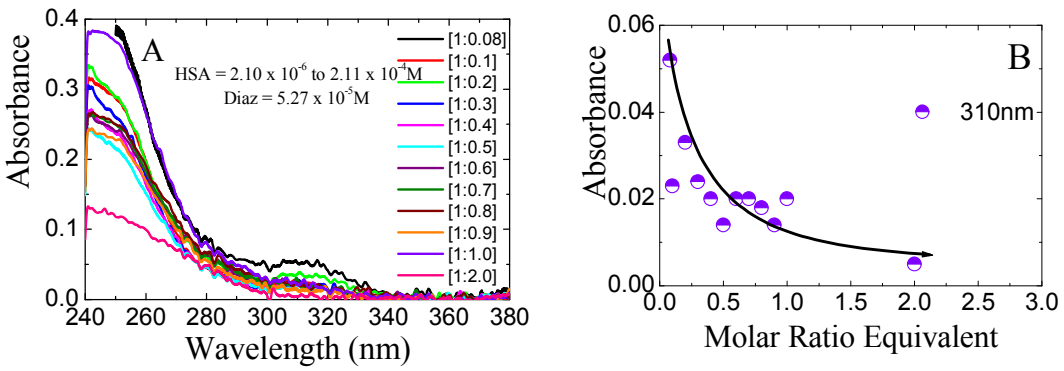

Figure 5.29. Determination of free diazepam by microfiltration of the Warf:rHSA complex.

A Micro-centifuged samples of the titration of Diaz:rHSA
B Fixed wavelength plot of the micro-centrifuged sample of the titration of Diaz:rHSA, 1cm cell

5.7.ii. Diazepam pH Studies.

The titration of the diazepam:rHSA complex (Diaz:rHSA) was investigated with changing pH, the results revealed that the pH perturbations mimicked those for HSA alone when monitored in the aromatic region where diazepam absorbs. Like rHSA alone, the Diaz:rHSA complex also showed three transitions throughout the whole range of the pH titration with a region of relative stability between pH8.5 10.5, Figure 5.30 highlights these findings. The CD spectra showed no spectral shifts or any compromising of its profile; the isosbestic point is maintained depicting the existence of two species in equilibrium. The dissociation of the drug was monitored as a collapse of the spectra indicating that both species were affected in the same way and by the same degree. What was also evident was that all the pK's were shifted by a significant amount, displaced to higher pH as shown in Table 5.4. It is possible that the presence of the bound diazepam stabilised the conformation of rHSA making it more resistant to pH perturbation. The pH titration revealed that the complex was more susceptible to low pH alterations than it was to high pH, losing binding by pH3 when the protein is in its extended form. Maximum binding was achieved when the protein was in the transition at pH5-6.

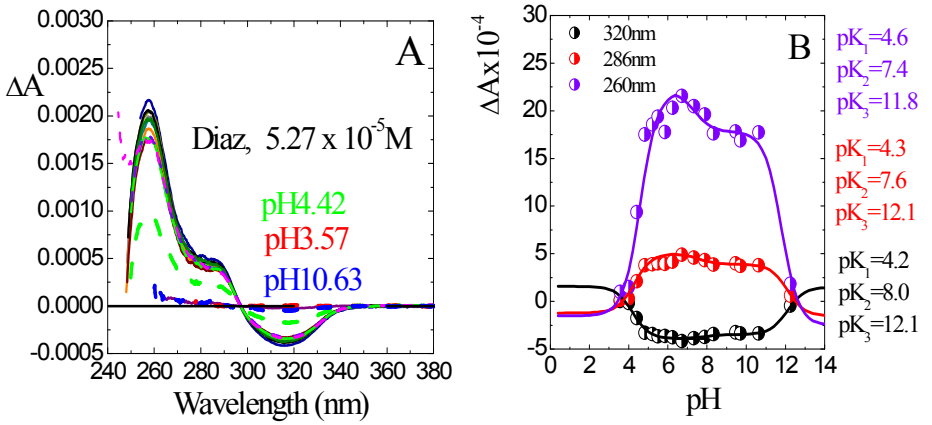

Figure 5.30. pH perturbations of Diaz:rHSA complex.

A The pH titration of a [1:1] molar ratio equivalent sample of Diaz:rHSA, 1cm cell
B Fixed wavelength plot of the pH titration of [1:1] molar ratio equivalent of Diaz:rHSA

rHSA				Diaz:rHSA			
λ (nm)	**pK_1**	**pK_2**	**pK_3**	**λ (nm)**	**pK_1**	**pK_2**	**pK_3**
				320	4.2	8.0	12.1
287	3.5	6.1	11.7	286	4.3	7.6	12.1
255	4.0		11.5	260	4.6	7.4	11.8

Table 5.4. Comparison of the pK values for rHSA &Diaz:rHSA complex.

Using the pH values isolated for the different forms of albumin conformations within the protein itself, diazepam binding was conducted at pH3.56, pH4.56, pH6.0 and pH 8.0 that represented the extended-form, the fast-form, the neutral-form and the aged form respectively. The results are drawn in Figure 5.31 with only the CD spectra shown for the pH titration at pH3.56 which could only be determined for the negative maxima. The fixed wavelength plots for the various pH's investigated are shown in Table 5.5.

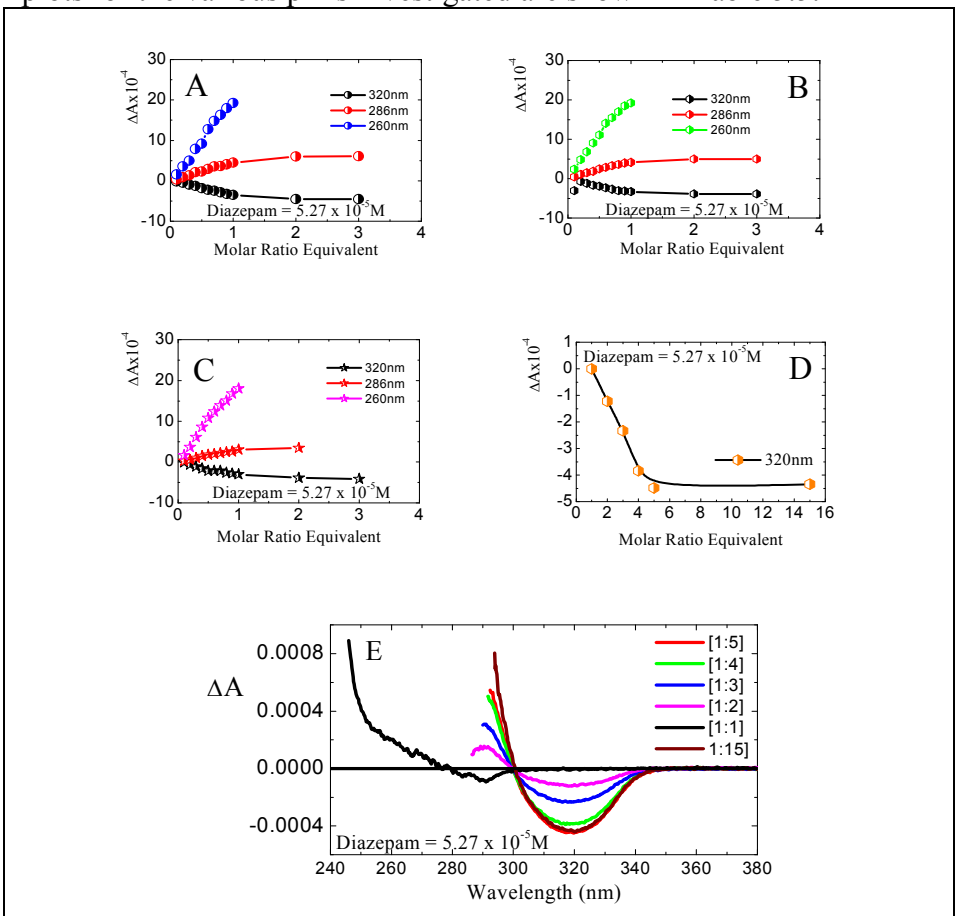

Figure 5.31. Binding studies of Diaz:rHSA at different pH values.

A Fixed wavelength plot of the titration of Diaz:rHSA in 10mM B/R, pH4.56, 1cm
B Fixed wavelength plot of the titration of Diaz:rHSA in 10mM P/B, pH6.0, 1cm
C Fixed wavelength plot of the titration of Diaz:Rhsa, 10mM Tris buffer, pH8.0, 1cm
D Fixed wavelength plot of the titration of Diaz:rHSA in 10mM B/R, pH3.56, 1cm
E CD Spectra of the titration of Diaz:rHSA in 10mM B/R, pH3.56, 1cm cell

The CD profiles for the complexes of Daiz:rHSA studied at the various pH values were all similar except for the titration made at pH3.56 that produced interference for wavelengths below 280nm.

Diaz:rHSA pH4.54		**Diaz:rHSA pH6.00**		**Diaz:rHSA pH7.20**		**Diaz:rHSA pH8.00**		**Diaz:rHSA pH3.56**	
λ (nm)	**K (M^{-1})**	**λ (nm)**	**K (M^{-1})**	**λ (nm)**	**K (M^{-1})**	**λ (nm)**	**K (M^{-1})**		
320	1.8 X 10^5	320	0.8 X 10^6	320	1.8 X 10^8	320	1.8 X 10^5	**λ (nm)**	**K (M^{-1})**
286	1.8 X 10^5	286	0.8 X 10^6	286	1.8 X 10^8	286	1.8 X 10^5	320	2.0 X 10^5
260	1.8 X 10^5	260	0.8 X 10^6	260	1.8 X 10^8	260	2.5 X 10^5		

Table 5.5. Comparison of the values of the binding constants for Diaz:rHSA complex at different pH values.

The binding titrations proved that although K at pH6.0 was high, the greatest binding constant was determined at pH7 when the protein was in its neutral conformation. All other pH solutions gave orders of magnitude lower values for K revealing conformations that were un-conducive to effective binding.

At all the pH values selected and studied, binding of diazepam occurred at varying amounts with albumin binding to the drug in the extended form of the protein being the most problematic. At pH3.56 albumin is in the extended form and produces binding with a ratio higher than the expected [D/P] ratio. Binding was not observed for a [D/P] molar ratio equivalent lower than 2M equivalent, with complete binding found at 5M equivalent (Figure 5.31.d.). In the extended form, it is thought that albumin offloads any bound ligands. However, it was found that in the extended form more diazepam ligands bind, suggesting more low affinity sites are created with a binding constant of 2.0 x $10^5 M^{-1}$. For pH4.55, albumin is in the fast form and binds with a [1:1] molar ratio equivalent detected at wavelengths 320nm and 286nm, but for the wavelength 260nm, which also lies under the aromatic region of the protein, binding seemed incomplete. As previously stated the existence of two species is depicted by the isosbestic point, and perhaps the second species is to be found at the wavelength of 260nm. Binding constants at all wavelengths for this pH was determined at 1.8 X $10^5 M^{-1}$, lower than that found at physiological conditions.

For pH6.0, the same criteria that existed for pH4.56 also existed at this pH with a binding constant determined at 0.8 X $10^6 M^{-1}$, this was found to be an order of magnitude greater than that found at the lower pH, and showed that by moving closer towards physiological conditions the maximum affinity of diazepam for albumin was achieved. Under physiological conditions, the binding constant was determined to be 1.8 X $10^8 M^{-1}$, the highest determined for the binding of diazepam. However, changing the pH to pH8.0 decreased the binding affinity producing a binding constant of 1.8 X 10^5 M^{-1}, decreasing it by an order of magnitude. Unlike warfarin, diazepam is affected by the base form of albumin that shows reduced binding. What is evident is that the site for diazepam binding reflects the conformational state of albumin, by its binding affinity it may be able to determine what conformational state albumin is in.

5.7.iii. Diazepam Temperature Studies.

Temperature investigations was conducted on the [1:1] molar ratio equivalent of Diaz:rHSA in two ways, the first was the sequential heating and quenching of the samples, scanning between each temperature increment and cooling once equilibrium was attained. The results can be found in Figure 5.32.

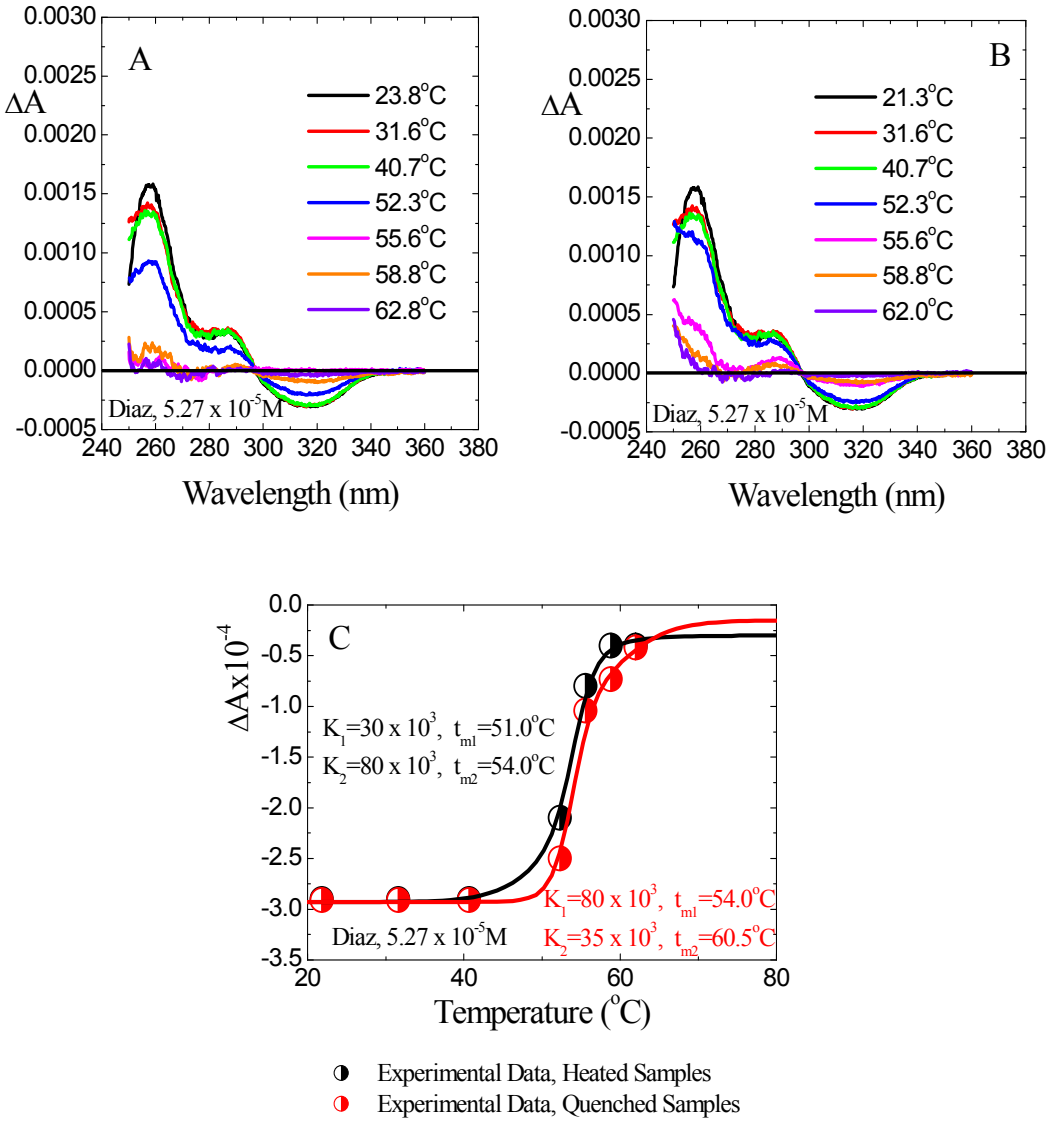

Figure 5.32. Temperature studies of Diaz:rHSA by sequential heating and quenching studies.

A Melting studies of a [1:1] molar ratio equivalent of Diaz:rHSA in 10mM P/B, pH7.2, 1cm cell
B Quenching studies of the [1:1] molar ratio equivalent of Diaz:rHSA in 10mM P/B, pH7.2, 1cm cell
C Fixed wavelength plot of the temperature studies of a [1:1] molar ratio equivalent of Diaz:rHSA

The heating curve shows the stability of the complex for temperatures up to 40^{o}C. Thereafter, there was a dramatic loss in binding spanning a 15^{o}C range with almost complete dissociation attained by 60^{o}C. The quenching curve almost mirrored the results seen in the melting curve; a small displacement was seen that suggested that a small but well defined recovery in structure of albumin was found that was sufficient to offer increased association of the drug towards the protein. Dissociation occurred at relatively low temperatures and was quite distinct from the dissociation seen for domain IIA in warfarin binding that covered a much broader temperature range (Figure 5.25.). Domain IIIA appears to be less resilient to temperature perturbations when compared to domain IIA, where domain IIIA seems to be affected by the onset of heating with re-association shown in the quenching curve to be minimal at low temperature. Initial observations show the dissociation of diazepam to site IIIA occurring between 50-60˚C, whereas in the case of warfarin binding to site IIA, dissociation occurred between 60-70˚C.

There were two transitions seen in both the heating and quenching curves that seemed to follow reverse paths in terms of K. In the heating curve the first transition was observed at a t_m=51.0˚C with K_1=30 x 10^3 (Figure 5.32.c.). The second transition lies very close to the first and is found at t_m 54.0˚C and a much higher value for K_2=80 X 10^3. Conversely, in the quenching curve, although exhibiting two transitions, its first was detected at a t_m 54.0˚C overlapping with that found for the second transition of the heating curve, and that may explain the high value for K. The second transition of the quenching curve was determined with a t_m 60.5˚C with K_2=35 X 10^3.

The second temperature investigation was undertaken by using pre-heated samples of albumin creating partial intermediates binding was carried out at room temperature and the results can be seen in Figure 5.33. The three CD maxima were monitored and compared

for similarities. At all the wavelengths studied, the results showed a relative stability of drug association to the protein for temperatures up to 48C. As with the heating and quenching studies, temperatures above 48˚C revealed a rapid loss in association of the drug towards the protein, with complete loss experienced by 60˚C. All wavelengths coalesce at 60˚C with each wavelength showing two transitions. The first transition was observed with a t_m = 50˚C that differed by 1˚C between the wavelengths, all values of K_1=40 x 10^3. The second transition was equally as close with a t_m = 55˚C, but this time only two of the three wavelengths studied produce identical values of K = 90 x 10^3, the third wavelength produced a value for K = 80 x 10^3, lower than for the other wavelengths. Here there is a difference between the negative CD maximum and the positive CD maxima at the point where the isosbestic point is found, this may be indicative of the relationship between the two species that are closely related but showing subtle differences.

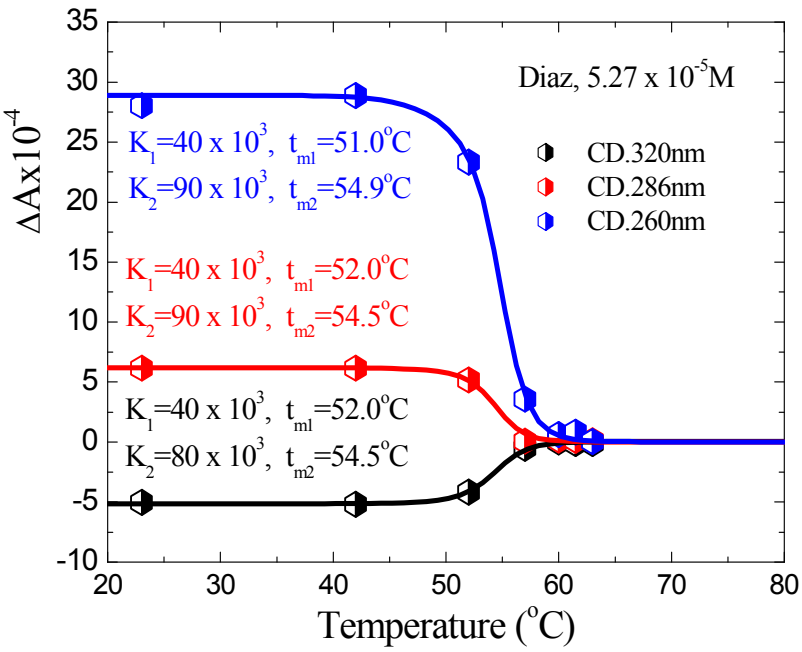

Figure 5.33. The binding of diazepam to pre-heated samples of rHSA.

Fixed wavelength plot of the temperature studies of a [1:1]molar ratio of Diaz:rHSA in 10mM P/B, pH7.2, 1cm

5.7.iv. Diazepam Denaturation Studies.

The last determination to be considered in this series of investigation was the denaturing effects of urea and GuHCl on a D/P ratio equivalent of [1:1] for the Diaz:rHSA complex, the results are shown in Figure 5.34 & 5.35. The end results for the two denaturants were the same on the complex producing dissociation with the collapse of the CD signal, but the means to which the end points were obtained was different. Considering the urea titration first, for addition up to 3M equivalent produced a relatively small but gradual loss in binding of diazepam. Within the defined region of 3M – 4M equivalent produced the dramatic loss in binding experienced by the protein with only a small association of the drug at this molarity (Figure 5.34.b.). The microcentrifuged samples revealed an increase in association of diazepam towards albumin for small additions of urea. For molar ratio equivalent of urea greater than 1M, successive loss of association was seen with the increase of free diazepam detected (Figure 5.34.d.). In the absence of ligand albumin unfolds in one step in urea with the midpoint of the transition found around 5M equivalent. The presence of diazepam ensures that complete binding was lost by the time the midpoint of the conformational change for albumin occurs.

The effect of GuHCl denaturation reflected a somewhat different picture than that shown for urea which produced a sigmoid relationship. The addition of GuHCl produced a steady loss in the association of the D/P complex with no real trend observed even though GuHCl in albumin only produces an intermediate conformational state. It is clear that this intermediate conformational state that was formed has no bearing on the activity of subdomain IIIA where diazepam resides.

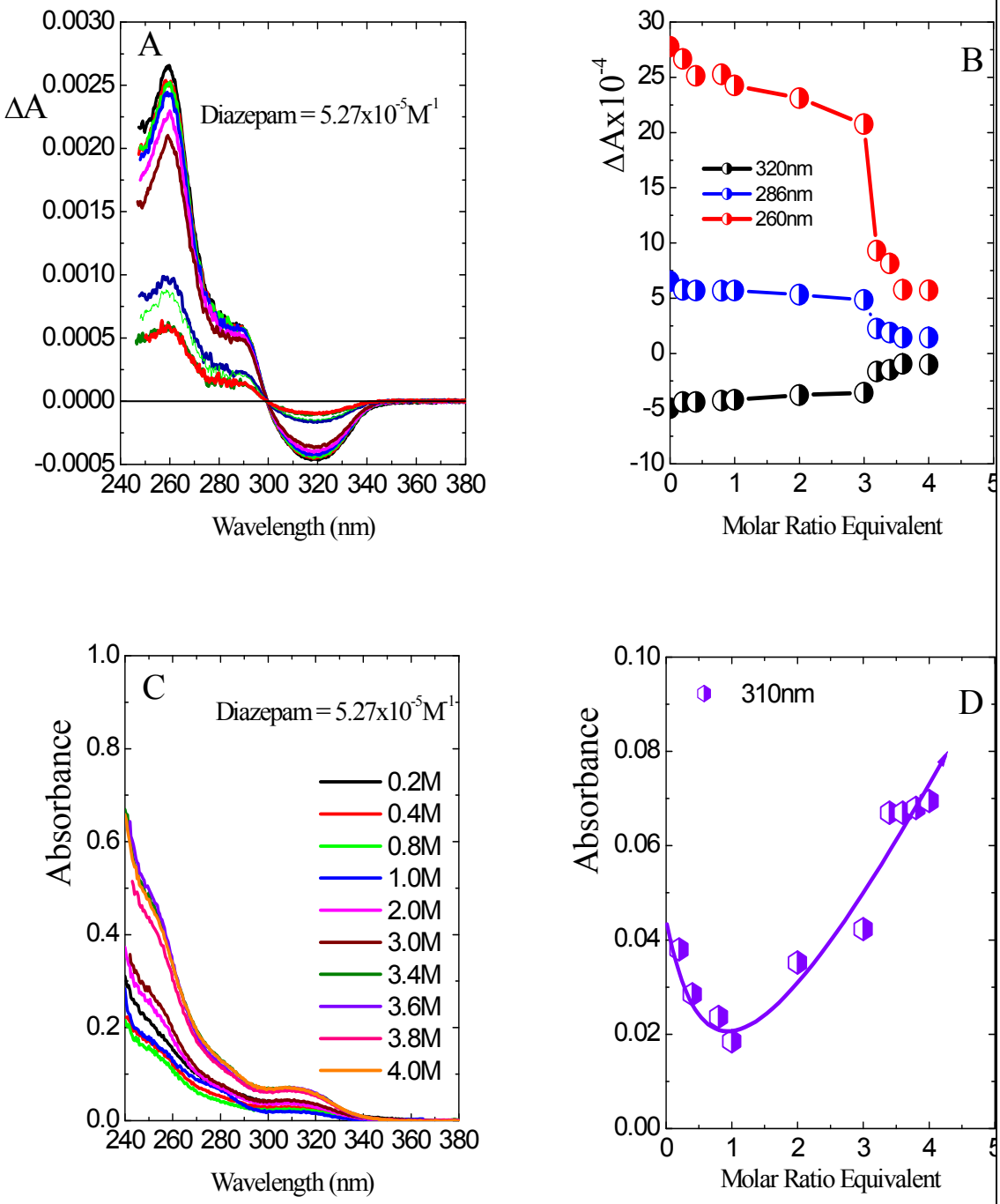

Figure 5.34. Denaturation studies of a [1:1] molar equivalent of Diaz:rHSA in urea.

A CD Titration of a [1:1] molar ratio equivalent of Diaz:rHSA in Urea, 1cm cell
B Fixed wavelength plot of Diaz:rHSA in Urea
C Microcentrifuged samples of a [1:1] molar ratio equivalent of Diaz:rHSA in the presence of Urea, 1cm
D Fixed wavelength plot of the titration of a [1:1] molar ratio equivalent sample of Diaz:rHSA in Urea

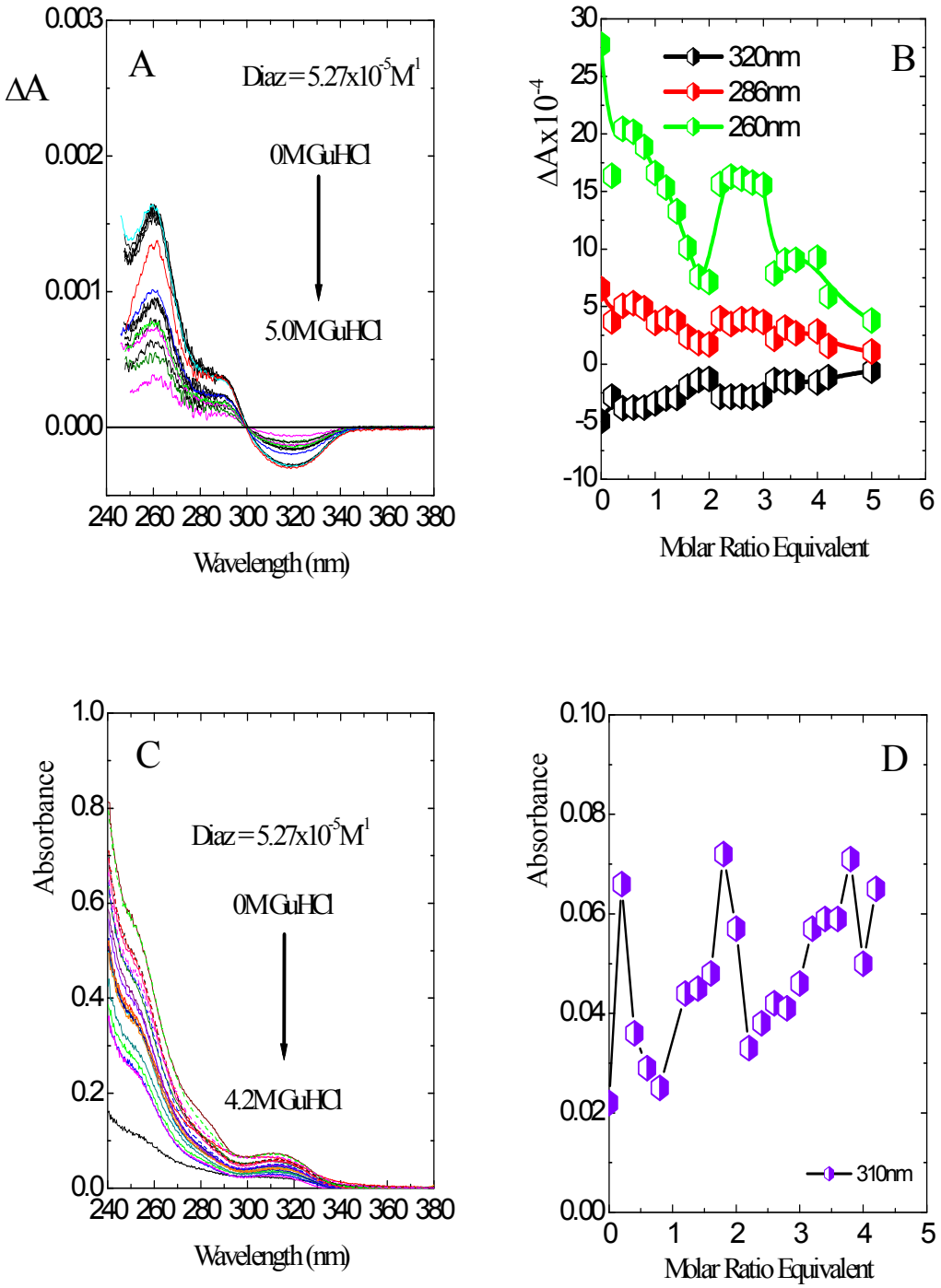

Figure 5.35. Denaturation studies of a [1:1] molar equivalent of Diaz:rHSA in GuHCl

A GuHCl binding to a [1:1] molar ratio equivalent of Diaz:rHSA in H_2O, 1cm cell
B Fixed wavelength plot of Diaz:rHSA in GuHCl
C Micro-centifuged samples of a [1:1] molar ratio equivalent of Diaz:rHSA in GuHCl, 1cm cell
D Fixed wavelength plot of the titration of a [1:1] molar equvalent sample of Diaz:rHSA

5.8.. Result of the Studies of Salicylic Acid and its Derivatives

5.8.i.a. Salicylic Acid Binding

Salicylic acid (SA) and its derivatives were studied in much the same way as warfarin and diazepam, looking for variations in environmental changes to distinguish between binding sites. SA, known to bind to both domain IIA and IIIA would give a good indication of the kinds of conditions that may affect either or both of the sites. Salicylic acid was the last in this group of drugs to be studied, the simplest of the trio of salicylates and can be considered as the parent compound since the other two derive from its structure. The main absorption of this drug was found at 295nm also reflected in the CD spectra as shown in Figure 5.36. SA has a single positive CD maximum centred on its absorption maximum at 295nm with the possibility of a second transition peak, a negative peak at 265nm which belongs to a secondary absorption that underlies the main absorption. The evidence of this was also confirmed in the absorption spectra where there seemed to be the resemblance of an isosbestic point located at around 325nm. There was also evidence of spectral shifts in the absorption maxima at the higher [D/P] ratios, with evidence of interference in the CD spectra also at high molar equivalent concentration.

A D/P ratio equivalent for [SA:rHSA] was found to be [2:1]. The absorption spectra of the drug was found to have two main absorption bands (Figure 5.37.a.), one at 295nm and the other at 230nm that would be masked in the titration by the protein backbone. The fixed wavelength plot of the drug titration was found to produce consistent increases in CD maxima for every additional increase for ratios up to and including 1M equivalent. The increase however, for the additions of 1M – 2M equivalent only produced a small increase in CD, smaller than that that was expected.

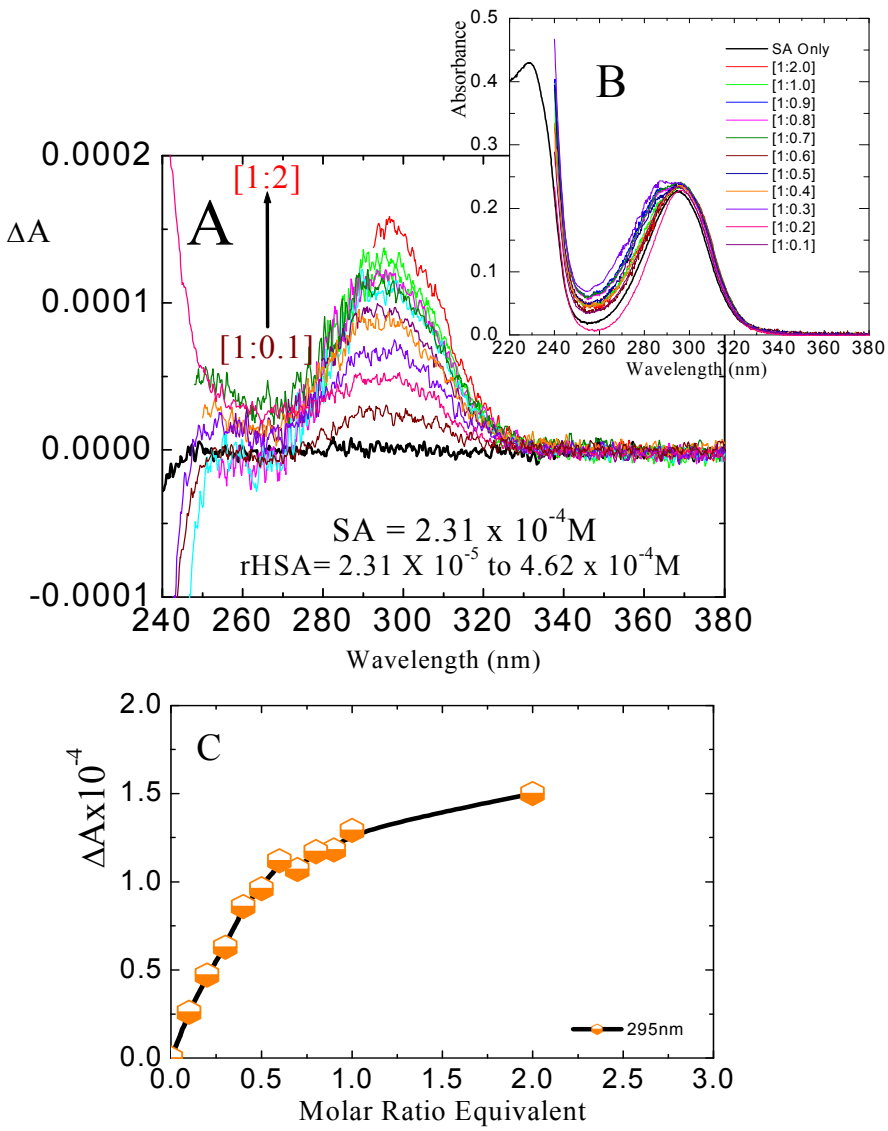

Figure 5.36. The binding of SA to rHSA.

A Titration of SA with rHSA in 10mM P/B, pH7.2, 1cm cell
B Absorption Spectra of the titration
C Fixed wavelength plot of SA with rHSA in 10mM P/B, pH7.2, 1cm

All the samples measured in the binding studies were filtered and the UV spectra measured to determine the amount of free drug, if any was present. The filter removed all the albumin molecules in the sample and the results can be seen in Figure 5.37. The fixed wavelength plot reflected the results seen in the titration in that there was a consistent loss of free drug for molar ratio equivalent up to [1:1], for concentrations exceeding that ratio produced only a minimal loss up to a molar ratio equivalent of [1:2]. The results suggested

that binding continued up to 2M equivalent of the protein.

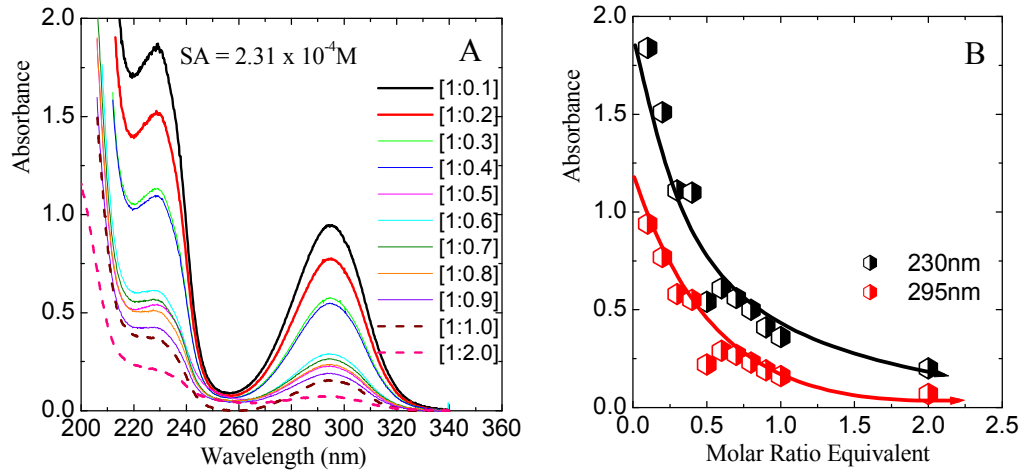

Figure 5.37. Micro-centrifuged samples of the titration of SA:rHSA.

A Absorbtion spectra of the micro-centrifuged samples of SA with rHSA, 1cm cell
B Fixed wavelength plot of the micro-centrifuged samples of SA:rHSA in 10mM P/B, pH7.2, 1cm cell

5.8.i.b. Salicylic Acid Temperature Studies

Temperature studies were conducted on the [2:1] molar ratio equivalent of the complex of [SA:rHSA] in response to the pre-heating of albumin samples prior to drug binding at room temperature. The binding revealed as expected full binding of the drug to the pre-heated samples of albumin for temperatures up to 52˚C, indicative of the temperature effects observed for diazepam. Once again there was a dramatic loss in binding between temperatures of 52^{o}C - 60^{o}C as demonstrated in Figure 5.38.a. Pre-heating the albumin samples brought about some structural changes within albumin that resulted in the negative peak at 265nm, not previously distinguished, now forming a prominent feature. At both the wavelengths studied two transitions were observed with t_m temperatures that varied no more that 2˚C. The first transition revealed a t_m = 52˚C & 54˚C for wavelengths 295nm & 265nm respectively, with the value of K_1=3x greater at 295nm that at 265nm. The second

transition equally reflected similar results and proved that the conformational species detected at 265nm was much more unstable than that detected at 295nm.

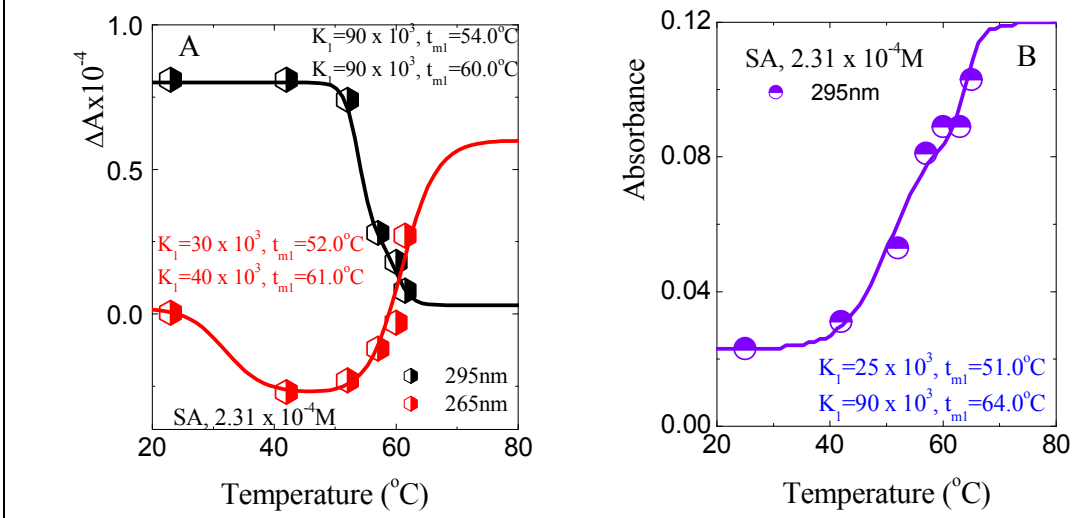

Figure 5.38. Temperature studies of SA:rHSA.

A Fixed wavelength plot of pre-heated rHSA samples added to SA, [2:1], 1cm
B Fixed wavelength plot of the microcentifuged samples of pre-heated rHSA bound to SA, 1cm

Analysing the micro-centrifuged samples of the pre-heated samples revealed a similar response to that found when measuring by CD (Figure 5.38.b.). Minimal amounts of unbound drug was found for temperatures up to 45°C, thereafter an increase in displaced drug was detected as the protein became more denatured. Two transitional states were detected that were almost identical to that found by CD analysis proving that the two techniques were monitoring the same changes.

5.8.i.c. Salicylic Acid Denaturation Studies

In keeping with the studies carried out on the other drugs the effects of denaturants were investigated with the [SA:rHSA] complex ([2:1]) and the results can be found in Figure 5.39. Considering urea denaturation first, for additions up to 3M equivalent of urea resulted

in the gradual displacement of the bound drug with the greatest loss seen between 2M – 3M equivalent. There was still a relatively high degree of association between the drug and the protein at these concentrations of urea. Additions between 3M – 3.2M equivalent revealed the greatest degree of dissociation where most of the drug was now in the free form (Figure 5.39.a.). When the samples were micro-centrifuged and the amount of free drug determined in the samples highlighted, the gradual loss in association over the entire range monitored was observed (Figure 5.39.b.). The dramatic loss seen by CD between the ratio of 3M – 3.2M equivalent was not evident in the filtered samples.

The effects of GuHCl were more profound showing the general differences monitored at the two wavelengths. A 295nm the CD revealed that for a small amount of GuHCL of 0.5M equivalent produced a stabilizing effect where no loss of binding was seem. For additions greater than that, a general loss in binding was detected up until 3M equivalent where total binding was lost. At 265nm up to 1M equivalent of GuHCL produced an inversion of the CD signal from negative to positive of almost equal magnitude. Further additions of GuHCL resulted in the gradual loss in CD back to the negative value of equal value to the value determined at the start (Figure 5.39.c.). The microcentrifuged samples of the GuHCL titration reflected first the reduction in free drug, then the gradual increase of drug detected.

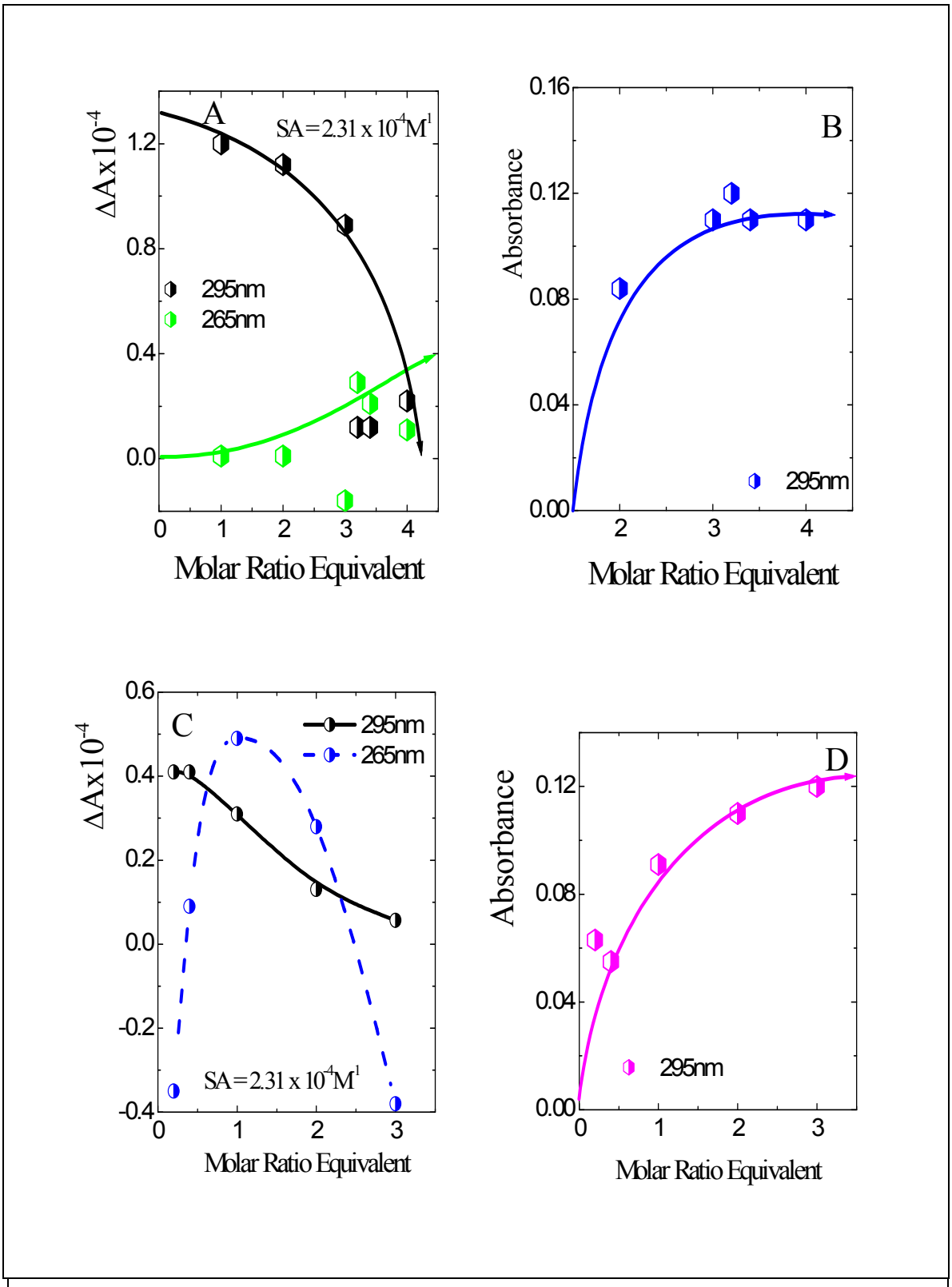

Figure 5.39. The effect of denaturants on the SA:rHSA complex.

A Titration of a [2:1] molar equivalent of SA:rHSA in increasing concentrations of Urea, 1cm cell
B Fixed wavelength plot of the micro-centrifuged samples of SA:rHSA in Urea, 1cm cell
C Titration of a [2:1] molar equivalent of SA:rHSA in increasing concentrations of GuHCl, 1cm cell
D Fixed wavelength plot of the microcentrifuged samples of SA:rHSA in GuHCl, 1cm cell

5.8.ii.a. 5-Iodosalicylic acid Binding Studies

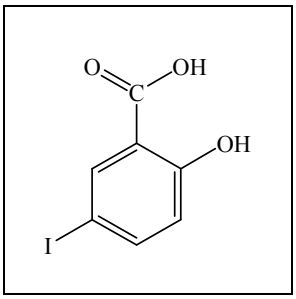

The titration of 5-iodosalicylic acid (5ISA) was conducted and compared with the results obtained from SA. Initially the pH titration of the 5ISA was conducted in water in the absence of protein and its spectral shifts observed. The absorption spectra was dominated by a single peak found at 300nm, shifted by 5nm to longer wavelength, with a second absorption found at lower wavelength too large to be investigated under these conditions (Figure 5.40.).

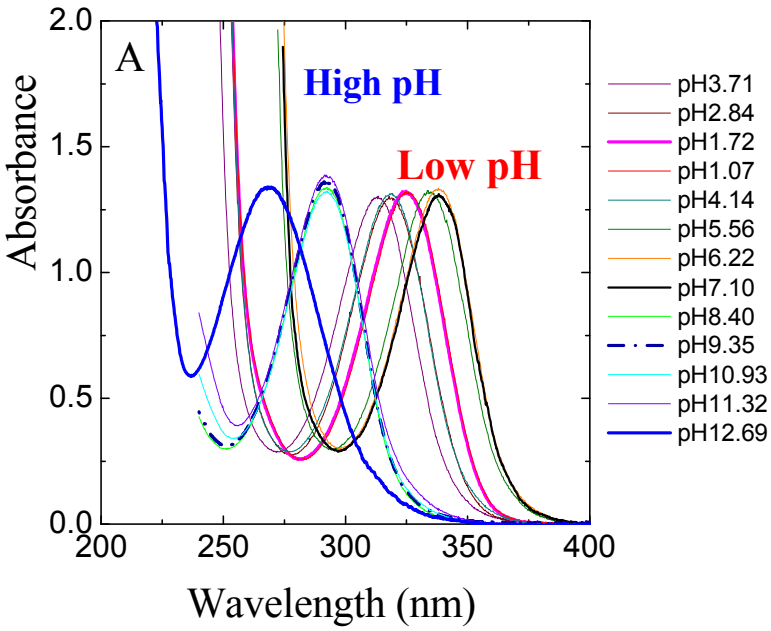

Figure 5.40. pH titration of 5ISA in H_2O.

Absorbance spectra of the pH titration of 5ISA, 4.73 x $10^{-4}M^{-1}$ in H_2O, 1cm cell

The titration of 5ISA with rHSA was conducted, determining the binding characteristics by CD and binding constant. 5ISA exhibited many of the characteristic features found in its

parent drug with the existence of two positive CD maxima found at 300nm and 320nm, but in this case the two peaks were well defined and separated. The addition of the iodine atom to SA produces a shift of one of the CD maxima by 20nm to 320nm, with the other maximum remaining around 300nm. As with SA, 2M equivalent of 5ISA was titrated against varying concentrations of albumin until a [2:1] molar ratio equivalent was measured (Figure 5.41.a.). The fixed wavelength plot of the titration revealed complete binding by [2:1] molar ratio equivalent (Figure 5.41.b.). The UV spectra shows shifts in the maximum absorption at 300nm with the resemblance of an isosbestic point at approximately 290nm, indicative of several species in equilibrium.

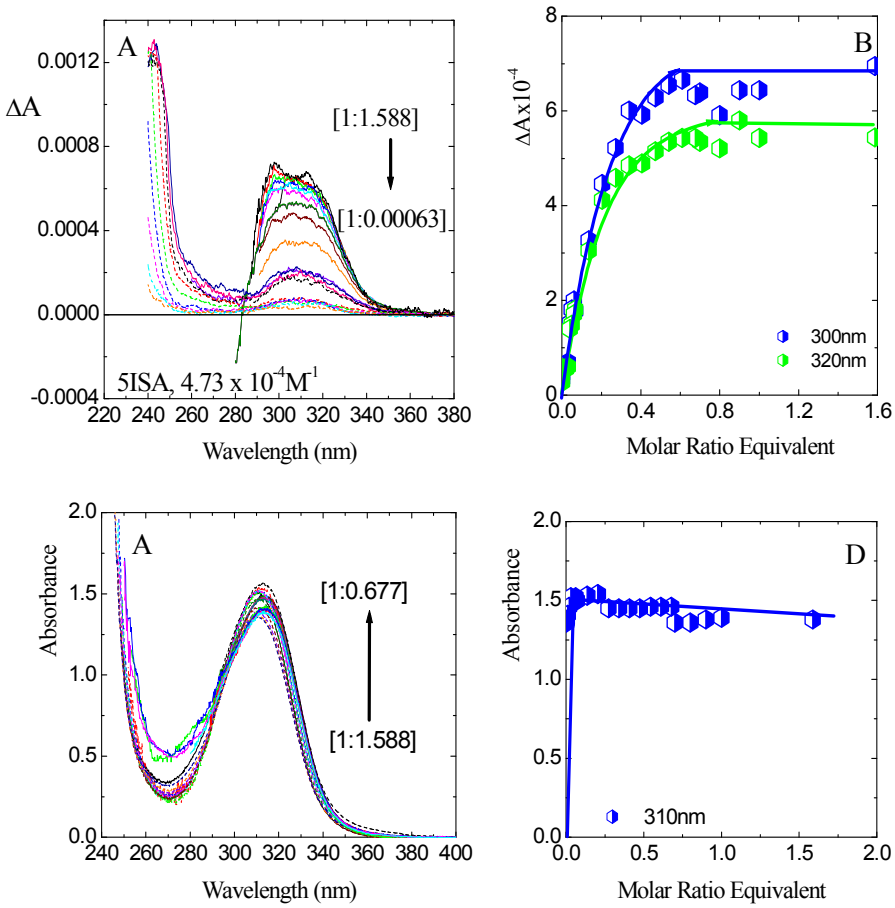

Figure 5.41. Titration of 5ISA with rHSA in P/B.

A Titration of 5ISA:rHSA in 10mM P/B, pH7.2, 1cm cell
B Fixed wavelength plot of the titration of 5ISA:rHSA
C Difference absorbance spectra of the titration of 5ISA:rHSA in 10mM P/B, 1cm cell
D Fixed wavelength plot of the difference absorbance spectra of 5ISA:rHSA in 10mM P/B, 1cm

The micro-centrifuged sample analysis for the titration of 5ISA:rHSA in P/B is shown in Figure 5.42.a. The main absorption is located at 320nm and shows for low level of rHSA the highest absorption of 5ISA was detected. As the titration progressed, the amount of detectable free ligand decreased until a minimum value was measured. The fixed wavelength plot shown in Figure 5.42.b. indicates the rapid decrease in the free ligand. By the time the titration reached a D/P ratio equivalent of [1:0.5] complete binding was detected indicative of a [2:1] molar ratio equivalent. An anomaly was seen centred around a ratio of [1:0.25], this could be the point where the first ligand has completely bound and the second ligand starts to bind.

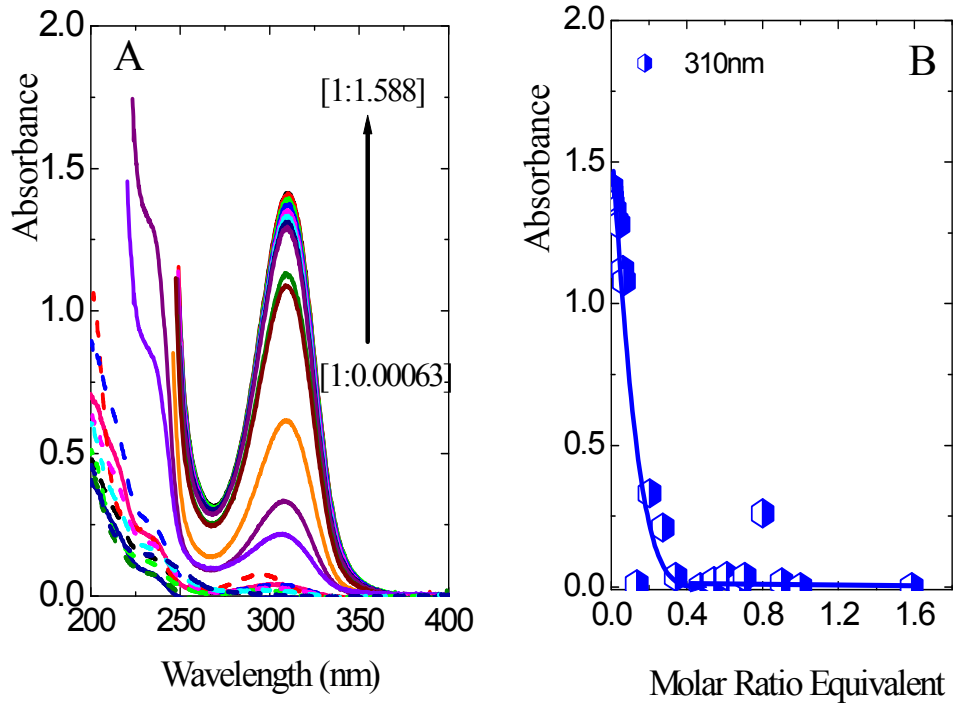

Figure 5.42. Microcentrifuged samples of 5ISA with rHSA in P/B.

A Microcentrifuged samples of the titration of 5ISA:rHSA in 10mM P/B, pH7.2, 1cm cell
B Fixed wavelength plot of the microcentrifuged samples of 5ISA:rHSA in 10mM P/B, 1cm

5.8.ii.b. 5-Iodosalicylic acid Temperature Studies

Temperature studies were conducted on a [2:1] molar ratio equivalent by the method of sequential heating and quenching, the results of the fixed wavelength plot are shown in Figure 5.43. The heating curves are characterised by two transitions with the different wavelengths reflecting different findings. Like the parent compound, 5ISA showed a certain amount of stability towards heating with complete association of the ligand found up to temperatures of 50˚C. At around 60˚C the first transition was seen for both wavelengths with the same values of K = 35 X 10^3. The second transition for both wavelengths gave identical values in terms of t_m = 70˚C and K = 90 X 10^3. The quenching studies revealed that by heating its effects caused internal rearrangement of the protein that enhanced binding for temperatures exceeding 40˚C and up to 65˚C. Above 65˚C produces a cascade effect with the dramatic loss of binding giving a t_m = 70-72˚C. However, what was evident was that even after the protein had been heated to temperatures above 70C binding of 5ISA was still very evident with still a high degree of association of the ligand to the partially denatured protein. This response is atypically as it was expected that at such high temperatures binding would be totally lost. 5ISA is a relatively smaller molecule, when rHSA is heated and cooled back down to room temperature the binding pocket/pockets are sufficiently conserved that binding was still achievable. Conformational changes in the protein coupled with the small size of the ligand have ensured binding even at such high temperatures. It has been demonstrated that heating albumin does not result in the complete collapse of its structure and that some secondary structural elements remain intact resulting in the binding of 5ISA, reinforces the fact that albumin still maintains sufficient structural integrity to maintain binding. This finding also confirms the theory that domain IIIA retains its structural integrity at extreme conditions.

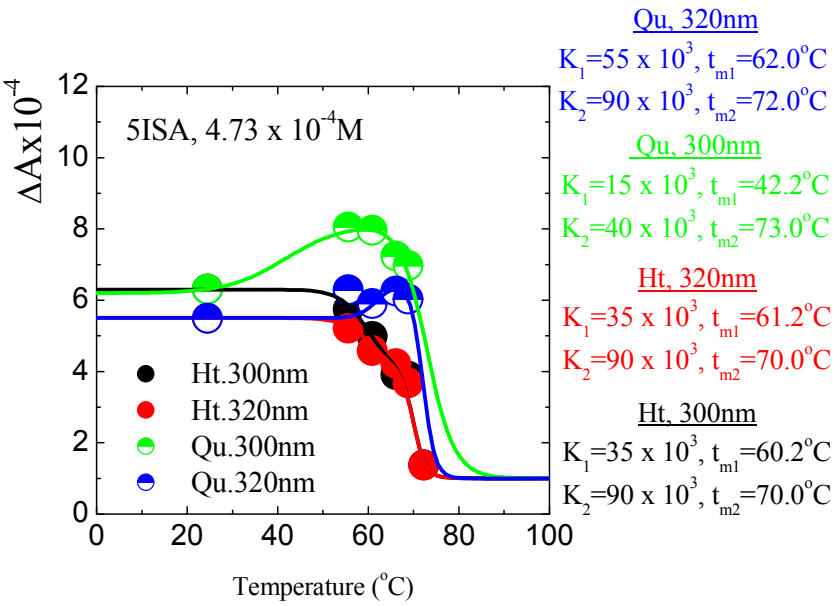

Figure 5.43. Heat denaturation studies of 5ISA:rHSA complex.

Fixed wavelength plot of the temperature cycling of a [2:1] molar ratio equivalent of 5ISA:rHSAin 10mM P/B, pH7.2,1cm cell

5.8.ii.c. 5-Iodosalicylic acid Denaturation Studies

Denaturation studies were conducted on 5ISA:rHSA [2:1] using urea as the first denaturant, the results are shown in Figure 5.44. As has been previously observed the addition of a small amount of urea (1M) can cause conformational changes beneficial to the binding of the ligand, all wavelengths studied reveal this positive enhancement to varying degrees. A further addition of 1M causes an increased affinity in the D/L association, and the inversion of the 270nm maximum from negative to positive was also observed (Figure 5.44.b.). Further additions of urea produced reduced binding of 5ISA with almost the complete loss of binding by 4M.

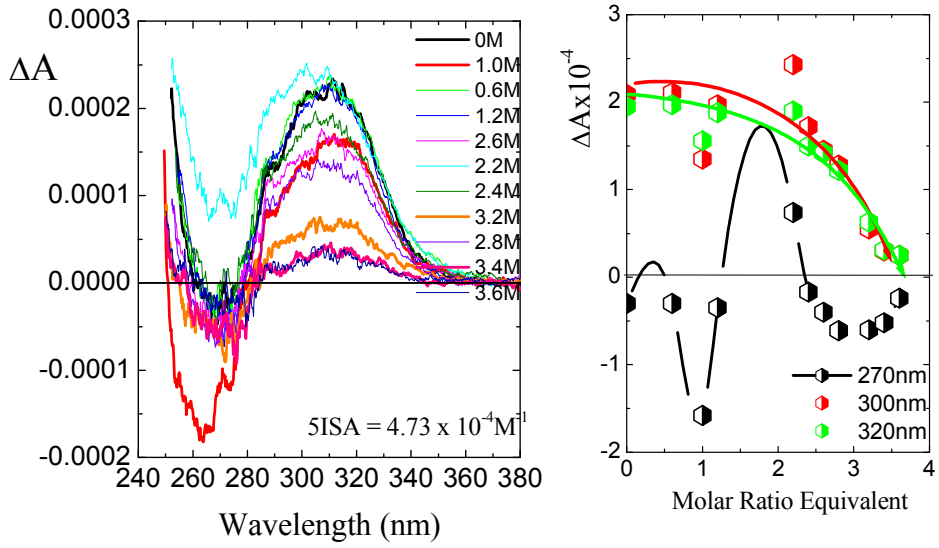

Figure 5.44. The denaturation of 5ISA:rHSA using urea.

A Titration of a[2:1] molar equivalent of 5ISA:rHSA with Urea in H_2O, 1cm
B Fixed wavelength plot of the urea titration of 5ISA:rHSA in H_2O, 1cm cell

The micro-centrifuged samples of the urea induced denaturation are shown in Figure 5.45. The initial addition of up to 2M of urea produces an increase association of ligand to protein and supports the findings in the titration data. There is a steady loss detected in association up to a concentration of 3.5M where complete dissociation is achieved.

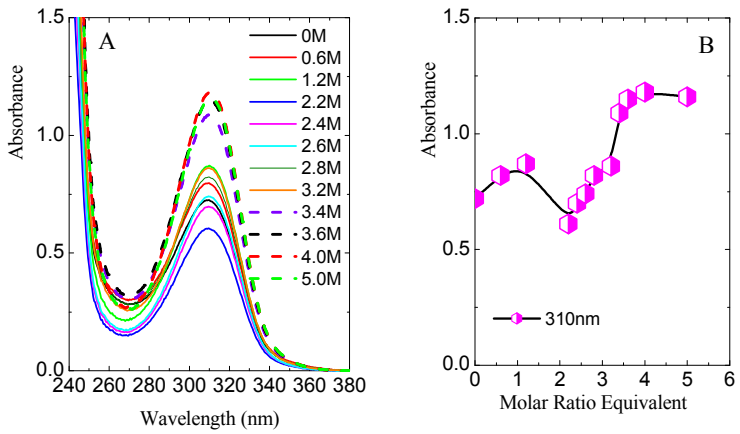

Figure 5.45. Absorption spectra of the microcentifuged samples of 5ISA:rHSA.

A Microcentrifuged samples of the [2:1] 5ISA:rHSA samples in urea, 1cm cell
B Absorbance spectra of the microcentrifuged samples of 5ISA:rHSA, [2:1], with Urea, 1cm

5.8.iii. 3,5 Diiodosalicylic Acid

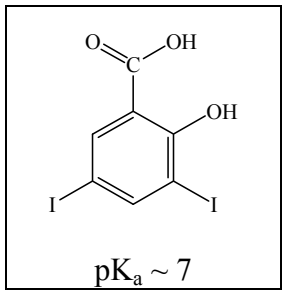

3,5 Diiodosalicylic acid (DIS) was extensively studied as the ligand that binds to two sites and used to represent the salicylate binding group as a whole. The substitution of iodine groups at positions 3 & 5 alters significantly the CD signal detected. The addition of iodine (one molecule in 5ISA and two molecules in DIS) produces two CD positive maxima at 300nm and 320nm. The absorption spectra associated with DIS in an aqueous solution (Figure 5.46.a.) produced an absorption maximum at 320nm with further absorptions at shorter wavelengths produced as a response to high pH conditions. The pH titration of the free drug in water produced a uniform response to pH changes at wavelength 320nm with one transition found at a pK=2.1. There was a shift in the absorption maximum detected at the extreme pH regions to produce a second absorption peak at 345nm. At the wavelength of 345nm two constants were revealed, one at pK=1.7 and the other at pK=11.5 as shown in Figure 5.46.b.

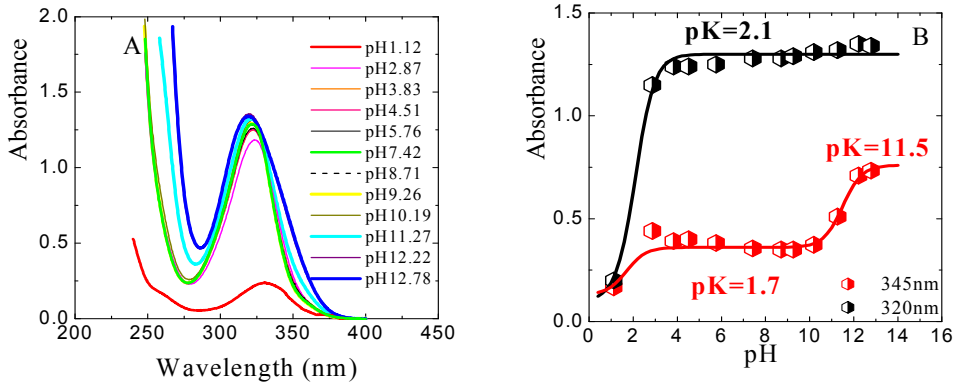

Figure 5.46. pH investigations of DIS only in water.

A Absorbance Spectra of the pH titration of free DIS in water, 3.26 X $10^{-4}M^{-1}$, 1cm cell
B Fixed wavelength plot of free DIS in water

5.8.iii.a. 3,5 Diiodosalicylic Acid Binding Studies

The CD spectra of the binding of DIS to rHSA showed similarities to the CD of warf:rHSA in that it possessed two overlapping positive peaks at 300nm and 330nm. However, the spectra in the case of DIS was more complex with two further maxima, a negative maximum located around 280nm and a positive maximum located below 240nm (Figure 5.47.a.). The fixed wavelength plot confirmed a D/P ratio equivalent of [2:1] with the two positive maxima reaching completion at different ratios (Figure 5.47.d.), this may be a reflection of the different species in equilibrium. The CD spectra also reflected the complexity of the titration with the generation of potentially two isosbestic points, one at approximately 290nm and the other at approximately 265nm. The UV data also exhibited an isosbestic point dissecting that which was found above and below 350nm.

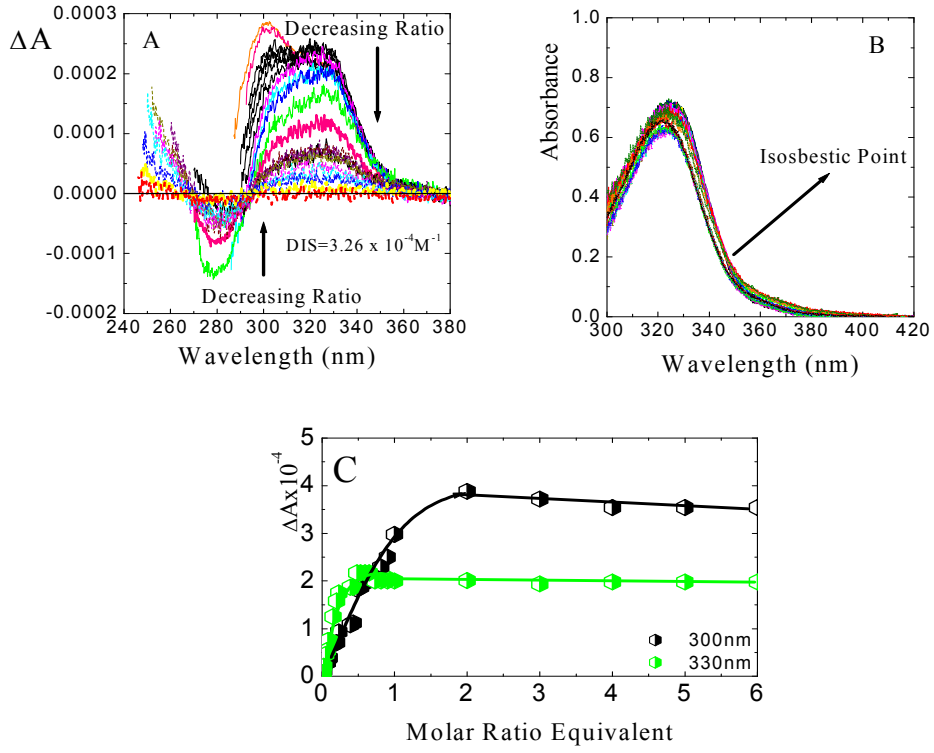

Figure 5.47. Binding studies of DIS:rHSA measured in a 5cm cell.

A CD Spectra of the titration of DIS with rHSA in P/B, pH7.2, 5cm cell
B Absorbance spectra of DIS:rHSA, (rHSA baseline subtracted), P/B, pH7.2, 5cm
C Fixed wavelength plot of DIS /rHSA, ratios [1:0.009] to [1:23] in P/D, pH7.2, 5cm

The data in Figure 5.47.c. showed the effect of concentration on the binding studies and revealed a perfectly symmetrical relationship that reflected no concentration dependencies. The binding relationship for DIS to rHSA remains the same as long as the D/P ratio remains the same regardless of the concentration used to attain that ratio. In optimising the conditions by increasing the D/P ratio equivalent to [1:25] and above revealed that there existed a higher complex than the [1:2] ratio previously thought to exist. Binding at the higher concentrations of rHSA meant that solubility became an issue. In order to compensate for that the concentration of DIS was reduced and ratios up to [1:70] were investigated and are shown in Figure 5.48. The loss of the positive maxima at 330nm that seem to shift to lower wavelength that stabilised at 312nm and changed signs to become increasing negativity for ratios up to [1:50]. The maximum at 300nm became increasingly more positive. The experimental limit of this experiment was reached and it was impossible to push the boundaries further in view of the solubility problems of albumin and its optical transparency at such high concentrations.

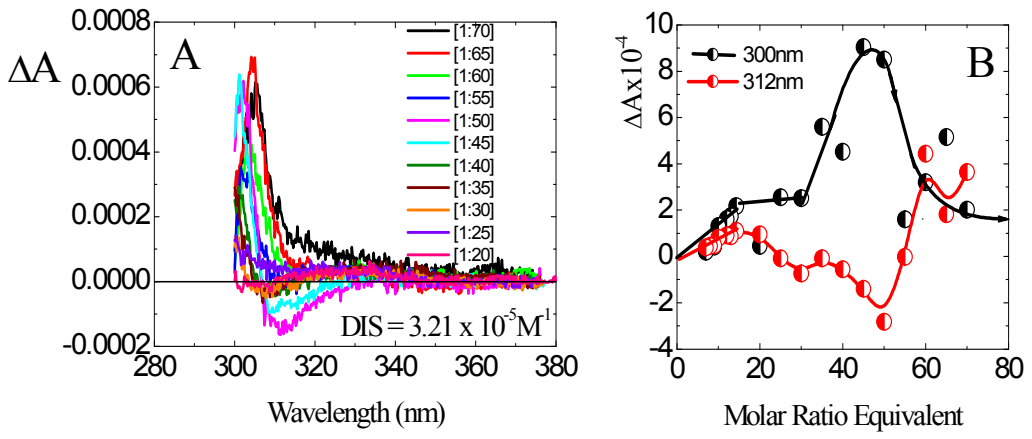

Figure 5.48. Titration of DIS with rHSA for high D/P ratios.

A Titration of a fixed concentration of DIS to rHSA in 10mM P/B, pH7.2, 1cm cell
B Fixed wavelength plot of DIS to an increasing concentration of rHSA in 10mM P/B, pH7.2, 1cm

The binding of DIS to rHSA was compared to nHSA, the results showed great similarities (Figure 5.49). The characteristic features associated with DIS binding were evident. However, the appearance of a more defined isosbestic point at a relatively low D/P ratio indicated a difference not so prominently observed with the DIS:rHSA titration. A further difference was seen in the end point observed at the 300nm maximum that reached completion at 2M equivalent. A [2:1] D/P ratio also existed under these conditions with a clear distinction between the behaviour of the two positive maxima that was more prominent in native albumin than in rHSA.

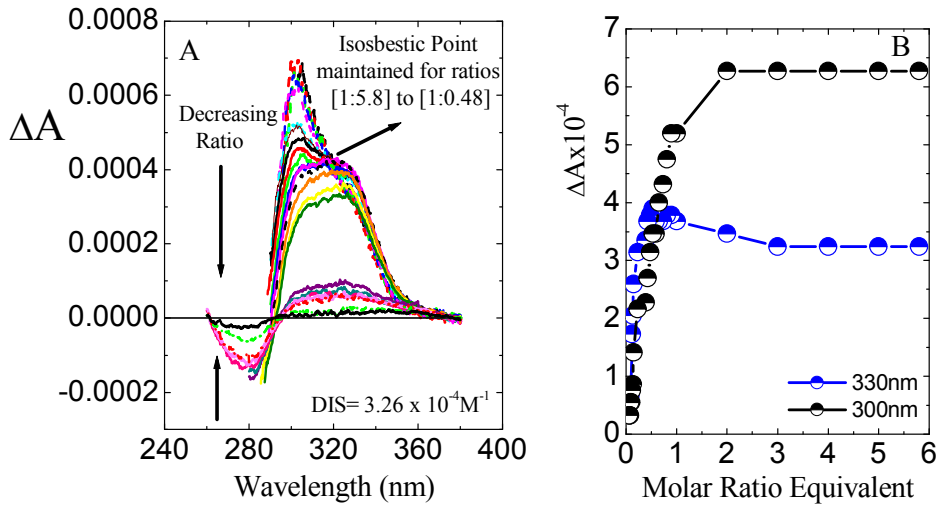

Figure 5.49. The binding of DIS to nHSA

A DIS : nHSA titration, molar ratio equivalent [1:5.8] to [1:0.0165] in P/B, pH7.2, 1cm
B Fixed wavelength plots of DIS:nHSA titration in P/B, pH7.2, 1cm

Elucidating the ultimate binding conditions for DIS:rHSA proved elusive, the extremely high concentration of albumin compared to that of the drug meant that monitoring the drug became increasingly difficult. The best possible data obtained for such a titration is shown in Figure 5.50. where the DIS concentration was increased and fixed at 3M equivalent, this provided a larger induced CD signal (i.e. 3x greater). As the D/P ratio increased the negative CD maximum shifts to longer wavelength and increases in magnitude. It was

possible to monitor the CD spectral changes in the far UV CD region and revealed a further two CD maxima together with the negative maximum previously detected and centred at 260nm. The first new maximum was seen as a negative peak centred on 240nm as shown in Figure 5.50., this peak shifts to longer wavelength and changes in intensity until at high D/P ratios a positive maximum results. The last new maximum detected was positioned around 230nm and was seen as a large positive peak. Again, spectral shifts were also associates with this peak. The existence of several conformational binding complexes was evident at high D/P ratios, the use of 3M equivalent DIS highlighted this. The spectral changes observed could be due to the redistribution on DIS on albumin that could account for the dramatic changes observed in the spectra.

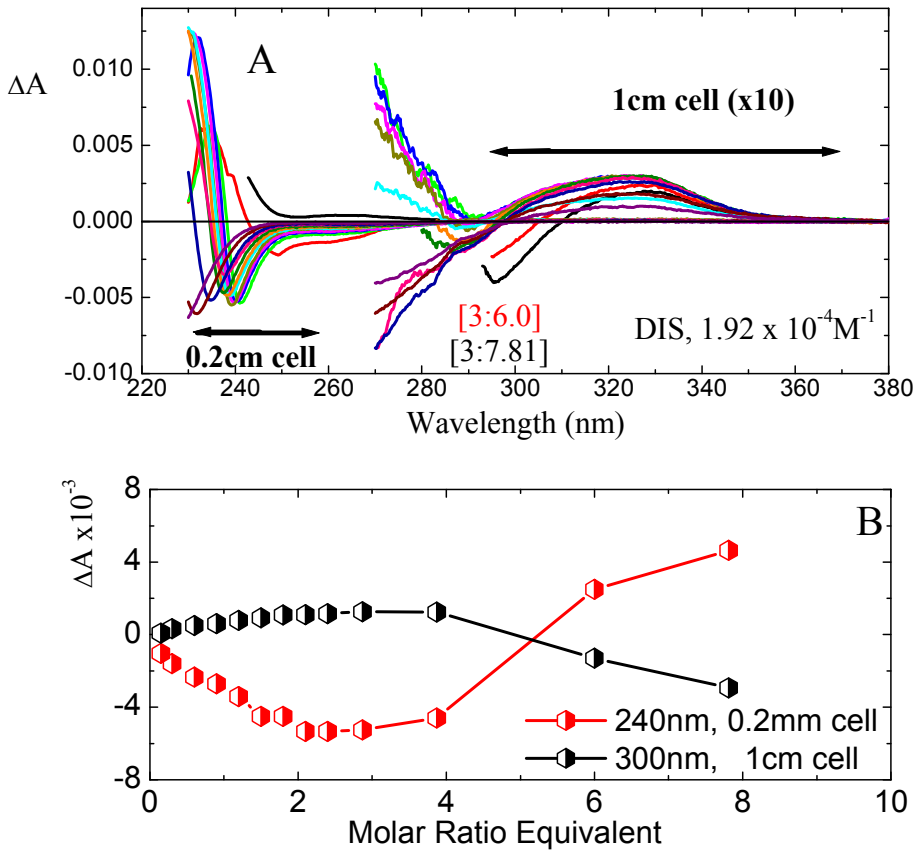

Figure 5.50. Ultimate titration of the binding of DIS to rHSA.

A Titration of DIS (fixed at 3 molar equivalent) with rHSA, 10mM P/B, pH7.2,1cm and 0.2cm
B Fixed wavelength plot of a fixed concentration of DIS (3M equivalent) to varying rHSA

5.8.iii.b. 3,5 Diiodosalicylic Acid Binding in the Presence of an Antagonist

The binding at site IIIA of a ligand can be antagonised by some ions, fatty acids and amino acids such as tryptophan (Trp). Tryptophan was chosen to be the antagonist and was titrated with a [2:1] molar ratio equivalent of DIS:rHSA. The presence of a small amount of Trp (0.1M) slightly enhances the binding of the ligand. However, further additions of Trp resulted in the displacement of DIS, shown in Figure 5.51.a. The affinity of Trp was not strong enough to displace DIS from binding pocket IIIA. However, the presence of a small amount of Trp (0.1M equivalent) was sufficient to produce enhances binding of the ligand. The titration of DIS was now carried in the presence of 0.1M equivalent Trp bound to rHSA, and as expected Trp was shown to enhance binding. Figure 5.51.b. supports these findings. From this study it seems that Trp does not act as an antagonist in the case of DIS but rather as an enhancer.

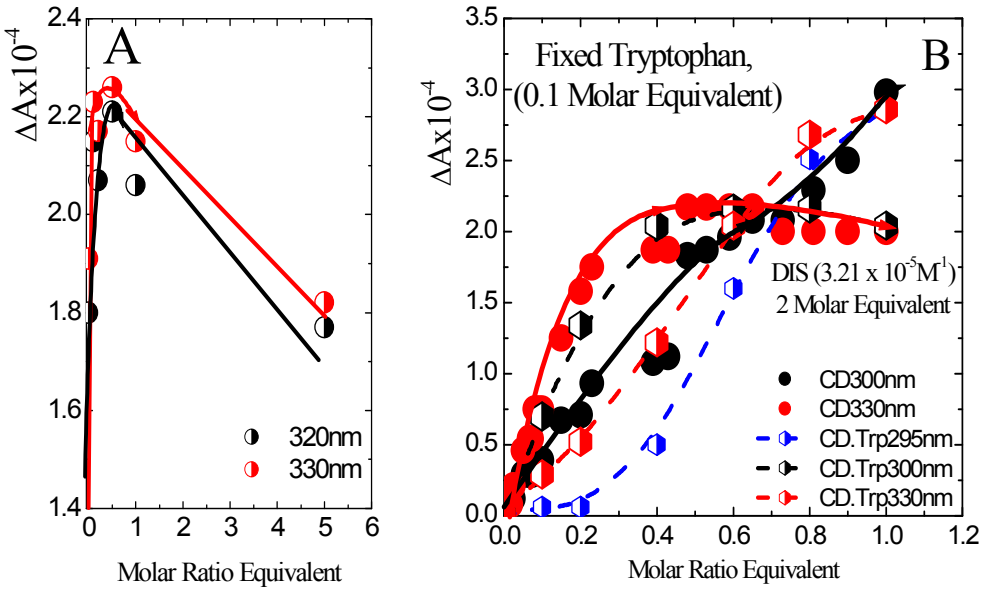

Figure 5.51. The binding of DIS to rHSA in the presence of Trp.

A Titration of tryptophan to fixed molar ratio equivalent of [2:1] DIS:rHSA, 10mM P/B, pH7.2, 5cm
B Titration of DIS:rHSA in the presence and absence of tryptophan, 10mM P/B, pH7.2, 5cm

5.8.iii.c. 3,5 Diiodosalicylic Acid Binding to a Fixed Concentration of rHSA

Binding studies can be conducted fixing either the concentration of the ligand or the protein. Whichever way the titration is performed the end result, in theory, should be the same. Carrying out the titration of DIS:rHSA to test this hypothesis, the concentration of rHSA was kept constant and fixed at 1.28 x $10^{-4}M^{-1}$, Figure 5.52. shows the results of that titration.

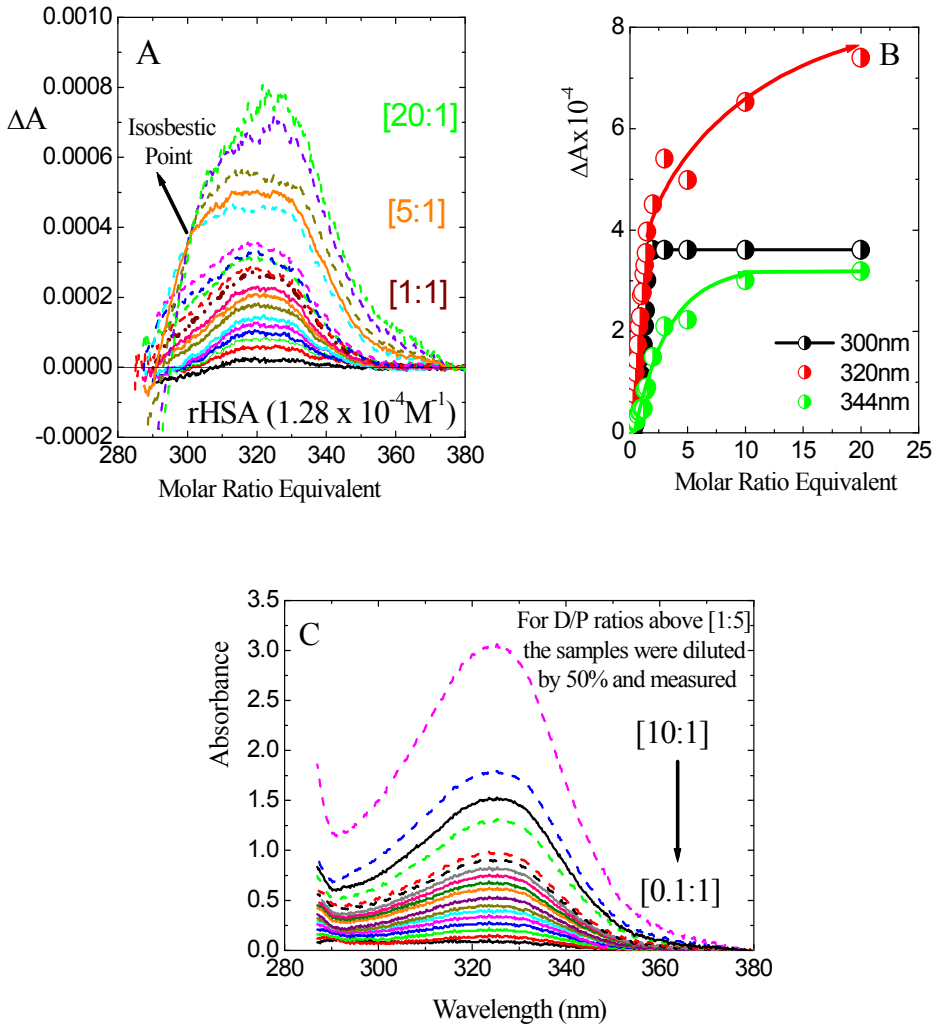

Figure 5.52. The titration of a variable concentration of DIS to fixed rHSA.

A Fixed rHSA (1M equivalent) to increasing concentrations of DIS, P/B, pH7.2, 5cm
B Fixed wavelength plot of rHSA at fixed concentration with increasing amounts of DIS
C Absorbance spectra of rHSA (fixed) with increasing amounts of DIS, P/B, pH7.2, 5cm

The CD profile of the titration was similar to the binding seen when the conditions are reversed (i.e. when the ligand concentration was constant). An isosbestic point was observed for ratios exceeding a D/P ratio equivalent of [4:1] suggesting the existence of two of more species in equilibrium. The end point of the titration was not reached with changes monitored up to a D/P ratio of [20:1], showing continuous changes for the main CD spectra at 320nm. An additional maximum at 344nm was now evident appearing as a shoulder on the main transition (Figure 5.52.a.). The binding of DIS to albumin seemed to occur in stages, the initial stage which reflected a D/P ratio of [2:1]. The initial stage was rapid as shown by the maxima at 300nm in Figure 5.52., and appeared to be stable resisting further perturbation until a point is reached where a second stage of binding dominates as demonstrated in Figures 5.48 & 5.52. Albumin triggered the binding of DIS at high D/P ratio, however, it was not possible to reach completion of the titration as the solubility of both DIS and albumin becomes a problem at such high concentrations.

5.8.iii.d. Variable Concentrations of both 3,5 Diiodosalicylic Acid and rHSA

The final set of experiments conducted was to investigate the chemical properties of the binding of DIS was to vary both the ligand and protein concentrations, this was achieved by taking a [2:1] molar ratio equivalent sample of the complex and titrating in 2M equivalent sample of DIS. The method adopted serves to dilute the rHSA concentration and subsequently increase the DIS concentration. The results are shown in Figure 5.53. and reflects similar characteristics to the transitions shown when titrated with fixed DIS and varying rHSA. The continuous changing conditions of both the ligand and the protein meant no final end point could be obtained.

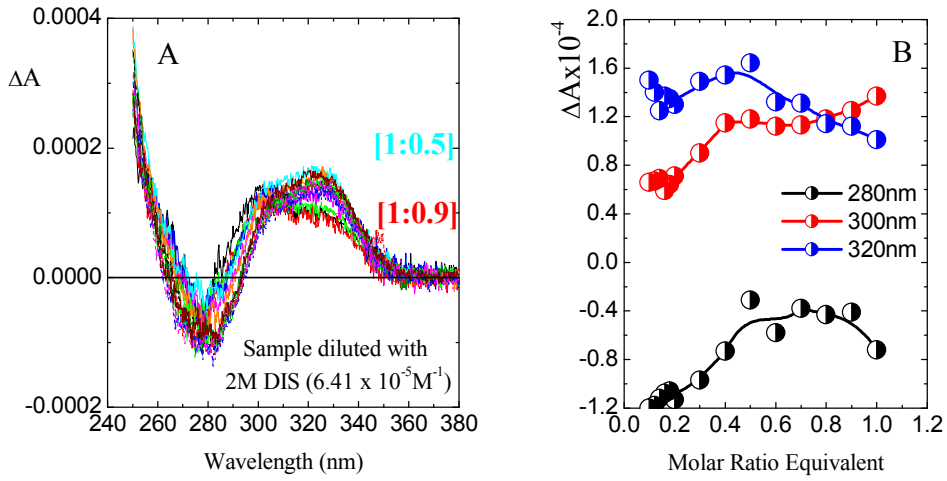

Figure 5.53. The titration of DIS:rHSA varying both concentrations

A Variable concentrations of DIS with changing rHSA concentration in P/B, pH7.2, 1cm
B Fixed wavelength plot of variable DIS and rHSA concentrations

5.8.iii.e. 3,5 Diiodosalicylic Acid pH Studies

The environment of the binding pockets of DIS:rHSA for a [2:1] molar ratio equivalent was investigated with changing pH and was found to be quite robust for the wavelength maximum of 382nm, withstanding pH changes between pH3.5 and pH10. For the other wavelengths studied this was not the case, pH variation was reflected throughout, with these wavelengths showing three transitions with the exception of wavelength 280nm that revealed four transitions. The results of all the pK can be found in Table 5.6.

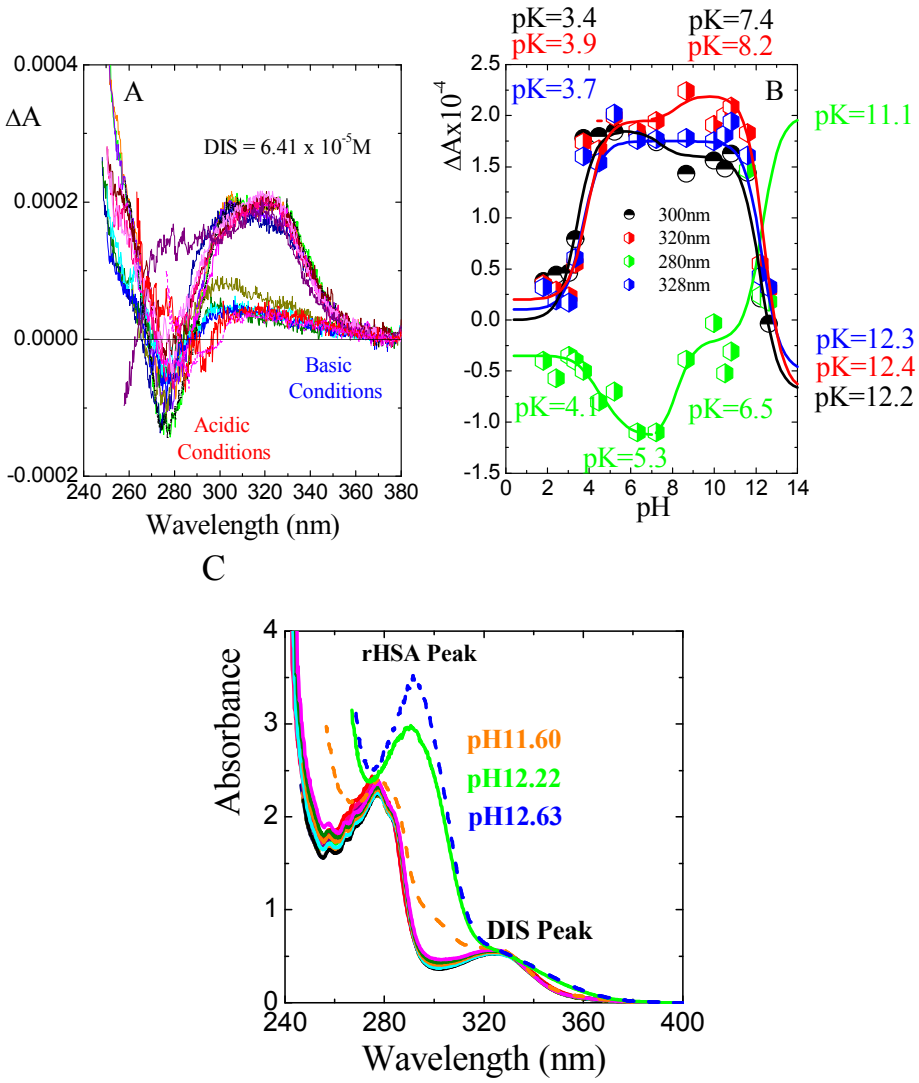

Figure 5.54. pH perturbation of a [2:1] ratio of DIS:rHSA.

A pH Titration of a [2:1] molar ratio sample of DIS:rHSA in water, 1cm cell
B Fixed wavelength plot of the pH titration of a [2:1] molar ratio equivalent of DIS:rHSA in water

C Absorption spectra of a [2:1] molar ratio equivalent of DIS:rHSA pH titration in water, 1cm cell

Wavelength (nm)	**Dis:rHSA [2:1]**			
	1st	2nd	3rd	4th
280	4.1	5.3	6.5	11.1
300	3.4	-	7.4	12.2
320	3.9	-	8.2	12.4
328	3.7	-	-	12.3
rHSA 287nm	3.5	-	6.1	11.7

Table 5.6. The pH transitions of Dis:rHSA

The wavelength in Dis:rHSA (300nm) closest to that of rHSA only wavelength maxima reflected similar transitions and values for pK, the other wavelengths were more distinctive. In order to ascertain whether the amount of bound DIS that gave different CD profiles over the same wavelength region investigated would respond differentially to pH perturbations, four different D/P ratio combinations were investigated. The ratios chosen were [0.2:1], [0.4:1], [0.6:1] and [0.8:1], and the results are shown in Figures 5.55. to 5.58. The data reflected spectral changes specific to the D/P ratios with good agreement reached the closer the D/P ratio moved towards the [2:1] molar ratio equivalent.

The ratios were chosen such that the two lowest ratios would mean only one molecule of DIS was bound at any one time to the protein. The higher ratios were chosen to reflect the possibility of two molecules of DIS molecules bound to the protein. From the results there was a clear distinction between the first two titrations and the last two. The ratios that contained one DIS bound produced three transition at the wavelength maximum of 250nm, for the other two wavelengths monitored only two transitions were seen. There was also a certain amount of spectral shift of the maxima towards longer wavelength.

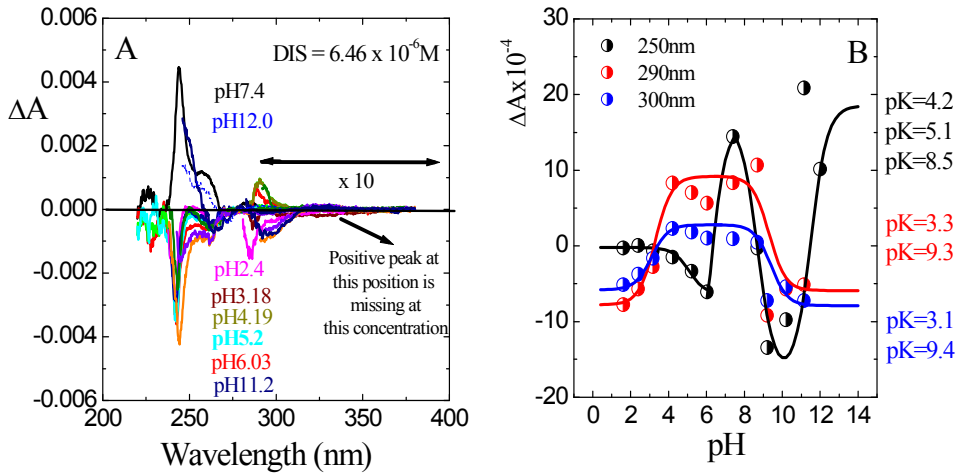

Figure 5.55. pH titration of [0.2:1] molar ratio of DIS:rHSA.

A pH Titration of a [0.2:1] molar ratio equivalent of DIS:rHSA in water, 2cm cell
B Fixed wavelength plot of the pH titration of a [0.2:1] molar ratio equivalent of DIS:rHSA in water

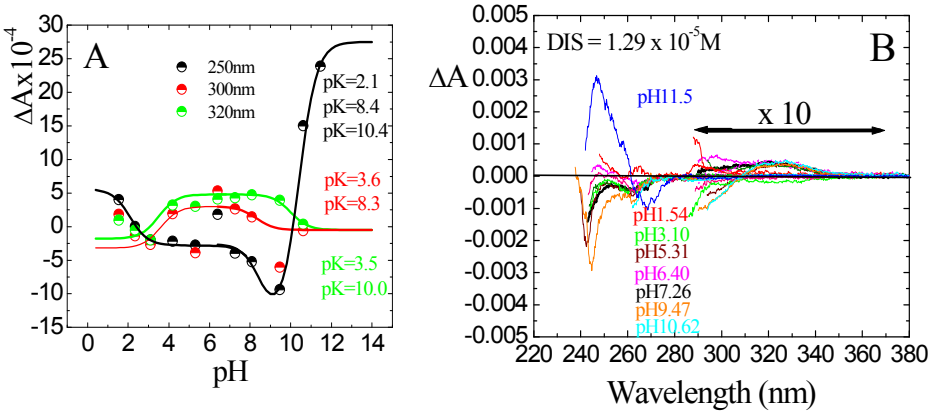

Figure 5.56. pH titration of [0.4:1] molar ratio of DIS:rHSA

A Fixed wavelength plot of the pH titration of a [0.4:1] molar ratio of DIS:rHSA in water
B pH titration of a [0.4:1] molar ratio equivalent sample of DIS:rHSA in water, 2cm cell

By the time the higher molar ratio equivalents were monitored the spectral shifts experienced at the lower ratios were not evident, but the maxima at 300nm and 320nm were firmly established.

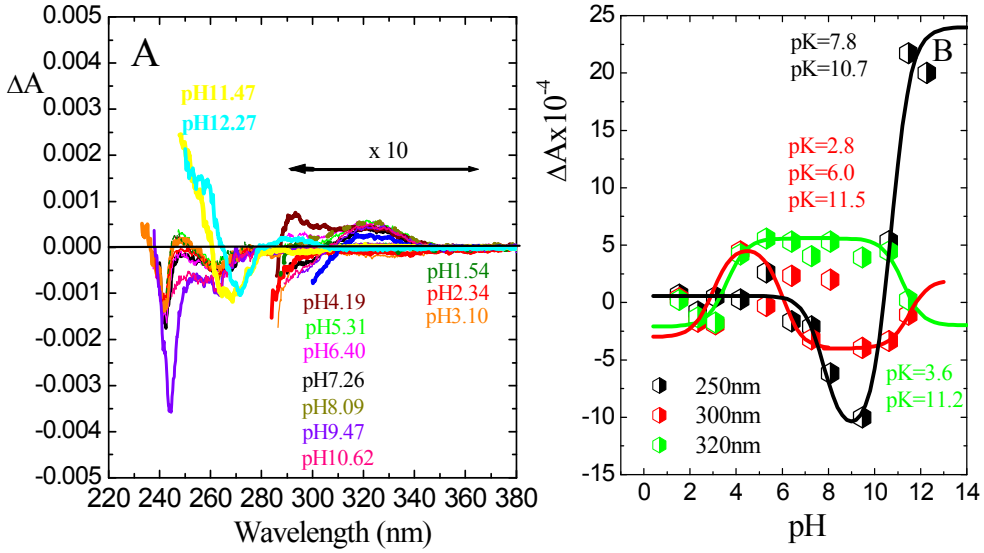

Figure 5.57. pH titration of [0.6:1] molar ratio of DIS:rHSA

A pH titration of a [0.6:1] molar ratio equivalent of DIS:rHSA in water, 2cm cell
B Fixed wavelength plot of the pH titration of [0.6:1] molar ratio equivalent of DIS:rHSA in water

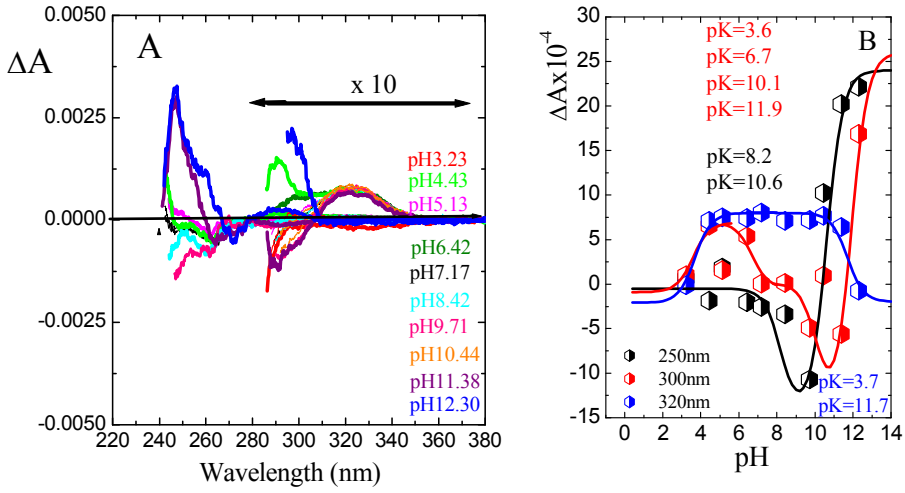

Figure 5.58. pH titration of [0.8:1] molar ratio of DIS:rHSA

A pH Titration of a [0.8:1] molar ratio sample of DIS:rHSA in water, 2cm cell
B Fixed wavelength plot of the pH titration of a [0.8:1] molar ratio sample of DIS:rHSA in water

Now shifts in the number of transitions were observed at the wavelengths monitored. At 250nm, previously three transitions were seen now reveals only two for the two higher ratios. However, at 300nm which showed two transitions now supported three transitions, a reversal in role between the two wavelengths. A table of all the transitions observed is shown in Table 5.7.

λ nm	**DIS:rHSA [0.2:1]**				**DIS:rHSA [0.4:1]**				**DIS:rHSA [0.6:1]**				**DIS:rHSA [0.8:1]**			
	1st	2nd	3rd	4th	1st	2nd	3rd	4th	1st	2nd	3rd	4th	1st	2nd	3rd	4th
250	4.5	5.1	8.1		2.1		8.4	10.4			7.8	10.7			8.2	10.6
290	3.3		9.3													
300	3.1		9.3		3.6		8.3		2.8	6.0		11.5	3.6	6.7	10.1	11.9
320					3.5			10.0	3.6			11.2	3.7			11.7

Table 5.7. Transitions in the different molar ratio equivalents with changing pH.

Clear trends could be seen from the table of results. At all ratios studied the final wavelengths monitored revealed two transitions for all samples, one in the extended form and the other in the basic form. At 250nm, ratios [0.2:1] & [0.4:1] revealed three transitions, one in the E-form, one in the N-form and the last in the B-form. For the higher

ratios, two transitions in the N-form & B-form were seen. The middle wavelength region was the area that revealed the greatest complexity with the higher ratios supporting three to four transitions, while at lower ratios only two transitions were observed in the E-form & B-form. It was clear that each conformational form experience by albumin had a direct effect on the binding of DIS and there was a dependency on the number of bound DIS present. In view of the pH susceptibility of DIS binding with respect to the conformation of albumin, the next experiment investigated the effects of binding at different pH values. The environment of HSA was altered, four pH regions were observed, pH3.56 with HSA in its extended form, pH4.57 where HSA was in the fast form, pH7 the neutral form of HSA, and lastly pH9.04 where HSA was in the basic form. At each specified pH, the titration of a fixed concentration of DIS was titrated to varying concentrations of albumin. The data is represented in Figure 5.59 – 5.62. In each case, the same concentration of DIS was used within a buffered environment to ensure continuity; the only parameter that varied was the pH.

The binding of DIS was shown to be pH dependent; the profiles of the spectra appeared different in each titration. When rHSA was in its extended form (pH3.56) the positive maximum at 300nm was markedly affected even at low D/P ratios. The only titration that was comparable at these low ratios to pH3.56 was that conducted at pH9, which showed a depression of the maximum at 320nm and 300nm. For D/P ratios up to [1:0.5] there was a continued increase in the peak at 320nm with the protein in the extended form reaching a plateau, further increases had no effect on this maximum and the peak remains steadfast. The intensity of ΔA at the plateau has also been compromised, attaining a lower level than was expected (Figure 5.59.a.). The maximum at 300nm however, continues to increase, this suggests that the two maxima work independently and may be indicative of the two binding sites. When albumin was in the fast form (pH4.57) the binding of DIS brought kayos with the loss in magnitude of the maximum at 300nm , now this peak was inferior to

the maximum at 320nm, suggesting that binding related to that peak has been compromised (Figure 5.59.b.). The spectra appeared noisy as the samples appeared to be quite affected when kept at that pH. Binding at 320nm had been slightly enhanced with an increased in ΔA by approximately a third to the expected value. Also noticeable was the loss of the negative maximum at 280nm, this suggests that perhaps the maxima at 300nm and 280nm were coupled and therefore the compromise at one will result in corresponding changes at the other peak.

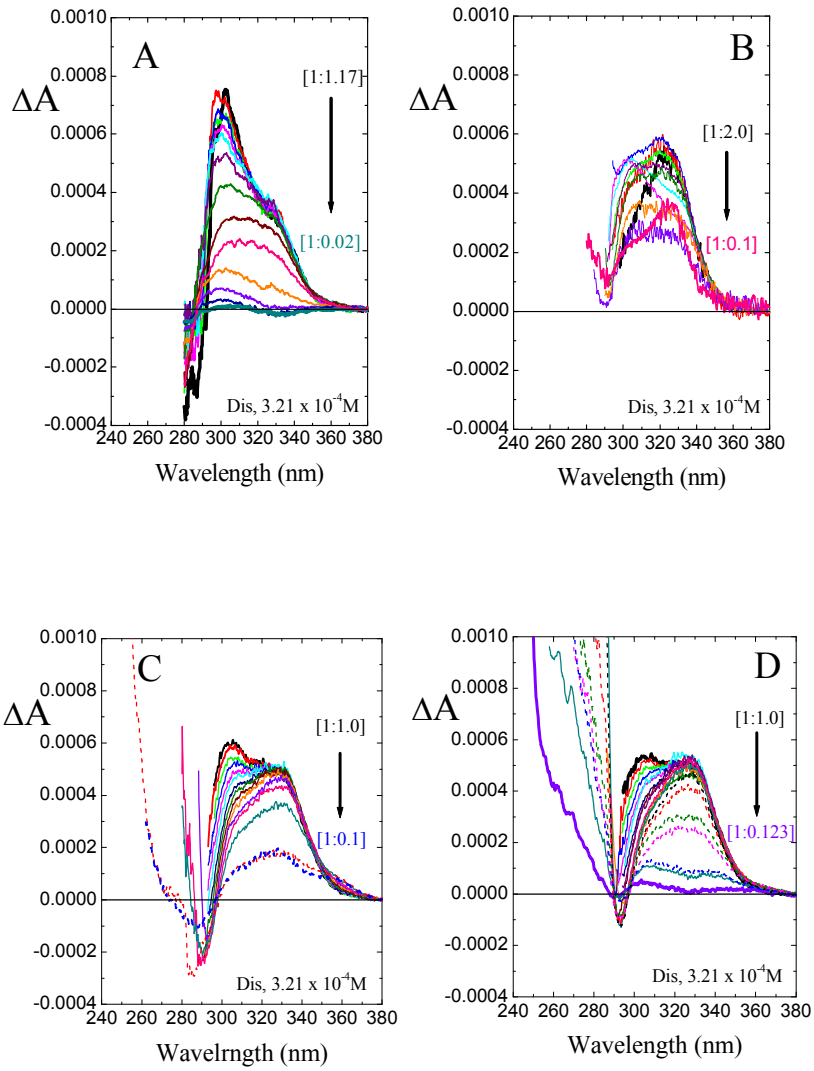

Figure 5.59. pH effects on the binding titration of DIS to rHSA

A Titration of DIS:rHSA in 10mM B/R buffer, pH3.56, 1cm cell
B Titration of DIS:rHSA in 10mM B/R buffer, pH4.57, 1cm cell
C Titration of fixed DIS with rHSA in 10mM Tris buffer, pH7.01, 1cm cell
D Titration of fixed DIS with rHSA in 10mM Tris buffer, pH9.04, 1cm cell

Binding at physiological conditions (Figure 5.59.c.) produced the typical spectra that were expected but with one exception, there appears to be the generation of a new peak relatively small in intensity that was generated for low D/P ratios. The new peak was formed at 360nm and reduces to a minimum for ratios greater than [1:0.35]. The last pH condition to be studied was when albumin was in the aged transition (pH9). At this pH binding behaved similar to that at physiological conditions but with two exceptions. Firstly the maximum at 300nm had been compromised with a magnitude more typical for that found at 320nm, the distinction between both wavelengths were minimal. Secondly, the negative peak at 280nm was very much reduced, once again supporting the hypothesis that the peaks at 280nm and 300nm were coupled. The fixed wavelength plots of the CD data can be found in Figure 5.60.

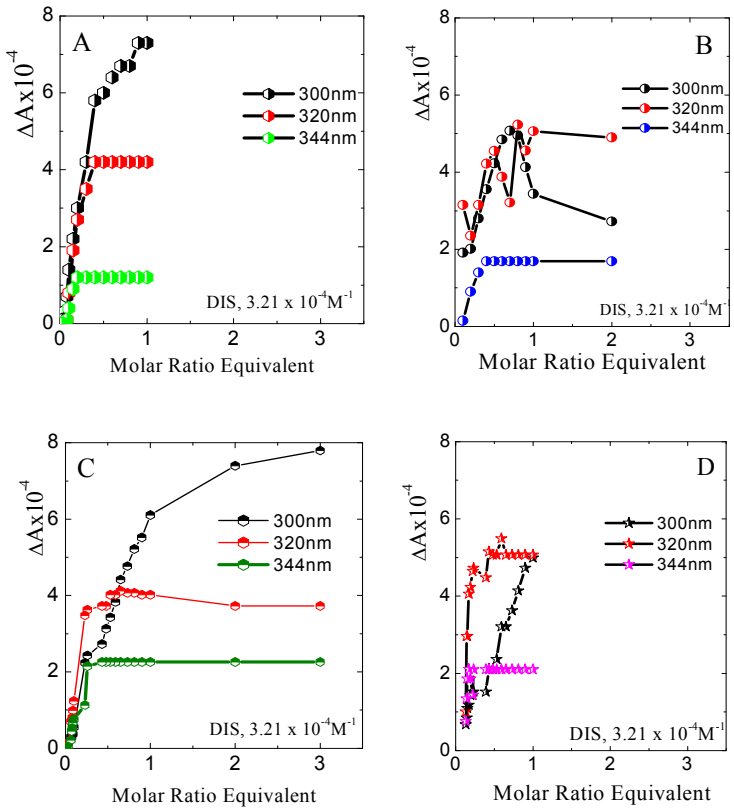

Figure 5.60. Fixed wavelength plots of the pH effects on the binding titration.

A Titration of a fixed concentration of DIS to increasing rHSA in B/R buffer, pH3.56, 1cm cell
B Titration of a fixed concentration of DIS to increasing rHSA in B/R buffer, pH4.57, 1cm cell
C Titration of a fixed concentration of DIS to increasing rHSA in Tris buffer, pH7.01, 1cm cell
D Titration of a fixed concentration of DIS to increasing rHSA in Tris buffer, pH9.04, 1cm cell

The fixed wavelength plots reflected the trends seen in the CD spectra. Each pH titration reflected its unique set of binding data.

5.8.iii.f. 3,5 Diiodosalicylic Acid Temperature Studies

Like previously, temperatures studies were conducted in two ways. First the binding of DIS to preheated samples of rHSA was investigated; the results are shown in Figure 5.61. The CD spectra revealed the loss of both positive maxima with increasing heat denaturation.

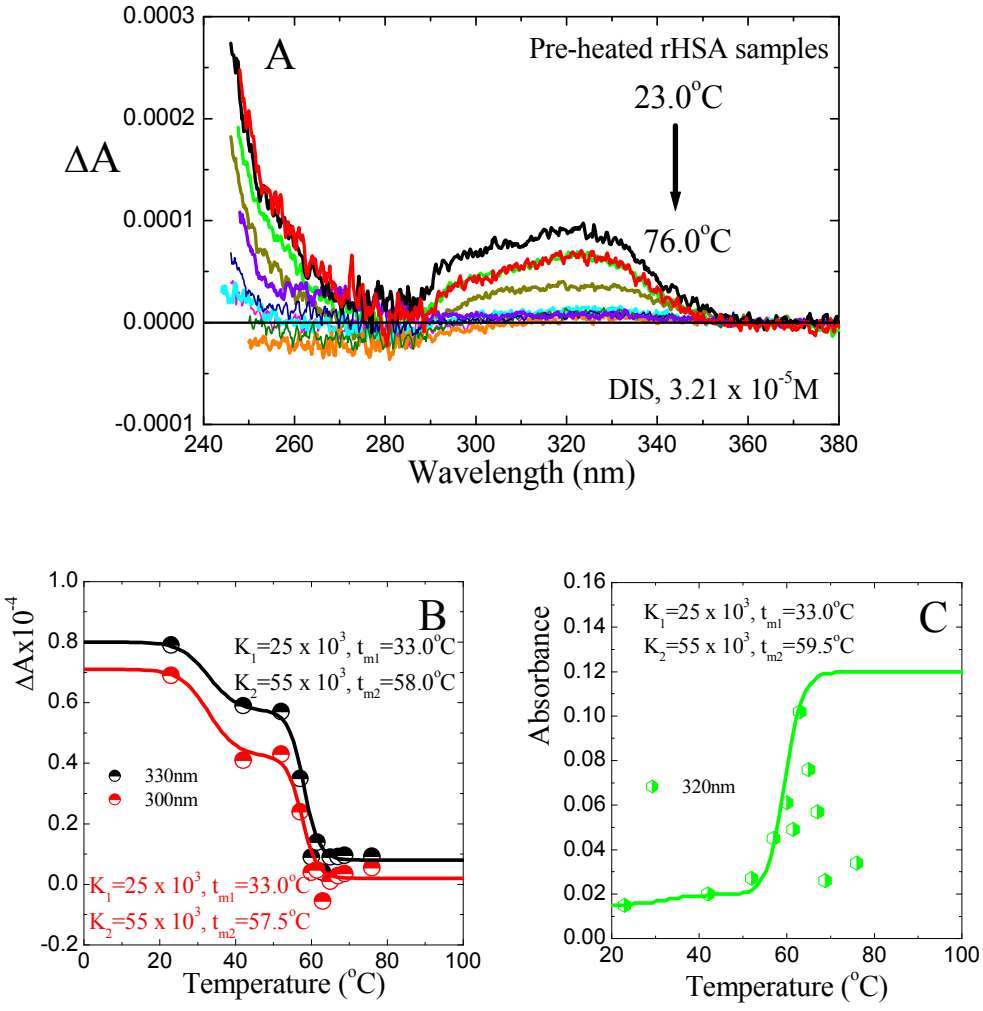

Figure 5.61. Binding studies of pre-heated rHSA with DIS.

A Temperature studies of a [2:1] molar ratio equivalent of DIS:rHSA in 10mM P/B, pH7.2, 1cm cell
B Fixed temperature plot of the pre-heated samples of rHSA bound to DIS in 10mM P/B, pH7.2, 1cm cell
C Microcentrifuged samples of the pre-heated rHSA bound to DIS in 10mM P/B, pH7.2, 1cm cell

The fixed wavelength plots showed the existence of two transitions for both of the positive maxima studied, both occurring within a degree of each other showing that they were both responsive to the conformational perturbations (Figure 5.61.b.). The first transition was determined at a t_m= 33.0˚C with a K = 25 x 10^3 for both maxima, this produces a reduction of approximately 50% of the CD signal. The second transition was more rapid and occurred at t_m= 57-58.0˚C with a K = 55 x 10^3 that represented the total loss of binding of DIS. The micro-centrifuged samples measured by absorption also supported the findings in the CD spectra that revealed two transitions with very similar numerical values (Figure 5.61.c.). The second temperature study was to measure the heating and quenching spectra for a [2:1] molar equivalent sample of DIS:rHSA. The observation of the heating curve revealed the gradual dissociation of the drug from albumin for temperatures up to 60^{o}C. For temperatures exceeding this, the loss was more significant with complete dissociation achieved around 85^{o}C (Figure 5.62). Three transitions were determined with the first t_m detected at 42.0˚C that produced the highest value of K=28 X 10^3. The other two transitions occur at 68.0^{o}C & 74.0^{o}C with lower values of K=10 X 10^3 & 20 X 10^3 respectively.

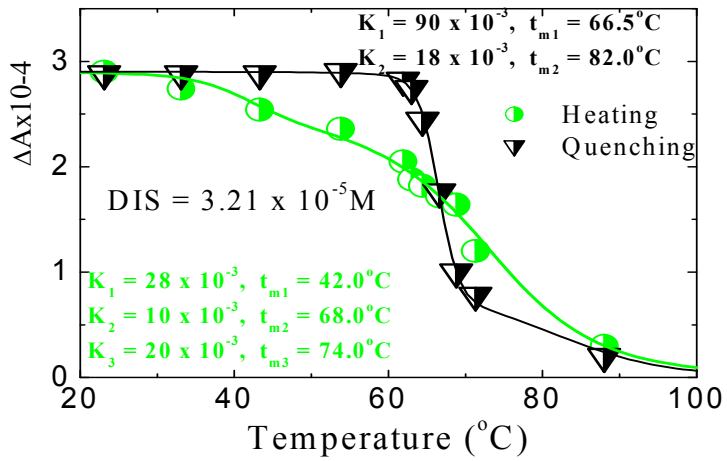

Figure 5.62. Temperature studies of a [2:1] molar ratio equivalent of DIS:rHSA.

Fixed wavelength plot of the [2:1] molar ratio equivalent of DIS:rHSA in 10mM P/B, pH7.2, 5cm cell

The quenching curve highlighted the relative stability of the DIS:rHSA association, and showed that temperatures up to 60^{o}C did not affect the binding pockets of DIS. Dissociation was very rapid between 60^{o}C and 70^{o}C with virtually the complete loss in binding attained by the end point. Two transitions were seen at 66.5^{o}C & 82.0^{o}C with values of K=90 x 10^3 & K=18 x 10^3 respectively, revealing the difficulties of the first transition and the relative ease of the second.

5.8.iii.g. 3,5 Diiodosalicylic Acid Denaturation Studies

The denaturation studies of both urea and GuHCl are shown in Figure 5.63., and reveal the robustness of the DIS:rHSA binding site. Even at very high denaturation conditions substantial binding remained, with both positive maxima compromised the negative maximum was enhanced. The absorption spectra for the guarnadinium complex is shown in Figures 5.63.a. & b. and revealed no significant spectral changes in either the DIS absorption or the rHSA. The absorption spectra also reflected the same results as the CD, revealing little changes in absorption, with the fixed wavelength plot revealing consistency of binding (Figures 5.64.a. & b).

Urea, like GuHCL, reflected similar changes with the endpoint of the titration still producing reduced binding of DIS to rHSA (Figures 5.63.c. & d.). Neither of the denaturants used was able to completely displace DIS from albumin. The response of albumin in the absence of ligand responded to either of the denaturants by completely unfolding, and indeed little structural integrity remains. However, in the presence of DIS, binding was maintained, albeit at a reduced amount.

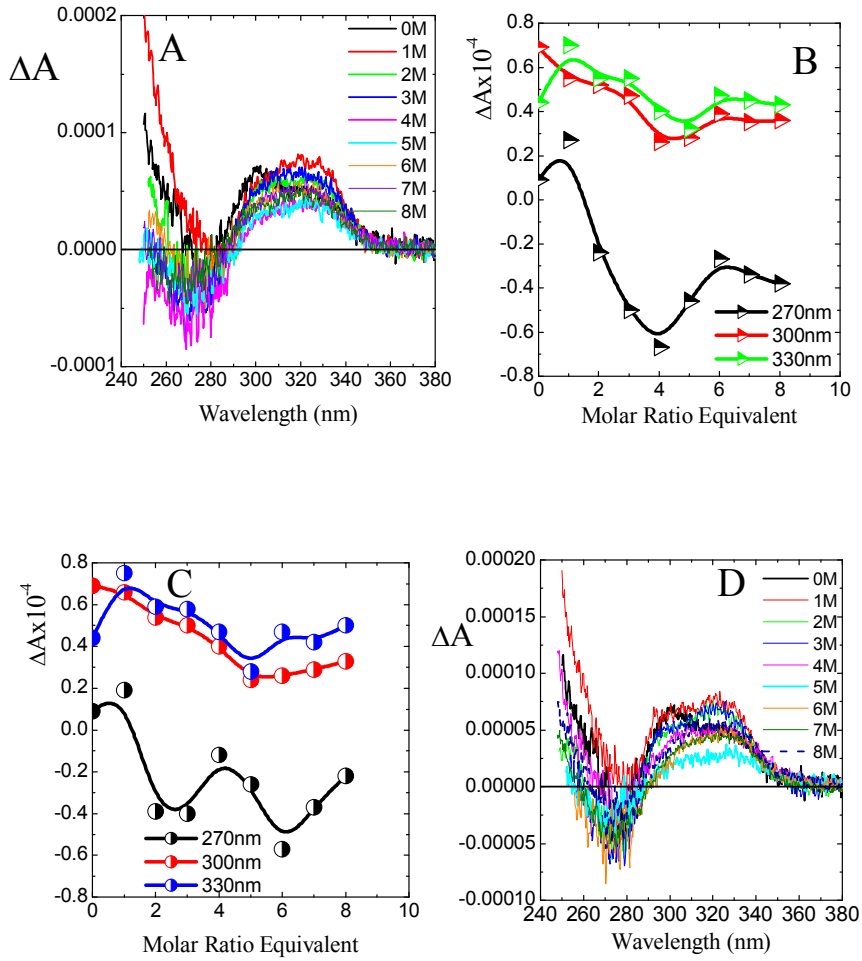

Figure 5.63. CD Spectra of DIS:rHSA, [2:1] molar ratio equivalent in denaturants.

A Titration of a [2:1] molar equivalent sample of DIS:rHSA with increasing GuHCl in water, 1cm cell
B Titration of a [2:1] molar ratio equivalent of DIS:rHSA with increasing concentrations of GuHCl, 1cm
C Titration of a [2:1] molar ratio equivalent of DIS:rHSA with increasing concentrations of Urea, 1cm
D Titration of a [2:1] molar equivalent sample of DIS:rHSA with increasing Urea in H\-(2)O, 1cm cell

The measurements derived from the micro-centrifuged samples revealed a steady increase in absorbance with increase in concentration of GuHCl, however, there was still a substantial amount of bound drug shown. The micro-centrifuged samples measured for the urea complex reflected similar trends to its counterpart (Figure 5.64.e.), with urea producing a slightly greater displacement of DIS relative to GuHCL. Both produced unexpected binding since the denaturants were known to denature domains I & II. In view of that, may be the integrity of the binding site IIIA still retained and this would explain the present findings.

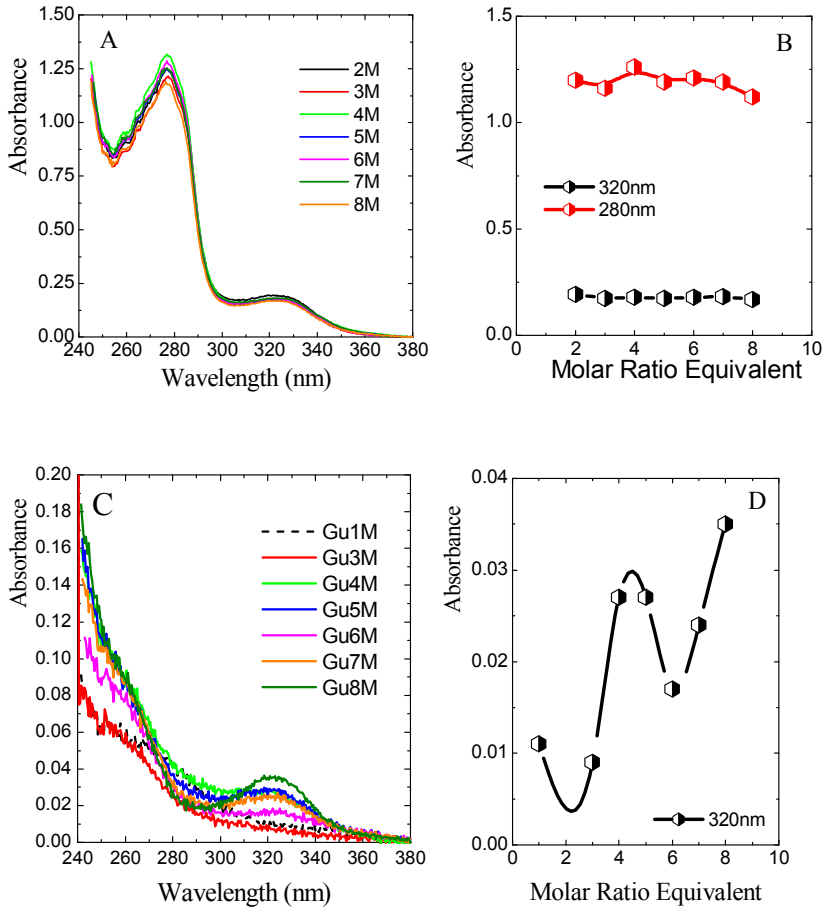

Figure 5.64.a, Absorbance spectra of the microcentrifuged samples of DIS:rHSA:GuHCL.

A UV Absorbtion of the tiration of a [2:1] molar ratio of DIS:rHSA in increasing concentrations of GuHCl
B Fixed wavelength plot of the UV absorption spectra of the titration of DIS:rHSA in GuHCl, 1cm
C Microcentrifuged samples of the titration of a [2:1] molar ratio equivalent of DIS:rHSA in GuHCl
D Fixed wavelength plot of the microenctrifuged samples of a [2:1] sample of DIS:rHSA in GuHCl, 1cm

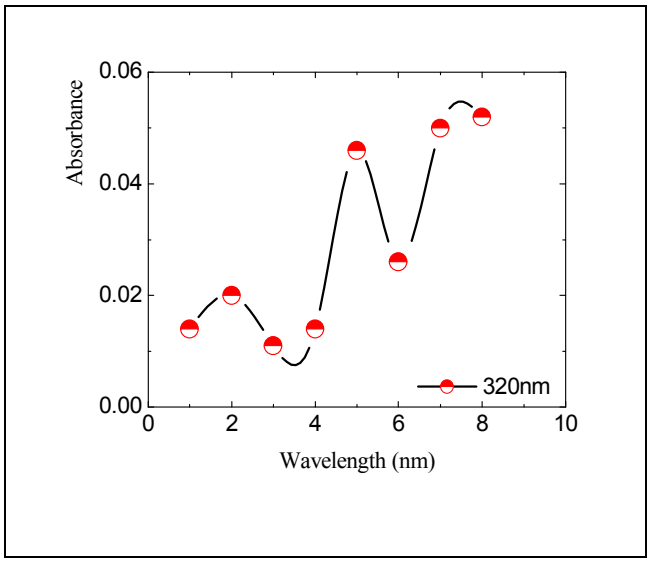

Figure 5.64.b. Fixed wavelength plot of microcentrifuged DIS:rHSA:Urea complex.

E Microcentrifuged samples of [2:1] molar equivalent of DIS:rHSA with Urea, 1cm cell

5.8.iv. DIS:Domain I+II Binding Studies

The binding of DIS to one of the domain fractions of albumin was studied and compared to whole albumin, domain I+II was selected since it contained one of the binding sites of DIS and therefore its CD profile should be similar to that of the whole sample. The results of the titration are shown in Figure 5.65. and shows that for high D/P ratios the similarities between the binding to domain I+II and the whole were strikingly similar, revealing both the 300nm and 320nm positive maxima. The difference in peak heights between the two positive maxima were more pronounced in the fragment then they were in the whole, making it very difficult to measure the negative maximum at 280nm (Figure 5.65.a.). For ratios below [1:2], but greater than [1:0.5], the results highlighted the fluidity of the positive maxima that seem to be concentration dependant (Figure 5.65.b.). Firstly, the consolidation of the two positive maxima into a single peak detected at 320nm was observed. Secondly, an inversion of the consolidated peak resulting in a negative maximum was found that was also detected at 320nm, and was almost the mirror image of that which was seen for the positive maxima, the negative maximum at 275nm was unaffected. Ratios below [1:0.5] gave the characteristic single positive CD maximum at 320nm, there was a noticeable lack of the 300nm peak. By all accounts, the CD profile of the fraction did not seem to be compromised in terms of binding ability by its preparation, its integrity seem to be intact at least where DIS binding was concerned.

The fixed wavelength plot revealed that even at a molar ratio equivalent of [1:17] complete binding was not attained. Initial assessments revealed that there was a substantial increase of the number of binding sites on the domain fraction, higher than could be explained under normal circumstances.

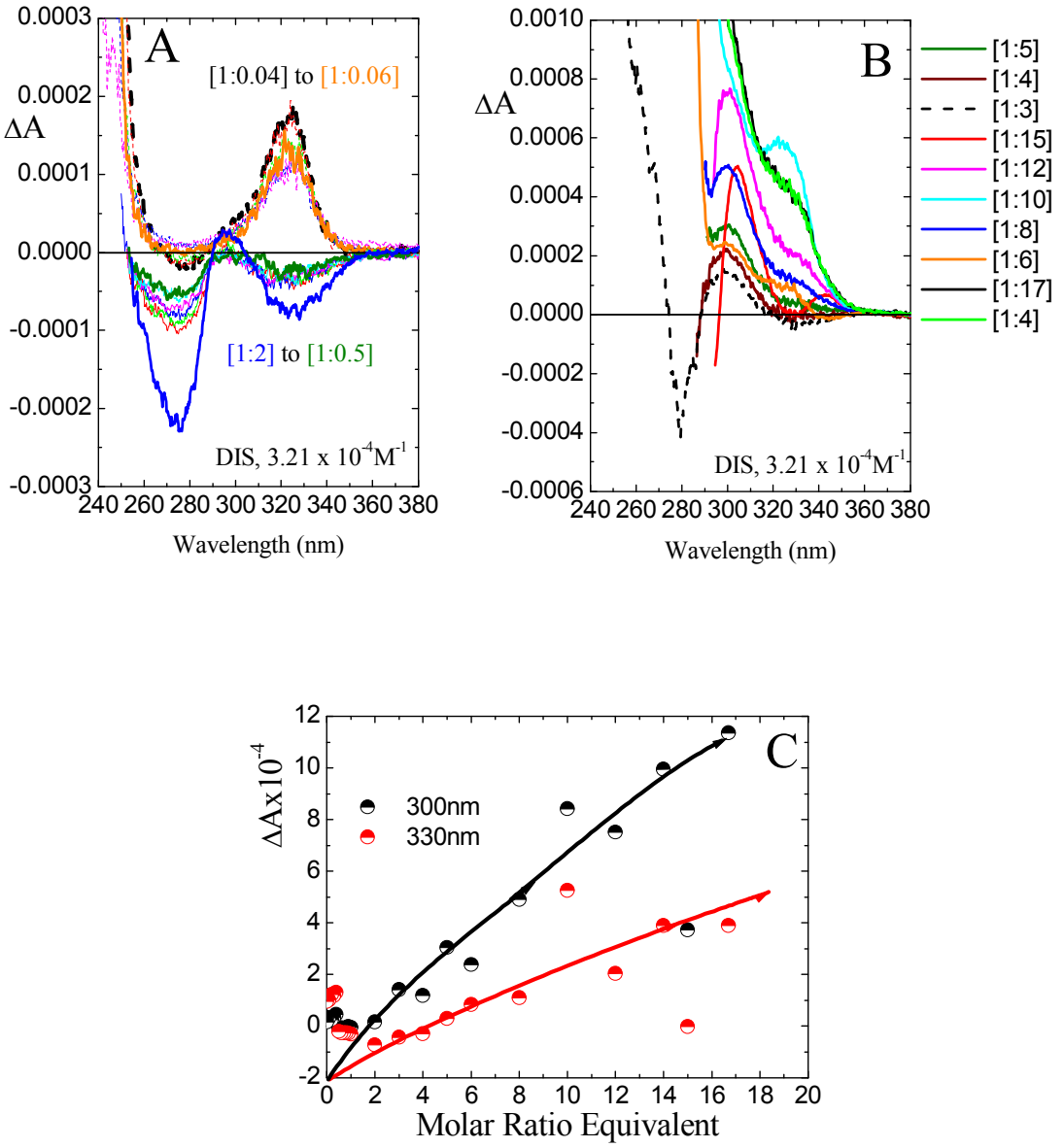

Figure 5.65. CD Spectra of the binding of DIS to domain I+II.

A Titration of a fixed concentration of DIS to varying concentrations of Domain 1+2, P/B,pH7.2, 1cm
B Titration of a fixed concentration of DIS to varying concentrations of Domain 1+2, P/B,pH7.2, 1cm
C Fixed wavelength plot of the titration of DIS with Domain1+2 in 10mM P/B, pH7.2, 1cm cell

The micro-centrifuged samples of the titration of DIS:domain I+II revealed that for very low D/P ratios the amount of unbound drug was high, but as the concentration of the domain fraction increased so to did the degree of binding. For the D/P ratio of [1:15] there was only a minuscule amount of free drug detected as shown in Figure 5.66; the fixed wavelength plot showed complete binding at a D/P ratio of [1:8] (refer to Figure 5.66.b.), but as shown in Figure 5.65.a. this was not the complete picture. There was a shift to shorter wavelength of the CD maximum at 300nm that could not be taken into account in the fixed wavelength plot.

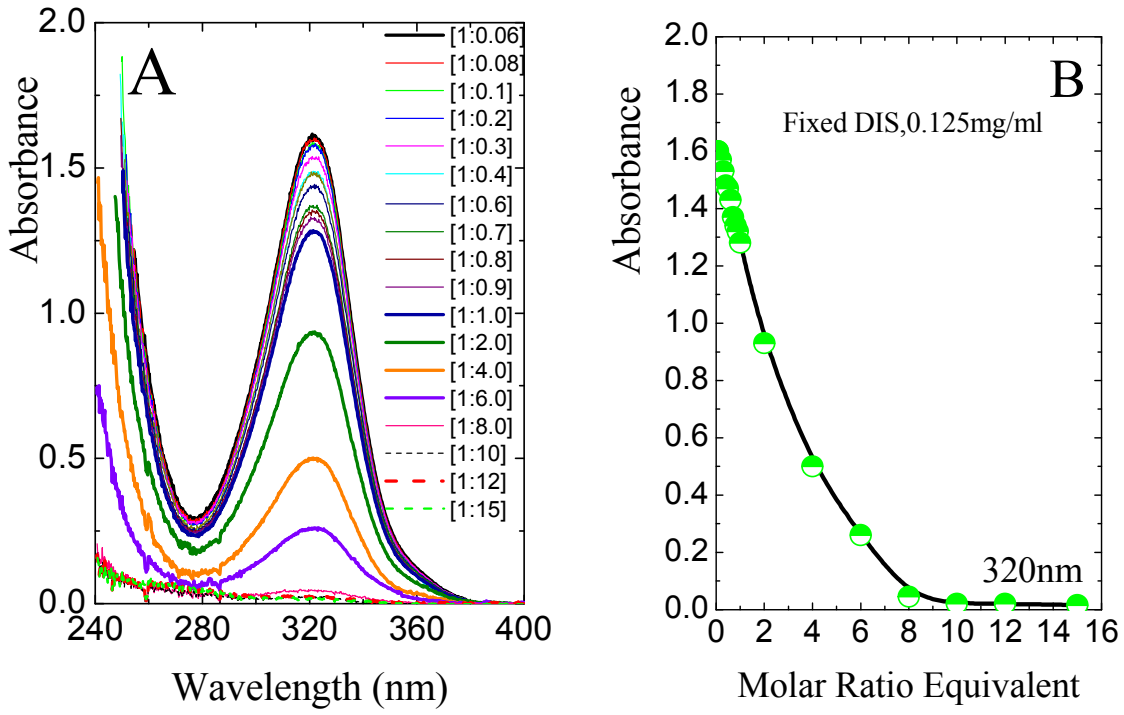

Figure 5.66. Absorbance spectra of the microcentrifuged samples of DIS:Domain I+II.

A Microcentrifuged samples of the titration of DIS:Domain I+II in 10mM P/B, pH7.2, 1cm cell
B Fixed wavelength plot of the microcentrifuged samples of the titration of DIS:Domain I+II, 1cm cell

5.9. Multiple Binding of Ligands to rHSA

Multiple binding studies to albumin was considered for three of the drugs/ligands previously studied with reference,

(a). to monitor the binding of DIS:rHSA:Diaz complex.

(b). War:rHSA:Diaz complexes.

Both the CD of the multiple complex (drug:rHSA:drug/antagonist) and the CD of the bound drug/or the antagonist (drug/antagonist:rHSA) complex were determined and are represented in Figures 5.67. & 5.68.

5.9.i. DIS:rHSA:Diaz complex

Considering the multiple complex first for DIS:rHSA complex and titrating with a 1M equivalent of diazepam, the CD of the combined drugs to rHSA gave a CD profile that was dominated by the DIS:rHSA signature. At high diazepam concentrations the peak at 320nm belonging to the DIS:rHSA interaction diminished as the negative effects of the diazepam maximum also at 320nm became evident (Figure 5.67.a.). The fixed wavelength plot (Figure 5.67.b.) revealed the continual influence of increasing diazepam binding. When the [2:1] molar ratio equivalent of DIS:rHSA baseline was removed the binding of diazepam signal became much more apparent (Figure 5.67.c.) albeit noisy compared to when diazepam binds to rHSA in the absence of any other perturbants. The fixed wavelength plot also supported the findings of a [1:1] molar ratio equivalent of diazepam binding to rHSA (Figure 5.67.d.). The CD for the corrected spectra revealed that 1M equivalent of diazepam had bound to rHSA in the presence of DIS. If 2M equivalent of DIS was also present at the same time that diazepam was present, then it was safe to assume that the binding site of DIS to IIIA had become displaced by diazepam and relocated to bind at IB. The presence of DIS to site IIA was unperturbed, thus supporting the theory that under certain conditions subdomain IIA becomes the dominant site for DIS,

with the weaker site moving to IB as found by crystal structural analysis.

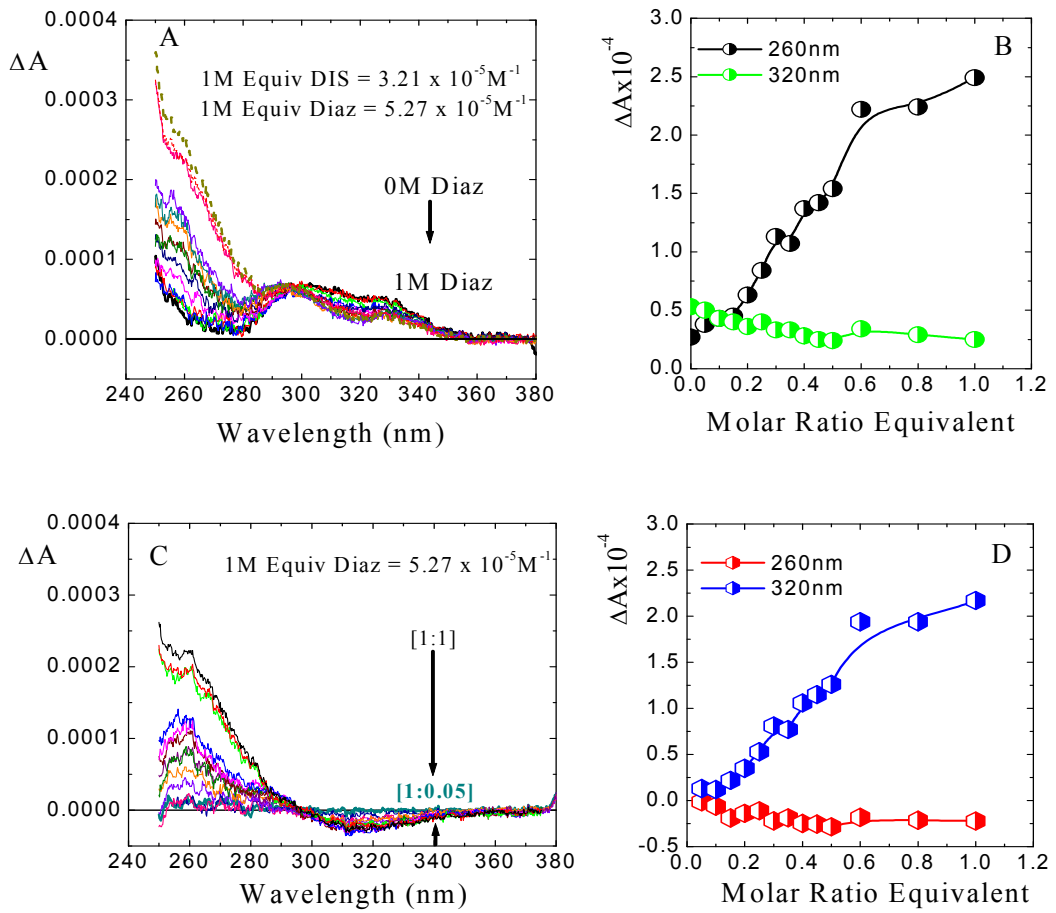

Figure 5.67. The study of diazepam binding to DIS:rHSA, [2:1] complex.

A Titration of a [2:1] molar equivalent of DIS:rHSA with increasing Diaz, 10mM P/B, pH7.2, 1cm
B Fixed wavelength plot of [2:1] DIS:rHSA with increasing concentration of diazepam
C Induced binding of a[2:1] molar ratio equivalent of DIS:rHSA with Diaz, (DIS:rHSA CD spectra has been removed), 1cm
D Fixed wavelength plot of DIS:rHSA:Diaz - DIS:rHSA

5.9.ii. War:rHSA:Diaz complexes

The other complex studied was the complex of War:rHSA binding to increasing concentrations of diazepam, monitored to investigate the possible coexistence of the two drugs to rHSA. The CD spectra reflected the combination of the two individual induced CD spectra; the results are shown in Figure 5.68. The results revealed the presence of a well defined isosbestic point highlighting a two state system. The distinct CD profile of the

warf:rHSA complex became increasingly dominated by the profile of the diazepam signal as it bound to albumin with the generation of a negative maximum located at 298nm(Figure 5.68.a.). The fixed wavelength plot revealed an increase in binding for D/P molar ratio equivalent up to [1:1:0.5], thereafter followed by a dramatic reduction in binding at those specified wavelengths (Figure 5.68.b.). When the War:rHSA baseline was subtracted from the mixture the true induced diazepam CD spectra was revealed and showed the characteristic CD profile for the corrected Diaz:rHSA complex (Figure 5.68.c.). The fixed wavelength plot obtained in Figure 5.67.d. mimicked the results found in the mixture (Figure 5.68.b.).

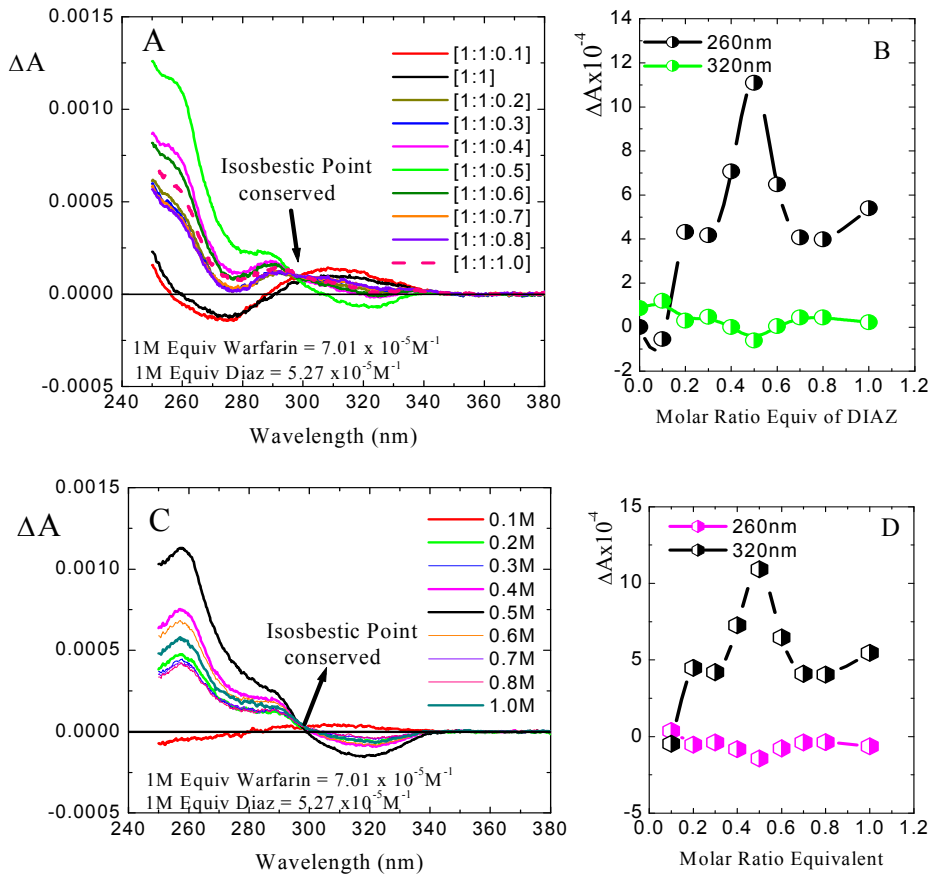

Figure 5.68. The multiple titration of Warf:rHSA [1:1] molar equivalent with diazepam.

A Titration of a [1:1] molar equivalent sample of War:rHSA with increasing Diaz, P/B, pH7.2, 1cm cell
B Fixed wavelength plot of the titration of [1:1] War:rHSA with increasing concentrations of Diaz
C Induced binding of a [1:1] molar ratio equivalent of War:rHSA with increasing Diaz, (War:rHSA spectra has been removed)
D Fixed wavelength plot of War:rHSA:Diaz - War:rHSA

CHAPTER 6

CHAPTER 6: Large Ligand:HSA Interaction, The Chemistry of Dyes

6.1. Introduction

The use of dyes in binding, structural and concentration studies of proteins is well established. Dyes are utilised because of their distinct colour and spectroscopic profiles. The absorption wavelength of a dye should be outside the spectroscopic range of the protein itself resulting in no spectral interference between the two; both the protein and the dye can be observed independently, a property utilised by UV and CD spectroscopy . HSA is no exception, the flexibility and adaptability of this protein is one of the main characteristics that allows it to bind numerous ligands with varying affinity. Locating binding sites however, has been problematic since HSA has the ability to present lower affinity binding sites as well as high. The specific binding of dyes can be used to provide excellent binding site markers, as they can be easily detected and monitored.

Three dyes, with similar core molecular structures, were chosen in this study. All three dyes were believed to bind to the same region on HSA located within domain IIA, between positions 182 - 283 in the protein (Kragh-Hansen, 1990), referred to as Site I by (*Sudlow et al., 1976*), with an association constant of the order 10^4 - 10^5 M^{-1}. Once Sudlow's site I is fully occupied, HSA may bind the dyes at one of up to five other weaker sites that have with $K \sim 10^{-3} M^{-1}$; subdomain IIA is one of the primary binding site on HSA, located near the surface of the molecule and is susceptible to environmental changes. Changes in pH causes changes in the protein conformation, which in turn potentially offsets the affinity of the weaker binding sites (*Peter, 1996*). It must be noted that subdomain IIIA is the strongest high affinity binding site of albumin, subdomain IIA has been found to be marginally weaker. There are four main forces that are responsible for the fixation of the dye, these are:

i. Ionic forces- Occurring between the positive charges of the protein and the negative charge of the dye and visa versa in an aqueous or dilute acidic environment, this results in the protonation of the amino group of the protein. The dye is usually delivered in the sodium salt form.

ii. Hydrogen Bonding- This is the involvement of 'lone pair' electrons from an electron donor atom.

iii. Van der Waal's Forces- These forces are small in comparison to hydrogen bonding and ionic forces, involving the interaction of the π orbital of the dye with its host. This force is particularly prevalent in linear dye molecules (i.e. long and flat), where the dye can approach very close to the host and when both the dye and the host contain alkyl or aryl groups.

iv. Covalent Bonds- Covalent bonds form as a result of chemical interaction between the dye with the host resulting in bond formation between the two. Covalent bonds are the strongest as they become an integral part of the product. This type of bonding is most commonly seen in reactive dyes.

6.2. Materials and Method

Both nHSA (batch number ABC-0292B14611), supplied by Bio Products Laboratory, Hertfordshire, and rHSA (batch number GA 92014) supplied by Dr John Woodrow, Delta Biotechnology, (Nottingham, UK), were purified by either dialysing in distilled water, using dialysis tubing (MW cut-off of 10,000, supplied courtesy of Delta Biotechnology, Nottingham) or by column chromatography. The dialysis tubing was pre-treated in a heated solution of 0.05% of EDTA (analar grade supplied from BDH) and 2% of sodium bicarbonate (analar grade supplied from BDH) made up in distilled water. This was done to clean and degrease the tubing prier to use. The treated tubing was then washed several times in distilled water to wash away any traces of impurities. Dialysis proved effective for

removing small contaminates such as salts but was ineffective for removing fatty acids, a component added to the preparation of both types of HSA (4%) as a stabiliser. The removal of fatty acids was achieved using Sephadex G 25m (PD-10) columns (Code Number-17-0851-01, Lot Number SA 15390, supplied from Pharmacia). All purified HSA solutions were freeze-dried and the purified product stored in the freezer. For consistency the same batch of HSA was used for experiments in the same series.

Phenol red (PR) (Lot Number 00775-024) was supplied by Aldrich, UK and was made up to a concentration of 7.05 x $10^{-5}M^{-1}$. Bromophenol blue (BPB) (Lot Number 14273G), concentration 1.49 x $10^{-5}M^{-1}$ and bromocresol green (BCG) (4.30 x $10^{-5}M^{-1}$) were obtained from BDH, UK. 8M equivalent stock solutions of the dye under investigation and 8M equivalent stock solution of the protein were made in either 10mM buffer solution adjusted to the required pH, or in distilled water. Two buffers were used, Britton Robinson (2.47g/L boric acid, 1.52ml/L acetic acid and 2.544ml/L o-phosphoric acid (Analar grade) supplied fby BDH) and phosphate buffer (Analar grade) also from BDH. Denaturation studies involved urea and GuHCl both supplied by BDH, UK. All other products used were of the highest analytical grade (Analar) to ensure the highest spectroscopic purity and transparency. Where necessary, the dye:protein solutions were spun in a microcentrifuge (Watman Microcentrifuge Force 14, model reference MOO 17279) using Millipore microcentrifuge tube filters with an ultrafiltration media (from Whatman, UK) having a nominal molecular weight limit of 10,000.

6.3. Experimental Procedure

Using the stock solutions, a series of sequential dilutions were made, each containing 1M equivalent of dye solution (fixed concentration) with varying concentrations of protein ranging from 3M equivalent to 0.02M equivalent. A series of solutions were prepared of

the dye:protein complex with varying concentrations of protein (a stock solution of 8M equivalent was used) to a fixed concentration of dye (1M equivalent at final dilution), using two stock solutions. A total 1ml volume of each complex solution was made. A reference HSA baseline was also measured containing the equivalent concentration of protein as the complex solution but without dye, this was subtracted from the complex solution spectrum to obtain the effects of the dye only when bound to the protein. Any interference due to the protein was thus eliminated and only the induced spectra of the dye measured.

When conducting denaturation studies with either GuHCl or urea, a 10M stock solution of each were made. Stock solutions of both 2M equivalent dye and 8M equivalent HSA were also prepared. Using the HSA and denaturant stock solutions a 2M equivalent solution of the protein in varying concentrations of the denaturant was prepared and stored overnight in the refrigerator so as to enable the denaturant to work and attain equilibrium (i.e. 2M equivalent of HSA in 1M equivalent denaturant, 2M equivalent HSA in 2M equivalent of denaturant etc. to produce the series was made). The following day, the protein : denaturant solutions were divided equally one to prepare the dye:HSA:denaturant complex, and the other to prepare the baseline (HSA:denaturant in water). Since the dye was not chiral, any surplus dye would be transparent when measured by CD, and therefore did not have to be considered in the data analysis.

6.4. UV Absorption Spectroscopy

The absorption spectrum of all the samples were measured on a AVIV 17DS spectrophotometer with a spectral band width of 0.2nm and a scan speed of 0.2nm/sec in a 1cm cell. Samples that had been spun in a microcentrifuge through microcentrifuge tube filters had low volumes (100 - 300μl); measurements were made with a 1cm pathlength rectangular micro-cuvette designed by Dr A.F. Drake (King College London) and

manufactured by Helma, UK. The total capacity of the cuvette was 300µl, the walls of the cell were black glass allowing a maximum light throughput through only the window of the cell. The cell holder of the spectrometer was modified such that the beam was concentrated only through the optical window of the cuvette.

6.5. Circular Dichroism Spectroscopy

Two instruments were used to measure the CD, either a JASCO J600 spectropolarimeter or the JASCO J720 spectropolarimeter using a 1nm spectral bandwidth, a scan speed of 10nm/min and a time constant of 4sec. Both instruments were calibrated against NH_4-d-Camphor-10-Sulphonate standard (supplied by Jasco, UK). All samples were measured in a 1cm cell between the wavelengths of 240 - 750nm and at room temperature, unless temperature studies were being conducted where a thermostatting water-bath was used to maintain the desired temperature. Quenched studies were conducted at room temperature after the sample had been heated to the desired temperature.

Results of Phenol Red : Human Serum Albumin Interaction Studies

6.6.i. Ultra-Violet / Visible Studies of Phenol Red

Phenol red (PR) or Sulfonphthalein ($C_{19}H_{14}O_5S$), MW 354.38, has two distinct pK_a related colour changes, one under acidic conditions and the other in more neutral/basic conditions. A sample of 7.05 x 10^{-5}M PR in distilled water was investigated, the pH equation is represented in Figure 6.1.a. and the UV spectral changes are shown in Figure 6.1.b. Changing pH shifted the observed absorption wavelength maxima and the peak intensities. Plotting absorption against pH at fixed wavelengths of 557nm and 451nm highlighted a sigmoidal relationship depicted in Figure 6.1.c., with an inflection point located at pH 7.6. Literature states the pKa for PR to be 7.9, experimental data gave a calculated pK_a at λ 431nm to be 7.7 and at λ 557nm as 8.0 showing close agreement with the published data.

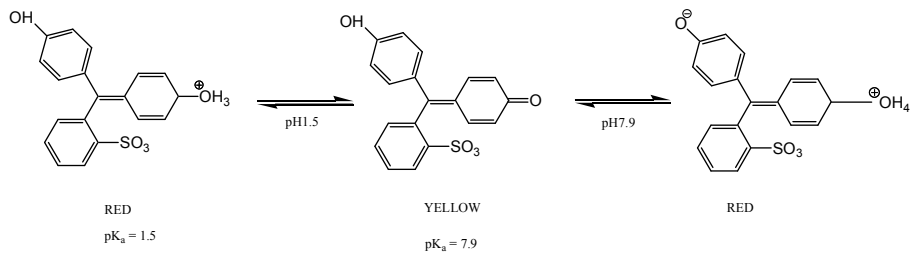

Figure 6.1.a. Schematic representation of the dissociation of PR.

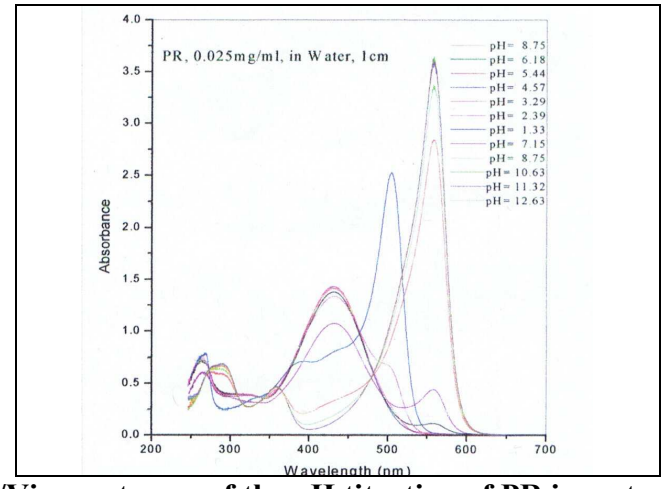

Figure 6.1b. UV/Vis spectrums of the pH titration of PR in water, 1cm cell.

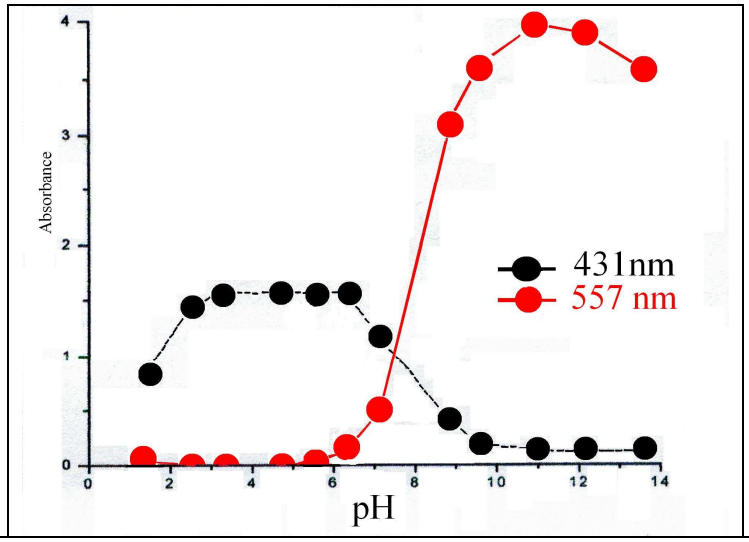

Figure 6.1.c. Fixed wavelength plot of PR pH titration in water, 1cm cell.

6.6.ii. Binding Studies of PR:HSA Interaction

The characterisation of PR:HSA binding studies was carried out at pH7.2, a fixed concentration of 7.05 x 10^{-3}M of dye solution was titrated with varying concentrations of HSA to determine the binding capacity of the dye to the protein. The absorption spectra of PR exhibits a single maximum at 450nm when dissolved in water at physiological conditions. However, when bound to albumin an additional peak was observed at 550nm that decreased in magnitude with increasing albumin concentration (Figure 6.2.a. &6.2.b.). The resulting CD spectra of the complex revealed three maxima, the largest, a positive maxima at 450nm matches the main absorbance band of the dye, followed by two features approximately equal in intensity but opposite in sign with maxima at 380nm and 330nm respectively, shown in Figure 6.2.c. & 6.2.d.. Two isosbestic points at 350nm and 400nm were observed indicative of two states in equilibrium. The binding of PR to rHSA revealed a [1:1] relationship indicative of only one ligand binding to a single protein molecule in agreement with previous findings that stated subdomain IIA as the active site.

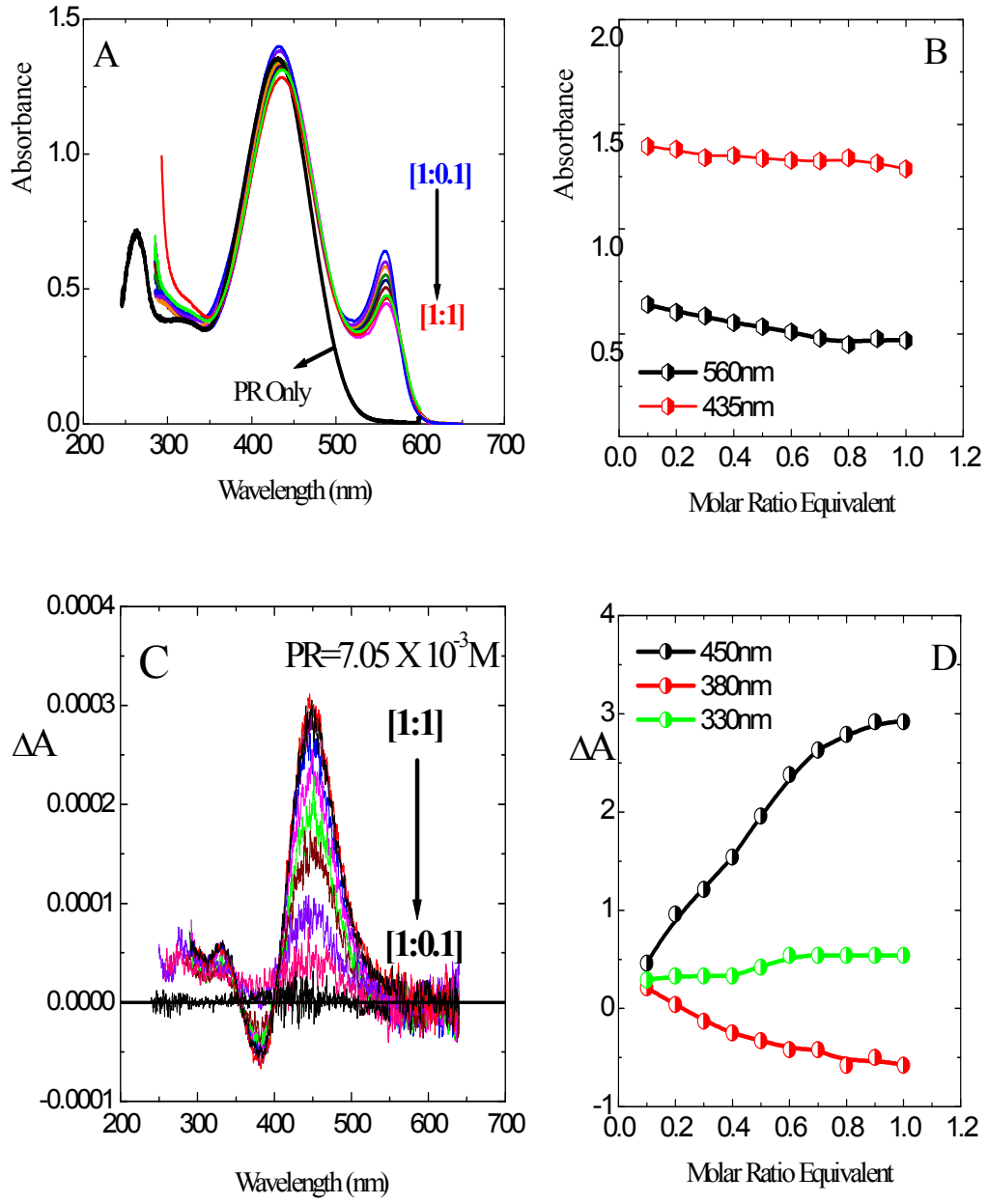

Figure 6.2. The CD of PR:rHSA titration at pH 7.19, 1cm cell.

A Absorption spectra of the titration of PR to rHSA in 10mM P/B, pH7.2,1 cm cell
B Absorption spectra of the titration of PR to rHSA in 10mM P/B, pH7.2,1 cm cell
C CD spectra of the titration of PR to rHSA in 10mM P/B, pH7.2, 1cm cell
D Fixed wavelength plot of the titration of PR:rHSA

6.6.iii. pH Studies of Phenol Red to Albumin

To elucidate the binding characteristics of subdomain IIA, the [1:1] complex of PR:rHSA was investigated against changing pH. Previous studies on the protein alone highlighted three main structural transition associated with changing pH (refer to Chapter 1 on Structure and Properties of HSA), the N-form at pH7.2, the F-form at pH4.3 and the E-form at <pH3 were highlighted as the areas of interest (*Peters et al, 1996*). The objective was to ascertain whether the observed changes seen in HSA only with changing pH were due to specific regional changes in the protein denaturing (reversibly), thus knocking out the specific binding site for that ligand or whether the observed changes in HSA were more global and non-specific. The UV of the pH titration in essence remained unchanged, similar in appearance to the pH titration of the dye in the absence of protein (Figure 6.1.b.). However, the CD reflects many changes especially at low pH values, at pH3.55 there was an inversion of the CD spectra found at pH7.14 and is shown in Figure 6.3. with the creation of a further isosbestic point at shorter wavelength totalling three in all. At high pH values the CD of the complex collapsed. The pH titration highlighted several areas of interest, that at pH7.9, pH4.44 and pH3.55 indicative of the areas of known structural changes within the protein. Therefore, the molar titrations, binding studies and temperature studies were investigated at these designated pH values. The fixed wavelength plots of the pH titration revealed three different species existing when the three distinct regions of concerns were monitored, each wavelength studied showed different transitions. It was clear that each wavelength studied reflected the structural changes that occurred in the protein and its response to the bound ligand.

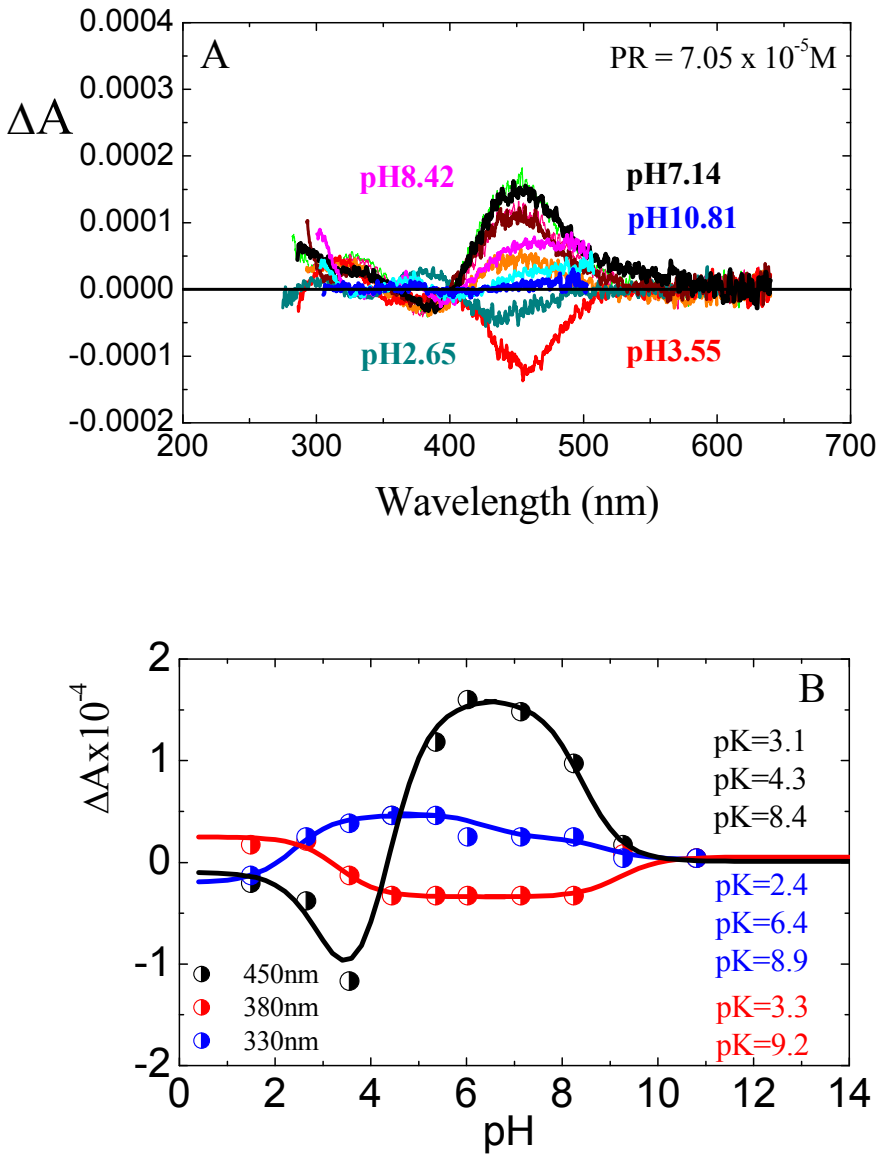

Figure 6.3. pH Titration of a [1:1] Molar Ratio of PR:rHSA

A CD spectra of the titration of a [1:1] molar ratio equivalent sample of PR:rHSA in water, 1cm
B Fixed wavelength plot of the titration of a [1:1] molar ratio equivalent of PR:rHSA

Associated with the main absorption maximum, three pH transitions were seen, one in the E-form, one in the F-form and the final one in the B-form (Figure 6.3.). In the E-form, the CD spectra of the 450nm maximum became inverted and of the same intensity, further reduction in pH produced CD spectra in the inverted position but very much reduced with the complete loss of CD detected by pH1.5. At 380nm, this CD maximum behaved more

akin to what was expected, revealing two transitions observed in the E-form and B-form, between those regions consistent changes were observed (Table 6.0.). At the final wavelength studied at 330nm, once again three transitions were observed two in different regions from that detected at the other wavelengths, the first lower than the E-form at very much reduced pH. The second transition was found surprisingly near the physiological conditions giving a pK_a=6.4, also not seen at the other wavelength. The final transition was observed in the recognised B-form bordering on the aged-form. The pH titration reflected the complexity of the binding processes between the dye and the protein.

rHSA				PR:rHSA			
λ (nm)	**pK_1**	**pK_2**	**pK_3**	**λ (nm)**	**pK_1**	**pK_2**	**pK_3**
255	4.0		11.5	330	2.4	6.4	8.9
287	3.5	6.1	11.7	380	3.3		9.2
				450	3.1	4.3	8.4

Table 6.0. Comparison of the pK values for rHSA &PR:rHSA complex

Lowering the pH to 4.40 and conducting a binding titration produced a CD profile similar to that found at pH7 but with the maximum at 450nm very much reduced, this reduction makes the other two maxima found at shorter wavelength appear much larger and more pronounced with a more apparent symmetry between them. At this pH increased binding was observed for a molar ratio equivalent of [3:1] for PR:rHSA, the structure perturbation of HSA was sufficient to induce increased binding of the dye (Figure 6.4.). At low molar ratio equivalents ([0.4:1] and below) little to no binding was observed in contrast to that found at pH7. The UV spectra of the binding at this pH revealed a decrease in absorption for ratios up to [1:1] molar equivalent. Thereafter, an increase was observed up to a ratio of [2:1] molar equivalent that stabilized (Figure 6.4.a. & b.). The UV fixed wavelength plot contradicted that found in the CD fixed wavelength plot, in that increasing CD was determined after the molar ratio equivalent of [2:1], with increase binding detected at [3:1] molar equivalent (Figure 6.4.c. & d.).

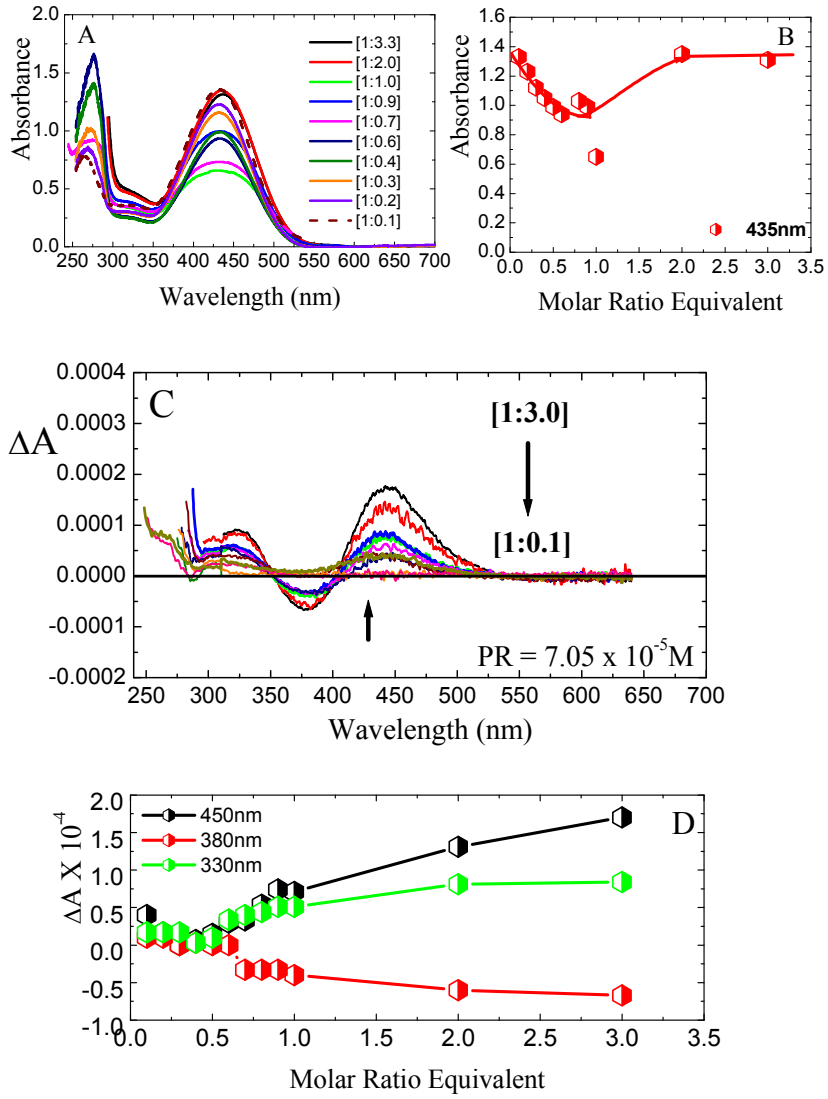

Figure 6.4. Molar titration of PR:rHSA at pH 4.40.

A Absorption spectra of the titration of PR:rHSA at pH4.40, 1cm cell
B Fixed wavelength plot of the absorption of PR:rHSA
C CD spectra of the titration of PR:rHSA in B/R buffer, pH4.4, 1cm cell
D Fixed wavelength plot of the titration of PR:rHSA in B/R buffer, pH4.40, 1cm cell

Lowering the pH further to pH3.56 produced changeable CD spectra that were dependent on the molar ratio equivalent of its components. The UV however, produced spectra that behaved as expected with increase absorption detected for increase D/P ratios, a plateau was observed for ratios greater than 1M equivalent of the protein. In contrast the CD produced for drug:protein ratios between [1:0.1] to [1:0.4] a single positive maximum at

420nm with a further positive peak observed at shorter wavelength, outside the measuring range of this experiment. The positive maximum previously located at 460nm had either been lost or had shifted to the newly determined maximum found at 420nm. At a ratio of [1:0.5], to ratio equivalents up to [1:0.9], the 460nm maximum became split forming a positive and negative doublet that appeared to be linked. As the D/P ratio increased, so to did the intensities of the doublet, changing from a relatively intense positive and weaker negative maxima to a relatively weak positive and stronger negative maxima (Figure 6.5.c.) until the [1:1] molar ratio equivalent was reached where only the negative maximum was found and the positive peak had disappeared. For the molar ratio equivalent of [1:2] the doublet peak returned but this time two negative peaks were determined of almost equal intensities. The binding of PR at pH3.56 proved to be concentration dependent more so than at any of the other pH values studied, with changing spectra that reflected the changes seen in concentration.

Plotting the CD against molar ratio at fixed wavelength for the titration at pH3.56 revealed variations within the binding site and in the protein as a whole, not consistent with that found at pH7. At this pH the protein is in the extended form, more of the protein is exposed to the solvent and therefore to environmental changes. From the profile of the CD binding spectra there appears to be mainly two types of profile present, one with a predominantly positive maxima at 420nm and a weak negative at 460nm, the other a predominant negative maxima at 460nm and another negative located at 380nm. It was possible that the dye's preferred binding site had become compromised or modified in such a way that an alternative location was used that may account for the changes in the CD profile, with the use of a non-specific site that may account for the changing CD profile as the titration progressed. The CD fixed wavelength plot highlighted the sigmoid relationship that exists.

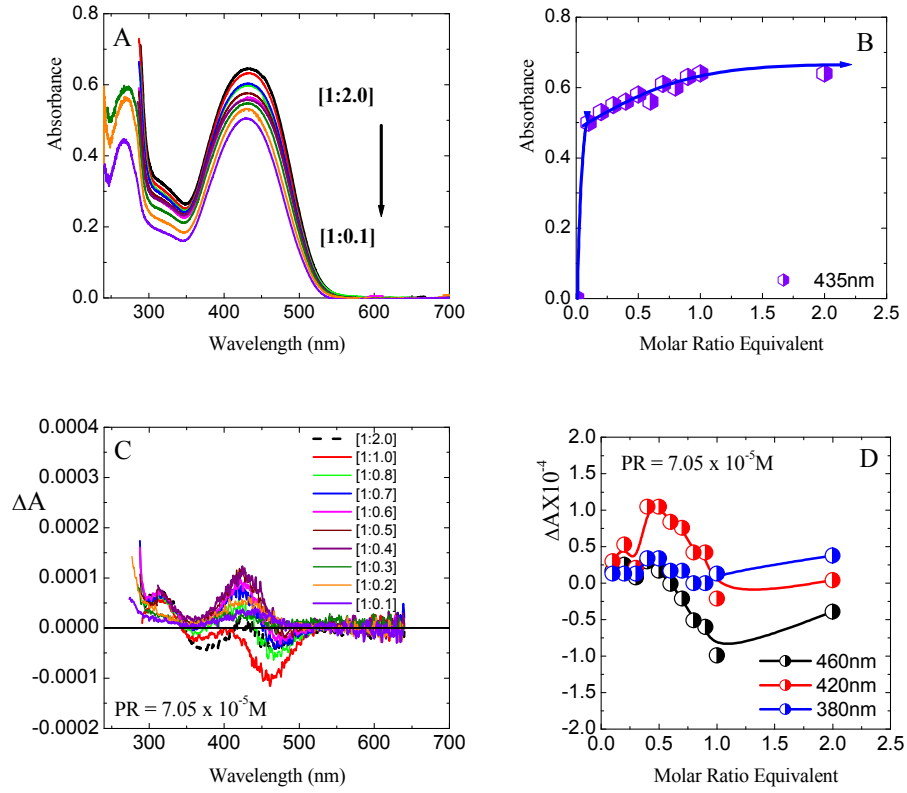

Figure 6.5. Molar titration of PR:rHSA at pH 3.56, 1cm.

A Absorption spectra for the titration of PR:rHSA in B/R buffer, pH3.56, 1cm
B Fixed wavelength plot of absorbance for of the titration of PR:rHSA IN B/R, pH3.56
C CD spectra of the titration of PR:rHSA in 10mM B/R buffer, pH3.56, 1cm cell
D Fixed wavelength plot of the CD measurements of PR:rHSA in 10mM B/B, pH3.56

The titration of PR to albumin at varying pH values revealed the changing CD profile that exists with the deterioration and changing signs of the maxima. The largest CD profile was determined at physiological conditions and revealed a [1:1] molar ratio equivalent. As the pH reduced so to did the magnitude of the spectra, with pH4.40 producing spectra that were approximately two thirds that found under physiological conditions with the profile in essence essentially the same. A further reduction in pH produced the spectra that revealed the most spectral changes and the greatest reduction in magnitude, reducing the spectra by approximately one third of that found at physiological conditions. Modification in the CD profile was also observed beyond that previously detected.

6.6.iv. Temperature Studies of Phenol Red:Human Serum Albumin

Temperature investigations were undertaken by heating and quenching studies. A [1:1] molar ratio equivalent of PR:rHSA was heated at various pH values predetermined by previous studies. pH7.2 was the first sample to be investigated and highlighted spectral changes in the CD that were associated with reduced binding with the onset of heating. Approximately two thirds of the binding of the dye was lost by the time the temperatures reaches 50°C, a characteristic previously observed with other ligands . Continued heating produced further decreases in the loss of binding resulting in total loss by 63°C (Figure 6.6.). Two transitions were observed for each wavelength studied with the first transition occurring easier than the second. At the main absorption band (450nm) $K_1=23x10^3$, and was the lowest determined at 42°C. At 330nm, t_{m1} determined was similar to that found at 450nm but the value of K had considerably increased. The results at 380nm found both high values for K and an especially high t_m for the first transition. The second transition at all three wavelengths studied gave consistently similar results.

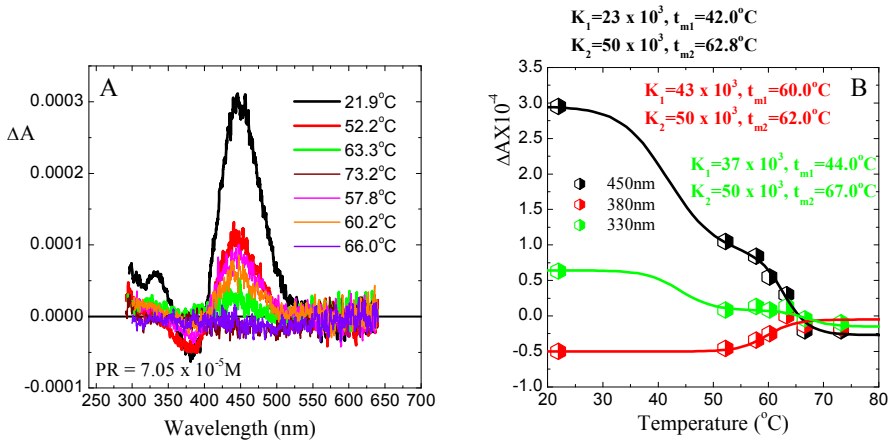

Figure 6.6. Temperature studies of a 1:1 molar ratio of PR:rHSA at pH 7.20.

A CD spectra of the temperature studies of a [1:1] molar ratio equivalent of PR:rHSA, P/B, pH7.2, 1cm
B Fixed wavelength plot of the temperature studies of a [1:1] molar ratio equivalent of PR:rHSA, 1cm

The quenched samples highlighted the stability of the protein for temperatures not exceeding 55°C as was expected, since HSA in isolation shows no denaturation when heated to temperatures up to 60°C. The onset of denaturation was evident by 60°C and by 67°C a dramatic decrease in binding of the dye was experienced with no binding evident by 73°C. As previously detected for site IIA binding, a rapid loss of binding was experienced between 58 - 67°C. The structural integrity of the protein had been compromised resulting in an inability of the dye to bind at 67° C, even though there was a considerable amount of structure in albumin retained at that temperature (Figure 6.7.). Only one transition was seen for each of the wavelengths monitored.

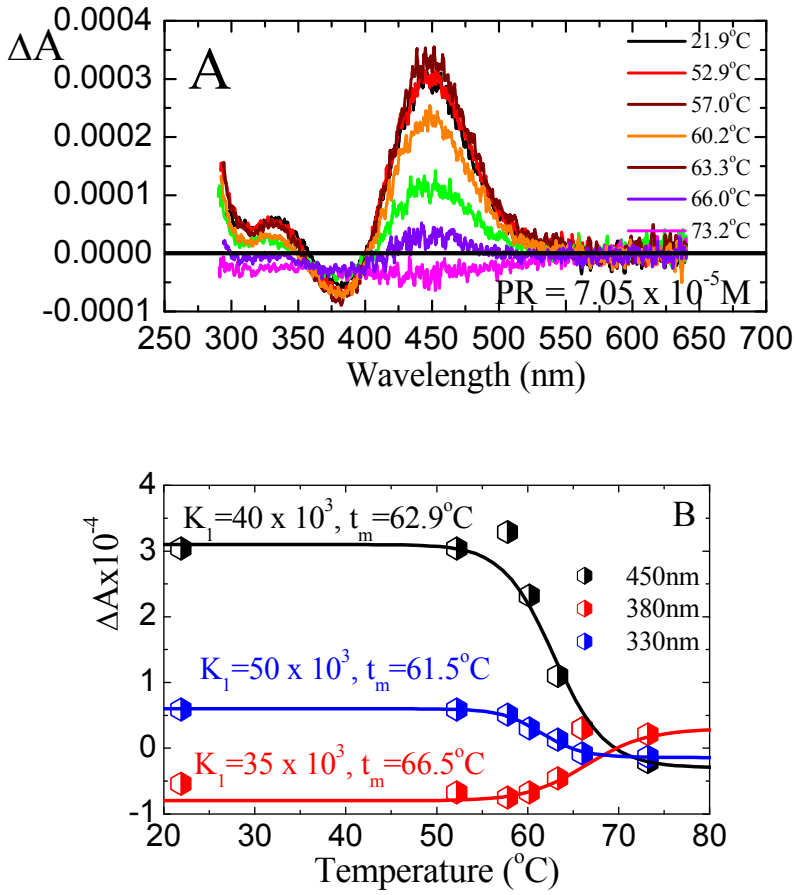

Figure 6.7. Quenched studies on a [1:1] molar ratio of PR:rHSA at pH 7.20.

A CD spectra of the quenched samples of a [1:1] molar ratio equivalent of PR:rHSA, 1cm cell

B Fixed wavelength plot of the quenched samples of a [1:1] molar ratio equivalent of PR:rHSA

Temperature studies were now conducted on a [1:1] molar ratio equivalent sample of PR:rHSA at pH4.40. Increasing the temperature of the complex from room temp to 48.2°C produced a decrease in the positive maxima at 450nm that initially stabilised between 48 - 66.3°C. At this pH, modifications in the protein were such that the binding pocket was conserved or protected from its environment to some degree, allowing a residual amount of binding to occur at higher temperatures than would normally be expected. Higher temperatures result in the collapse of the binding pocket as demonstrated in Figure 6.8. Binding was still evident at 75°C with the CD at all maxima reversed. Wavelength 330nm revealed the first transition to be relatively easy, $K=13x10^3$ at a t_m=44.5°C, the second transition was considerably higher with $K = 50x10^3$ and a t_m=71.0°C.

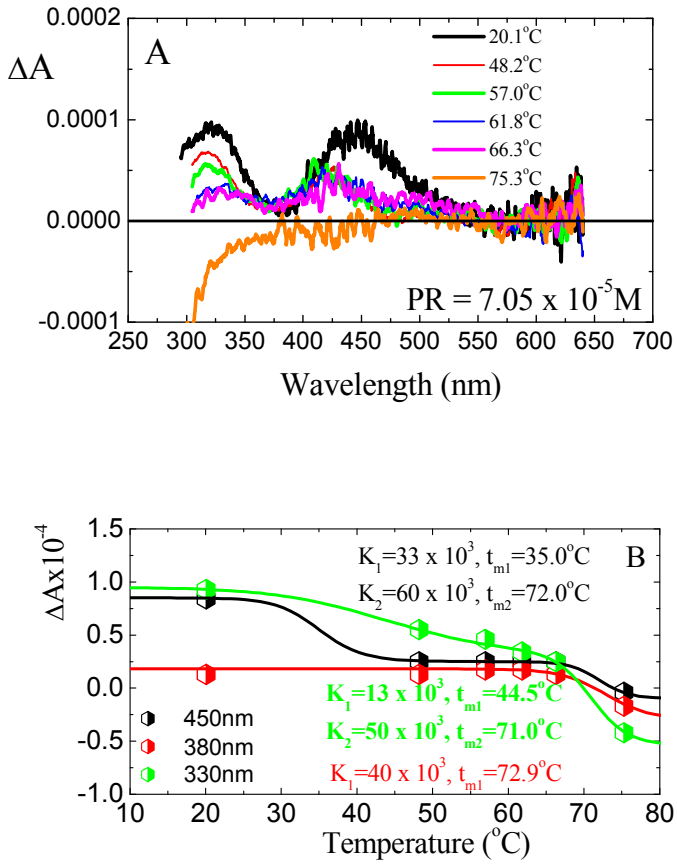

Figure 6.8. Temperature studies of a [1:1] molar ratio of PR:rHSA at pH4.40.

A Temperature studies of a [1:1] molar ratio equivalent of PR:rHSA, 10mM B/R, pH4.56, 1cm
B Fixed wavelength plot of the temperature studies of [1:1] molar ratio equivalent of PR:rHSA in 10mM B/R, pH4.56

The quenching studies revealed no loss in structural integrity of the binding site for temperatures below 50°C. Heating the samples above 50°C produced a steady decrease in the binding of the dye with an inversion of the CD maxima observed for all the peaks, almost equal but opposite for temperatures up to 75.3°C with a similarity in the CD profile to that observed at pH3.56. Heating had allowed the protein to adopt a structure similar to that induced by adjusting the pH to 3.56. Binding was still evident even after heating rHSA to 75.3°C (Figure 6.9.), but the binding observed was not the same as that found at room temperature for that pH. The results reflected that either the same binding pocket had been modified to accommodate the changing conditions or that another site had been used, bearing in mind that subdomain IIA has three chambers that the dye can be located in.

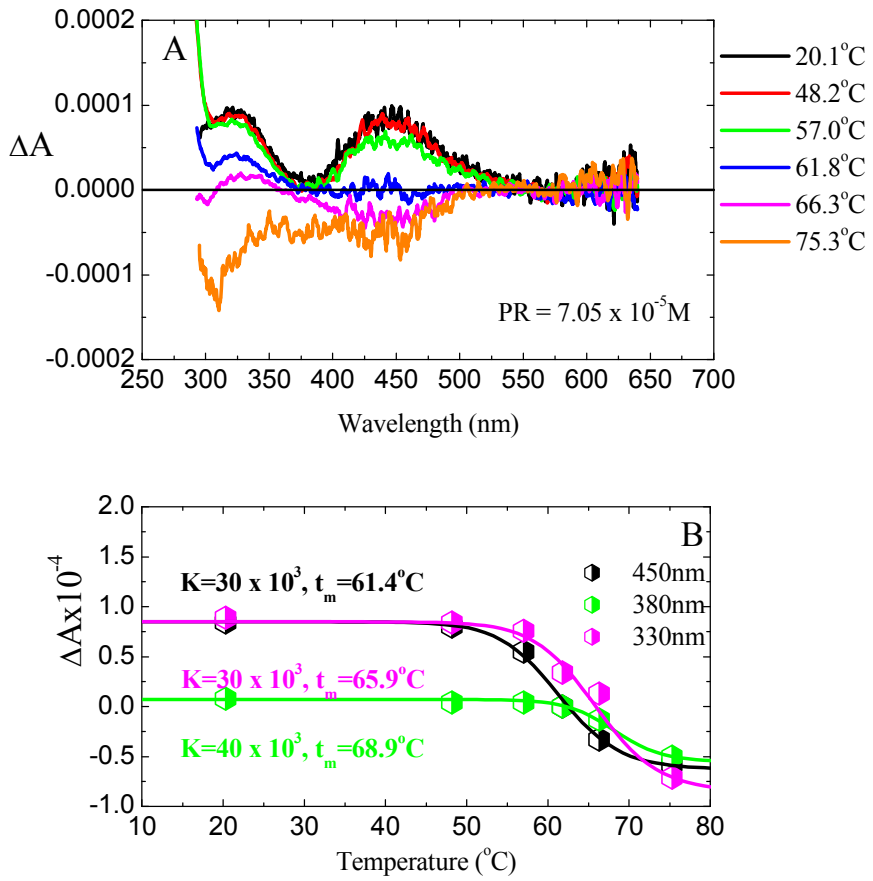

Figure 6.9. Quenching studies of a [1:1] molar ratio of PR:rHSA at pH4.40.

A Quenching studies of a [1:1] molar ratio equivalent of PR:Rhsa, 10mM B/R, pH4.35, 1cm
B Fixed wavelength plot of the quenched temperature studies of a [1:1] molar ratio equivalent of PR:rHSA in 10mM B/R, pH4.56

Once the pH of the [1:1] molar ratio equivalent complex of PR:rHSA was lowered to 3.56, as may be expected the complex offers no resistance to heating as demonstrated in Figure 6.10a & b. The CD spectra collapses in the region of 450nm as soon as heating was initiated revealing the exposure of the binding pocket under these conditions. The CD was measured for samples heated up to 88.4°C, and even though the profile of the spectra had changed, reverting back to that found at high temperatures at pH7.2, increased binding was observed suggesting modification of the site (Figure 6.10.) or the possibilities of a lower affinity binding site being used. Heating HSA to such high temperatures at pH3.56 revealed that PR was still able to induce binding even though the protein had become denatured. It should be noted that the heated samples of HSA in isolation never produced the complete collapse of the protein, there was always a residual amount of structure that was retained estimated to be greater than 35% structured. The possibility existed that one of the lower affinity sites existed within that region and was utilised by PR. What was evident was that the appearance of the CD profiled had significantly altered such that the main maximum at 450nm collapsed, however, binding was still evident at 330nm and at 380nm.

The quenched samples of albumin offered a bit more insight into the binding ability of albumin showing the resilience of the association of PR to albumin. The binding remained steadfast for temperatures up to 60°C. For temperatures greater than 60°C the complex deteriorated and altered but PR retained bound to the altered state for temperatures up to 80°C (Figures 6.10.c. & d.). Once again the CD profiles at high temperatures were different to that seen at pH7, however, pH4.56 and pH3.56 both showed the reverse CD spectra at 450nm as the samples were heated to higher temperatures. Both the heated and quenched samples at pH3.56 revealed two transitions at all the wavelengths monitored, this was in contrast to the other pH values that all revealed only one transition for the quenched

samples. Also evident was the existence of a new transition that occurred at longer wavelength with the resemblance of a maximum starting at 650nm, this was also observed at pH4.56. Table 6.1. compares all the transitions that occurred for the complex at the three pH values studied and reveals the complexity of the melting process.

Studying the transitions for the samples at pH3.56 highlighted the instability of the protein and revealed the ease of the first transition. With the exception of the first transition at 330nm the other two occurred at very low t_m temperatures in the heating cycle, the transition at the main absorption maximum occurs at a temperature little higher than RT.

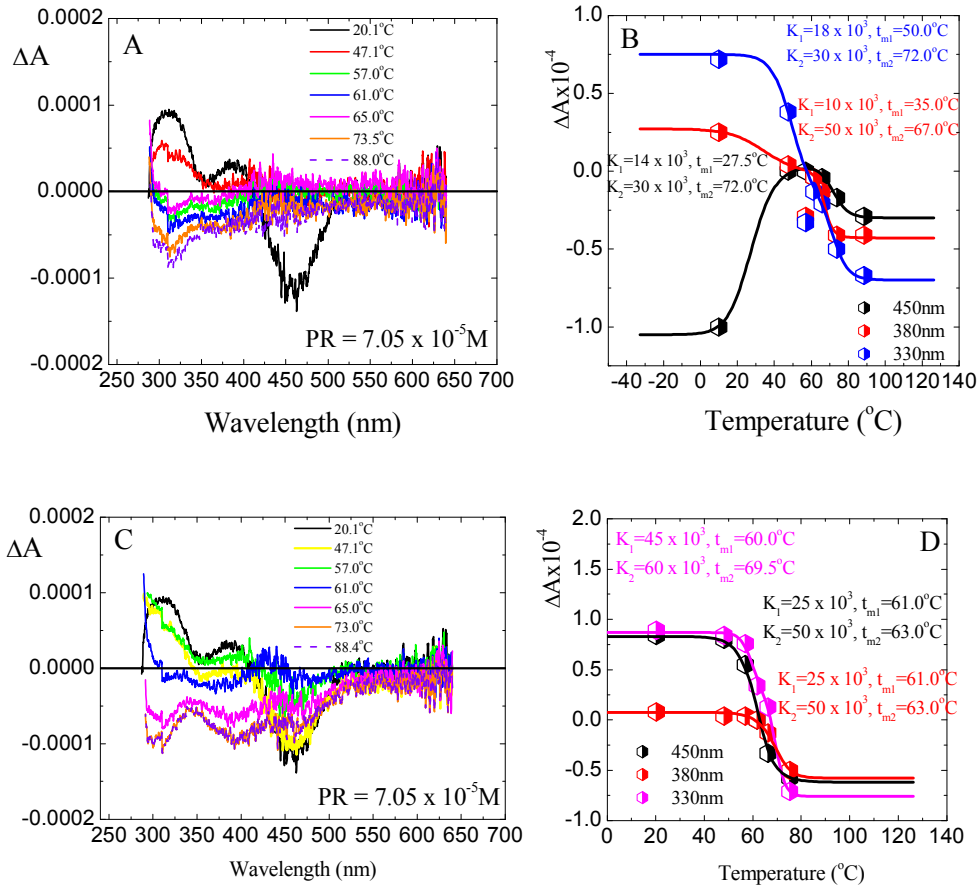

Figure 6.10. Temperature studies and quenched samples of a [1:1] molar ratio equivalent of PR:rHSA at pH3.56, 1cm cell.

A Temperature studies of a [1:1] molar ratio equivalent of PR:rHSA in 10mM B/R, pH3.56, 1cm
B Fixed wavelength plot of the temperature studies of [1:1] molar ratio equivalent of PR:rHSA, 10mM B/R, pH3.56
C Temperature studies of the quenched samples of PR:rHSA, [1:1], in 10mM B/R, pH3.56, 1cm cell
D Fixed wavelength plot of the quenched samples of [1:1], of PR:rHSA in 10mM B/R, pH3.56

		PR:rHSA pH7.20 Heating		**PR:rHSA pH7.20 Quenching**		**PR:rHSA pH4.40 Heating**		**PR:rHSA pH4.40 Quenching**		**PR:rHSA pH3.56 Heating**		**PR:rHSA pH3.56 Quenching**	
λ (nm)	**Transition**	**t_m (°C)**	**K**	**t_m (°C)**	**K**	**t_m (°C)**	**K**	**t_m (°C)**	**K**	**t_m (°C)**	**K**	**t_m (°C)**	**K**
450	1st	42.0	23 X 10^3	**62.9**	**40 X 10^3**	35.0	50 X 10^3	**61.4**	**30 X 10^3**	27.5	14 X 10^3	**61.0**	**25 X 10^3**
	2nd	62.8	50 X 10^3			72.0	50 X 10^3			72.0	30 X 10^3	**63.0**	**50 X 10^3**
380	1st	60.0	43 X 10^3	**61.5**	**50 X 10^3**	72.9	40 X 10^3	**65.9**	**30 X 10^3**	35.0	10 X 10^3	**60.0**	**45 X 10^3**
	2nd	62.0	50 X 10^3							67.0	50 X 10^3	**69.5**	**60 X 10^3**
330	1st	44.0	37 X 10^3	**66.5**	**35 X 10^3**	44.5	13 X 10^3	**68.9**	**40 X 10^3**	50.0	10 X 10^3	**61.0**	**25 X 10^3**
	2nd	67.0	50 X 10^3			71.0	50 X 10^3			72.0	30 X 10^3	**63.0**	**50 X 10^3**

Table 6.1. Results of the transitions of the heating and quenching curves of the complex of PR:rHSA at different pH values.

6.6.v. Denaturation Studies of Phenol Red:Human Serum Albumin

Both urea and guanadiniun chloride were used as denaturants in protein assays, unfolding the protein by varying degrees depending on the amount of denaturant added. Considering urea binding to a [1:1] molar ratio equivalent of the complex of PR:rHSA, small additions in the region of up to 0.2M of urea produces an immediate decreased in the observed CD spectra with approximately a half reduction in magnitude in the presence of 0.4M of urea. Spectral shifts in the CD maxima were observed especially for the maximum at 380nm where an inversion of the peak was witnessed, this was also seen for the peak at 330nm. The main absorption at 450nm was now represented by a couplet comprising of a positive and negative peak (except for the first addition of urea that produced the single positive maximum at 450nm). Between 1M - 3M of urea the CD produced by the complex showed a region of stability. The greatest loss in binding was detected between 3 – 3.5M with greater than 90% of binding lost. One significant feature detected at longer wavelengths greater than 600nm was the appearance of a new maximum that increased in magnitude with increasing urea concentration shown in Figure 6.11. Although the main absorption at 450nm was lost, the absorption at longer wavelength continued to grow. The definition in the spectra of the other two maxima (380nm & 330nm) were also lost at high concentrations of urea. For 5M urea a positive CD was observed at 330nm with no characterising features. The fixed wavelength plot revealed a two transition step process that did not reflect the transitions seen in albumin alone that exhibited only one in the presence of urea.

Beyond this point no further measurements in CD was conducted as it was impossible to determine a region of zero CD in which to normalize the data on. What was evident was that binding still existed at high concentrations of urea even if it was not necessary at the same site. Previous studies have shown there to be a single transition in the denaturation of

albumin with urea, it was unclear which regions were affected and at which point in the titration that they occurred. What was certain was that PR still remained bound to albumin even if the characteristic features of the spectra were unrecognisable.

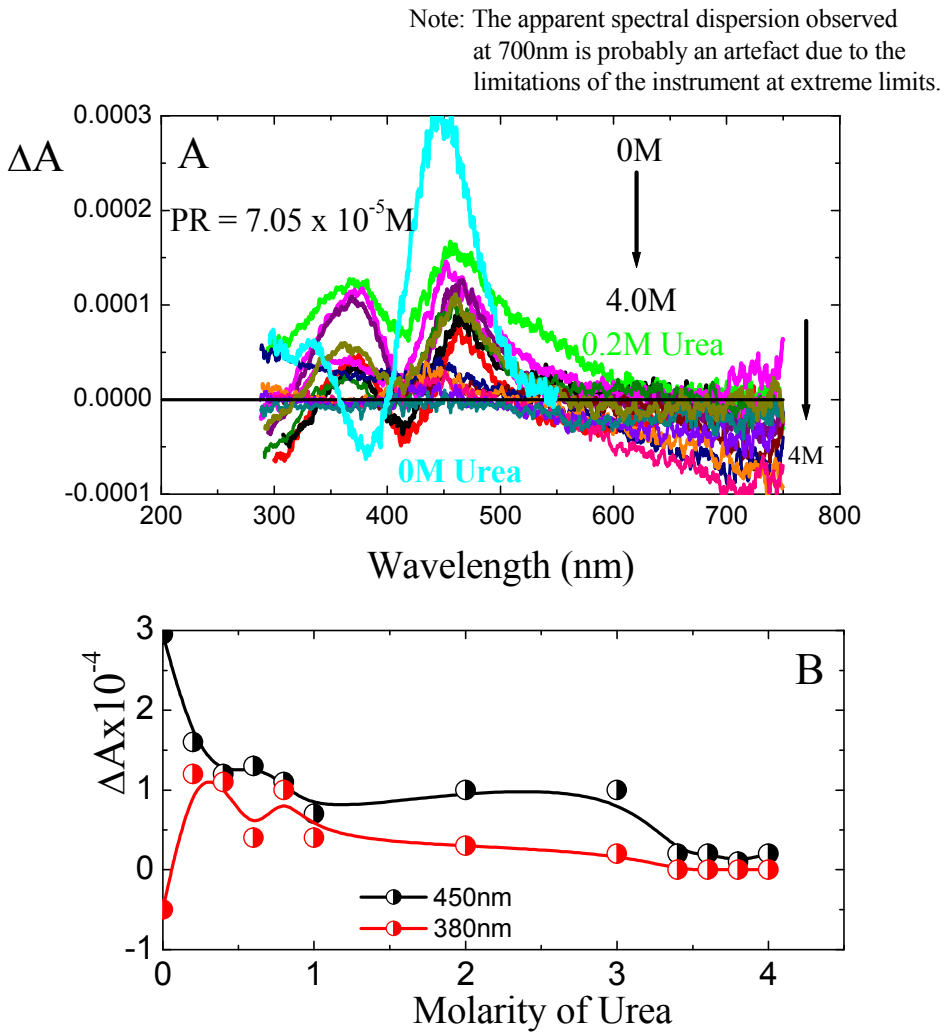

Figure 6.11. Urea titration of PR:rHSA in water, 1cm cell.

A Titration of a [1:1] molar ratio equivalent of PR:rHSA with increasing urea, 1cm
B Fixed wavelength plot of the titration of PR:rHSA in increasing concentrations of urea

The addition of GuHCl as the denaturant agent to the PR:rHSA complex affected the folding of HSA with relatively small additions, causing adverse effects as shown in Figure 6.12. The integrity of the CD profile remained intact with conservation of all the maxima unlike that seen by urea that resulted in spectral shifts. 1M of GuHCl produced effectively

an 80% reduction in the binding of the dye with the loss shown by the maximum at 450nm, and by 2M GuHCl all the binding at this maximum was lost. The other wavelengths also reflected similar trends with the collapse of their peaks. However, also seen with increasing concentration of denaturant was an additional maximum at longer wavelength, greater than 700nm (Figure 6.12.). Similar to the urea denaturation studies, the presence of GuHCl induces changes in the protein that could allow weaker affinity sites to become active. At wavelengths greater than 700nm increased binding was observed, this occurred to the detriment of the other absorptions.

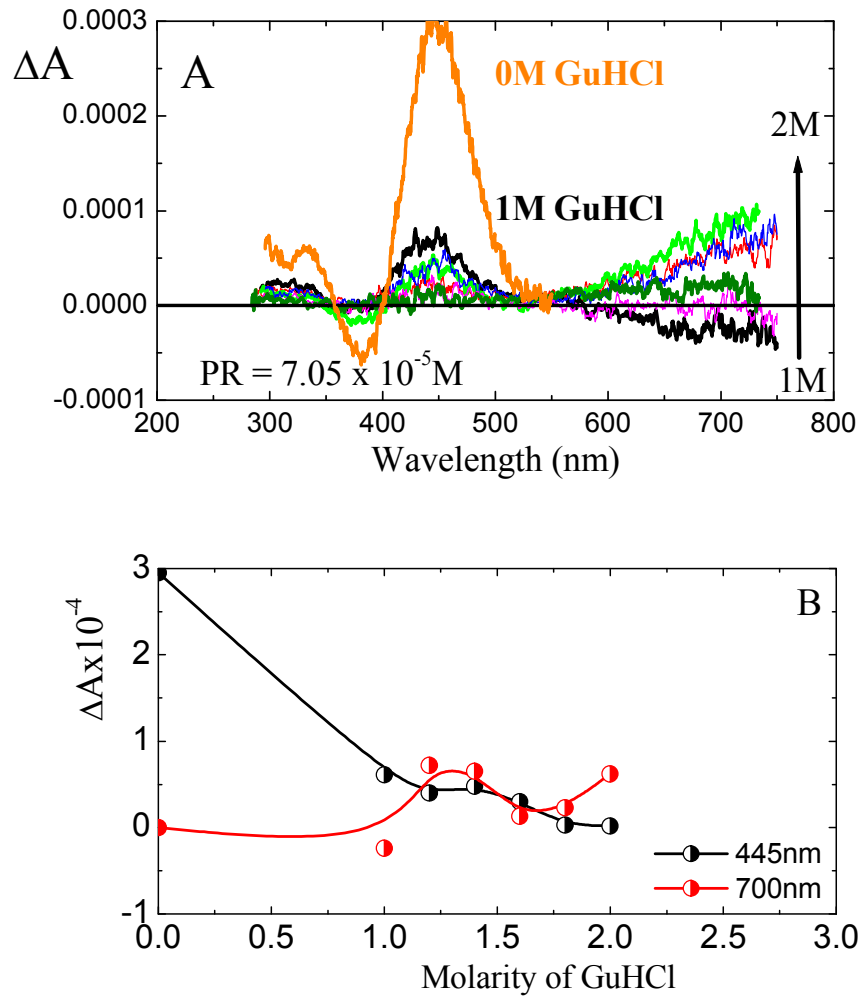

Figure 6.12. GuHCl titration of PR:rHSA, [1:1], in water, 1cm.

A Titration of a [1:1] molar ratio equivalent sample of PR:rHSA with GuHCl,
B Fixed wavelength plot of PR:rHSA with increasing concentrations of GuHCl

6.6.vi. Microcentrefuged Samples

Considering the PR:rHSA titration in P/B at pH7.20, for low molar ratios equivalent of the complex the largest quantity of free dye was detected (Figure 6.13.). At low concentrations of protein, the availability of dye will be high since there will only be a small quantity of protein to interact with the dye. Therefore, at that concentration it would be expected to have a high detection level of dye. As the concentration of the protein increases so will the rate of formation of the complex, therefore there will be less dye detected in the mixture that will be proportional to the rate of formation of the complex and limited by the dye concentration since it is that quantity that has been fixed, a fact found in the results shown in Figure 6.13. The detection of free dye was not a smooth transition but peaks were determined at [1:0.2] & [1:0.6] molar ratio equivalent of the complex, a fact mimicked at both wavelengths studied.

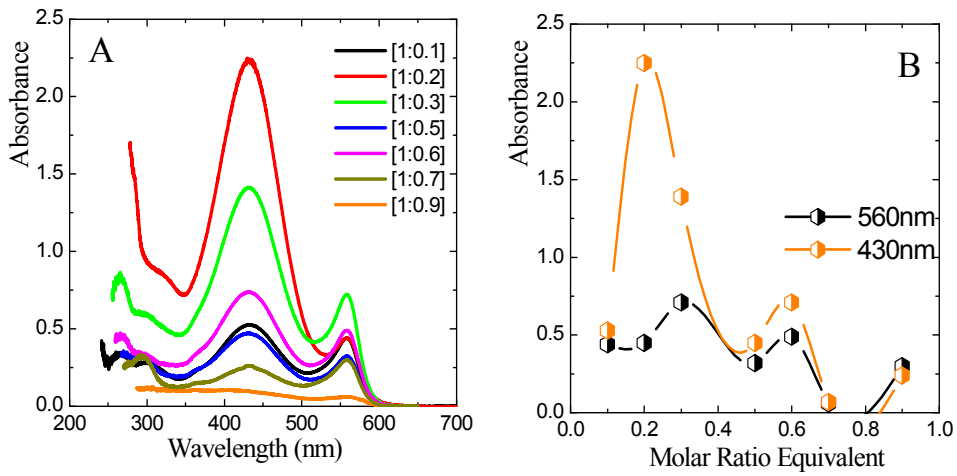

Figure 6.13 Microcentrifuged samples of PR:rHSA titration at pH7.19, 1cm.

A Absorbance spectra of the microcentrifuged samples of PR:rHSA titration, P/B, pH7.2, 1cm
B Fixed wavelength plot of the microcentrifuged samples of PR:rHSA in 10mM P/B, pH7.2, 1cm

Next studied was the microcentrifuged samples of the pre-heated complex of PR:rHSA (Figure 6.14.) that produced more characteristic results, supporting the results found for the

albumin samples in isolation. Samples heated to temperatures up to 55°C produced small UV absorption spectra, confirming that most of the dye was bound to the protein at these temperatures. Raising the temperatures resulted in more of the free dye being detected as more of the protein becomes denatured displacing the dye; thus larger absorption maxima observed for the free dye was detected until a point where all the dye had been displaced from the protein. Displacement was rapid, occurring within a specific and well defined temperature region with a t_m=55.6°C and K=70 x 10^3. From these results that look at the binding from the prospective of the dye only, it can be seen that only in the first thermal transition in the protein (t_m=57.0°C with K=18 x 10^3) is the dye dissociation detected. Since PR only binds to site IIA on albumin, it is reasonable to infer that it is site IIA that is first affected by heating in the protein, the other two thermal transitions were not detected in terms of this dye binding. The CD data of the quenched samples reflected different results with t_m=62.9°C and K=40 x 10^3 for the main absorption, there will be re-association of the dye that will influence the CD detected and this may explain the higher values obtained.

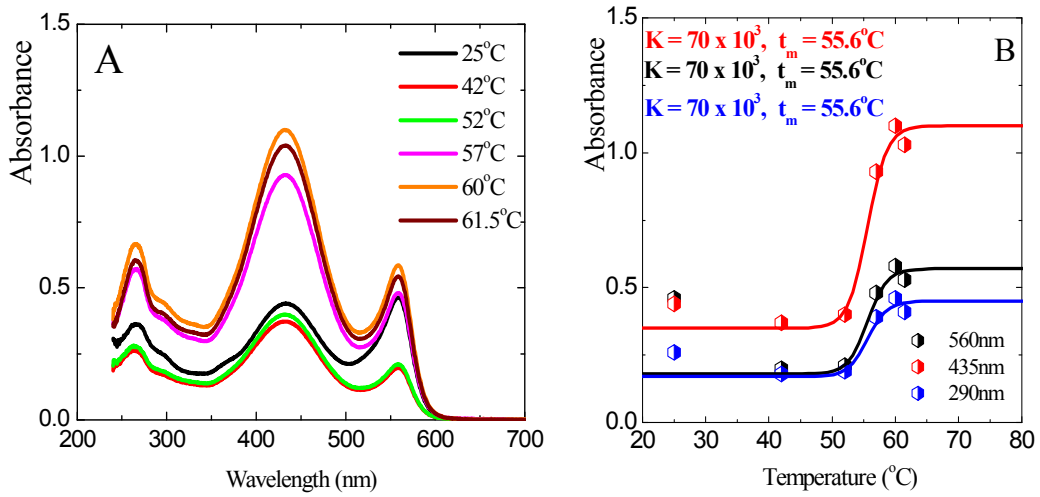

Figure 6.14. Microcentrifuged samples of pre-heated PR:rHSA, pH7.19, 1cm.

A Absorbance spectra of the microcentrifuged samples of quenched rHSA samples and PR in P/B, 1cm
B Fixed wavelength plot of the quenched samples of rHSA bound to PR

The microcentrifuged samples containing urea was investigated (Figure 6.15.). For low molar ratios of urea the UV of the free dye was shown to be small, showing that most of the dye was bound. A steady loss in binding was detected between 1M - 3M of urea, with the greatest loss in binding detected between 3.0M – 3.5M where approximately 80% of binding was lost. For ratios higher than that the residual dye remaining was lost resulting in the total loss of binding supporting the results measured by CD.

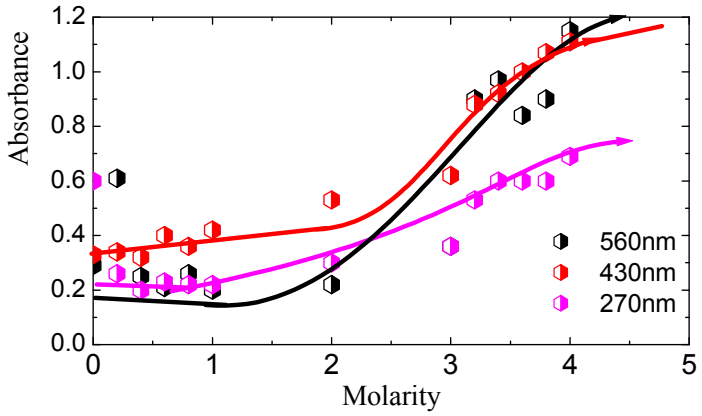

Figure 6.15. Absorbance spectra of the microcentrifuged samples of PR:rHSA in urea, water, 1cm

Conversely, for samples containing GuHCl the absorption measured remained relatively constant (Figure 6.16.) even though the main absorption of the complex detected by CD collapsed. It was evident that small additions of GuHCl caused substantial displacement of the dye, the CD was sensitive enough to detect the residual binding.

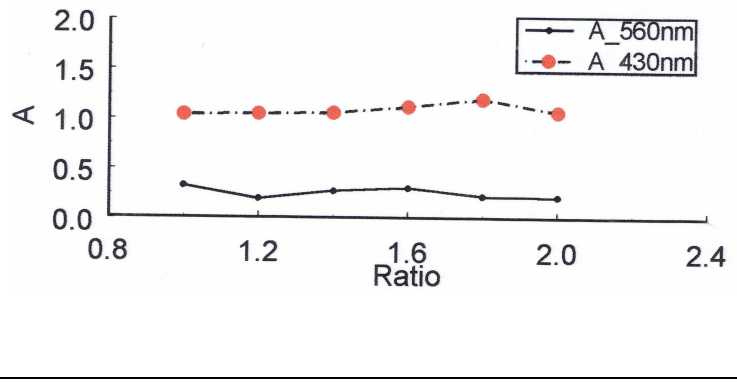

Figure 6.16. Microcentrifuged samples of PR:rHSA in GuHCl , 1cm

6.7. Bromophenol Blue : Human Serum Albumin Interaction

The second in the series of dyes to be considered with increased complexity was Bromophenol Blue (BPB) chemically known as 3'3"5'5"Tetrabromophenolsufonphthalein ($C_{19}H_{10}BR_4O_5S$), MW 669.99, and has a pH working range of between pH3.8 to pH5.4, (Figure 6.17.). BPB's pH titration curve is represented in Figure 6.18. with the titration producing four isosbestic points indicating several species in existence at the same time. The isosbestic points produced by BPB were well defined in contrast to PR whose points were not as distinct.

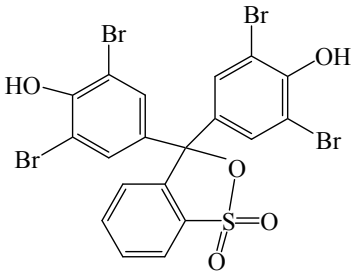

Figure 6.17. Structure of BPB.

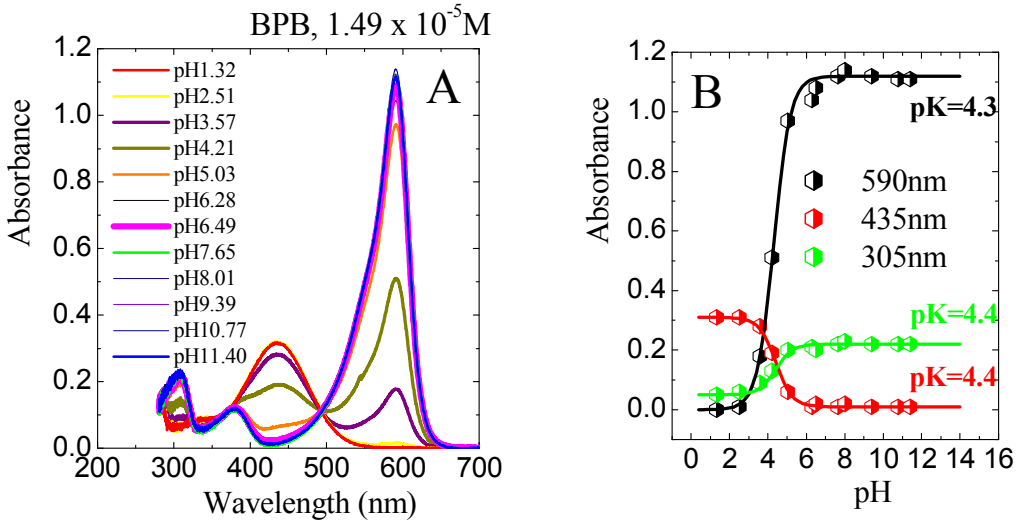

Figure 6.18. pH titration of BPB in water, 1cm cell.

A UV Spectra of the pH Titration of BPB in water, 1cm
B Fixed wavelength plot of BPB in water, 1cm

BPB differs from PR in the addition of two bromides to each of the two phenolic rings (compare with Figure 6.1.a.). Although BPB is a bulkier molecule its binding site on HSA is still reported as being located within subdomain IIA.

6.7.i. Binding Studies of Bromophenol Blue : Human Serum Albumin

The presence of rHSA on binding with BPB revealed distinct changes in the UV spectral profile with absorption maxima distinct from that of PR, the main difference was in the main absorption maxima. PR absorbs at the wavelength 435nm at pH7 with a shoulder at 560nm, whereas with BPB the absorption experienced a bathochromic shift to 610nm with a shoulder situated at 560nm in the same position as the minor absorption as the shoulder in PR (Figure 6.19.a.). The fixed wavelength plot of the UV absorption of the titration of BPB:rHSA expressed complete binding at a ratio of [0.5:1] of dye:protein respectively, showing a 2:1 binding ratio as shown in Figure 6.19.b. The CD reflected the same changes observed for the UV absorption. Four maxima were seen, two positive that were smaller in comparison to the other two peaks that were negative and larger, with the main CD absorption found at 610nm. Literature quotes a 1:1 relationship with the possibilities of other sites being available if the primary affinity site had been blocked or occupied, but at pH7.20 two sites were found, one established in site IIA and the other was as yet known.

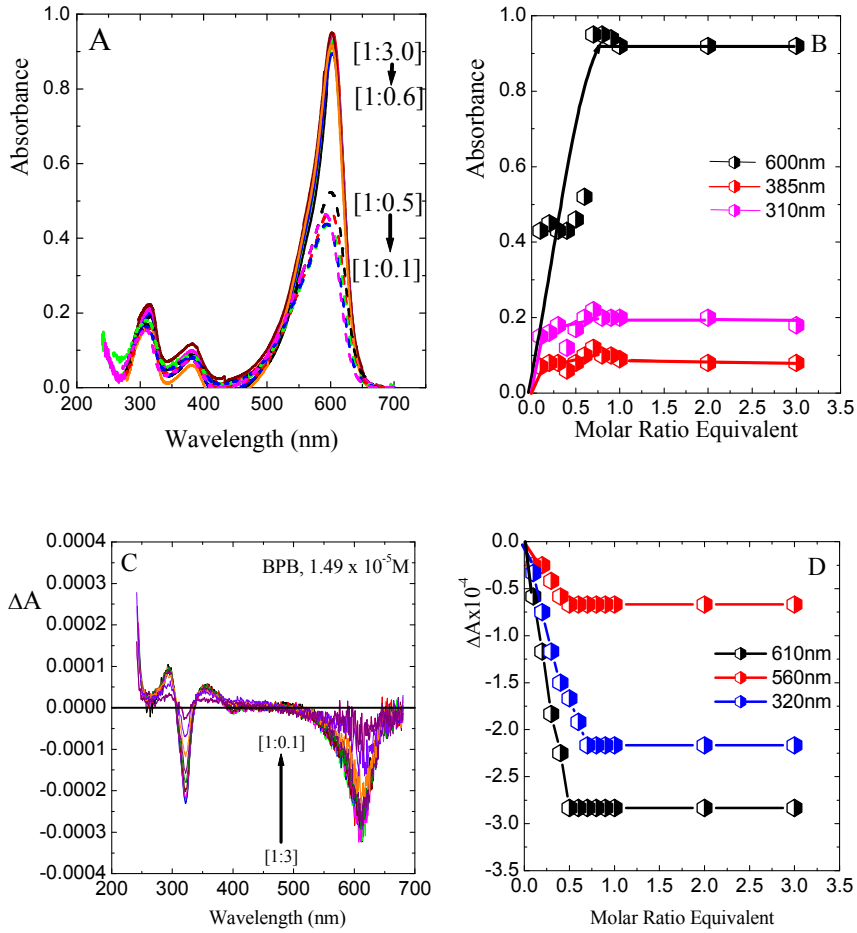

Figure 6.19. UV and CD spectra of the molar titration of BPB:rHSA at pH 7.20, 1cm

A Absorbance spectra of the titration of BPB:rHSA, 1cm
B Fixed wavelength plot of the titration of BPB:rHSA
C CD spectra of the titration of BPB:rHSA in 10mM P/B, pH7.2, 1cm cell
D Fixed wavelength plot of the CD spectra of the titration of BPB:rHSA in 10mM P/B

A pH titration was conducted of the [2:1] complex of BPB:rHSA that revealed a general increase in absorption for all the major absorptions maxima considered with increasing pH. The profile of the UV spectra did not change in quite the same way as BPB in isolation that exhibited a greater range of spectral shifts. Two transitions were found at each wavelength studied, the first under acidic conditions and the other in the alkaline region. The UV was detecting only the effects of the dye at the wavelengths studied. The CD spectra revealed the complex to be affected by neutral conditions and alkaline pH, with a change in the

profile of the complex specifically detected at pH 3.56 as shown in Figure 6.20. These findings were consistent with PR that also showed the biggest change at this pH and like PR, BPB revealed a reversal in some of its CD maxima at this pH. The CD like the UV highlighted a general increase in magnitude for pH values up to pH11, by pH 12 the CD collapses.

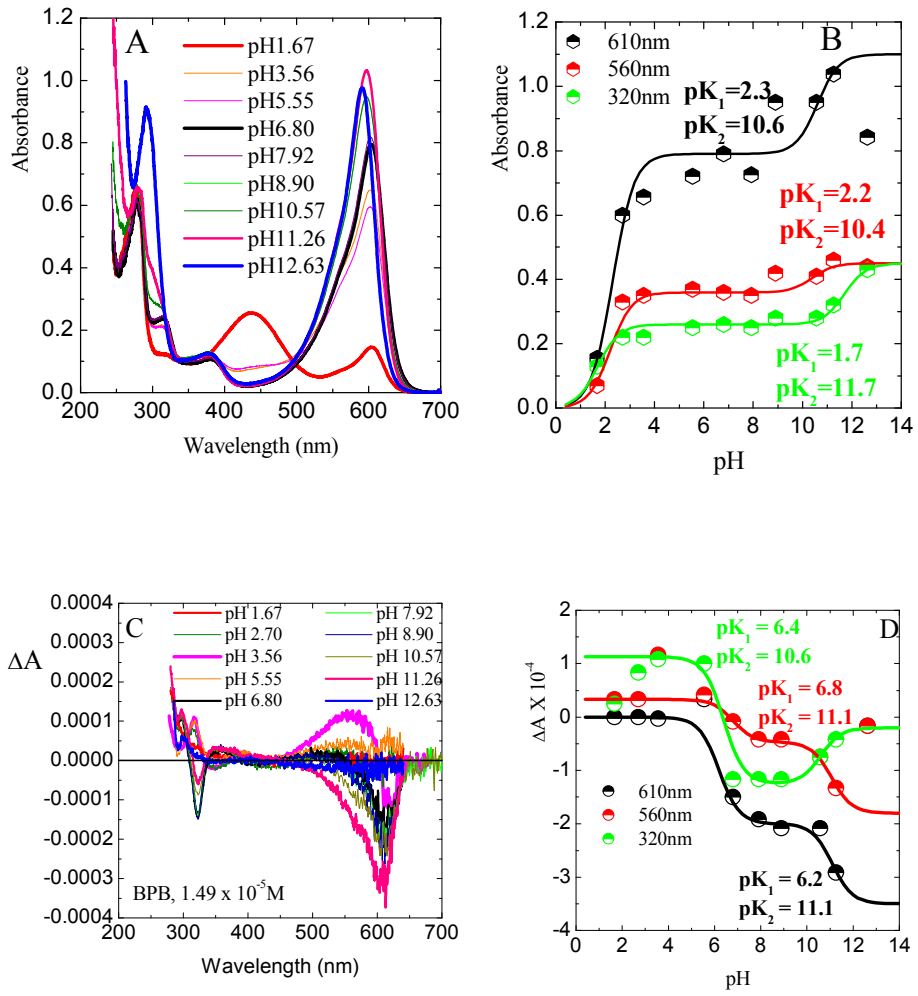

Figure 6.20. pH titration of BPB:rHSA complex [1:1] in water, 1cm cell.

A Absorption Spectra of the pH Titration of BPB:rHSA, [2:1] in water, 1cm
B Fixed wavelength plot of the absorbance spectra of the complex
C CD Spectra of the pH titration of the complex, 1cm cell
D Fixed wavelength plot of the CD spectra of the complex

As with all the other ligands monitored, the titration of the BPB:rHSA complex was investigated at pH4.56. When titrated under these conditions the BPB:rHSA complex exhibited a [2:1] molar ratio equivalent binding relationship consistent with that found at

pH7.19, and in contravene to that expected (Figure 6.21.). Both the UV and CD spectra was markedly changed from that determined at physiological conditions with the UV spectra showing a pronounced shoulder at 565nm in addition to the other two peaks found at shorter wavelength. In response to the formation of the shoulder seen in the absorption spectra the CD spectra reflected this change with the generation of positive and negative couplet, the negative peak being larger than the positive.

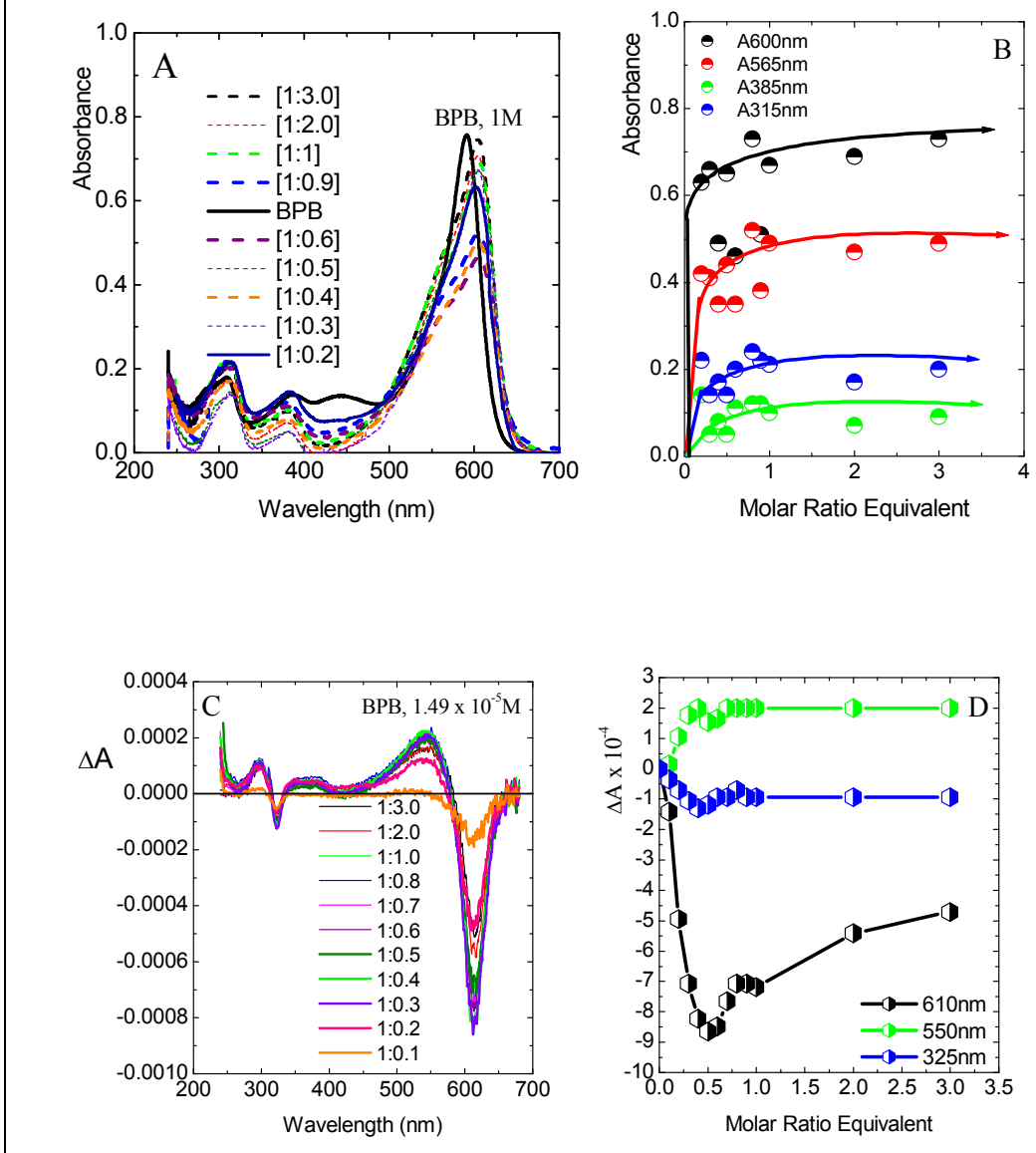

Figure 6.21. Molar titration of BPB:rHSA at pH 4.56, 1cm.

A Absorption spectra of the titration ot BPB to rHSA in 10mM B/R, pH4.56, 1cm
B Fixed wavelength plot of the absorption spectra of the titration
C CD spectra of the titration of BPB:rHSA at pH4.56, 1cm
D Fixed wavelength plot of the CD spectra of BPB:rHSA

Reducing the pH further to pH3.57 and conducting the binding titrations under these conditions revealed a [2:1] binding relationship as shown in Figure 6.22. The reduction in pH exposed more of the binding sites that the dye made use of.

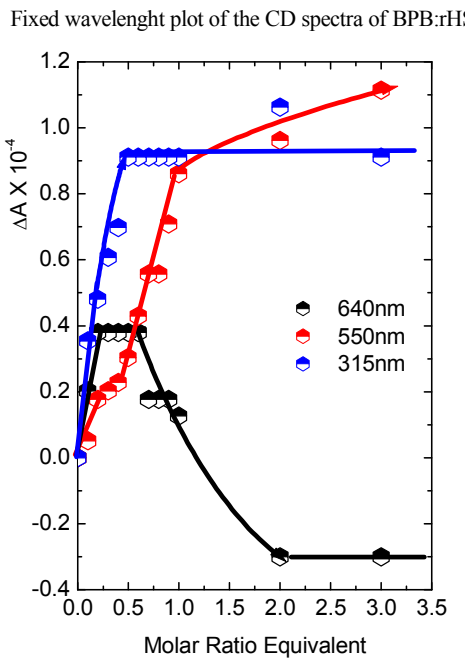

Figure 6.22. Molar titration of BPB:rHSA at pH 3.56, 1cm cell.

6.7.ii. Temperature Studies of Bromophenol blue: Recombinant Human Serum Albumin

Like PR, BPB at pH7.2 offers little resistance to increasing temperatures above 40°C, the dye becomes displaced and the CD signal lost (Figure 6.23.). Only a small quantity of dye is lost up to temperatures of 55°C. However, between the temperatures of 55°C and 65°C most of the binding was lost, but complete dissociation was never achieved. At 610nm binding was still evident at 70°C as a strong negative CD signal was still seen. At 67°C the CD spectra obtained showed close similarities to the CD measured at pH3.56, it was evident that the structural changes induced by heating albumin to high temperature also produces similar changes in binding BPB by lowering the pH specifically to pH3.57. What

was not clear was if at high temperatures the BPB molecules were bound to the same site on albumin or if they had found alternative positions.

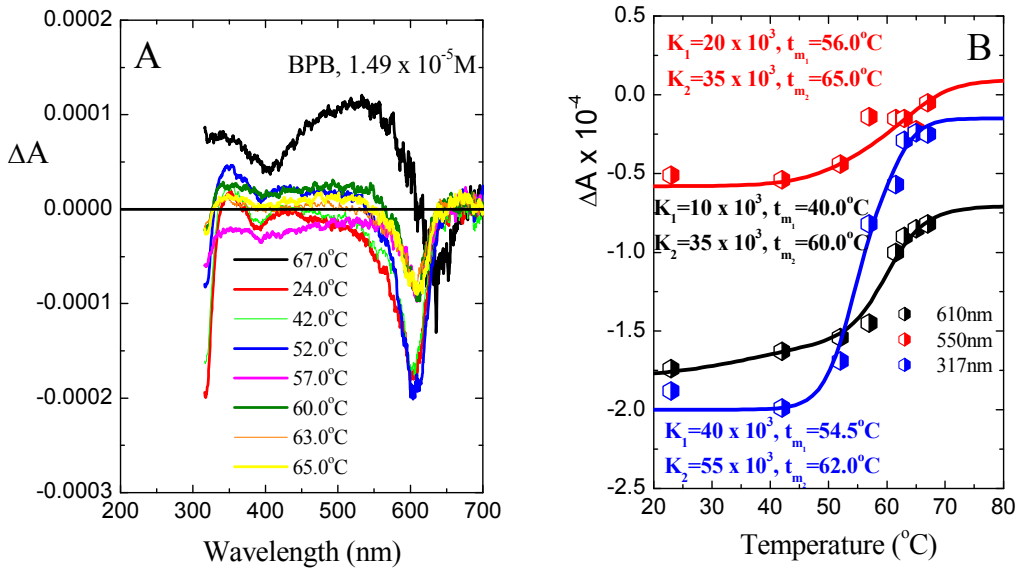

Figure 6.23. Temperature studies of a [2:1] molar ratio complex of BPB:rHSA in P/B, 1cm.

A CD spectra of complex in P/B, pH 7.19, 1cm
B Fixed wavelength plot of the CD spectra of the temperature studies of BPB:rHSA, 1cm

Conducting temperature studies at reduced pH for the [2:1] molar ratio equivalent complex of BPB:rHSA, reducing to pH3.56 revealed the reverse situation from that found at the other two pH values studied, thus highlighting the special conditions that pH3.56 produces in albumin. At the other pH values the heating curve produced at least two transition for each wavelength studied, and a single transition for the quenched curves. At pH3.56, only a singe transition was produced for the heating curve, however, surprisingly two transitions were produced for all the wavelengths investigated. Considering the heating curve first, of the three maxima studied the absorption peak at 315nm behaved distinctly different from the other two, requiring a higher K and t_m. The peaks at 550nm and 620nm appeared coupled producing virtually identical values for K and t_m that were both relatively low with

both curves coalescing to the same point, confirming the instability of the complex (Figure 6.24.a.). The peak at 620nm also experienced a reversal in sign changing from negative to positive as soon as the complex was heated. Once again residual binding was also detected with the incomplete collapse in binding as detected with other ligands.

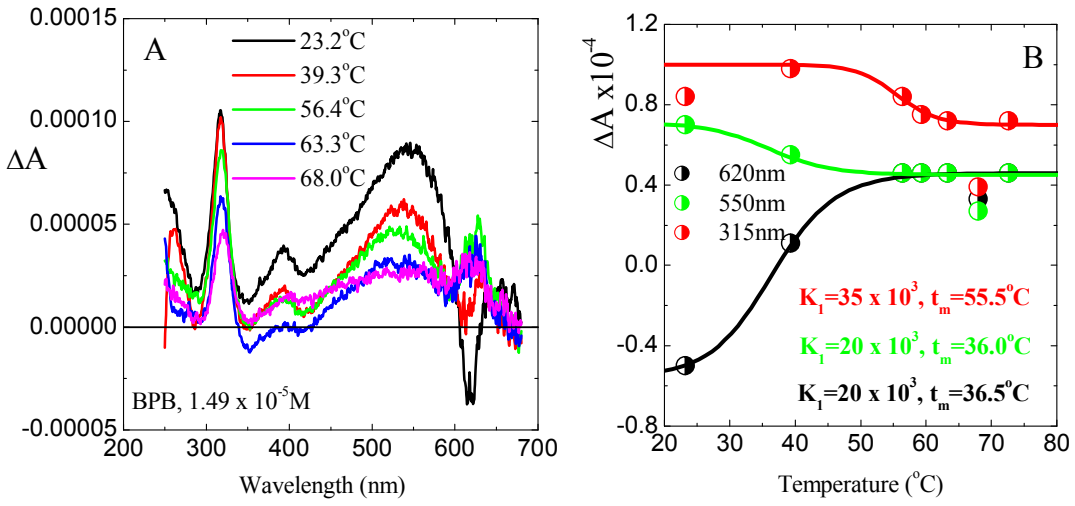

Figure 6.24.a. Temperature studies of a [2:1] complex of BPB:rHSA at pH 3.56, 1cm.

A CD spectra of the temperature study at pH3.56, 1cm
B Fixed wavelength plot of the CD Spectra of the titration

The quenched samples reinforced that which was seen in the heating studies with the peaks at 620nm and 550nm behaving similarly and almost coalescing. However, unlike the heating curve the first transition for wavelengths 315nm and 620nm now behaved very similarly with K_1=20 X 10^3 for both and t_m's of 61.5°C and 58.5°C respectively. The transition at 550nm occurred at a much higher value of K that increased by 10 x 10^3 at a t_{m1} = 47°C. The second transition reverts back to that which was expected with the values at 550nm and 620nm behave very similarly with identical values of K_2=45 X 10^3 and t_m's of 69.0°C and 67.0°C respectively. At 315nm, again a 10 x 10^3 increase was experienced in K_2 with a t_{m2} = 66.2°C. Once again at wavelength 620nm a change in sign of the CD signal was experienced for temperatures greater than 60.0°C, (Figure 6.24.b.)

Binding was still evident in spite of the albumin samples being heated to temperature that caused irreversible damage, although greatly reduced at the main absorption, it was still significant to be prominent at all the wavelengths studied. Albumin when heated retains approximately one third of its original structure when cooked, and it must be that part that the BPB molecules/molecule binds to. Again it is difficult to say whether one or two binding sites are in use and their apparent location/s within the albumin molecule.

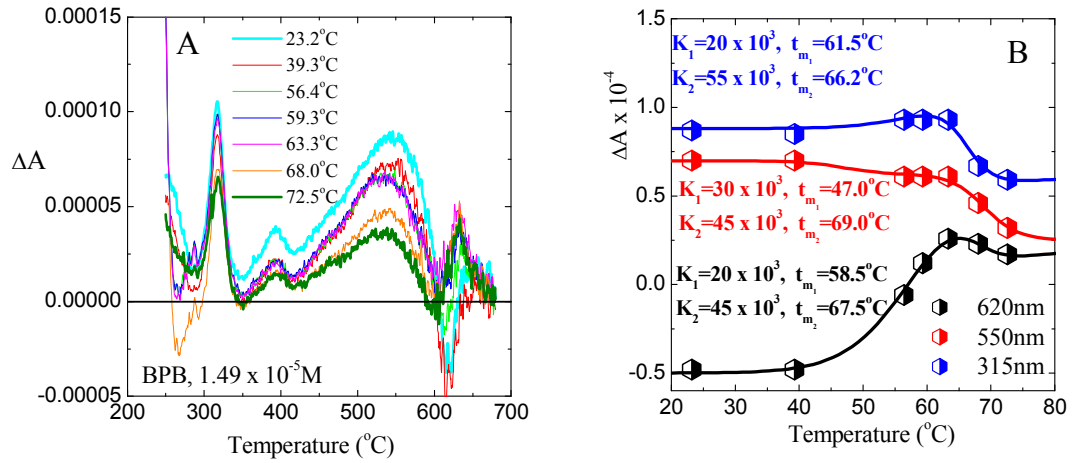

Figure 6.24.b. Temperature studies of the quenched samples of BPB:rHSA at pH 3.56, 1cm.

A CD spectra of the quenched samples of a [2:1] complex sample at pH3.56, 1cm
B Fixed wavelength plot of the CD spectra of the quenched samples at pH3.56, 1cm

6.7.iii. Denaturation Studies on Bromophenol Blue:Recombinant Human Serum Albumin

The addition of urea to the [2:1] molar equivalent complex samples revealed by UV spectroscopy that binding was maintained throughout the entire titration for the main absorption maximum at 600nm, the other wavelengths showed only 36% binding at 380nm and 46% at 310nm (Figure 6.25.a.). Indeed, for the peak at 600nm, enhanced absorption was detected for additions of between 2M – 4M of urea. CD spectroscopy highlighted a different trends, at 600nm, for urea concentrations up to 6M equivalent an increase in the magnitude of the negative maximum was observed with a small loss detected for ratios of

7M – 8M equivalent (Figure 6.25.b.). The peak at 390nm remained fairly steadfast with a slight loss in its negative CD observed. Like that seen at 600nm, the peak at 390nm between 4M – 6M equivalent proved significant with the biggest loss in CD detected at those concentrations, a slight recovery was detected for concentrations of urea between 7M – 8M equivalent. The spectral changes that occurred at 390nm was mirrored at 315nm but to a greater extent. Once again it was the spectral changes at 600nm that proved atypical.

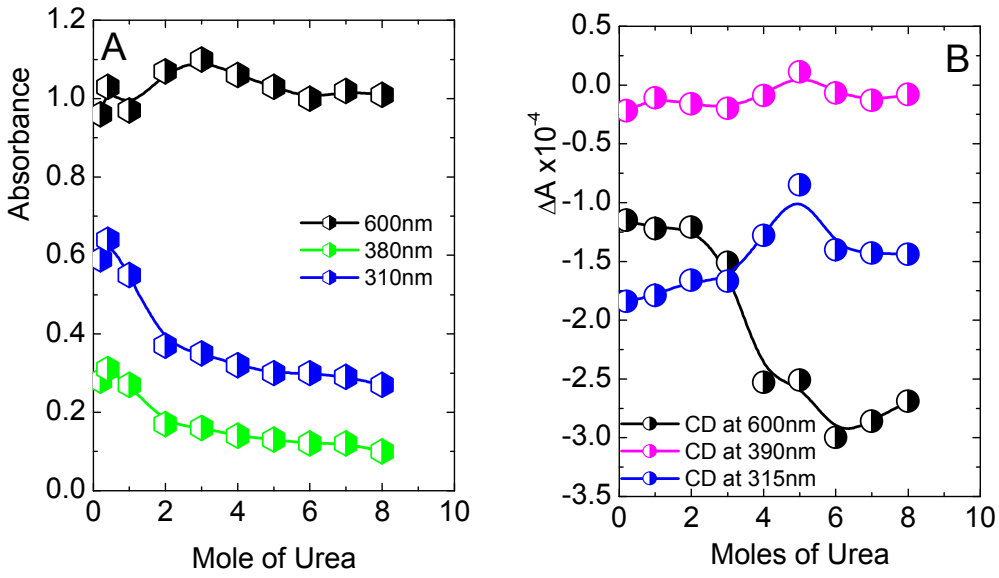

Figure 6.25. Denaturation studies of BPB:rHSA complex in urea, 1cm.

A Fixed wavelength plot of the absorption spectra of the urea titration of the complex
B Fixed wavelength plot of the CD spectra in the presence of Urea, water, 1cm

Denaturation studies involving GuHCl produced similar results as that experienced with the urea titrations, with the results confirming that it was the maximum at 600nm proving atypical. The UV spectra revealed the enhanced binding experienced at 600nm with a gradual sequential increase in the magnitude of the absorption (Figure 6.26.a.). However, there were spectral changes that occurred for the peaks at lower wavelengths with the peak detected previously at 380nm now shifted to shorter wavelength located at 350nm, and the other located at 310nm now positioned at 320nm. Once again for concentrations between

1M – 3M equivalent produced decreases in association of the dye to the protein that was detected at wavelengths 350nm and 320nm, that then became stable with no further losses experienced at either wavelength. Likewise, the CD also observed shifts in the absorption maxima obtained with the main absorption still detected at 600nm, but additional peaks shifted from 390nm to 350nm, and from 315nm to 320nm (Figure 6.26.b.). The CD spectra revealed that for increasing concentrations of GuHCl up to 8M equivalent, generally a decrease in CD absorption was detected. However, binding was not totally lost as a significant amount of association of the dye was still detected, this suggested that binding was observed in regions of the protein that remained unaffected by the additions of GuHCl. The findings differed from that of PR that produced a complete collapse in the complex by 1.8M equivalent of GuHCl.

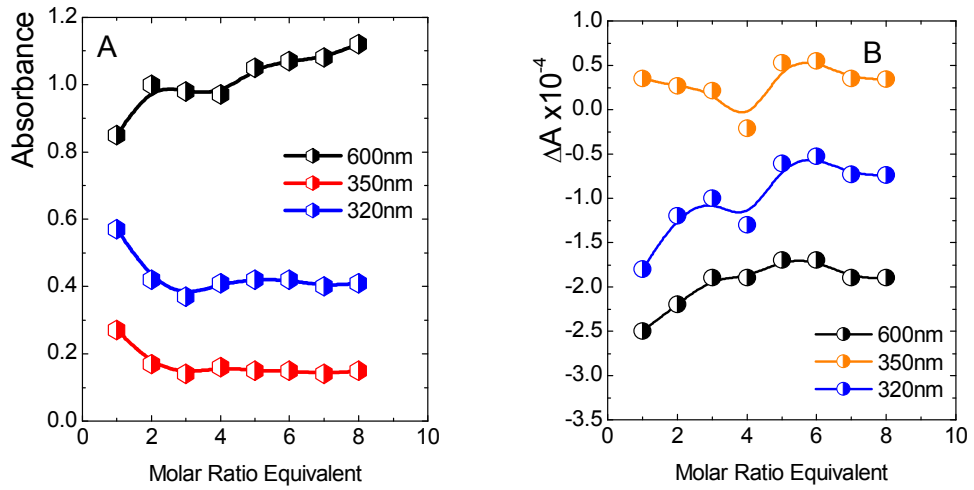

Figure 6.26. Denaturation studies of BPB:rHSA complex in GuHCl, 1cm.

A Fixed wavelength plot of the absorption spectra in GuHCl
B Fixed wavelength plot of the CD spectra of the complex in GuHCl

6.7.iv. Microcentrefuged Samples of Bromophenol Blue:Recombinant Human Serum Albumin

Considering the titration conducted at the three pH values chosen expressed that for low molar ratios equivalents of BPB:rHSA and up to [2:1] the microcentrifuged samples showed the presence of decreasing amounts of free dye in solution. For molar ratio equivalents above a value of [2:1], all the dye was in the bound state and no free dye could be detected (Figure 6.27.).

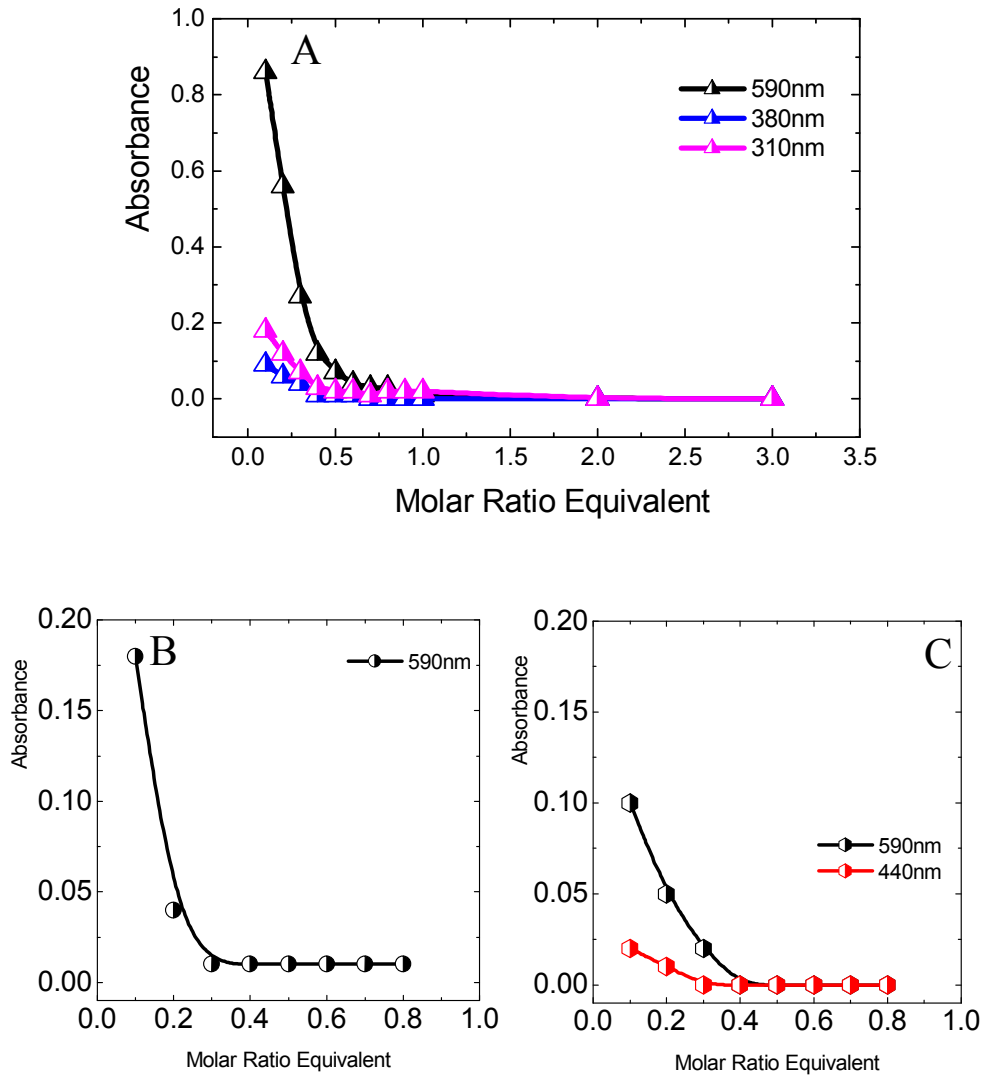

Figure 6.27. Microcentrifuged samples of the titrations of BPB:rHSA conducted at different pH values.

A Microcentrifuged samples of the BPB:rHSA titration in P/B, pH7.19, 1cm cell
B Microcentrifuged samples of BPB:rHSA in B/R buffer, pH4.56, 1cm cell
C Microcentrifuged samples of BPB:rHSA in B/R buffer, pH3.57, 1cm cell

Temperature studies on the pre-heated samples of the complex indicated no free dye present for samples heated to 50°C; above that temperature increasing amounts of free dye was visible, supporting the theory that as the protein becomes denatured its ability to bind ligands was increasingly debilitated. It also suggests that one of the binding sites may be exposed or close to the surface of the protein and had lost its ability to bind. The fixed wavelength plot in Figure 6.28. shows that there was greater than 50% of the dye still bound at temperatures exceeding 70°C, suggesting more than one binding site existed (Figure 6.28.a.). Two transitions were observed at each wavelength that supported the previous finding of the relationship between wavelengths 380nm and 310nm, and revealed that the first transition was much easier to achieve then the second. This was the reverse of that found at the main absorption peak that found both the first and second transitions were equally as difficult All three wavelengths gave identical values for both K and t_m at all wavelengths, supporting that one of the binding sites previously determined was incapacitates at a t_m = 65.2°C. The second site was unperturbed at these temperatures.

The micro-centrifuged samples of BPB:rHSA in urea were measured and shown that for small additions of urea up to 3M equivalent produced small amounts of free dye that was detected (Figure 6.28.b.). Additions greater than 3M equivalent produced more of the dye being displaced from the protein resulting in larger absorptions detected at the main absorption band, that never attained maximum levels, indicating incomplete displacement of the dye. The greatest amount of unbound dye was detected for the complex in 5M equivalent of urea, this supported the findings in the CD where the greatest change was seen at this concentration. Additions of urea greater than 5M equivalent produced decreasing amounts of free dye at the main absorption band, suggesting increased association of the dye:protein complex. This contradicted the findings at the other two wavelengths that highlighted maximum binding of the dye at 5M equivalent urea that

became increasingly displaced for amounts higher that that. For the GuHCl samples, only the main absorption band was monitored and showed that only at 4M equivalent was the concentration of GuHCl sufficiently high enough to produce any appreciable levels of dye that could be detected. For concentrations above 4M equivalent, negligible amounts of free dye was found (see Figure 6.28.c.) reinforcing previous finding that full dye binding is maintained in the GuHCl samples.

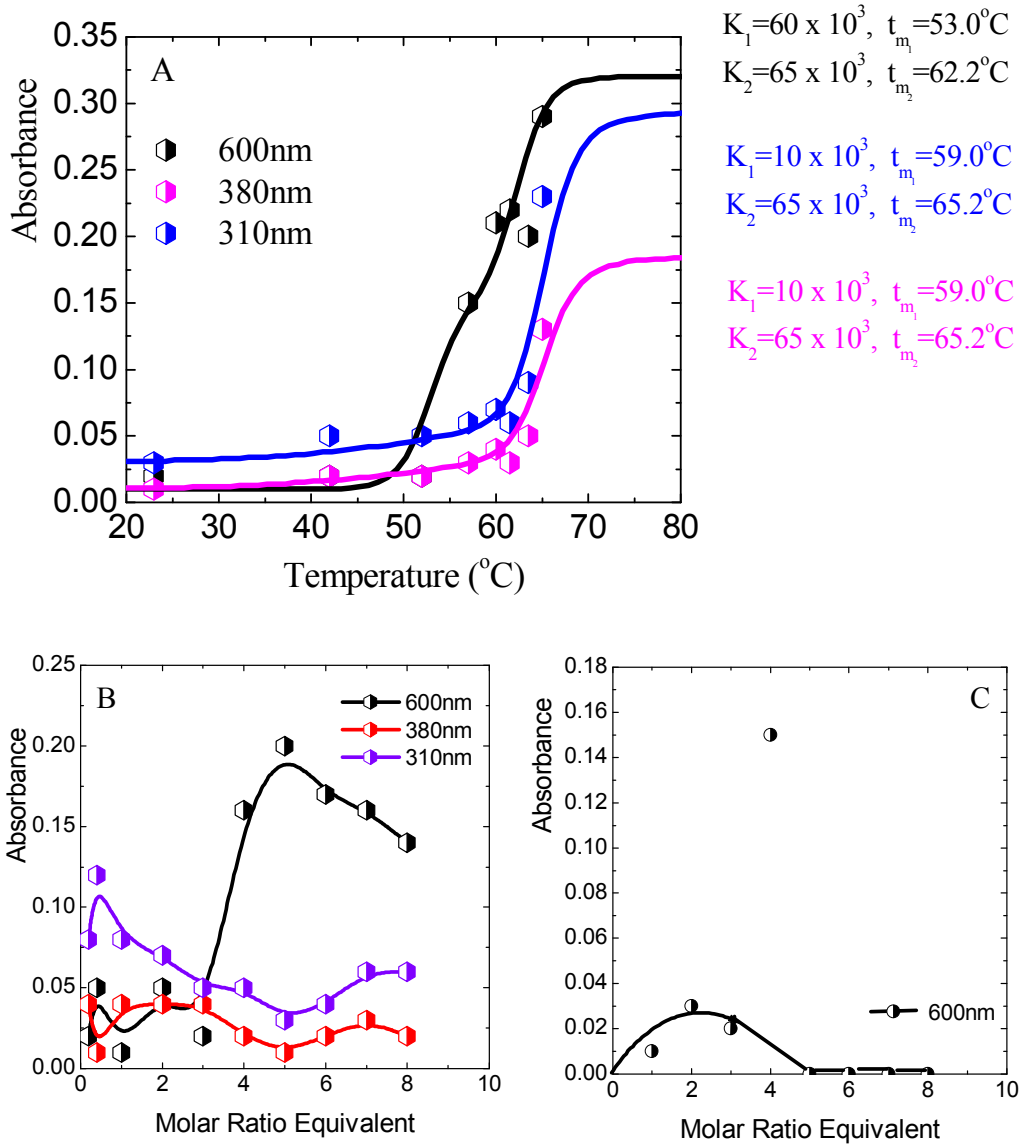

Figure 6.28. Denaturation studies on BPB:rHSA complex, 1:2, 1cm cell.

A Microcentrifuged samples of the pre-heated samples of BPB:rHSA in P/B, pH7.19, 1cm
B Microcentrifuged samples of the complex in urea, 1cm
C Microcentrifuged samples of the complex in GuHCl, 1cm

6.8. Bromocresol Green : Human Serum Albumin Interaction

The last in the series of dyes to be considered with increasing complexity was Bromocresol Green (BCG) or 3'3"5'5"Tetrabromo-m-cresolsufonphthalein ($C_{21}H_{14}BR_4O_5S$), MW 698.04, this has a working pH range of 3.8 - 5.4. BCG differs from BPB in the addition of two methyl groups one in each of the dibromophenol rings (Figure 6.29.).

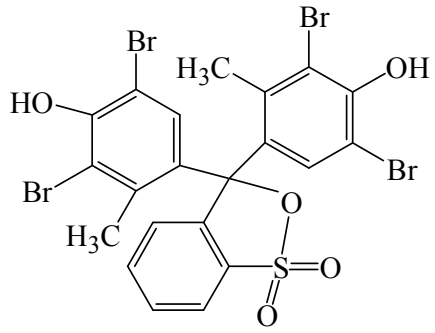

Figure 6.29. Schematic representation of BCG.

6.8.i. Binding Studies of Bromocresol Green to Recombinant Human Serum Albumin

Binding studies at physiological conditions (pH 7.19) were conducted and revealed that the binding of BCR was not straight forward in that the CD underwent several spectroscopic changes depending on the molar ratio equivalent present (Figure 6.30.). For low molar ratio equivalents, at the main absorption a positive CD maximum was seen. As the ratio increased, so the positive peak transformed to a positive and negative couplet, then through to a negative peak of increasing magnitude. The other peaks present behaved more typically increasing in magnitude as the molar ratio equivalent increased. An increase in CD magnitude was observed at all the wavelengths studied for molar ratio equivalents up to [1:0.5], after that, a decrease was experienced at all wavelengths up to a ratios of [1:1] molar equivalent. A small loss was observed after that for molar ratio equivalents up to [1:3]. The initial experimental interpretation of the CD spectra suggests that a [2:1]

relationship exists in the BCG:rHSA, the same as for BPB which was not unexpected since they both share similar complexities of structure.

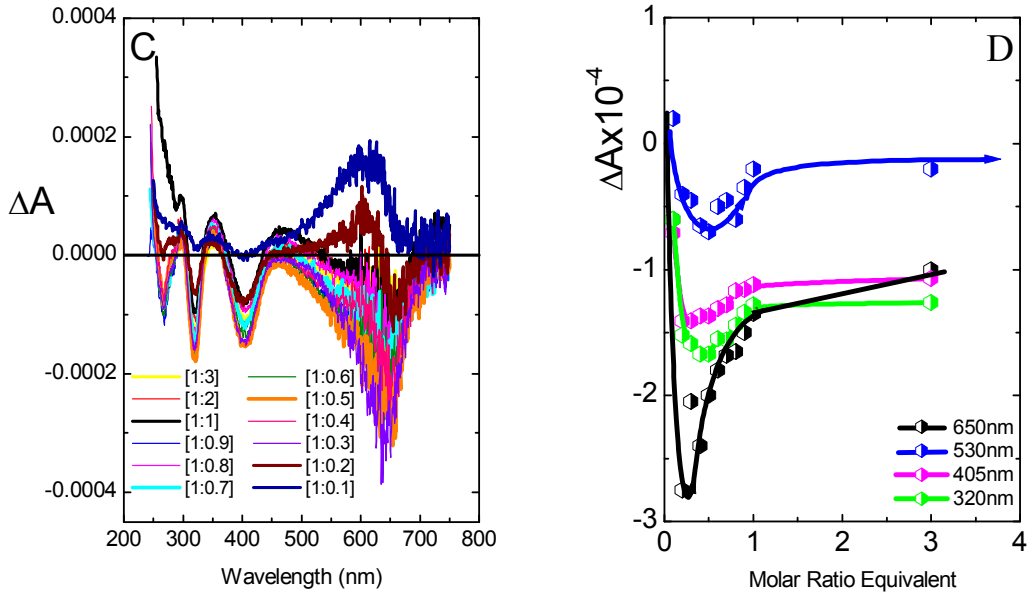

Figure 6.30. Titration of BCG:rHSA in P/B, pH 7.2, 1cm.

C CD spectra of the titration of the complex in P/B, 1cm
D Fixed wavelength plot of the CD spectra of the titration in P/B, pH 7.45, 1cm cell

6.8.ii. pH Studies of Bromocresol Green to Albumin

Considering the pH titration and comparing the effects of native protein with the recombinant, the titration was conducted under identical conditions for both. The CD profile of BCG:nHSA complex for a [2:1] molar ratio equivalent bears similarities with its counterpart the BPB:rHSA complex, with the CD maxima located in similar positions and with the same sign, however, the detection wavelengths were not the same (Figure 6.31. & 6.32.). Although the UV showed a general increase in the main absorption band at 630nm with increasing pH as detected with BPB:rHSA complex, the fixed wavelength plots for the CD spectra revealed spectral changes that were complex. Between pH5 & pH10 the CD maximum at wavelength 420nm for the BCG:rHSA complex seemed relatively unperturbed, this was not the so for the other wavelengths that changed radically. When

comparing the changes between the complexes of nHSA and rHSA bound to BCG diversities were observed with the two complexes producing CD maxima at different wavelengths. The use of this dye was the first ligand to show such diversities between the two proteins (Figure 6.31. & 6.32.). For both proteins, the UV spectra revealed the fluidity of the absorptions and also their complexities that gave rise to such complex CD spectra. The CD showed the existence of coupling of two of the main absorptions, and the existence of independent absorption that responded to changing pH in isolation to the other absorptions. It was evident that the increase in complexity of the dye molecule had profound effects that changed its binding abilities to albumin.

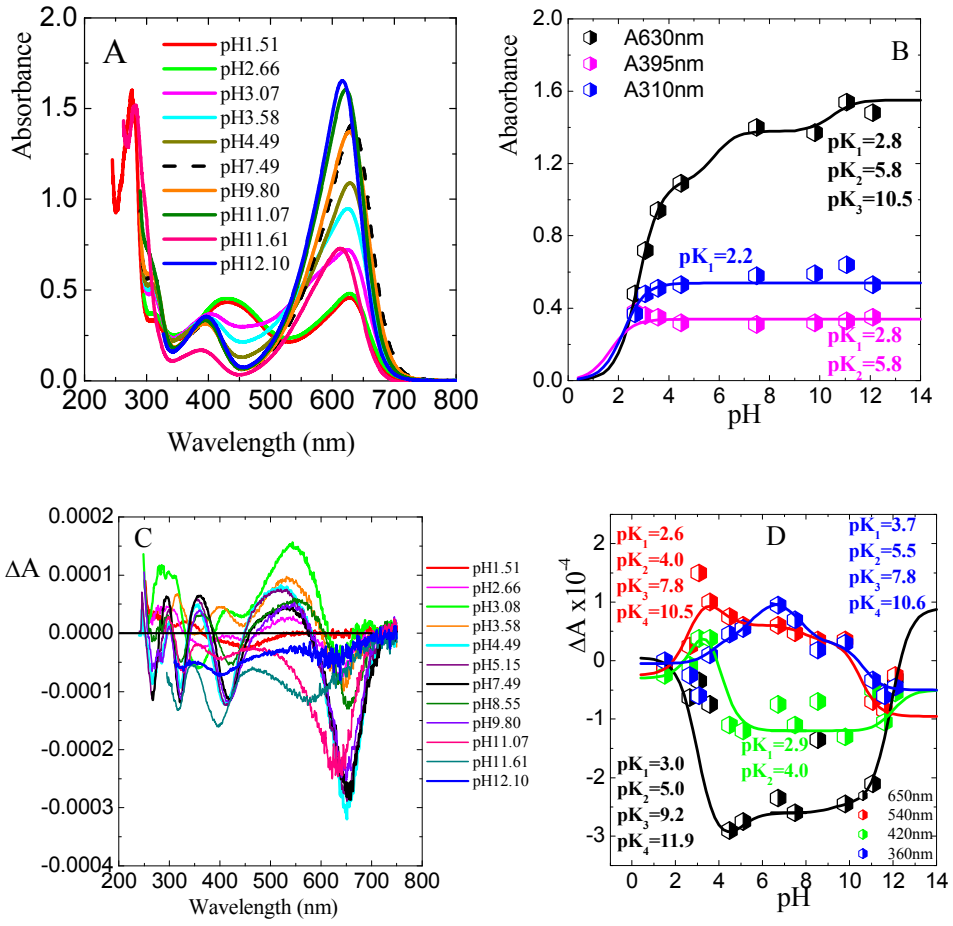

Figure 6.31. pH titration of BCG:rHSA in a 1cm cell.

A Absorbance spectra of the pH titration of the complex, 1cm cell
B Fixed wavelength plot of the absorbance of the pH titration of [2:1] complex
C CD spectra of the pH titration of the complex in H\-(2)O, 1cm
D Fixed wavelength plot of the CD spectra of the complex

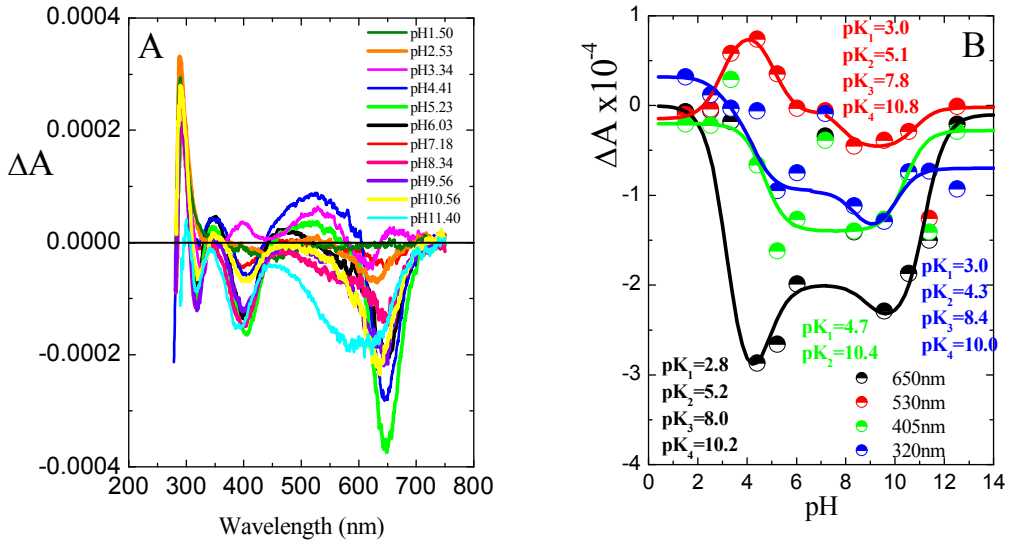

Figure 6.32. pH titration of BCG:nHSA in a 1cm cell.

A CD spectra of the pH titration of the [2:1] complex, 1cm
B Fixed wavelength plot of the pH titration of BCG:nHSA in water

Comparisons of the pK_a values for each protein has been tabulated in Table 6.1. and highlighted subtle differences that exists together with minor spectral shifts. Overall the two proteins behave similarly. In keeping with all the other experiments, work was conducted on the recombinant protein.

rHSA	nHSA	[2:1] BRG:nHSA Complex				[2:1] BRG:rHSA Complex			
λ (nm)	λ (nm)	pK_1	pK_2	pK_3	pK_4	pK_1	pK_2	pK_3	pK_4
650	650	2.9	5.2	8.0	10.2	3.0	5.0	9.2	11.9
540	530	3.0	5.1	7.8	10.8	2.6	4.0	7.8	10.5
420	405	4.7	10.4			2.9	4.0		
360	320	2.8	5.2	8.0	10.2	3.7	5.5	7.8	10.6

Table 6.2. Comparison of rHSA and nHSA in response to pH changes

Further binding titration were conducted at pH4.40 and pH3.56. Dropping the pH to pH4.40 the titration of BCG:rHSA revealed a [2:1] relationship similar to that found for BPB:rHSA (Figure 6.33.). At pH4.40, the titration was conducted within the working pH range of the dye and gave the best fixed wavelength plot results. However, when the pH was decreased further to pH3.56, outside the range of the dye, CD spectral changes were still detected even for a molar ratio equivalent of [3:1] suggesting that maximum binding

was not attained. rHSA at pH3.56 was able to bind more than 3M equivalent of dye when the protein was in the E-form as shown in Figure 6.34.

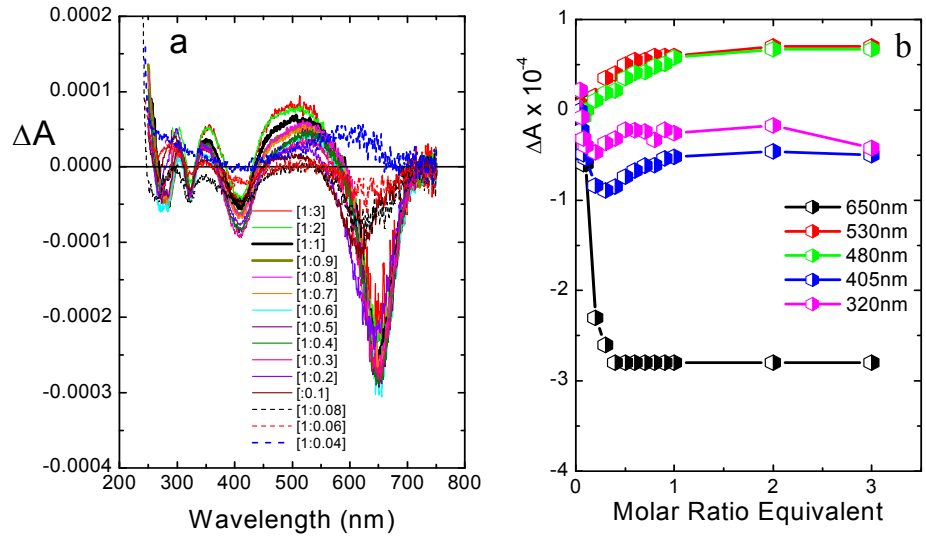

Figure 6.33. Molar titration of BCG:rHSA at pH4.4, 1cm.

a CD spectra of the titration in B/R buffer, pH 4.40, 1cm
b Fixed wavelength plot of the CD titration at pH4.41

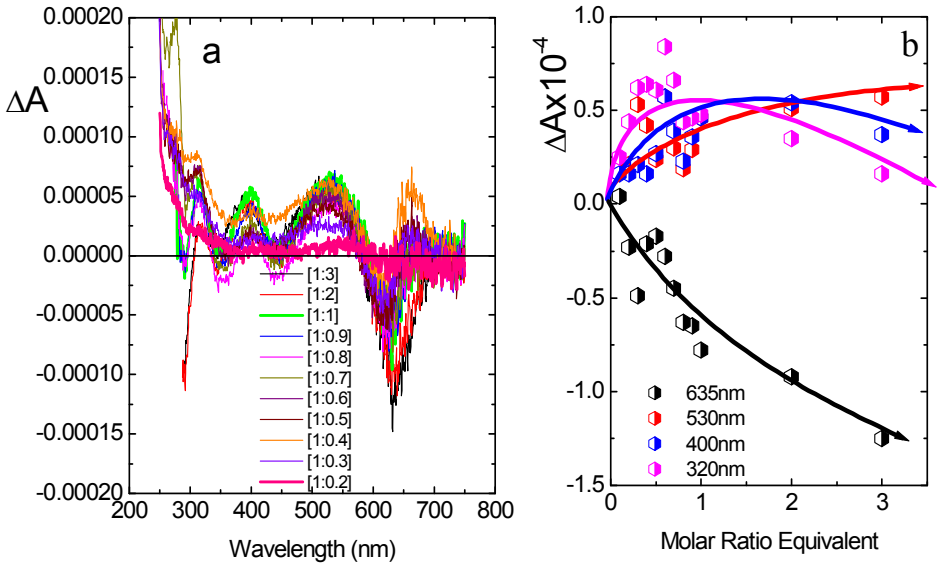

Figure 6.34. Molar titration of BCG:rHSA at pH3.56, 1cm.

a CD spectra of the titration in B/R buffer, pH3.56, 1cm
b Fixed wavelength plot of the CD spectra of the titration in B/R, pH3.56, 1cm

6.8.iii. Temperature Studies of Bromocresol Green:Human Serum Albumin

When a [2:1] complex of BCG:rHSA at pH7.19 was heated, the complex revealed stability to temperatures up to 50°C (Figure 6.35.). Between the temperatures of 50 - 60°C a steady decrease in binding was detected that partially stabilised between 60 - 68°C. For temperatures exceeding 68°C highlighted the greatest loss in binding resulting in almost complete loss by 78°C. Once again there were several spectral changes observed that included a change in the sign of some of the peaks determined. Two transitions were observed at every wavelength monitored, and the data revealed that there was increasing difficulty as the value for K_1 increased as you moved from 530nm, 405nm and 320nm respectively, with the transition at 650nm being the hardest to achieve and occurred at the highest t_m. The second transitions all gave identical values for $K_2=80x10^{-3}$ with the exception of wavelength 650nm that was extremely low ($K_2=20x10^{-3}$). Binding at the main absorption was always detected even though most of the other absorptions were lost.

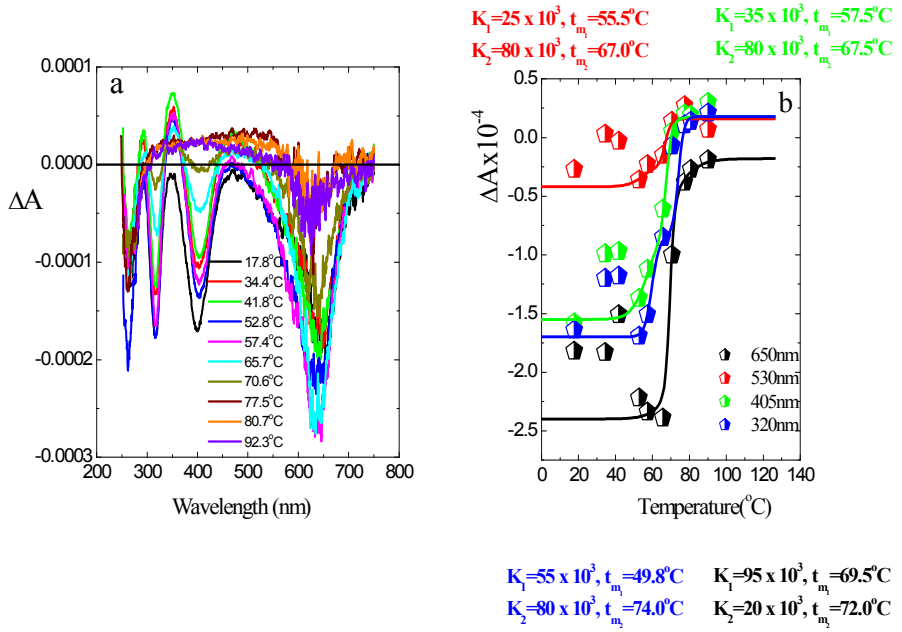

Figure 6.35. Melting of a [2:1] Complex of BCG:rHSA at pH7.19, 1cm cell.

a Temperature studies in P/B, pH7.19, 1cm
b Fixed wavelength plot of the CD temperature spectra

The quenched samples of the [2:1] complex of BCG:rHSA at pH7.19 revealed the stability to temperatures not exceeding 55°C, for higher temperature the results revealed a loss of binding with negligible amounts bound at 92.3°C (Figure 6.36.). The fixed wavelength plot of the quenched curve at pH7.19 revealed stepwise sequential unfolding transitions similar to those observed in the melting studies, with two transitions observed except for that found at wavelength 650nm that only produced one. Three of the wavelengths studied produced similar results for values of K_1 and t_{m1}, with the second transition being that much harder to achieve as would be expected. Once again the main absorption found at 650nm proved atypical producing a K_1 and t_{m1} much higher than that found at the other wavelengths. At wavelength 530nm there was a change in sign of the peak from negative to positive that then reversed again to form the negative CD peak. As seen before, binding of the dye was maintained with at least 50% of the dye remaining in situate, this suggests that one of the possible two dye molecules have become displaced and reinforces the theory of there being two dye molecules bound to the protein.

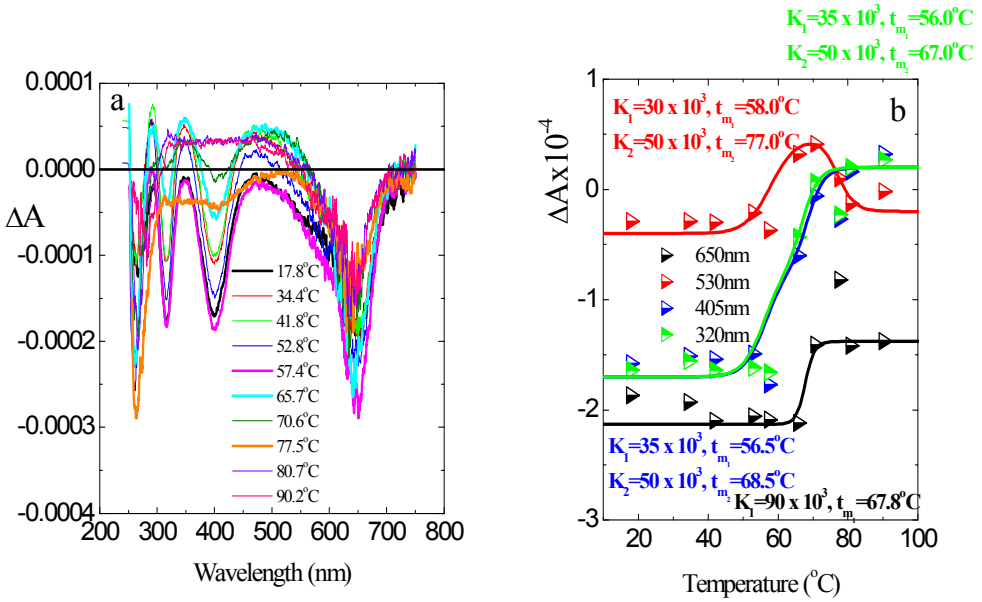

Figure 6.36. Temperature studies of quenched BCG:rHSA at pH7.19, 1cm cell.

a CD spectra of the quenched samples of the complex, in P/B, pH7.19, 1cm
b Fixed wavelength plot of the quenched samples of the complex in P/B, pH7.19, 1cm

In order to perturb the stability of the [2:1] binding complex of BCG:rHSA the temperature study of the complex was conducted under reduced pH conditions (Figure 6.37.). Lowing the pH values to pH4.40 revealed the fragility of the complex with the loss of binding experienced at the main absorption band of 650nm once the sample was heated. At the three other wavelengths studied, there was an increase in binding detected for temperatures up to 55°C, the location of the first of two transitions that occurred with relative ease at low temperature, suggesting some sort of reorganisation of the protein . For temperatures above 55°C, all wavelengths monitored followed very similar paths with the loss of binding detected. Again spectral shifts were observed, the biggest was the creation of a positive CD band at shorter wavelength at the temperature of 72.8°C.

The second transition also occurred with relative ease with all the values of K_2 found to be identical and the t_{m2} occurring between 62°C – 68°C, a sharp decrease in binding was determined. Once again most of the binding was seen at the main absorption band of 650nm with only approximately a 25% loss in binding.

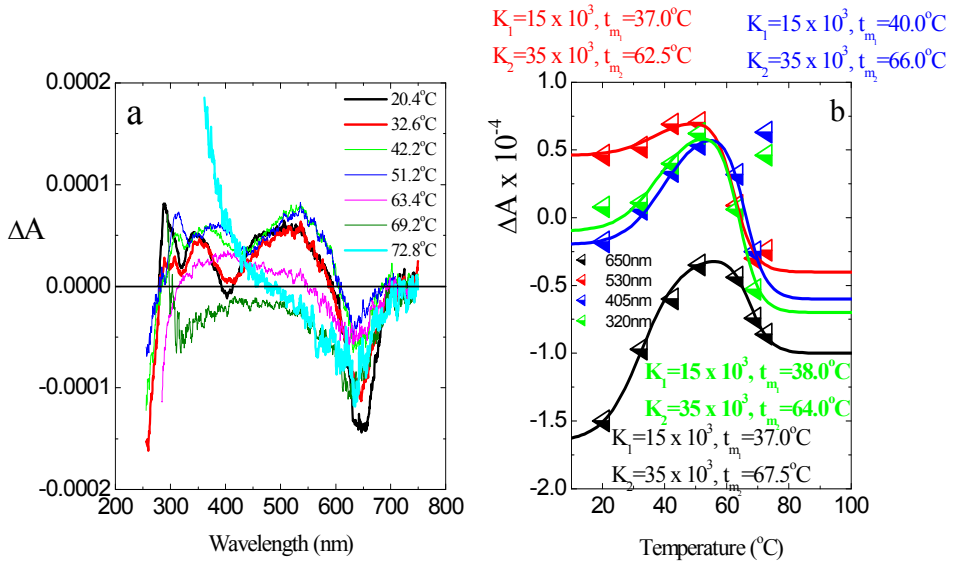

Figure 6.37.a. & b. Temperature studies of BCG:rHSA at pH4.40, 1cm cell.

a CD spectra of the temperature studies of BCE:rHSA in B/R, pH4.42, 1cm
b Fixed wavelength plot of the CD spectra of the heated samples of the complex

The quenching curve reflected similar trends as that seen in the heating curve at the same pH, but its changes were not as pronounced. There was a variation in the relative ease of the two transitions found at each wavelength, and like the heating curve a high proportion of binding was still maintained even after cooking the protein.

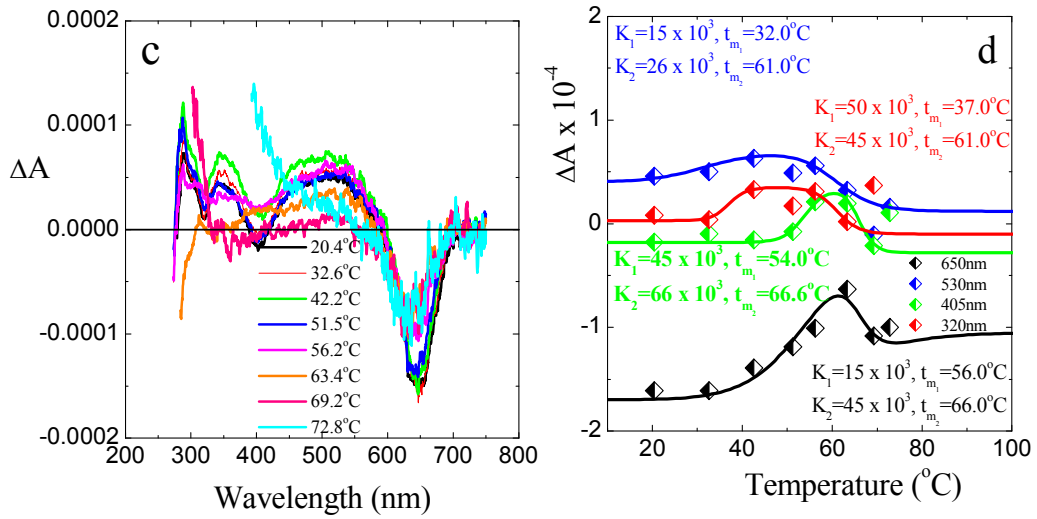

Figure 6.37.c. & d. Temperature studies of the quenched samples of BCG:rHSA at pH4.40, 1cm cell.

c CD spectra of the quenched samples of the BCG:rHSA complex in B/R buffer, pH4.42, 1cm
d Fixed wavelength plot of the quenched samples of the complex

Decreasing the pH further to pH3.56 resulted in the initial reorganisation in binding for temperatures up to 57°C, but also revealed were many spectral changes in the CD, indicative of what would be expected for the protein once in the extended form. For temperatures above 57°C an increase in binding was observed with binding at 80°C greater than that detected for the unheated samples. rHSA in the E-form once heated to high temperatures seem to facilitate binding of the comparably large dye molecule. Denaturation of the protein did not affect this binding site at very low pH values, suggesting that this site was shielded in some way thus preserving its integrity. Both the heated and quenched samples reflected this trend as demonstrated in Figure 6.38.

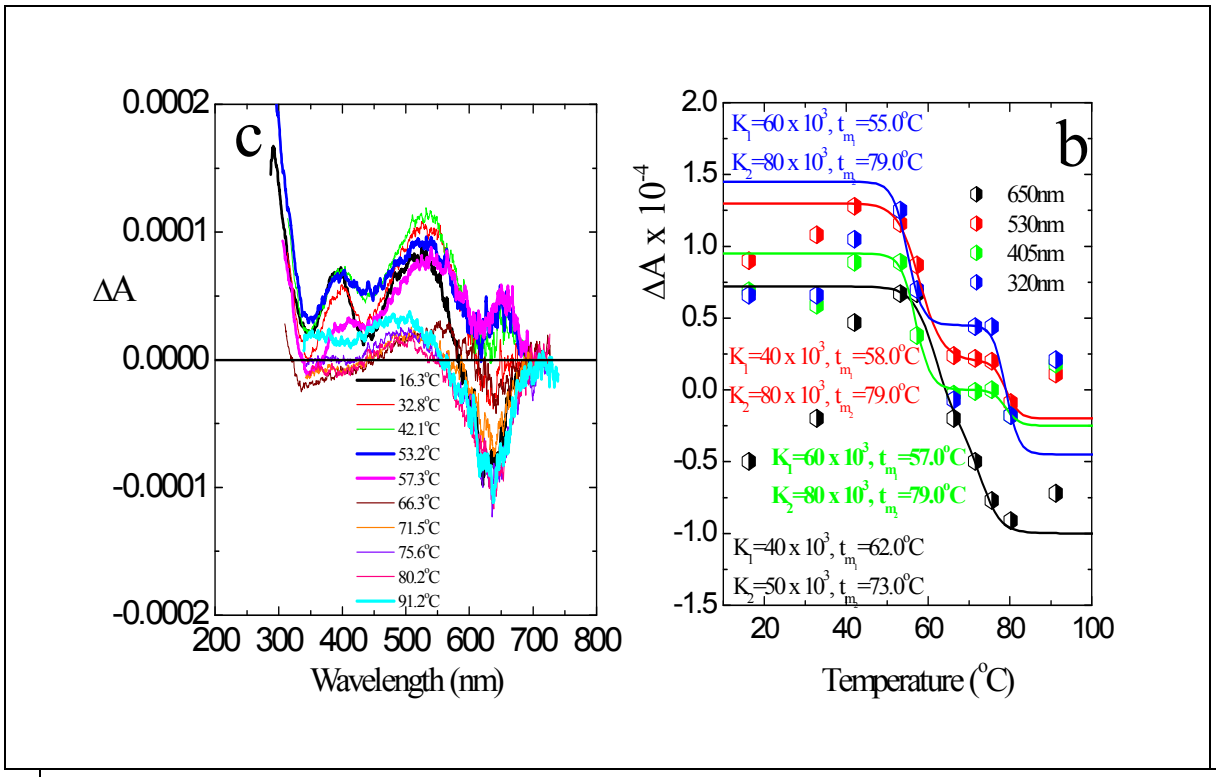

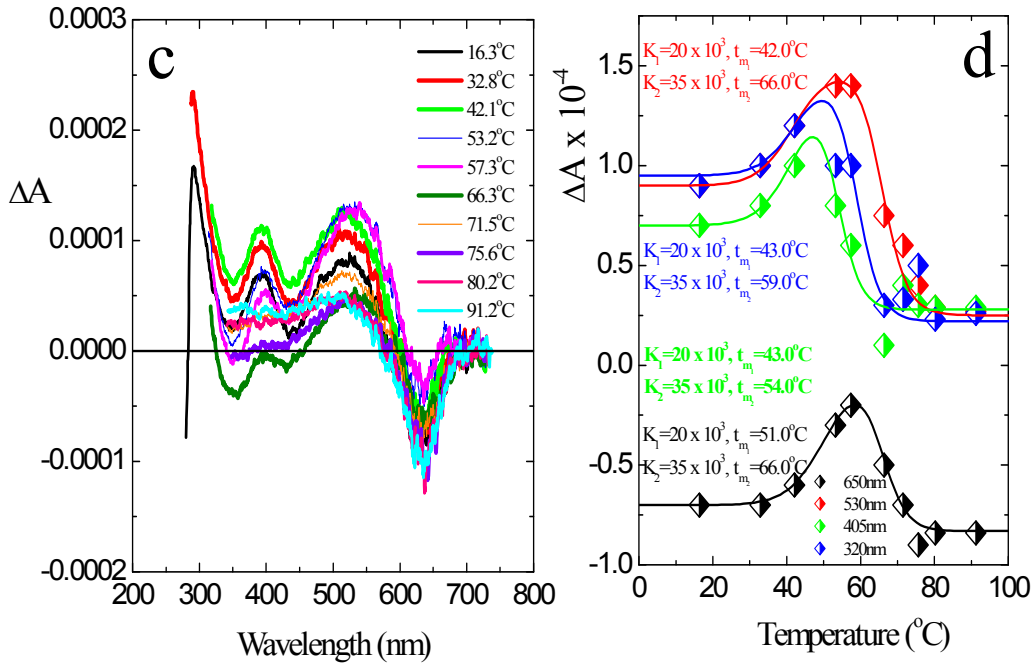

Figure 6.38 Temperature studies of BCG:rHSA at pH 3.56, 1cm cell.

a CD spectra of the temperature study of the complex in B/R buffer, pH3.56, 1cm
b Fixed wavelength plot of the CD spectra of the temperature study at pH3.56
c CD spectra of the quenched temperature samples of the complex in B/R buffer, pH3.56, 1cm
d Fixed wavelength plot of the quenched samples of the complex

6.8.iv. Denaturation Studies of Bromocresol Green:Human Serum Albumin

The addition of small amounts of urea (up to 3M equivalent) to samples of the [2:1] molar ratio equivalent of BCG:rHSA resulted in little to no effect. There was however, loss in binding for samples containing between 4M - 5M equivalent addition of urea. For molar ratios in excess of 5M of urea, an increase in binding of the dye was observed with maximum effect detected at 7M. The value of ΔA at 7M was greater than that found in the absence of urea suggesting facilitated binding and enhancement, and is represented in Figure 6.39.

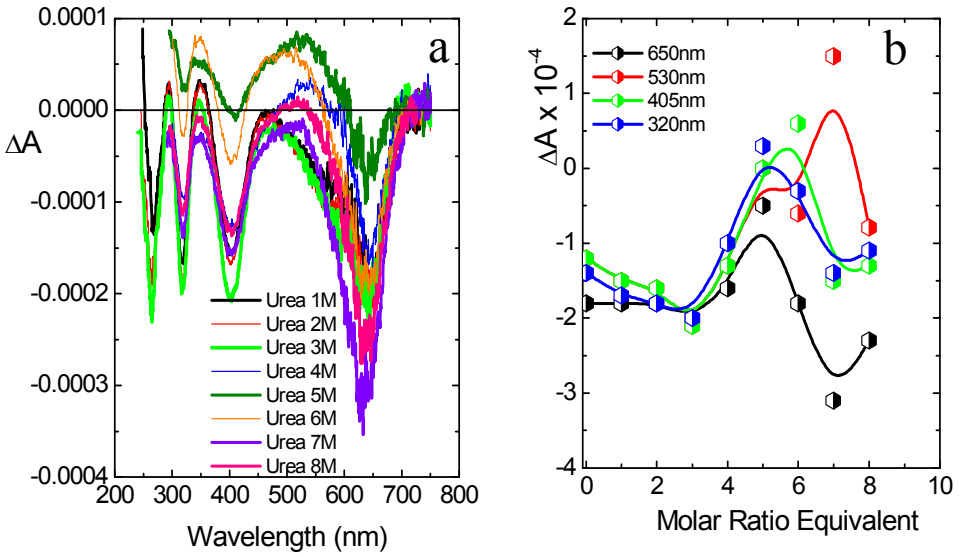

Figure 6.39. Molar titration of BCG:rHSA in Urea, 1cm cell.

a CD spectra of the complex of BCG:rHSA with increasing concentrations of urea in water, 1cm
b Fixed wavelength plot of the CD spectra of the urea titration

6.8.v Microcentrifuged Samples of Bromocresol green:Recombinant Human Serum Albumin

Considering the temperature studies conducted at physiological conditions, the concentration of free dye detected at the lower temperatures were low, indicative that most

of the dye was bound to the protein (Figure 6.40.). For temperatures above 52°C, increasing amounts of free dye were found as the protein became denatured. Between 68 - 76°C a plateau was obtained for wavelength 610nm at the main absorption band. At the other wavelengths, fluctuations where observed with wavelength 590nm producing the greatest absorption of 0.4 at 65°C, after that a small amount of re-association was observed. At wavelength 385nm, low levels of free dye was detected. The micro-centrifuged samples revealed that more than 50% of BCG remained bound to albumin at the end of the experiment, the equivalent of potentially one of the two dye molecules bound.

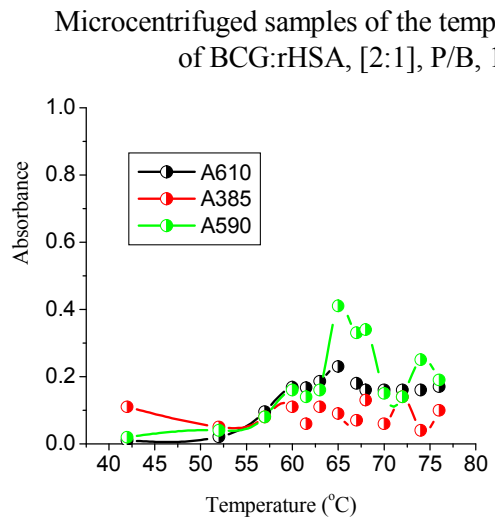

Figure 6.40. Temperature studies of BCG:rHSA at pH7.19, 1cm cell.

Microcentrifuged samples of the temperature studies of BCG:rHSA, [2:1], P/B, 1cm

Considering BCG:rHSA in the denaturant urea, at low molar ratio equivalents, there was little to no detection of the free dye, all the dye was found to be bound to albumin. A 5M equivalent concentration of urea seemed to be the pivotal point where the most significant displacement of dye was observed at all the wavelengths monitored, and specifically at 598nm the absorption detected was 0.7, this equates to 70% displacement of the dye. Again a small amount of BCG remained associated with albumin even under extreme

denaturation conditions, this fact was further supported by the CD measurements that revealed the magnitude and sign of the CD spectra.

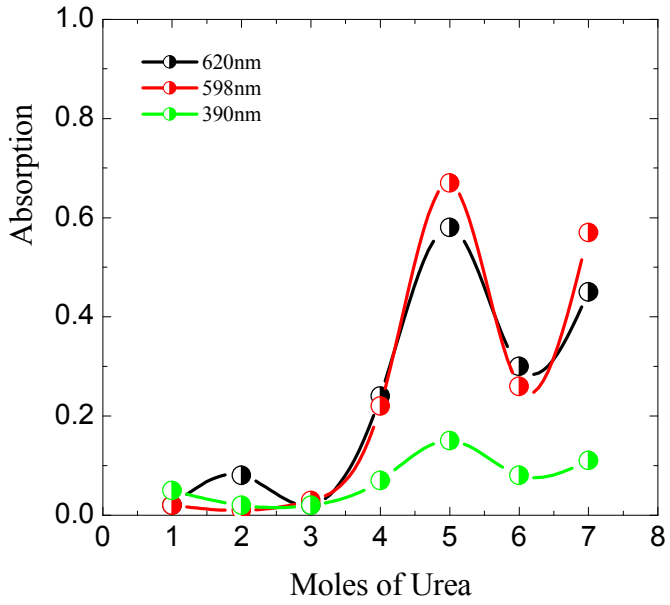

Figure 6.41. Microcentrifuged Samples of the BCG:rHSA complex

CHAPTER 7

CHAPTER 7: Conclusion and Further Discussion

7.1. Final Conclusion

Albumin has lived up to it reputation of being a multi-faceted, resilient protein, willing to participate in any biological activities, facilitating the fast, but effective transport of ligands that bind with high affinity. Albumin's resilience to heat denaturation was demonstrated when heating the protein to temperatures exceeding 85^{o}C (Figure 4.7. – 4.11.). The anticipated collapse in structure was not achieved, there was still a noticeable amount of secondary structure detected with estimations of between 15 - 20% of α-helix and the same amount in β–sheet found. The loss in secondary structure was found to come from the conversion of α-helix that was converted mainly into irregular structure with a minimal gain in β-sheet. There was a mirrored effect observed between changes in irregular structure and β-sheet, a trend what was reflected in all of the albumin samples studied including the glycosylated sample (L27). The only exception was found in the domain I fraction that contained an unusually high amount of irregular structure (Figure 4.10.c.). The high irregularity may be an artefact of the method of preparation of the fraction, or more likely to be caused by the incomplete folding of the remaining protein in the absence of the other domains. Whatever the reason, domain I's predominant structure was found to be irregular structure that was in contrast to that found in the other samples.

Considering the glycoylated sample, the modifications seen in the secondary structure did not influence the performance of this protein towards heat; the structural changes seen in the other forms were evident here. Heating all the whole albumin samples through a second temperature cycle did not evoke much spectral changes. Most of the denaturation was caused in the first temperature cycle, and further changes in the protein were shielded, and suggested that there was a core of residual structure that could not be penetrated. This

core was thought to exist in domain III, with domain II seeming to be the most susceptible to heat denaturation.

Albumin unfolded occurred in a series of transitions or steps that appeared to reflect subdomain denaturation (Figure 4.12.b.), suggested the hypothesis that heat could be used as a means of partially unfolding the protein, thus selectively interfering with possible binding sited. The hypothesis was further supported by the fact that albumin retained the structure to which it was heated (Figure4.14) with little to no recovery on cooling. The resultant protein acted like a template for partial denaturation. The effects on the binding of albumin in the presence of a drug with increasing temperature revealed that for domain IIA binding ligands (e.g. warfarin), the dissociation was almost instant (Figure 5.25.). However, re-association of the drug occurred once the temperature dropped, provided that the protein was not heated to temperatures above 60 ^{o}C. The loss in binding was evoked on initiation of heating. For domain IIIA binding (e.g. diazepam), a state of equilibrium existed for temperature up to 45^{o}C, above this temperature displacement was seen with the rapid loss in binding (Figure 5.32.). By comparison, the two melting and quenching profiles of the association between albumin and warfarin and diazepam were completely different, possible being a reflection of the different sites that the two drugs bind to. DIS, being an example of a ligand that binds to both sites, reflected a combination of both sites (Figure 5.61. & 62.).

Dye binding was also investigated with temperature, with the use of different pH values coupled to the reaction. Dyes, also bind to domain IIA, like other site-specific markers displayed dissociation on heated (Figure 6.6.). Lowering the pH to pH4.4 and pH 3.56 evoked greater stability in both cases (Figure 6.8. & 6.10.) in the region where loss was previously detected, although the amount of dye that bound was greatly reduced, a trend that was exhibited for all the dyes studied.

pH effects were shown to play a pivotal role on structural conformations of albumin, promoting elongation of the molecule with decreasing pH. The robustness of albumin in isolation, with changing pH, demonstrated the relative stability that exists between the pH values of pH4 to pH10. Several ions while bound to albumin were chosen for further investigations on their pH effects, and were found not to be drastically affected by the physical changes in albumin within the range of pH3 to pH10. The dyes proved to be the ligands that showed significant change with changing pH. In PR there was a complete CD spectral reversal at pH3.55 and pH2.65. The effect of pH in conjunction with temperature with the dyes highlighted the relative stability of the binding site to temperatures approaching 50^{o}C.

The effects of multiple binding to albumin proved promising when studied by CD. It was possible to see the effect of both drugs binding to albumin for non-competitive ligands binding to different sites, and it was possible to subtract the effects of one drug to reveal the effect of the other. Monitoring was possible in the cocktail for ligands that absorb at different wavelengths of the absorption, sufficiently removed to distinguish their absorption maxima. The results postulated the possibility of taking a ligand whose binding properties to albumin was unknown, and by the use of ligands of known binding sites on albumin it may be possible to determine which binding site the unknown ligand binds.

7.2. Further Discussion

The results in this thesis are exciting, revealing possibilities for further work that can be done in order to further characterise the albumin molecule. pH studies are known to induce different conformational structure, however, the use of temperature was not appreciated. Temperature studies in the thesis has highlighted the conformational rigidity of albumin and the ability to isolate different conformational forms, perturbing the different domains in albumin depending on what temperature the protein is heated to. More work is needed to isolate and fully characterise the conformations formed with a view to elucidate the binding sites present. Further work is also needed to look at the unfamiliar subdomains such as subdomain IB, suggested to play a pivotal role in the binding activity of some ligands binding to subdomain IIA. The possibility of the temperature studies may well offer a possible route of clarification.

rHSA offered a possible therapeutic alternative to natural human albumin. The results obtained in this thesis showed that it was equally as good as its human counterpart without the obvious health risk. It was also possible to produce is in sufficiently large quantities relative cheaply. More work is needed on a more diverse range of drugs and ligands to validate better the initial finding. If proven correct over an adequate range of ligands then its findings will be significant.

Finally, the Mathcad fits of single site binding proved to be an essential asset for determining binding constants of a simple one to one binding relationship. However, when two or more ligands were involved involving more than one site, it became disproportionately difficult to fit with no obvious or simple solution. More work is needed to properly formalise this with a view to making the determination of multiple binding and the determination of their associated binding constants easier.

CHAPTER 8

CHAPTER 8: References

A

Abrahart, E., 1977, Dyes & Their Interactions, Edward Arnold (Publishers) Ltd.

Abrahant, E. N., 1977, Dyes and their Intermediates, 2"d Editon, published by Edward Arnold Ltd.

Aguanno, J. and Ladenson, J., 1982, J. Biol. Chem., 257, 8745-8748.

Ahmad, B., Khursheed, M., Khan, A., Khatun Haq, S. and Hasan Khan, R.,2003, Biochem. Biophys. Research Commum., Vol 314, 166-173.

Ahmad, B., Ahmed, M., Haq, S. and Khan, R., 2005, Biochim. et Biophy.- Proteins & Proteomics, Vol 1750, Iss. 1, 93-102.

Aki, H. and Yamamoto, M., 1992, Chem. Pharm. Bull., 40, 1553-1558.

Aki,H. and Yamamoto, M., J. Pharmaceutical Sci., 1994, 83, 12, 1712-1716.

Alebić-Kolbah, T., Kajfež, Rendić, S., Sinjić, V., Konowa, A. and Snatzie, G., 1979, Biochem. Pharm., 28, Iss, 16, 2457-2464.

Alexander, P. and Hamilton, I, 1968, Arch. Biochem. Biophys., 88, 128-135.

Alexander, M., Ambre, J., Liskow, B. and Trost, D., 1979, J. Am. Med. Assoc., 241, 2527-2529.

Anderegg, J., Beeman, W., Shulman, S. and Karsberg, P., 1955, J. Am. Chem. Soc., 77, 2927-2937.

Anderson, L. O., 1966, Biochem. Biophys. Acta, 117, 115-133.

Anderson, O., 1969, Arch. Biochem. Biophys., 133, 277-285.

Anderson, S. and Weber, G., 1969, Biochem., 8, 371-377.

Anfinsen, C. and Haber, E., 1961, J. Biol. Chem., 236, 1361-1363.

Aoki, K. and Foster, J. F., 1957, J. Am. Chem. Soc., 79, 3393-3396.

Aoki, F., Sato, K., Nagoaka, S., Kamada, M. and Hiramatsu, K., 1973, Biochim. Biophys. Acta, 328, 323-333.

Arakawa, T. and Timashelf, S., 1984, Biochem., 23, 5912-5923.

Artali, R., Bombieri, G., Calabi, L. and Del Pra, A., 2005, II Faemaco, 60, Iss. 6-7, 485-495.

Ascenzi, P., Bocedi, A., Notari, S., Fanali, G., Fesce, R. and Fasano, H., 2006, Med. Chem. 6,

No: 4, 483-489.

Ascoli, G., Bertucci, C. and Salvadori, J. Pharmaceutical Sci., 84, 6, 737-741.

Ashbrook, J., Spector, A. and Fletcher, J., 1972, J. Biol. Chem., 247, 7038-7042.

Ashbrook, J., Spector, A., Santos, E. and Fletcher, J., 1975, J. Biol. Chem., 250, 2333-2338.

Atkinson, A., Hammond, P., Hartwell, R., Hughes, P., Scawen, M., Sherwood, R., Small, D., Bruton, C., Harvey, M. and Lowe, C., 1981, Biochem. Soc. Trans., 9, 290.

B

Banaskak, L., Winter, N., Xu, Z., Bernlohr, D., Cowan, S. and Jones, T., 1994, Adv. Protein Chem., 45, 89-151.

Banfield, C., O'Reilly, R., Rowland, E. and Rowland, M., 1983, Br. J. Clin. Pharmac., 16, 669-675.

Bargren, G. and Routh, J., 1974, Clin. Biochem., 7, 290-296.

Barlow, W. and Klopfenstein, W., 1980, Biochim Biophys. Acta, 620. 18-23.

Batra, P., Sasa, K., Uchi, T. and Takeda, K., Int. J., 1989, Biochem., 21, 857-862.

Baxter, J., 1964, Arch. Biochem. Biophys., 108, 375-383.

Bayner, J. and Thorpe, S., 1981, Arch. Biochem. Biophys., 206, 372-379.

Beaven et al., 1973, Eur. J. Biochem, 33, 500-510.

Beaven, G., Chen, s., Albis, A. and Gratzer, W., 1974, Eur. J. Biochen,41, 539-546.

Behrens, P., Spickerman, A. and Brown, J. 1975, Fed. Proc., 34, 591

Bendedouch, D. and Chen, S., 1983, J. Phys. Chem., 87, 1473-1477.

Benson, E. and Hallaway, B., 1970, J. Biol. Chem., 245, 4144-4149.

Berfucci, C., Canepa. A., Ascoil, G., Guimmaraes, L. and Felix,G., 1999, Chirality, 11, 675-679.

Betsy, J., Hart, T., Wilting, J. and De Gier, J., 1986, Biochemical Pharmacol. 35, 6, 1005-1009.

Bhattacharya, A., Grune, T. and Curry, S., 2000, J.Mol. Biol. 303, 721-732.

Bifriger, Wright and Thompson, 1975, Biophys. Biophys. J. 15, 137-141.

Biochemical & Biophys. Research Communications, 2000, 277, 83-88.

Biophys Acta, 328, 323-333.

Birkett, D., Myers, S. and Sudlow, G., 1977, Mol, Pharmacol., 13, 987-992.

Birkett, D., Myres, S. and Sudlow, G., 1978, Clin. Chim. Acta, 85, 253-258.

Blaabjerg, O. and Hyltoft, P., 1979, J. Clin. Lab. Invest., 39, 751-757.

Blauer, G. and Sund, H., 1978, Transport by Proteins, Walter de Gruyter & Co., Berlin – New York

Bloomfield, V., 1966, Biochem., 5, 684-689.

Bloomfield, V., 1967, Biopolymer, 5, 135.

Bohney, J. and Feldhoff, R., 1992, Biochem. Pharmacol., 43, 1829-1834.

Booker et al, 1942, Rev. Mod. Phys., 1942, 275.

Bos, O., Remijn, J., Fischer, M., Wilting, J. and Janssen. L., 1988, Biochem. Pharmacol., 37, 3905-3909.

Bos, O., Fischer, M., Wilting, J. and Janssen, L., 1988, Biochim. et Biophys. Acta, 37-47.

Bos, O., Ladro, J., Fischer, M., Wilting, J. and Janssen, l, 1989, J. Biol. Chem., 264, 953-959.

Bothorel, P. and Desmazes, J., 1974, Biochim. et Biophys. Acta, 365, 181-192.

Bowman, B., 1969, Biochem., 8, 4327-4335.

Bowmer, C. and Landup, W., 1982, Biochen. Pharmacol. 31, 319-323.

Boyer, P., Lum, f., Ballou, G., Luck, J. and Rice, 1946, J. Biol. Chem., 162, 181-196.

Bradbury, J. and Norton, R., 1973, Biochim. Biophys.Acta, 328, 10-19.

Bradford, A., 1976, Anal. Biochem. 72, 248-254.

Bramanti, E. and Benedetti, E., 1996, Biopolymers, 38, 639-653.

Brand, J. and Toribara,U., 1972, Mol. Pharmoc., 8, 751-758.

Brandt, J. and Andersson, L., 1976, Int. J. Peptide Protein Res., 8, 33-37.

Brodersen, R., Sjödin, T. & Sjöholm, 1977, J. Biol. Chem., 252, 5067-5072.

Brown, J., 1974, Fed. Proc., 33, 1389.

Brown, J., 1975, Fed. Proc., 34, 591.

Brown, N. A., Jahnchen, E., Muller and Wollert, U., 1976, Mol. Pharmac., 13, 70-79.

Brown, J., 1977, Rosenoer, V., Oratz, M. and Rothschild, M., Albumin, Structure, Function and Use, Pergamon Press, Oxford, 27-51.

Brown, N., Jahnchem, E., Miller, W. and Wollert, U., Mol. Pharmacol., 1977, 13, 70-79.

Buchholz, L., Cai, C., Andress, L., Cleton, A., Brodfuehrer, J. and Cohen, L., 2002, Eur. J. Pharm. Sci.,15, 209-215.

Bui, T., 1998, Thesis, Kings College London.

Bull, H., 1944, J. Am. Chem. Soc., 66, 1499

Burkbard, R. Moore, F. and Louloude, S., 1961, Arch. Biochem. Biophys., 94., 291-300.

Burton, S. Quirk, A. and Wood, P., Eur. J. Biochem., 179, 379-387.

Bury, L., 1935, J. Amer. Chem. Soc., 57, 2115.

C

Callaghan, P. and Martin, N., 1962, Biochem. J., 83, 144-151.

Campbell, I. and Dwek, R., Biological Spectroscopy, Uni. of Oxford, The Benjamin/Cummings Publishing Company Inc.

Carter, C. C., Min He, X., Munson, S. H., Twigg, P. D., Gemert, K. M., Broom, M. B. and Miller, T. Y., 1989, Science, 244, 1195-1198.

Carter, C. C. and Min He, X., 1990, Science, 249, 302.

Carter, C. C. and Min He, X., 1992, Nature, 358, 209-214.

Carter, D. and X. Ho., J., 1994, Adv. Protein Chem., 45, 153-203.

Chatterjee & chatterjee, 1965, J. Mol. Biol., 11, 432-437.

Chen, R., 1966, Biochim. Biophys. Acta, 120, 169-171.

Chen, R. F., 1967, J. Biol. Chem., 242, 173-181.

Chen, R., Yang, J. and Martinez, H., 1972, Biochem., 11, 4120-4131.

Chen, J. and Hage, D.,2004, Nature Biotechnology, 22, 1445-1448.

Chignell, C. F., 1970, Molec. Pharmac., 6, 1.

Chignell, C. F., and Starkweather, D. K., 1971, Molec. Pharmac., 7, 227.

Chignell, C. F., and Starkweather, D. K., 1971, Molec. Pharmac., 7, 229.

Choonara, A., Chohton, S., Hayes, B. P., Brickenridge, A. M. and Park, B., Br. J. Clin. Pharmac., 1986, 21, 271-277.

Chou. P and Fasman, G., 1974, Biochem. 13, 222-245.

Chuang, V. and Otagiri, M., 2006, Chirality, 18, 159-166.

Clark, D, Smith, L. and Wilson, D., 1988, J. Colloidal Interface Sci. 121, 136-137.

Clonis, Y., Goldfinch, M. and Lowe, C., Biochem. J., 1981, 197, 203.

Coates et al., 1967, J.S.D.C., 83, 101.

Cohen, E., 1941, Chem. Rev., 28, 395-417.

Compton, L. and Johnson., W., 1986, An. Biochem. 155, 155-167.

Cornell, C. and Kaplan, L., 1978, Biochem., 17, 1750-1754.

Cornell, C. and Kaplan, L., 1978, Biochem., 17, 1755-1758.

Curry, S., Mandelkow, H., Brick, P. and Franks, N., 1998, Nature Structural Biol., 5, 827-835.

Curry, S., Brick, P. and Franks, N., 1999, Biochim. Biophys.Acta, 1441, 131-140.

Curry, S., Ghuman. J., Zunszain. P., Petitpas, I., Bhattacharya. A., and Otangiri. M., 2005, Journal of Molec. Bio., Vol 353, Iss 1, 38-55.

Curry et al., 1935, J. Amer. Chem. Soc., 57, 345.

D

Damodaran, s., 1986, Int.J. Pept. Protein Res, 27, 589-596.

Dean, J., Lange's Handbook of Chemistry, 14th Ed.

Deutch et al, 1991, Adv. Cancer Res., 56, 253-312.

Devlin, T., 1997, Textbook of Biochemistry with Clinical Correlation, Wiley-Liss Inc., New York Publishers.

Diana, F., Veronich, K. and Kapoor. A., 1987, J. Pharmaceutical Sci., 78, 3, 195-199.

Dill, K. and Shortle, D., 1991, Annu. Rev. Biochem., 60, 795-825.

Dockal, M., Carter, D. and Ruker, F., 1999, J. Biol. Chem., 274, No. 41, 29303-29310.

Dockal, M., Carter, D. and Ruker, F., 1999, J. Biol. Chem., 275, 5, 3042-3050.

Dockal, M., Carter, D. and Ruker, F., 2000, J. Biol Chem., 275, Iss. 5, 3042-3050.

Dockal, M., Chang, M., Carter, D. and Ruker, F., 2000, Protein Sci., 9, 1455-1465.

Doumas, B., Watson, W. and Biggs, H., 1971, Clin. ChimActa, 31, 87-96.

Drake,A., 1994, Methods in Mol. Biol., 22, Ed. Jones, C., Mulloy, B. and Thomas, A.

Drake, A., 2001, Protein-Ligand Interactions, Structure & Spectroscopy, Ed. S. Harding, & B. Chowdhry, Oxford University Press.

Dröge, A., Janssen, L. and Wilting, J., 1982, Biochem. Pharmacol., 31, 3781-3786.

Dröge, A., Janssen, L. and Wilting, J., 1983, Pharm. Weekbl. Sci., 5, 5, 228-233.

Dröge, A., Janssen, L. and Wilting, J., 1988, Biochem.. J., 250, 443-446.

E

Edwards, R. and Woody, 1979, Biochem., 18, 5197.

Edsall, J., Edelhoch, H., Lontie, R. and Morrison, P., 1950,

Edsall, J. and Gutfreund, 1983, Biothermodynamics. The Study of Biochemical Processes at Equilibrium, John Wiley & Sons Ltd.

Edward, F., Rombauer, R. and Campbell, B., 1969, Biochim. Biophys. Acta, 194, 234-245.

Ellis, R. and Van der Vies, M., 1991, Annu. Rev. Biochem., 60, 321-347.

F

Fanali. G., Ascenzi. P. and Fasano M., 2007, Biophy. Chem. Vol 129, Iss. 1, 29-35.

Fehske, K., Schlafer, U., Wollert, U. and Muller. W., 1981, Mol. Pharmacol., 21, 387-393.

Fehske, K., Muller, W. and Wollert, U., 1981, Biochem. Pharmacol., 30, 7, 687-692.

Feng, H., Vu, N. and Bal, Y., 2004, J. Mol. Biol., 343, Iss. 5, 1477-1485.

Figge et al., J. Clin. Med., 117, 453-467.

Fitos, I., Visy, J., Simonyl, M. and Hermansson, J., 1999, Chirality, 11, 115-120.

Fitos, I., Visy, J. and Kardos, J., 2002, Chirality, 14, 5, 442-448.

Fitos, I., Visy, J., Zsila, F., Mády, G. and Simonyi, M., 2007, Biooranic & Med. Chem., 15, Iss. 14, 4857-4862.

Fiume, L., Bassi, B., Bongini, A., 1988, Pharm Acta. Helv., 63, 137-139.

Flora, K., Brennan, J., Baker, G., Doody, M. and Bright, F., 1998, Biophys. J., 75, 1084-1096.

Foster, j., 1960, The Plasma Proteins, Vol. I, Putnam, F. W., Ed., New York, Academic Press, 179-239.

Foster et al., 1974, Biochem., 13, 17, 3465-3471.

Foster, J., 1977, Albumin Structure, Function and Uses, Rosenoer, V., Oratz, M. and Rotthschild, M., Pergamon, Oxford, 58-84.

G

Geisow, M. and Beaven, G., 1977, Biochem. J., 161, 619-625.

Geisow, M. and Beaven, G., 1977, Biochem. J., 163, 477-484.

Gerig, J., Katz, K. and Reinheimer, J., 1981, Organic Magnetic Resonance, 15, 2, 158-161.

Ghuman, J., Zunszain, P., Petitpas, I., Bhattacherga, A., Otagim, M. and Curry, S., 2005, J. Mol. Biol., 353, 38-52.

Gill, S. and Hippel, P., 1989, Analytical Biochem., 182, 319-326.

Glaumann, H., 1970, Biochim. et Biophys. Acta, 224, 206-218.

Goldsworthy, P. and Volwiler, 1958, J. Biol. Chem., 230, 817.

Gronenborn, M. and Clore, G., 1994, Protein, Structure, Functionand Genetics,19, 273-276.

Guillaume, Y., Guinchard, C. and Berthelot, A., 2000, Talanta, 53, Iss. 3, 561-569.

Gulyassy, P., Bottini, A., Stanfel, B., Jarrard, E. and Depner,T., 1986, Kidney International, 30, 391-398.

Gurachevsky, A., Shimanovitch, E., Gurachevskaya, T. and Muravsky, V., 2007, Bioche. Biophys. Research Communication, 360, Iss. 4, 7, 852-856.

H

Haddock, R., and Trager, 1975, J. Med. Chem., 18, 5, 519-523.

Hamer, et al., 1936, Proc. Roy. Soc. Lon., A154, 73.

Hamer, et al., 1937, Proc. Roy. Soc. Lon., A163, 138.

Hammes, G., 2000, Thermodynamics and Kinetics For The Biological Science, Wiley Interscience, A John Wiley & Son, Inc., Publication.

Hanai, T., Koseki, A., Yoshikawa, R., Ueno, M., Kinoshita, T. and Homma, H., 2002, Analytica Chimica Acta, 454,101-108..

Hanggi, D. and Carr, P., 1985, 149, 91-104.

Harmsen, B., De Bruin, S., Janssen, L., Rodrigues de Miranda, J. and Van Os, G., 1971, Biochem., 10,3217-3221.

Harris, D. and Bashford, c., Spectrophotometry & Spectrofluorimetry, a Practical Approach.

Hart et al, 1986, Biochem. Pharmacol., 35, 1005-1009

He, X. and Carter,D. 1992, Nature, 358, 209-215.

Hennessey, J. and Johnson, C., 1981, Biochemistry, 20, 1085-1094.

Herskovitz, T. and Laskowski, M., 1962, J. Biol. Chem., 237, 2481-2492.

Heyningen, S., 1973, Biochim. et Biophys. Acta, 328, 303-313.

Ho, J., Holowachuk, E., Norton, E. Twigg, P. and Carter, D. 1993, Eur. J. Biochem., 215, 205-212.

Honoré, B. and Brodersen, R., 1988, Anal. Biochem, 171, 55-56.

Hughes, W., 1954, The Protein, Edited By: Neurath, H. and Beley, K, 26, 663, Academic Press, New York.

Hughes, W. L., 1954, The Protein, H. Academic Press, New York, Vol. IIB.

Huges, P., Lowe, C. and Sherwood, R., 1982, Biochim. Biophys. Acta, 700, 90.

Huges, P., Lowe, C. and Sherwood, R., 1982, Biochem. J., 205, 453.

Hulim, A., Kadir, H. and Tayyab, S., 2008, J. Biolchem., 144, 32-38 (doi:10.1093/jb/mvn036)

I

Itoh, T., Nakashima, K., Tsuda, Y. and Yamada, H., 1996, Chirality, 8, 201-206.

J

Janssen, L., Wilgenburg, M. and Wilting, J., 1981, Biochem. Biophys. Acta., 669, 2, 244-250.

Janssen, L., Dröge, J., Durlinger, F. and Fruytier, F., 1985, J. Biolog. Chem., 260, 21, 11442-11445.

Janssen, L, Dröge, A. and Wilting, J., 1988, Biochem.. J., 250, 443-446.

Johnson, W. C., 1996, Circular Dichroism and the Conformational Analysis of Biomolecules, Ed. Gerald D. Fasman Plenum Press, New York.

Jones, C., Mulloy, B. and Thomas, A., 1994, Methods in Molecular Biology, 22, Microscopy, Optical Stectroscopy, and Macroscopic Techniques, Humana Press Inc., Totowa, NJ.

Jones, G. and Clarke, D., 2003, Faraday Discuss., 126, 223-236.

K

Kaminsky, L., Dunbar, D., Wang, P., Beaune, p., Larrey, D., Guengerich, F., Schnellmann, R. and Sipes, I., 1984, Am. Soc. Pharmacol. Experim. Therapeutics, 12, 4, 470-477.

Kamisaka, K., Listowsky, I., Betheil, J. and Arias, I., 1974, Biochim.et Piophys. Acta, 365, 169-180.

Khan et al., 1986, Biochem. J., 236, 307-310.

Kim, B., Kadir, H. and Tayyab, S., 2008, 11, 20, 2418-2422, (ISSN 1028-8880)

King, T. and Spencer, M., 1970, J. Biolog. Chem., 245, 22, 6134-6148.

Klotz, I., 1946, Arch. Biochem, 9, 109-117.

Klotz, I. and Hunston, D., 1979, Arch. Biochem. & Biophys., 193, 2, 314-328.

Klotz et al., 1961, Am. J. Physiol., 2000, 1301-1306.

Kober, A., Ekman, B. and Sjöholm, 1978, J. Pharmaceut. Science, 67, 1, 107-109.

Kratochwil N. A., Huber W., Muller F., Kansy M., and Gerber P. R., 2002, Biochem Pharmacol,

64 (9): 1355 — 74.

Kragh-Hansen, U., 1983, Biochem. Pharmacol., 32, 18, 2679-2681.

Kragh-Hansen, U., 1985, Biochem. Pharm., 32, No. 8, 2679-2681.

Kragh-Hansen, U., 1985, Biochem. J., 225, 629-638.

Kragh-Hansen, U., 1988, Mol. Phamacol., 34, 160-171.

Kragh-Hansen, U., 1990, Danish Medical Bulletin, 37, 57-85.

Kragh-Hansen, U., Brennan, S. O., Galliano, M. and Sugita, O., 2000 Mol. Pharmacol. 37, 238-242.

Kragh-Hansen, U., Chuang, V. and Otagiri, 2002, Biol. Pharm. Bull., 25, 6, 695-704.

Kranjc, Z. and Lapanje, S., 1993, Int. J. Peptide Protein Res., 42, 320-325.

Kratochwell, N., Humber, W., Muller, F., Kansy, M. and Gerber, 2002, Biochem. Pharmacol., 64, 1355.

Krishnakumar, S. and Panda, D., 2002, Biochemistry, 41, 7443-7452.

Kuntz, I. D. Jr. and Kauzmami, W., 1974, Adv. Protein Chem., 28, 239-345.

L

Labaune,J., Handbook of Pharmacokinetics, Toxicity Assessment of Chemicals, Ellis Horwood Ltd.

Lagercrantz, C. and Larsson, T., Biochem. J., 1983, 213, 387-390.

Lee, J. and Hirose, M., 1992, J. Biolog. Chem., 267, 21, 14753-14758.

Leonard, W., Vijai, V. Foster, J., 1961, J. Biol. Chem. 236, 2662-2669.

Leonard, W., Vijai, V. Foster, J., 1963, J. Biol. Chem. 238, 1984.

Lightner, D. and Gurst, J., 2000, Organic Conformational Analysis and Stereochemistry from CD Spectroscopy, John Wiley & Sons Inc.

Loannides,C., 2008, Cytochromes P450: Role in the Metabolism ans Toxicity of Drugs and other Xenobiotics, Royal Soiety of Chemistry, p521.

Lowe, C., Spibey, H. and Drabble, W., 1980, Anal. Biochem., 104, 23.

Lowe, C., Small, D. and Atkinson, A., 1981, Int. J. Biochem., 13, 33.

Luetscher, J. A., 1939, J. Am. Chem. Soc., 61, 2888-2890.

Luft et al., 1983, Biochem., 22, 5978-5981.

M

Maes, V., Hoebeke, J., Varcugsse, A. and Kanarek, L., 1979, Molec. Pharmac., 16, 147.

Mc.Ardell, j., Atkinson, A. and Bruron, C., 1982, Eur. J. Biochem., 125, 361.

MacKay, D., Panjehshahin, M. and Bowmer, C., 1991, Biochem. Pharmacol., 41, 12, 2011-2018.

Mc.Lachlan, A. D., Walker, J. E., 1977, J. Mol. Biol., 112, 543-558.

Malik, K., 1997, Thesis, Birkbeck College, University of London.

Maruyama, K., Nishigori, H. and lwatsuru, M., 1985, Che. Pharm. Bull. 33, 11, 5002-5012.

Maruyama, T., Lin, C., Yamasaski, K., Miyoshi, T., Imai, T., Yamasaski, M. and Otagill, M., 1993, Biochem. Pharmac., 45, No. 5, 1017-1026.

Mason, S. F., 1988, Biochem. Pharmacol., 37, 1-7.

Mason, S. F., 1989, Chirality, 1, 183-191.

Meloun, B., Moravek, L. and Kostka, V., 1975, FEBS Letters, 58, 134-137.

Mendham, J., Penney, R., Barnes, J. and Thomas, M., 2000, Vogel's Textbook of Quantitative Chemical Analysis, 6th Ed.

Miller, J. and Smail, G., 1977, J. Pharm. Pharmacol., 29, 330.

Minghetti, P. P., Ruffner, D. E., Kuang, W. J., Demiison, O. E., Hawkins, J. W., Beattie, W. G. and Dugaiczyk, A., 1986, J. Biol. Chem., 261, 6747-6757.

Moreno, F., Cortijo, M. and Gonzalez-Jimenez, J., 1999, Photochem. & Photobiol.,

Murachi, T., Biochim. Biophys. Acta, 71, 1963, 239-241.

Mullert, W. E., Wollert, U. and Naunyn-Schmiederberg, 1973, Arch. Pharmac., 280, 22.

Mullert, W. E., Wollert, U. and Naunyn-Schmiederberg, 1974, Arch. Pharmac., 283, 67.

Muzammil, S., Kumar, Y. and Tayyab, S., 2000, Protein: Structure, Function and Genetics, 40, 29-38.

N

Nakanishi, K., Berova, N. and Woody, R., 1994, Circular Dichroism, Principles and Applications, VCH Publishers Inc.

Nishio, T., Takamura, N., Nashii, R., Takamura, J., Yoshimoto, M. and Kawai,K., 2008, 23, 2304-2310.

Noel, J. and Hunter, M., 1972, J. Biol. Chem, 247, 7391-7406.

Notterman, D., Drayer, D., Metakis,L. and Reidenberg, M., 1986, Clin. Pharmacol. And Therapeutics, 40, 5, 511-517.

O

Octaaf, J. M., Fischer, J., Wilting, J. and Janssen, L., 1988, Biochem. Pharmacol., 953, 37-47.

Octaaf, J. M., Fischer, J., Wilting, J. and Janssen, L., 1989, Biochem. Pharmacol., 38, 12, 1979-1989.

Otagiri, M. and Otagiri, Y, and Perrin, 1979, Int. J, Pharm. (Amst.), 2, 283-294.

P

Panjehshahin, M. R., Browmer, C. J. and Yates, M. S., 1989, Biochem. Pharmacol. 38, 155-159.

Panjehshahin, M. R., Browmer, C. J. and Yates, M. S., 1989, Biochem. Pharmacol. 41, 2011-2018.

Panjehshahin, M. R., Browmer, C. J. and Yates, M. S., 1989, Biochem. Pharmacol. 44, 873-879.

Panjehshahin, M. R., Browmer, C. J. and Yates, M. S., 1991, Biochem. Pharmacol. 41, 1227-1233.

Panjehshahin, M. R., Browmer, C. J. and Yates, M. S., 1991, Biochem. Pharmacol. 41, 2011-2018.

Panjehshahin, M. R., Browmer, C. J. and Yates, M. S., 1992, Biochem. Pharmacol. 44, 873-879.

Panjehshahin, M. R., Browmer, C. J. and Yates, M. S., 1993, Proceedings of the 2"d European Conference on Vetinary Drug Residues (European Conference ll), Vol. II, 509-513.

Patersen, C., Ha, C.,Curry, S. and Bhagavan, N., 2002, Protein: Structure, Function and Genetics,

47, 116-125.

Paulsen, O., Nilsson,L., Saint-Salva, B., Manuel, E. and Lunell, E., 1988, Pharmacol. & Toxicol., 63, 215-220.

Pearce, A., Irons, L., Robinson, A. and Seabrook, R., 1992, 283, 823-828.

Pearson, W. R., 1990, Methods in Enzymology, 183, 63-98.

Pedersen, A. O. and Jacobsen, J., 1980, Eur. J. Biochem, 106, 291-295.

Penniston, J., 1982, Exp. Eye. Res., 34, 435-443.

Perrin, H. J. and Nelson, D., 1973, J. Pharm. Pharmac., 25, 125-130.

Perry, J., Goldsmith, M., Williams, T., Radack, K., Christensen, T., Gorham, J., Pasquinell, M., Toone, E., Beratan, D. and Simon, J., 2006, Photochemistry and Photobiology, 82, 1365-1369.

Peters, T. Jr., 1985, Adv. Protein Chem, 37, 161-249.

Peters, T. Jr., All About Albumin, Academic Press Ltd., U.K. Publishers, 1996,

Petitpas, I., Grune,T., Bhattacharya, A. and Curry, S., 2001, J. Mol. Biol., 314, 955-960.

Patitpas, I., Bhattacanrya, A., Twine, S., East, Malcolm and Curry, S., 2001, J. Biol. Chem., 276, 22804-22809.

Phillips, R. and Marmorstein, R., 1988, Arc. Biochem. Biophys., 262, 1, 337-344.

Pinckard,R., Hawkins,D. and Farr, 1970, Arthritis and Rheumatism, 13, 4, 361-368.

Pinnell,A and Northan, B., 1978, Clin. Chem., 24, 1, 80-86.

Pistolozzi, M and Bertucci,C., 2008, Chirality,20, 552-558.

Privalov, P., 1989, Annu. Rev. Biophys. Biophys. Chem., 18, 47-69.

Provencher, S. and Glockner, J., 1981, Biochemistry, 20, 33-37.

Q

Qin, C., Xie, M. and Liu, Y., 2007, Biomacromolecules, 8, 2182-2189.

Quirk, A. V., Geisow, M. J., Woodrow, J. R., Burton, S. J., Wood, P. C., Sutton, A. D., Jolmson, R. J. and Dodsworth, N., Biotechnol. Appl. Biochem, 11, 273-287.

R

Rachinsky, M. and Foster, J., 1975, Arch. Biochem. Biophys., 70, 283.

Rahman, M., Maruyama, T., Okada, T., Imai T. and Otagiri, M., 1993, Biochem. Pharmacol. 46, 10, 1733-1740.

Reed, R., Feldhoff, R.,Clute, O. and Peters Jr, T., 1975, Biochemistry, 14, 4578-4583.

Research Communications, 2000, 277, 83-88.

Rezaei-Tavirani, M., Moghaddamnia, S., Ranjbar, B., Amani, M. and Marashi, S., 2006, J. Biochem. Mol. Bio., 39, 5, 530-536.

Rodger, A. and Nordén, 1997, Circular Dichroism and Linear Dichroism, Oxford University Press.

Roenoer, V., Oratz, M., and Rothschild, M., 1977, Albumin structure, function and uses, Pergamon Press,

Rosen, A., 1970, Bioclin. Pharmacol., 19, 2075-2081.

Rosenheck, 1961, Proc. Natl. Acad. Sci., USA, 47, 1775-1788.

Ross, P., Finlayson, J. and Shrake, A., 1984, Vox Sang, 47, 19-27.

Rudolph, R., Holler, E. and Jaenicke, r., 1975, Biophys. Chem., 3, 226-233.

Rupley, J. A. and Careri, G., 1991, Adv. Protein. Chem, 41, 37-172.

S

Sadler, P. J., Tucker, A. and Viles, J. H., 1994, Eur. J. Biochem., 220, 193-200.

Sanger, F., 1963, Proc. Chem. Soc. 76-83.

Scheider, W., 1979, Prac. Natl Acad. Sci. USA., 76, 5, 2283-2287.

Schindel, W., 1979, Proc. Natl. Acad. Sci. USA., 5, 2283-2287.

Schindel, F., Andersen, C. and Bosse, D., J. Clinical Pharmac., 2003, 43, 1032.

Schulz, G. E. and Schirmer, R. H., Principles of Protein Structure, Springer Advanced Text Chem., editor, Charles C. Cantor.

Schwartz, B. and Gray, G., 1977, Arch. Biochem. Biophys, 181, 542.

Seckler, R. and Jaenicke, R., 1992, The FASEB Journal, 6, 2545-2552

Sereikaite, J., Bumeliene, Z. and Bumelis, V., 2005, Acta. Chromatographica, 15,

Sellers, E. and Koch-Weser, J., Clinical Implications of Drug-Albumin Interaction., 159-167.

Shaklai, N., Garlick, R. and Bunn, F., 1984, 259, 6, 3812-3817.

Shrake, A., Finlayson, J. and Ross, P., 1984, Vox. Sang., 47, 7-18.

Shrake, A. and Ross,P., 1988, J. Biol. Chem., 263, 15392-15399.

Simard, J., Zunszain,P., Hamilton, J. and Curry, S., 2006, J. Mol. Biol., 361, 1552, 336-351.

Simonyi, M., Maksay, G., Kovacs, I., Tegyey, Z., Parkanyi, L., Kalman, A. and Otvos, L.,1990, The Problems and Wonders of Chiral Molecules, edited M. Simonyi, 293-311.

Simpson, R. and Valle, B, 1966, Biochem., 5, 2531- 2538.

Sinha, S., Mitra, R and Pal, S., 2008, J. Phys. Chem. B., 112, 16, 4884-4891.

Sjodin, T., Roosdrorp, N. and Sjoholm, L., 1976, 25, 2131-2140.

Sjo$holm, l. and Ljungstedt, I., 1973, J. Biol. Chem., 248, 8434-8441.

Sjo$din, T., Hansson, R. and Sjo$hohn, I., 1977, Biochim. Biophys. Acta, 494, 61-75.

Sjoholm, I. and Ljungstedt, I., 1973, 248, 24, 8434-8441.

Sjöholm, I., Kober, A., Odar-Cederlöft, I and Borga, o., Biochem. Pharmacol. 25, 12o5-1213.

Sjoholm, I., Ekman, B., Kober, A., Ljungstedt-pahiman, I., Seiving, B. and Sjodin, T., 1979, Mol. Pharmacol., 16, 767-777.

Skoog, D., Fundamentals of Analytical Chem., 6th Ed.

Slayter, E. M., 1965, J. Mol. Biol., 14, 443-452.

Sogami, M., Itoh, K. and Nemoto, Y., 1975, Biochim. Biophys. Acta, 393, 446-459.

Sogami, M. and Foster, J., 1968, Biochem., 7, 2172-2182.

Sogami, M., Era, S., Nagaoka, S. and Inouye, H., 1982, Int. J. Peptide Protein Res., 19, 263-269.

Sönnichsen, F. D., Van Eyk, J. E., Hodge, R. S. and Sykes, B. D., 1992, 31, 8790-8798.

Sowell,J., Mason, J., Strekoski, L. and Patonay, G., 2001, Electophoresis, 22, 18512, 2512-2517.

Spencer M. and King, T. P., 1970. J. Biol. Chem, 245, No. 22, 6134-6148.

Steinhardt, J., 1973, Biochem., 12, 1789-1797.

Squire, P. O., Moser, P. and Konski, O., 1966, J. Phys. Chem., 70, 744-756.

Squire, P. O., Moser, P. and Konski, O., 1968, Biochem, 7, 4261-4272.

Strat, D., 1998 Thesis, Application and Validation of a New Generation CD Spectrometer Based on Diode-Array Detection.

Stroupe, S. D. and Foster, J. F., 1973, Biochem. 10. 4479.

Sudlow, G., Brikket, D. and Wade, d., 1975,Mol. Pharmacol., 824-832.

Sudlow, G., Birkett, D. J. and Wade, D. N., 1976, Mol. Pharmacol., 12, 1052-1061.

Sugio, S., Kashima, A., Mochizuki, S., Noda, M. and Kobayashi, K., 1999, Protein Eng., 12, 6, 439-446.

Suzuki, Y., 2005, Analytical Sci., 21, 83-89.

Swaney, J. D. and Klotz, I. M., 1970, Biochem., 9, 2570.

T

Takagi, T., Tsujii, K. Shirahama, K., 1975, J. Biochem., 77, 939-947.

Tavirani, M., Moghaddamnia., Ranjbar, B., Amani, M. Amir-Marashi, S., 2006, J. Biochem. & Mol. Biol., 39, 5, 530-536.

Te Plio King and Spencer, M., 1970, J. Biol. Chem. 245, 22, 6134-6148.

Timberlake, C. and Bridle, P., 1967,

Toumadje, A., Alcorn, S. and Johnson, W, Jr., 1992, An. Biochem., 200, 321-331.

Toumadje, A. and Johnson, W, Jr., 1993, An. Biochem., 211, 258-260.

Trotman, G. E. R., 1975, Dying and Chemical Technology of Textile Fibres, 5th Edition, Charles Griffin and Company Ltd.

Trynda-Lemiesz, L. and Luczkowshi, M., 2004, J. Inorganic Biochem., 98, 1 85 1 -1 856.

U

Uddin, S., Shilpi, J., Murshid, G., Rahman, A., Sarder, N. and Alam, 2004, J. Biolog. Sci., 4 (5), 609-612, (ISSN 1727-3048)

V

Vorum, H., Fisker, K. and Brodersen, R., 1994, Biochimica et Biophysica Acta, 1205, 2, 178-182.

Vorum, H. and Honoré, B., 1996, J. Pharm. Pharmacol., 48, 870-875.

W

Walker, J., 1976, Febs. Letters, 66,2,173-175.

Wallace, B. and Teeters, C., 1987, Amer. Chem. Soc., 26, 1, 5-10.

Wallevik, K., 1973, J. Biol. Chem., 248, 2650-2655.

Watanabe, H., Kragh-Hansen, U., Tanase, U., Nakajou, K., Mitarai, M., Iwao, Y., Maruyama, T. and Otagiri, M., 2000, Biochem. J., 349, 813-819.

Watanabe, H., Kragh-Hansen, U., Tanase, U., Nakajou, K., Mitarai, M., Iwao, Y., Maruyama, T. and Otagiri, M., 2001, Biochem. J., 357, 269-274.

Weber, B., Willeford, K., Moe, J. and Piszkiewiecz, W., 1979, Biochem. Biophys.Res. Commun., 86, 252.

Wetlaufer, D., 1981, Adv. Protein Chem., 34, 61-92.

Wetzel, R., Becker, M., Behlke, J., Billwitz, H., Bohm, S., Ebert, B., Hamann, H., Krumbiegel, j. and Lassmann, G., 1980, Eur. J. Biochem. 104, 469-478.

Williams, K., 1991, Adv. In Pharmacol., 22, 57-135.

Wilson, J., 1976, Biochem. Biophys. Research Communication, 72, 3, 816-823.

Wilson, J., J. 1978, Biol. Chem., 253, 2070.

Wilting, J., Van Der Giesen w. f., Jassen , L., Weideman, M., Otagiri, M. and Perrin, J., 1980, J. Biol. Chem., 255, 3032-3037.

Wilting, J., ‘t Hart, B. and De Gier, J., 1980, Biochem. Biophys. Acta, 626, 5300-5303.

Wiseman, T., Williston, S., Brandts, J. and Lin, L., 1989, Analyt. Biochem., 179, 131-137.

Woody, R. W., Nakanishi, K. and Berova, N., 1992, Circular Dichroism, Principles and Application.

Wright, A. K. and Thompson, M. R., 1975, Biophys. J., 15, 137-141.

Wu and Lloyd, 1988, Clin. Physiol. Biochem., 6, 50-56.

Y

Yamasaki, K., Maruyama, T., Kragh-Hansen, U. and Otagiri, M., 1996, Biochem, Biophys, Acta., 147-157.

Yamasaki, K., Maruyama,T., Yoshimoto, K., Tsutsumi, Y., Narazaki, R., Fukuhara, A., Kragh-Henson, U. and otagiri, M., 1999, Biochemica et Biophysica Acta, (BBA) 1432, 2, 313-323.

Yang, F., Bian., C., Zhu, L., Zhao, G., Huang, Z. and Huang, M., 2007, J. Struc. Bio., 157, 2, 348-355.

Yu, M. and Finlayson, J., 1984, Vox Sang, 47, 28-40.

Z

Zhu, L., Yang, F., Chen, L., Mecham, E. and Huang, M., 2008, J. Structural Biol., 162, 40-41.

Zsila, F., Bikadi. Z. and Simonyi. M., 2003, Biochemical Pharmacology, 65, 447-456.

Zunszain, P., Ghuman, J., Komastsu, T., Tsuchida, E. and Curry,S., 2003, BMC Struct. Biol., 7, 3(1), 6.

Zurawski, V. Jr. and Foster, J, F., 1974, Biochem., 13, 3465-3471.